

## **ABSTRACT**

Title of Document: FORENSIC INVESTIGATION TECHNIQUES  
FOR INSPECTING ELECTRICAL  
CONDUCTORS INVOLVED IN FIRES FOR ARC  
AND MELT BEADS

Nasir Hussain, M.S. 2012

Directed by: Dr. Peter B. Sunderland  
Department of Fire Protection Engineering  
University of Maryland, College Park

The objective of this research was to determine, experimentally, if distinguishing characteristics exist between the beads formed on energized and non-energized wires exposed to various thermal insults. Most of research published in the literature has not tested energized and non-energized wires under the same thermal conditions. The tests in this study were conducted using convective, radiative and combined convective/radiative thermal exposures. Wires were tested in both energized and non-energized states. Energized wires were tested under “load” and “no load” conditions. Beads formed on both the energized and non-energized wires as results of thermal exposure. Beads were analyzed externally and internally with stereo microscope, SEM/EDS, and a metallurgical microscope. No clear trends or distinguishing visual or microscopic characteristics between the beads formed on energized and non-energized wires were found. The bead analysis methods used during this research showed that it is not possible to distinguish between the beads formed on energized and non-energized wires exposed to various thermal insults.

FORENSIC INVESTIGATION FOR INSPECTING ELECTRICAL CONDUCTORS  
INVOLVED IN FIRES FOR ARC AND MELT BEADS

By

Nasir Hussain

Thesis submitted to the Faculty of the Graduate School of the  
University of Maryland, College Park, in partial fulfillment  
of the requirements for the degree of  
Master of Science  
2012

Advisory Committee:  
Dr. Peter Sunderland, Chair  
Dr. Stanislav Stoliarov  
Dr. Richard Roby

© Copyright by  
Nasir Hussain  
2012

## **Acknowledgements**

**This research has been supported and funded by National Institute of Justice, award number 2010-DN-BX-K246, and Combustion Science & Engineering, Inc.**

The author would like to thank the advisory committee Dr. Peter Sunderland, Dr. Stanislav Stoliarov, and Dr. Richard Roby for the guidance throughout the project.

The author would like to thank, Dr. Jamie McAllister and Dr. Michael Klassen at Combustion Science & Eng., Inc. for their technical assistance and guidance throughout duration of the project. The author would also like to acknowledge Christopher Schooler, Maclain Holton, Casey Fuller and Brent Turner for their assistance in setup of the experimental apparatuses and testing and Dr. Esteban Gonzalez for help with heat transfer simulation.

Special thanks to Dr. Elizabeth Buc of Fire and Materials Research Laboratory in Lavonia, MI and Dr. Lori Streit of Unified Engineering in Illinois for helping with SEM/EDS analysis of the samples. Special thanks to Dr. Charles Manning and his group at Accident Reconstruction Analysis, Inc. for analysis of the samples with preparation, mounting, and grain structure analysis of the samples.

Also, special thanks to Michael Donhue, David Cusatic, Barry Grimm and Mark Teufert at the National Fire Academy in Emmitsburg, MD for helping with the Full-Scale compartment testing.

Most importantly, the author will thank his wife Asifa and children (Omar, Sameer, and Shan) for allowing him time to work on the project.

# Table of Contents

ABSTRACTI	
ACKNOWLEDGEMENTS.....	II
TABLE OF CONTENTS.....	III
LIST OF FIGURES .....	V
LIST OF TABLES.....	VII
NOMENCLATURE .....	VIII
CHAPTER 1: INTRODUCTION.....	1
CHAPTER 2: LITERATURE RESEARCH.....	5
CHAPTER 3: EXPERIMENTAL DESIGN AND SETUP .....	11
3.1 Current and Voltage Data Acquisition.....	12
3.2 Direct Flame Impingement Tests.....	13
3.3 Radiant Tunnel Tests .....	14
3.4 2/5-Scale Compartment Tests.....	17
3.5 Full-Scale Compartment Tests.....	20
3.6 Sample Analysis.....	22
CHAPTER 4: DATA AND RESULTS .....	24
4.1 Summary of Results.....	24
4.2 Testing Data and Results .....	25
4.2.1 Direct Flame Impingement Tests.....	25
4.2.2 Radiant Tunnel Tests .....	31
4.2.3 2/5-Scale Compartment Tests.....	36
4.2.4 Full-Scale Compartment Tests.....	41
4.2.5 Stereo Microscope Results.....	46
4.2.6 Scanning Electron Microscope and EDS .....	50
4.2.7 Analysis with Metallurgical Microscope .....	54
4.2.8 Heat Transfer Analysis .....	60
CHAPTER 5: DISCUSSION.....	64
5.1 Summary.....	64
5.1.1 Direct Flame Impingement Tests.....	64
5.1.2 Radiant Tunnel Tests .....	66
5.1.3 2/5-Scaled Compartment Tests.....	68

5.1.4	Full-Scale Compartment Tests.....	70
5.1.5	Comparisons between Various Exposures.....	72
5.1.6	Bead Characteristics.....	77
5.1.7	Analysis with Metallurgical Microscope.....	80
5.1.8	Heat Transfer Analysis.....	82
CHAPTER 6:	CONCLUSIONS AND FUTURE WORK.....	83
6.1	Conclusions and Summary.....	83
6.2	Future Work.....	86
APPENDIX 1	.....	88
APPENDIX 2	.....	170
APPENDIX 3	.....	180
APPENDIX 4	.....	213
REFERENCES	.....	232

## List of Figures

Figure 3-1: Data Acquisition Setup for Current and Voltage Measurements.....	13
Figure 3-2: Direct Flame Testing Setup (DF).....	14
Figure 3-3: Radiation Tunnel Setup (Units in Inches).....	15
Figure 3-4: Sketch of the Compartment Testing Setup .....	18
Figure 3-5: Flashover Scaled Compartment (SC).....	19
Figure 3-6: Wire Samples in the Ceiling with Thermocouple Tree-Full-Scale Compartment Tests (FSC) .....	21
Figure 4-1: Average Time to Break or Trip for All Wire Types-Direct Flame Tests (DF).....	27
Figure 4-2: Average Time to Break or Trip for Energized and Loaded-Direct Flame Tests (DF) .....	28
Figure 4-3: Typical Amperage and Voltage Graph-Direct Flame Tests (Loaded Wire DF) .....	29
Figure 4-4: Arcing Through Char-Direct Flame Tests (DF) .....	30
Figure 4-5: Average Break Time-Radiation Tunnel Tests (R-All).....	33
Figure 4-6: Average Trip Time-Radiation Tunnel Tests (E and L-R).....	34
Figure 4-7: Average Break Time and Trip Time –Radiation Tunnel Tests (R) .....	35
Figure 4-8: Average Trip Time-Scaled Compartment Tests (SC).....	38
Figure 4-9: Heat Flux at Circuit Trip Time-Scaled Compartment Tests (SC) .....	39
Figure 4-10: Temperature at Circuit Trip Time-Scaled Compartment Tests (SC).....	40
Figure 4-11: TEA at Trip Time for the Scaled Compartment Tests (SC) .....	41
Figure 4-12: Circuit Trip Time for Full-Scale Compartment Tests (FSC).....	44
Figure 4-13: Average Temperature at Trip Time for Full-Scale Compartment Tests (FSC).....	44
Figure 4-14: Average Heat Flux at Trip Time for Full-Scale Tests (FSC).....	45
Figure 4-15: TEA for Full-Scale Compartment Tests (FSC).....	45
Figure 4-16: Beads Produced with Direct Flame Exposure (12-gauge: NE, E (center), and L).....	47
Figure 4-17: Beads Produced with Radiant Tunnel Exposure (16-gauge: NE, 12- gauge: E (center) and L) .....	47
Figure 4-18: Beads Produced with Scaled Compartment Exposure (12-gauge: NE, E (center), and L).....	47
Figure 4-19: Beads Produced with Full-Scale Compartment Exposure (16-gauge: E, 18-gauge: L).....	47
Figure 4-20: Mounted Samples (Cut and Etched) .....	48
Figure 4-21: SM Images of Loaded Wires under Direct Flame Exposure (12-gauge: L-DF) .....	48
Figure 4-22: SM Images Loaded Wire under Scaled Compartment Exposure (12- gauge: L-SC).....	48
Figure 4-23: SM Images of Loaded Wires under Radiant Tunnel Exposure (12-gauge: L-R).....	49
Figure 4-24: SM Images of Non-energized wires under direct flame Exposure (18- gauge: NE-DF).....	49

Figure 4-25: SM Images of Non-energized Wires under Scaled Compartment Exposure (18-gauge: NE-SC) .....	49
Figure 4-26: SM Images of Non-energized Wires under Radiant Tunnel Exposure (18-gauge: NE-R).....	49
Figure 4-27: SM and SEM Images of MS Wires under different Electrical Conditions. ....	51
Figure 4-28: EDS Graph for a Bead Surface formed on an Energized Wire (DF).....	52
Figure 4-29: EDS Graph for a Bead Surface formed on a Non-energized Wire (DF)	53
Figure 4-30: Grain Structures of Wire Control Samples (Unexposed Wires: Solid (Top) and Stranded (Bottom)) .....	56
Figure 4-31: Metallurgical Microscope Images of Beads formed under Direct Flame Exposure (All Loaded 12-R Wires) .....	57
Figure 4-32: Metallurgical Microscope Images of Beads formed under Scaled Compartment Exposure (All Loaded 18-MS Wires).....	58
Figure 4-33: Metallurgical Microscope Images of Beads formed under Direct Flame Exposure (12-R NE (A) and 12-R L (B)) .....	59
Figure 4-34: Metallurgical Microscope Images of Beads formed under Scaled Compartment Exposure (12-R L (A)) and Radiation (14-R NE (B)) .....	60
Figure 4-35: Metallurgical Microscope Images of Beads formed under Scaled Compartment Exposure (18-MS NE (A) and 18-MS L(B)).....	60
Figure 4-36: Copper Wire Sample Setup for Heat Transfer Simulation .....	61
Figure 4-37: Heat Transfer Simulation Results-Temperature Change with Time.....	62
Figure 4-38: Axial Temperature Change along Wire Length (Dc similar to 12-R conductors).....	63
Figure 5-1: Maximum Heat Flux (averaged for each wire type) Measured During Testing. (FSC v SC).....	73
Figure 5-2: : Maximum Temperature (averaged for each wire type) Measured.....	74
Figure 5-3: Average Trip Times for Compartment Testing (FSC v SC).....	75
Figure 5-4: Full-Scale Compartment Trip Time Analysis (FSC) .....	76
Figure 5-5: Scaled Compartment Trip Time Analysis (SC).....	76
Figure 5-6: Total Energy per Area Comparison (SC and FSC).....	77
Figure 5-7: Comparison of Loaded and Non-energized Beads for various Exposures (SM Images).....	79
Figure 5-8: Internal Pattern Comparison of Loaded and Non-energized Beads for various Exposures (SM Images) .....	80
Figure 5-9: Internal Lines of Demarcation (Direct Flame (A and B) and Radiation (C)).....	81
Figure 5-10: : Internal Line of Demarcation (Scaled Compartment-All).....	82



## List of Tables

Table 3-1: Wire Specifications .....	12
Table 4-1: Direct Flame Testing Results (DF) .....	26
Table 4-2: Radiation Testing Results (R) .....	32
Table 4-3: Scaled Compartment Testing Results (SC) .....	37
Table 4-4: Full-Scale Compartment Testing Results (FSC) .....	42
Table 5-1 Average Failure Time-All Exposures .....	72
Table 5-2: Percentage of Samples with Bead Formation .....	77
Table 5-3: Average Bead Diameter .....	79

## NOMENCLATURE

12R	12 AWG Romex Wire
14R	14 AWG Romex Wire
16MS	16 AWG Multi-stranded Wire
18MS	18 AWG Multi-stranded Wire
ARAI	Accident Reconstruction Analysis, Inc.
BT	Time to Break
CFM	Cubic Feet per Minute
CSE	Combustion Science & Engineering, Inc.
Dc	Diameter of Copper Conductor or Strand in Wire
DF	Direct Flame Exposure
E	Electrical Wire with Potential only
E-SC	Energized Wire tested in Scaled Compartment
EDS	Energy Dispersive X-ray Spectrometry
FEMA	Federal Emergency Management Agency
FSC	Full-Scale Compartment Exposure
h	Convective Heat Transfer Coefficient
IR	Infrared (Bulbs)
L	Wire with Load
L-SC	Loaded Wire tested in Scaled Compartment
L-R	Loaded Wire tested in Radiation Tunnel
MS	Multi-Stranded Wire
NE	Non-Energized Electrical Wire
$q_c$	Convective Heat Flux
$q_f$	Flame Heat Flux
R	Radiation Exposure
SC	Scaled Compartment Exposure
SEM	Scanning Electron Microscope
SIMS	Secondary Ion Mass Spectroscopy
SM	Stereo Microscope
TEA	Total Energy per Unit Area (Area under the Curve)
TT	Circuit Time to Trip
V-AC	Alternating Current Voltage (AC)

## **Chapter 1: INTRODUCTION**

According to a National Fire Protection Association (NFPA) report (20) on home electrical fires, about 44,800 home structure fires reported to fire departments across the United States in 2009 included some type of electrical failure that caused fire ignition. These electrical fires resulted in 472 deaths, 1500 civilian injuries, and approximately \$1.6 billion in property damage. The report also highlighted that from 2005-2009, on average, electrical fires represented 13% of all fires, 17% of all casualties caused by fires, and 21% of the property damage caused by all fires in the United States during 2005-2009.

Electricity and fire is perhaps one of the most controversial couplings in the fire investigation field. Citing the cause of fire as electrical in origin is often misused, unused, and overused due to the lack of resources and information available to the investigation community. *NFPA 921, A Guide for Fire and Explosion Investigation* (NFPA, 2010), devotes an entire chapter to electrically initiated fires; this chapter includes descriptions of various modes of wire failure. Several images of damaged wires and the causes of that damage are presented as examples for investigators to use in their analysis of electrical wires. Specifically, these images focus on the production of arc beads on different types of electrical cords. Fire investigators often, rely on the appearance of electrical wires and the presence of arc-beads to assess the potential involvement of the wires or attached appliances in the initiation of the fire. Many times, a fire investigator will conclude that a device was electrically energized at the time of a fire and therefore could have potentially caused the fire, based on the presence of an arc bead on a wire. Unfortunately, there are many limitations in the

current state of the art for electrical wire analysis. Although many researchers have attempted to define the conditions under which particular characteristics occur on electrical wires, many, if not all, of these studies did not test a control (a non-energized wire). For example, if it is believed that arc beads are only formed in energized wires, then a control study must be performed to ensure that the same characteristic “bead” cannot be formed on non-energized wires.

The main objective of this research was to determine, experimentally, if distinguishing characteristics exist between energized and non-energized wires exposed to various types of thermal insults: direct flame impingement, radiant heating, and combined radiant/convective heating. Electrical copper conductors were tested under three electrical conditions that included non-energized, energized with potential only, and energized with load. After thermal testing was completed, the wires were analyzed with a high resolution stereomicroscope, a Scanning Electron Microscope (SEM) and Electron Dispersive Spectrometry (EDS) to define visual and elemental characteristics and patterns in and on the wires particularly the beads. . The internal grain structure of the beads was also studied with a metallurgical microscope by mounting the samples in epoxy, and then cutting, polishing, and etching each sample to reveal the inner grain structures.

There have been many studies that focused on the role of energized electrical wires in the initiation of fires, and many researchers have studied the causes of beads on electrical wires. However, most of this research has focused on distinguishing between beads formed due to a failure condition which resulted in a fire (cause) versus beads formed from exposure to a fire (effect). All of these studies have

focused on the energized wires with the assumption that beads only form on energized wires. Limited research has been performed to establish the ability of a “bead” to form on a non-energized wire. Therefore, the inherency of the formation of “beads” on energized wire and the relevance of these beads in the context of the fire cause is unknown. The overriding purpose of this research was to address whether any distinguishing characteristics exist between beads found on energized wires versus those found on non-energized wires.

As discussed in detail in the Literature Research Chapter below, there have been many studies that focused on the role of energized electrical wires in the initiation of fires; however, most of this research has focused on distinguishing between beads formed due to a failure condition which resulted in a fire (cause) versus beads formed from exposure to a fire (effect). Even with an extensive volume of research, there is still little agreement on an appropriate methodology for evaluating beads. Furthermore, there is little agreement on the usefulness and validity of the information gathered from the analysis of a wire bead in the context of fire origin and cause investigation. Additionally, one of the largest potential flaws in the research is the assumption that beads only form on energized wires. Limited research has been performed to establish the ability of a “bead” to form on a non-energized wire. Therefore, the inherency of the formation of “beads” on energized wire and the relevance of these beads in the context of the fire cause is unknown.

The goal of this research was to address whether any distinguishing characteristics exist between beads found on energized wires versus those found on non-energized wires. Based on preliminary findings, it was hypothesized that the

formation of a bead on a wire is not inherently related to the energized state of the wire, but rather is a function of the thermal kinetics of the copper. This hypothesis is contrary to the belief that beads can only be formed on energized electrical wires. However, the theory that beads can only be formed on energized wires is contrary to the phenomenon of surface tension. The basic laws of physics show that the same theories that apply to water droplets can be applied to other liquids; surface tension is the true cause of the “bead” shape that forms when copper melts. According to White [40] liquids form their spherical shape due to cohesive surface forces, and the necessity to minimize “wall tension”. All liquids would be “perfectly spherical” if no other forces (e.g. gravity) existed. Therefore, it is the liquidification (melting) of the metal that results in the formation of a bead. Whether this melting occurs as a result of fire exposure or arcing is irrelevant, since the outcome is independent of the melting conditions. Hence, it is hypothesized that the characteristic “bead”, typically defined as a round globule with a clear line of demarcation, can form on both non-energized and energized wires. Furthermore, it was hypothesized that the porosity and chemical composition of the beads will vary based on the conditions under which the beads are formed. The study of beads with SEM/EDS will show distinguishing characteristics between beads formed on energized and non-energized wires.

## **Chapter 2: LITERATURE RESEARCH**

Gray et al. [18] performed a series of experiments to distinguish between beads formed from overloading the wire with current versus beads formed from flame exposure. In both cases, the wires were energized. In the first test, an overload (7-10 times the amperage rating) was passed through the wires until heat caused the insulation to melt and the wires to short circuit. Flaming was only observed when 5 amp rated wires were exposed to currents above 30 amps. In the second test, wires were subjected to normal or slightly elevated current conditions and exposed to a flame. Once the wire insulation burned off, arcing occurred and typically resulted in the formation of a bead.

A Scanning Electron Microscope (SEM) was used to study the difference between the beads. Beads produced under overload conditions clearly showed small holes on the bead surface; this characteristic was not present on the wires exposed to a flame under normal load conditions. Gray et al. hypothesized that the holes found in the overloaded wire samples were caused by resistive heating of the copper above 260°C during the overload event. The heating, then caused the expulsion of minute crystals from the bead surface. Furthermore, Gray et al. hypothesized that the crystallization did not happen on the wires exposed to flame because the wire insulation provided “some degree of thermal insulation” which prevented the wires from overheating prior to failure. Gray et al. also hypothesized that the holes were due to the copper being heated throughout its entire length during overload, as opposed to localized surface heating which occurred during the flame exposure. The total number of experiments performed was not discussed; therefore, the level of

certainty in the analysis is unclear.

Anderson [1 and 2] used Auger Electron Spectroscopy (AES) to study wires damaged in fire. AES is used to outline elements found below the residue in an arc bead. AES works by scanning the surface of the bead using a focused electron beam and measuring the kinetic energy produced by collision between the element and the impacting electron. In Anderson's study, the bead was studied for the presence of different chemicals to better understand the environmental conditions under which the bead was formed.

Anderson focused on the presence of common combustion products in fires such as carbon, sulfur, chlorine, and calcium. Anderson hypothesized that beads formed prior to a fire (cause) would have a different chemical composition when compared to beads formed after the fire initiation (effect). Specifically, Anderson stated that combustion products would not be present in "cause" beads but would be present in "effect" beads. Three case studies were conducted on copper beads from actual fires. In the first case, a refrigerator cord was involved, which was assumed to have started the fire. AES analysis showed high levels of carbon, calcium, and chlorine, and low levels of oxygen. Anderson concluded that the bead was not formed prior to the fire but was an effect of fire exposure because it contained elements of combustion products.

In the second case, arcing was found in the copper coils of a heater fan. In this case, bead analysis showed low levels of carbon, calcium, and chlorine, and high levels of oxygen. Anderson concluded that the fire must have started in the fan based on the lack of high levels of combustion products. In the final case, a crock-pot



power cord was involved in a restaurant fire. AES analysis was used to indicate that the bead was created from fire exposure and was not the cause of the fire due to the presence of combustion products. Anderson did not set any quantitative standards on the presence of elements in beads for concluding that a bead was the cause of the fire or an effect of the fire.

Beland [10] discussed the difficulties of analyzing an arc bead due to its varying composition and was critical of Anderson's work, stating that the AES method was not effective in distinguishing between cause and effect beads. Beland's opinion of Anderson's AES method was based on the fact that the same elements (calcium, chloride, carbon, oxygen, etc.) would be present regardless of whether the bead was formed from cause or effect; these elements are produced from the melting and burning of the wire insulation, which would occur during a failure condition prior to arcing or would occur during fire exposure. Beland tested several similarly prepared wire samples for chlorine, carbon and oxygen. Beads were created by subjecting energized wires to flame or by creating a short-circuiting in the wires. The elemental composition of the beads formed under these conditions did not show consistent concentration of elements trapped in beads. This finding was true for different beads as well as for different locations in a given bead. No significant patterns were observed to indicate that a bead was the cause or effect of a fire. Beland stated that Anderson's method might be effective for bare wires but not for insulated wires.

Howitt [26] reviewed the literature on the solubility of gases in liquid copper. He determined that there was no scientific justification for the hypothesis that

atmospheric gases will become trapped in a bead as it solidifies. Howitt was able to conclude that the solubility of oxygen in copper is much lower than the detectable level of AES analysis, and oxygen is more soluble in copper in the solid state than in the liquid state where beads are formed. Howitt concluded that the AES spectra of arc beads contain no relevant information to conclude whether a bead was the cause or effect of a fire.

Hoffman [24] tested more than 700 electrical appliance power cords under various thermal conditions to assess their performance in fires and to evaluate the type of material damage sustained by the power cords. Power cords were exposed to radiant heating and direct flame impingement. Hoffman concluded that energized wires do not always produce evidence of electrical faults when exposed to radiant heating, that appearance of tested samples does not depend on the type of exposure, and that electrical damage to wire conductors produced in laboratories does not differ from that found in actual fires.

Lee et al [32] used SEM to analyze beads formed on energized wires. They evaluated the beads for graphitized and amorphous carbon. Lee et al. concluded that the beads produced from exposure to fire had only amorphous carbon, whereas beads produced from an electrical fault had both graphitized and amorphous carbon. However, only 26% of the beads produced from electrical activity showed both types of carbons; hence, this trend is not consistent throughout all the samples. The study did not test or analyze non-energized wires.

Other researchers also have disagreed with Anderson's analysis. According to Babrauskas [5], Satoh et al. showed that AES analysis is not as good as Secondary

Ion Mass Spectrometry [SIMS] in measuring the concentration of impurities found in beads. Babrauskas [5] strongly disagreed with Anderson based on the fact that wires have insulation that is made of carbon containing polymers. If a wire is heated to the point of shorting due to over-current, then the insulation will vaporize. A bead produced under these pre-fire conditions will possibly contain carbon from the vaporizing insulation. Babrauskas also pointed out that calcium carbonate is common filler in wire insulations and that PVC insulation consists of chloride, which could possibly result in the presence of calcium and chlorine in both cause beads and effect beads.

Levinson [34] studied micro and macro structures of copper conductors. According to Levinson, the untested copper contains only elongated copper structures and is considered single phase. This wire is highly pure and oxygen free also known as OFHC (oxygen-free high conductivity) copper wire. The second type of copper wire is known as ETP (Electrolytic tough-pitch). This copper has similar microstructures except it also contains copper oxide which is visible as small gray micro-structures within copper structure.

Copper wires start to recrystallize if they are heated above 260°C. The recrystallization time decreases from hours at 260°C to seconds at 540°C or above. If enough oxygen is absorbed,  $\text{Cu}_2\text{O}$  dendrites may form. Microstructures will be porous if the wire was heated or arced in presence of insulation or any carbonaceous materials. This characteristic cannot be attributed to heating or arcing of the wire. Melting of the wires with heat or arcing will lead to formation of droplets (beads) at the broken ends and the presence of droplets on wire ends is not proof that the wire

was under load and arced when it broke.

As discussed above, there have been many studies that focused on the role of energized electrical wires in the initiation of fires. Many researchers have specifically studied the causes of arc beads in energized electrical wires. The main areas of research have focused on distinguishing between cause and effect, i.e. an arc bead which is formed due to a failure condition which causes a fire versus an arc bead that is formed from exposure to a fire (effect). Based on the literature review, there is apparent disagreement between researchers in placing a value on the analysis of arc beads. Additionally, no research has been performed on non-energized conductors, so no one has yet provided a comparison between energized and non-energized wire damage. The present research will address the limitations of the current methods available to fire investigators and thereby enhance the accuracy of fire origin and cause determinations.

### **Chapter 3:           EXPERIMENTAL DESIGN AND SETUP**

The use of various types of exposure conditions ensured that the characteristics on the wires (or lack thereof) were not caused by one specific thermal insult. The wire tests in this study were conducted using direct flame apparatus, a radiant tunnel apparatus, a 2/5-scale fire compartment, and a full-scale compartment. Wires were tested in an energized and non-energized state. Energized wires were tested under “load” and “no load” conditions. Under load conditions, the energized wires were plugged into a 110-120 volt (V-AC) power source with 9-13 amps of load. Under “no load” conditions, the wires were plugged into the power supply but no load (i.e. current flow) was placed on the circuit.

Four types of electrical wires with copper conductors were chosen in order to represent most of the types of wires commonly found in households: 12-gauge solid, 14-gauge solid, 16-gauge stranded, and 18-gauge stranded. The wires chosen included two multi-stranded (MS) and two single stranded Romex wires. The specific wire details are provided in Table 3-1.

Multi-stranded wires were chosen based on an at-home survey of power cords including those used to power all lights and small appliances. It was discovered that most of the power cords were made of 18-gauge or 16-gauge, two-conductor, multi-stranded copper wires. Also, the most common branch-circuit wiring was 2-conductor, 14-gauge and 12-gauge Romex. The same Romex wiring brand was utilized for all tests; however, this was not the case for the stranded wires. The 16-gauge Southwire brand (black) and 18-gauge I-Sheng brand wires were utilized for direct flame testing. The 16-gauge Southwire brand (brown) and 18-gauge Weber

brand wires were utilized for all other testing.

**Table 3-1: Wire Specifications**

	Romex	Romex	MS W1	MS W2	MS W3	MS W4
<b>Manufacturer</b>	Southwire	Southwire	Southwire	Southwire	I-Sheng	Weber
<b>UL Listing</b>	E18679	E18679	E46194	E46194	E315167	E157652
<b>Size (AWG)</b>	12	14	16	16	18	18
<b>Conductors</b>	2	2	2	2	2	2
<b>Strands (per Conductor)</b>	1	1	26	65	41	41
<b>Strand Diam. (mm)</b>	2.00	1.59	0.25	0.16	0.16	0.16
<b>Type</b>	NM-B	NM-B	SPT-2	SPT-2	SPT-2	SPT-2
<b>Temperature (°C)</b>	90	90	105	105	60	105
<b>Voltage (V)</b>	600	600	300	300	300	300
<b>Ampacity (Amps)</b>	20	15	13	13	10	10
<b>Flame Rating</b>	N/A	N/A	VW-1	VW-1	VW-1	VW-1
<b>Insulation Thickness (mm)</b>	0.483 C 0.762 J	0.483 C 0.762 J	1.14	1.14	1.14	Unknown
<b>Insulation Material</b>	PVC/Nyln	PVC/Nyln	PVC	PVC	PVC	PVC
<b>Insulation Color</b>	Yellow	White	Black	Brown	Black	Green

### ***3.1 Current and Voltage Data Acquisition***

Various combinations of Labview and Pdaq View software and hardware were used to acquire and record data during each testing set. The voltage on the energized wires ranged from 110-120 volts and the amperage on the loaded wires ranged from 9-13 amps. An Avtron Model K490 load bank was used to generate current on the wire to be tested under loaded condition. Electrical activity and time to failure were monitored in the energized wires using a Ohio Semitronics, model VT-120E, voltage transducer and a CR Magnetics, model CR-4320-20, current transmitter. Continuous data was recorded with the acquisition system for the entire duration of each test. A schematic of this data acquisition system and current and voltage setup are shown in Figure 3-1 below. In this schematic, the Test Cell represents the method of exposure, a torch, a radiation tunnel or a compartment.

Energized with load, energized with no-load, and non-energized wires were tested simultaneously in both full and scaled compartment tests (Sections 3.3 and 3.4). In direct flame (Section 3.2) and in radiation testing (Section 3.3) wires were tested individually.

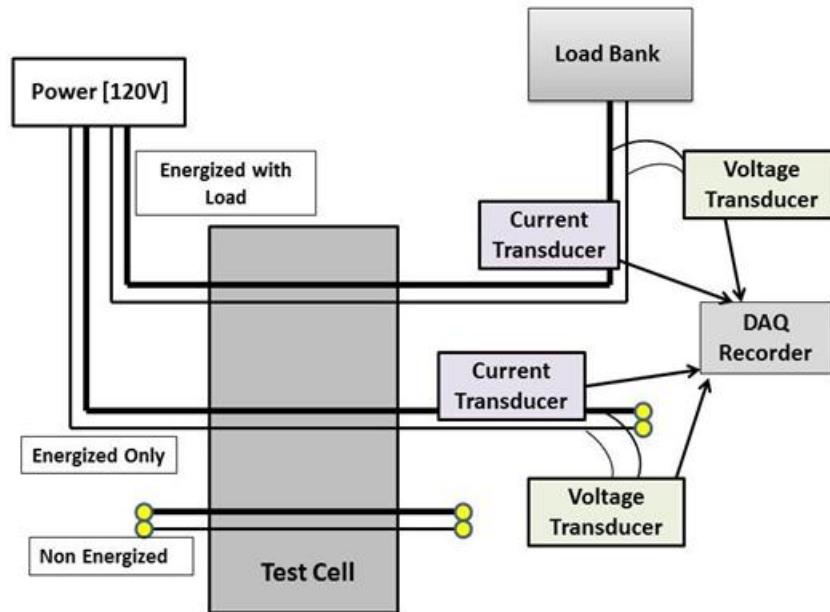


**Figure 3-1: Data Acquisition Setup for Current and Voltage Measurements**

### ***3.2 Direct Flame Impingement Tests***

A Bernzomatic Max Power Propylene torch was used to expose all four wire types (12-gauge solid, 14-gauge solid, 16-gauge stranded, and 18-gauge stranded) to direct flame impingement. Wires were tested under three electrical scenarios: energized with load, energized with no load, and non-energized

A wooden holder, shown in Figure 3-2 was utilized to ensure consistent wire placement relative to the torch. The wire was held about  $\frac{3}{4}$  of an inch away from the tip of the torch. The adiabatic flame temperature for a propylene torch is approximately 1982 °C (3600 °F) and the flame temperature with a thermocouple was

between 1280 °C-1300 °C. The mass loss rate of the fuel from the canister was  $1.18 \times 10^{-6}$  kg/s. The heat of combustion of propylene is about 48,820 kJ/kg therefore the heat release rate per area (heat flux) of the torch (based on the nozzle diameter of the torch of 0.91 cm and flame surface area from nozzle to the wire) was approximately 90 kW/m<sup>2</sup>.



**Figure 3-2: Direct Flame Testing Setup (DF)**

The wire was held in the flame, tension free, by clamps until it broke due to melting, arcing, or shorting. Each test variation was repeated six times resulting in a total of 72 tests.

### ***3.3 Radiant Tunnel Tests***

A radiant tunnel apparatus shown in Figure 3-3 was designed for this study. This apparatus was utilized to expose all four wire types (12-gauge solid, 14-gauge solid, 16-gauge stranded, and 18-gauge stranded) to approximately 125 kW/m<sup>2</sup> and 1050-1100 °C temperature until failure. Wires were tested under three electrical scenarios: energized with load, energized with no-load, and non-energized. The voltage on the energized wires ranged from 110-120 volts (V-AC), and the amperage on the loaded wires ranged from 9-13 amps. Voltage and amperage data was



recorded with the acquisition system described in Section 3.1 above. Time to failure was documented for each non-energized wire using a stopwatch.

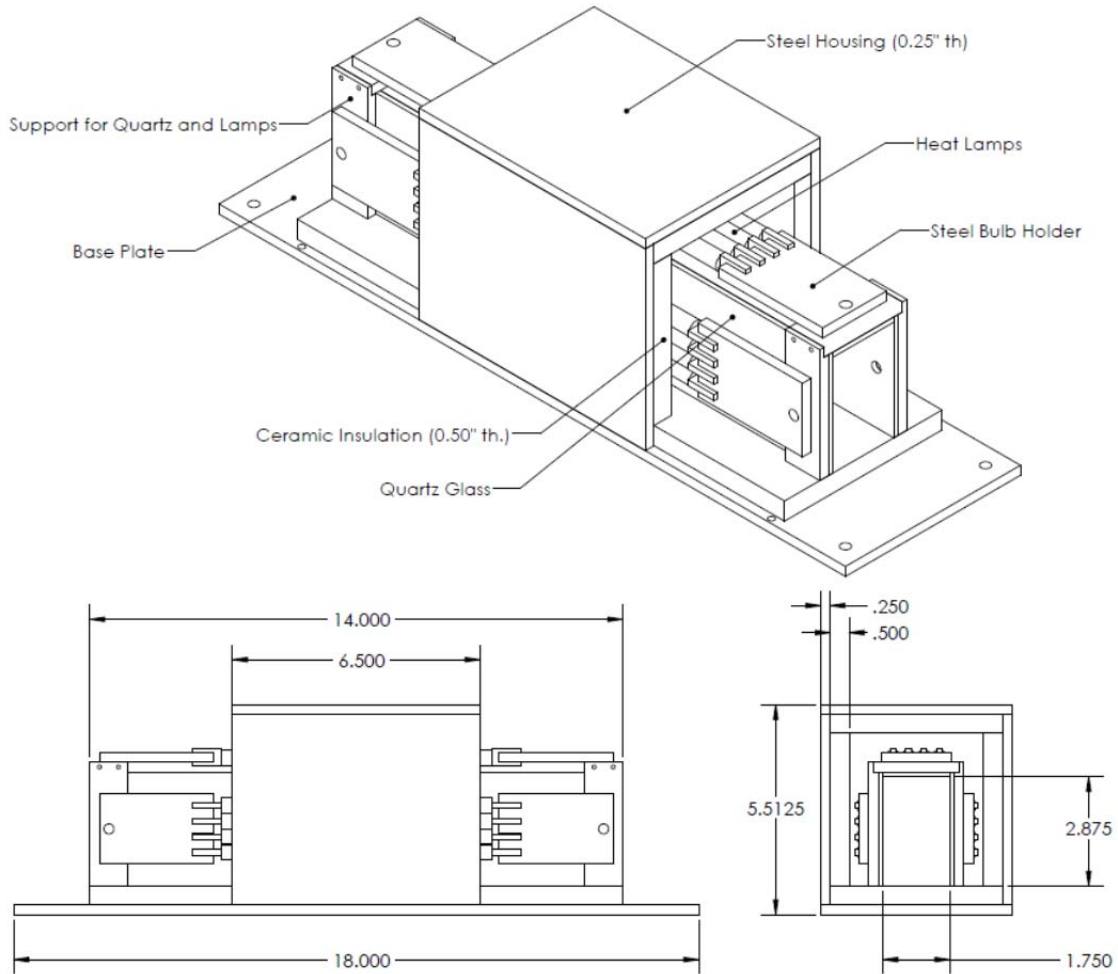


**Figure 3-3: Radiation Tunnel Setup (Units in Inches)**

The radiation apparatus contained twelve (12), 120 volt, 1200 watt Infrared (IR) bulbs inside a 14-inch long tunnel. Four bulbs were installed on each of the two vertical walls as well as the ceiling. Wires were run horizontally through the tunnel and supported on each end with clamps. The exterior of the tunnel was constructed of 1/4 inch steel, and the interior of the tunnel was lined with marinite. The bulbs were mounted on the marinite and a protective quartz glass shield was used in front of the

bulbs to prevent breakage due to arc spatter of copper pellets. Voltage and amperage to the bulbs were adjusted using a Model 18D Solid State Power Supply manufactured by Payne Engineering. The tunnel was calibrated before the start of each test to ensure that the heat flux and temperature output was consistent. A Vatel Corporation circular foil heat flux transducer (Model TG1000-30, maximum flux: 150 kW/m<sup>2</sup>) was used for the calibration.

In order to avoid pre-heating of the samples during placement inside the tunnel, a heavily insulated, fiberglass sample holder was utilized. The wire was placed in the sample holder and clamped at one end of the tunnel. The sample holder was then removed from the wire when the test was ready to begin. Once the sample holder was removed, the wire was clamped on the other end of the tunnel. No tension was placed on the wire. The wire was exposed to radiation until it broke due to heat and/or electrical activity.

The design of the radiant tunnel apparatus was improved throughout the testing process as issues arose; however, there were still some challenges that were faced when performing tests using this piece of equipment. In particular, some of the IR bulbs intermittently or completely failed between tests. The failures appeared to be caused by the premature aging of the bulbs and their connections due to the dramatic thermal cycling of the apparatus. The bulbs were replaced several times in order to continue testing. Finally, it was decided that the tunnel would be run continuously for one day to eliminate the thermal cycling. By running the tunnel continuously, a large number of tests were completed and no bulb replacement was necessary due to the

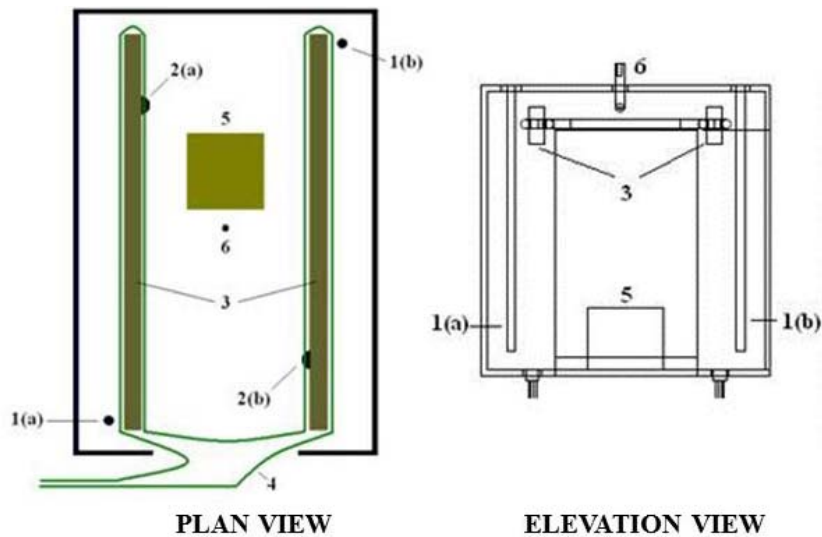
elimination of the heating and cooling cycle. Each test variation was repeated three times resulting in a total of 36 tests.

### ***3.4 2/5-Scale Compartment Tests***

A 2/5-scaled compartment was utilized to expose all four wire types (12-gauge solid, 14-gauge solid, 16-gauge stranded, and 18-gauge stranded) to a fire from an incipient stage to a fully-developed stage or post flashover stage. Wires were tested under three electrical scenarios: energized with load, energized with no load, and non-energized. The voltage on the energized wires ranged from 110-120 volts, and the amperage on the loaded wires ranged from 9-13 amps. The current and voltage were monitored with the setup described in Section 3.1 above. Temperatures within the compartment were monitored by two thermocouples trees located in the front left and middle of the compartment. Each tree contained eight (8) Type K thermocouples spaced approximately 6 inches apart from ceiling to floor. Heat flux within the compartment was monitored with two Medtherm Corporation heat flux transducers (Model 64-10-20, 100 kW/m<sup>2</sup>) located at floor level in the front right and back left corners. Temperature, heat flux, and electrical data were recorded with an acquisition system utilizing Labview software.

The 2/5-scale compartment was modeled after the ASTM E1822 full-scale compartment. The interior dimensions of the compartment measured 38.5 inches wide by 58.3 inches long by 38.5 inches high. The ventilation opening at the front of the compartment measured 18 inches wide by 32 inches high as shown in Figure 3-4 below. The interior walls were constructed of 1/2 inch gypsum wallboard covered with a 1/2 inch layer of marinite. The exterior walls of the compartment were built

with 3/4 inch plywood on (2 x 4)-inch wood studs. The compartment was constructed to withstand temperatures in excess of 900°C which are typically found during room flashover conditions. Wire samples were mounted on 2-inch by 4-inch wood studs and hung from the ceiling of the compartment as seen in the Plan View of Figure 3-4. The wiring was secured to the wood with metal staples. The staples were loosely secured into the wood in order to prevent any excessive pressure on the cable insulation and to minimize the potential for localized electrical activity between the wires and the staples. Each tested wire was about 40 feet long, which provided a sufficient length of wire to be routed through the ceiling of the compartment and out to the data acquisition system.



- 1(a) – TC Tree (4 inches from front and left wall)
- 1(b) – TC Tree (4 inches from back and right wall)
- 2(a) – Radiometer (12 inches from front wall, 8 inches from left wall)
- 2(b) – Radiometer (12 inches from back, 8 inches from right wall)
- 3 – 2x4 Wood Beams (6 inches from sides, 3 inches below ceiling)
- 4 – Wire (attached to wood beams via metal staples)
- 5 – Wood Crib ((10X10X9) inches on top of - inch diameter dish)

**Figure 3-4: Sketch of the Compartment Testing Setup**

After preliminary tests were conducted in the compartment, it was determined that the compartment reached a maximum temperature of only 930°C during post-flashover conditions. This temperature was not sufficient to melt the non-energized copper wires which have an average melting temperature of 1083°C. In order to increase the temperature within the compartment, the amount of oxygen available for combustion was increased using a forced air blower. The blower fan was ducted to the bottom portion of the doorway of the compartment. The ducting was 8 inches in diameter and was fitted with a 4 inches by 18 inches adapter at the compartment doorway. Figure 3-5 shows the general layout of the compartment and ducting using in a prior study [19]. The original adapter size was modified for the purposes of this study to run the entire doorway width.



**Figure 3-5: Flashover Scaled Compartment (SC)**

Because test samples were placed near the ceiling, the ventilation ducting was positioned at the bottom of the doorway to minimize disruption of the upper thermal layer development within the compartment. The blower produced an air flow velocity of approximately 6 m/s measured at the 8-inch diameter duct opening, so the

flow rate was slightly higher than 400 CFM. Each test variation was repeated six times resulting in a total of 72 tests.

### ***3.5 Full-Scale Compartment Tests***

Full-scale compartment fire tests were performed at the National Fire Academy (NFA) in Emmitsburg, Maryland in conjunction with the Academy's fire Origin and Cause Investigations course. NFA utilizes up to eight (8) test cells to simulate various types of fire scenes that investigators may encounter in the field. Most of the test cells are furnished with carpeting, couches, armchairs, coffee tables, televisions, lamps, and various other household effects. Each compartment measured 156 inches (13 feet) long by 108 inches (9 feet) wide by 96 inches (8 feet) high with a 23 inch wide by 35 inch high window and a 32 inch wide by 82 inch high doorway. In some cases, the window was partially open during the entire test. In all cases, the degree to which door was open was varied throughout the test to control the ventilation: If the fire growth slowed down, the door was opened and if the fire growth was too fast, the door was closed. This positioning was done until flashover conditions were reached in the test room. In most cases, the fire was extinguished by the fire fighters immediately after flashover conditions were observed.

The compartments were utilized to expose all four wire types (12-gauge solid, 14-gauge solid, 16-gauge stranded, and 18-gauge stranded) to a fire from an incipient stage to a fully-developed stage. Wires were tested under three electrical scenarios: energized with load, energized with no load, and non-energized. The voltage on the energized wires ranged from 110-120 volts (V-AC), and the amperage on the loaded wires ranged from 9-13 amps. The current and voltage were monitored with the setup

described in Section 3.1 above. Temperatures within the compartment were monitored with a thermocouples tree located in the center of the room. The tree contained eight (8) Type K thermocouples spaced approximately 12 inches apart from ceiling to floor. The heat flux within the compartment was monitored with a Medtherm Corporation heat flux transducers (Model 64-5-20, 50 kW/m<sup>2</sup>) located at floor level in the center of the room. Temperature, heat flux, and electrical data were recorded with an acquisition system utilizing Labview software.

The electrical wire samples were hung from the ceiling in a manner similar to the 2/5-scale compartment testing. The orientation of the wires is shown Figure 3-6.



**Figure 3-6: Wire Samples in the Ceiling with Thermocouple Tree-Full-Scale Compartment Tests (FSC)**

As was encountered with the small-scale tests, it was difficult to achieve temperatures in the compartment that exceeded 900°C. This difficulty was partly because of ventilation conditions within the compartments, and partly because of the need to leave the cells in suitable condition for post-fire investigation. Since the test

cells were being utilized for investigation training, it was important to have some remnants of the burn(s) for the student to evaluate. Therefore, the test fires were not allowed to remain in a fully-developed stage for a long period of time. In a few instances, the temperature did exceed the melting point of copper, and effects were seen on the non-energized copper wires; however, this was not the case for every test. Each test variation was repeated three times resulting in a total of 36 tests.

### ***3.6 Sample Analysis***

After each set of four thermal exposure testing was completed, damage on each wire sample was photographed using a Nikon SMZ800 stereomicroscope with 40x magnification. Some samples were analyzed with an SEM at the University of Maryland at College Park or at Unified Engineering (Aurora, IL). Samples analyzed at the University of Maryland were not mounted, cut, polished, or etched; only the exterior surface of each sample was analyzed. Samples analyzed at Unified Engineering, Inc. were mounted in Buehler epomet epoxy, rough sanded with 100 grit paper until the features were exposed, and then progressively sanded to a final polish of 3  $\mu\text{m}$ . After being polished, the samples were etched for 20 -30 seconds with a solution of 1 gram  $\text{FeNO}_3$ , 15 mL  $\text{H}_2\text{O}$  and 5 Ml  $\text{HCl}$ . These samples were also photographed with a stereomicroscope.

For further analysis, these samples were sent to Accident Reconstruction Analysis, Inc. (ARAI) for analysis with a metallurgical microscope to study the inner structures of the beads. The ARAI staff, particularly Dr. Charles Manning, has vast experience in dealing with copper wires on metallurgical bases. Samples were remounted and re-etched with an Ammonium Hydroxide-Hydrogen Peroxide



solution. A metallurgical microscope was used to take images of bead grain structures.

A one dimensional heat transfer calculation was also performed for the direct flame case of the solid wires to determine the axial heat transfer within the copper conductor away from the section being heated by the flame. A simple conduction model was used to perform the simulation.

## **Chapter 4: DATA AND RESULTS**

### ***4.1 Summary of Results***

A total of 190 wire samples were tested. Wire types included 12-gauge and 14-gauge solid and 16-gauge and 18-gauge stranded conductors. The tests were conducted using a bench-scale, direct, premixed flame impingement apparatus, a bench-scale 125 kW/m<sup>2</sup> radiant tunnel apparatus, and 2/5-scale and full-scale flashover compartments.

Temperature, heat flux, current, voltage, trip time (TT), and break time (BT) were recorded for each test. All of the collected data was analyzed for commonalities and trends between test sets. All of the wire samples were photographed, and the location and number of failure points were documented. Additionally, some of the wire samples were mounted, cut, polished, etched and analyzed using a combination of stereomicroscopic, SEM, and EDS techniques. After this analysis, samples were remounted and re-etched for copper grain structures analysis with a metallurgical microscope.

Based on preliminary studies, it was hypothesized that characteristic “arc-beads” could be formed on energized wires as well as non-energized wires. Additionally, it was hypothesized that the formation of a bead on a wire was not a function of its “energized state”, but a function of its “thermal state”. These hypotheses have been further validated by the research results discussed below. No trends or distinguishing visual or microscopic characteristics have been found in the samples reviewed with SM and SEM/EDS. Although metallurgical analysis showed some useful results that can be used on occasion to differentiate between energized

and non-energized wires, such evidence was not apparent in every situation

Whether a wire was energized with load, energized with no load, or non-energized had no significant effect on the visual or microscopic characteristics of the wire. Round copper globules with clear lines of demarcation, traditionally defined as “beads”, were produced on both energized and non-energized wires. Some energized wires that did arc failed to produce round copper globules with clear lines of demarcation, while some non-energized wires that could not arc did produce these characteristic beads. Under a microscope, beads from some of the energized wires were porous and contained a large quantity of internal void spaces, while other beads contained no void spaces. This same trend was true for non-energized wires. A preliminary view of the samples under SEM/EDS also showed no trends in grain structure or chemical compositions. A detailed study by ARAI of the inner grain structures of the beads did reveal some significant distinguishing trends between energized and non-energized wires but not in all samples.

## ***4.2 Testing Data and Results***

Data and results are presented in four subsections and separated according to thermal exposure type: direct flame impingement (4.2.1), radiant tunnel (4.2.2), 2/5 scale compartment (4.2.3.), and full-scale compartment (4.2.3).

### **4.2.1 Direct Flame Impingement Tests**

A Bernzomatic Max Power Propylene torch was utilized to expose wires to direct flame impingement. The wire samples were held near the center of the premixed flame until they broke due to melting and/or electrical activity. Testing was discontinued after a break in the wire occurred or the circuit breaker tripped due to

short-circuiting or arcing. As seen below, Table 4-1 shows the breakage times (BT) or trip times (TT) for each wire type under all three electrical conditions.

**Table 4-1: Direct Flame Testing Results (DF)**

Test No.	Romex 12/2			Romex 14/2		
	NE	E	L	NE	E	L
<b>Time to Break or Trip (Minutes)</b>						
<b>1</b>	2.92	1.04	0.75 (T)	3.50	0.79	0.77
<b>2</b>	2.25	0.73 (T)	0.64 (T)	3.50	0.57	0.65
<b>3</b>	1.68	0.63	0.50 (T)	3.38	0.48	0.82
<b>4</b>	2.67	0.76 (T)	0.56 (T)	3.20	0.83	0.75
<b>5</b>	2.33	0.86 (T)	0.63 (T)	3.40	0.51	0.58
<b>6</b>	2.48	0.68 (T)	0.67 (T)	5.43	0.84	0.75
<b>Average</b>	<b>2.39</b>	<b>0.78</b>	<b>0.62</b>	<b>3.74</b>	<b>0.67</b>	<b>0.72</b>
Test No.	Multi-Strand 16/2			Multi-Strand 18/2		
<b>1</b>	1.13	0.42	0.37 (T)	2.00	0.42	0.30
<b>2</b>	0.49	0.32	0.30	1.72	0.25	0.27 (T)
<b>3</b>	0.49	0.33	0.38 (T)	1.18	0.25	0.23 (T)
<b>4</b>	0.61	0.33	0.26 (T)	0.73	0.25	0.24 (T)
<b>5</b>	0.49	0.29	0.30	1.52	0.25 (T)	0.26 (T)
<b>6</b>	0.69	0.28	0.34	2.67	0.25	0.39
<b>Average</b>	<b>0.65</b>	<b>0.33</b>	<b>0.33</b>	<b>1.64</b>	<b>0.28</b>	<b>0.28</b>
NE = Non-Energized, E = Energized, No Load and L = Energized, Loaded (T) Circuit tripped but wire did not break						

In the 12-gauge solid wire tests, TT occurred before BT in 4 out of 6 tests for the energized, no-load conditions, and 6 out of 6 tests for the energized, loaded conditions. No circuit breaker trips occurred in any of the 14-gauge solid wire tests. The times for stranded wire tests were variable, with circuit tripping occurring in 3 out of 6 tests of 16-gauge, energized, loaded wires. In the stranded, 18-gauge wires, circuit tripping occurred in 1 out of 6 tests of energized, non-loaded wires, and 4 out of 6 tests of energized, loaded wires. However, between all wire types the difference between the trip times (TT) and the breakage times (BT) was not significant. Hence,

TT did not seem to occur any earlier or later than BT.

The data from Table 4-1 was plotted for each wire type under all three electrical conditions as shown in Figure 4-1.

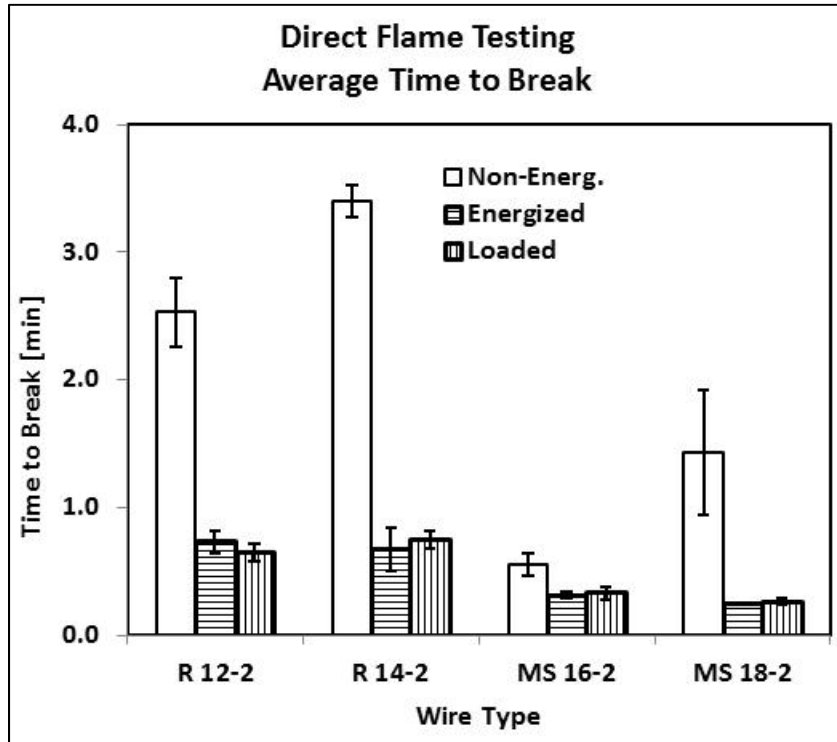


**Figure 4-1: Average Time to Break or Trip for All Wire Types-Direct Flame Tests (DF)**

The results for the energized wires were plotted again, in Figure 4-2, to provide easier visual comparison. The remaining plots for the direct flame testing are presented in Appendix 1.

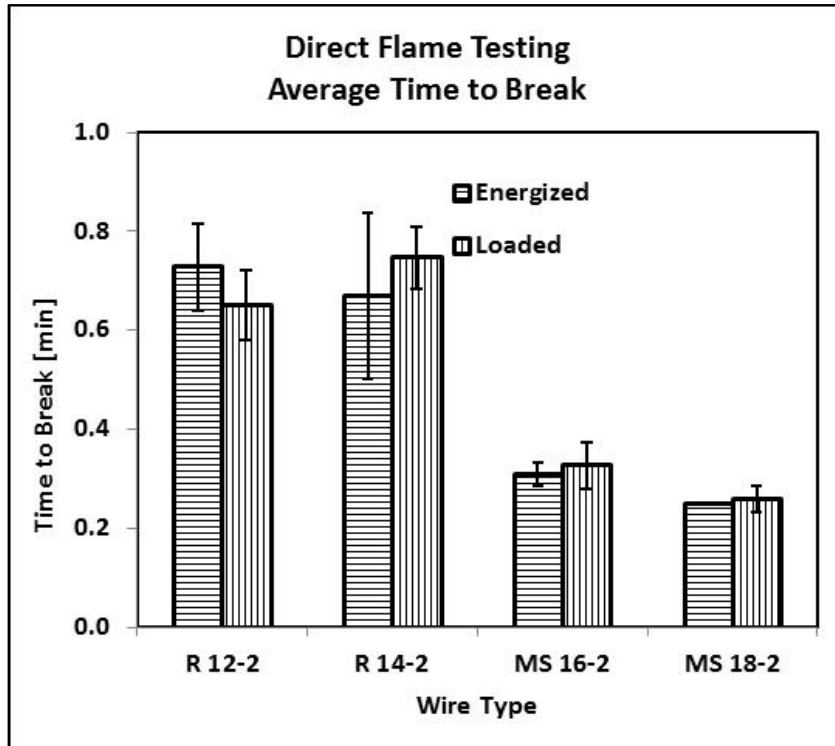


**Figure 4-2: Average Time to Break or Trip for Energized and Loaded-Direct Flame Tests (DF)**

A significant difference was present between the breakage times under the non-energized conditions when compared to the energized conditions. A significant difference was not present between the BT in the energized with load and energized with no-load wires, as seen in Figure 4-2 above. However, when comparing different wire types, the BT was longer for the solid (14 and 12) gauge energized wires (loaded and non-loaded) than for the stranded (16 and 18) gauge energized wires; the same was true for the non-energized wires. Hence, overall, it took a longer period of time, regardless of energized state, for the solid wires to break when compared to the stranded wires. When evaluating within the solid, non-energized wire group, however, longer BT were not associated with larger wire gauges; the same was true for the stranded wire group. The 14-gauge solid wires (smaller) had a significantly longer BT than the 12-gauge solid wires (larger), as did the 18-gauge stranded wires

when compared to the 16-gauge stranded wires. Hence, the dissipation of heat in the wires does not appear to be solely based on wire diameter, but is also dependent on wire geometry (stranded versus solid). The longer breakage times in the smaller wire gauges may also be related to wire insulation. Information about the wire insulation is currently being sought from distributors and manufacturers to identify any compositional differences between the four wire types.

For the loaded and energized wires, current and voltage data were recorded to monitor any electrical activity in the wire before failure. A representative graph of this data is shown in Figure 4-3: Typical Amperage and Voltage Graph-Direct Flame Tests (Loaded Wire DF) and Figure 4-4.

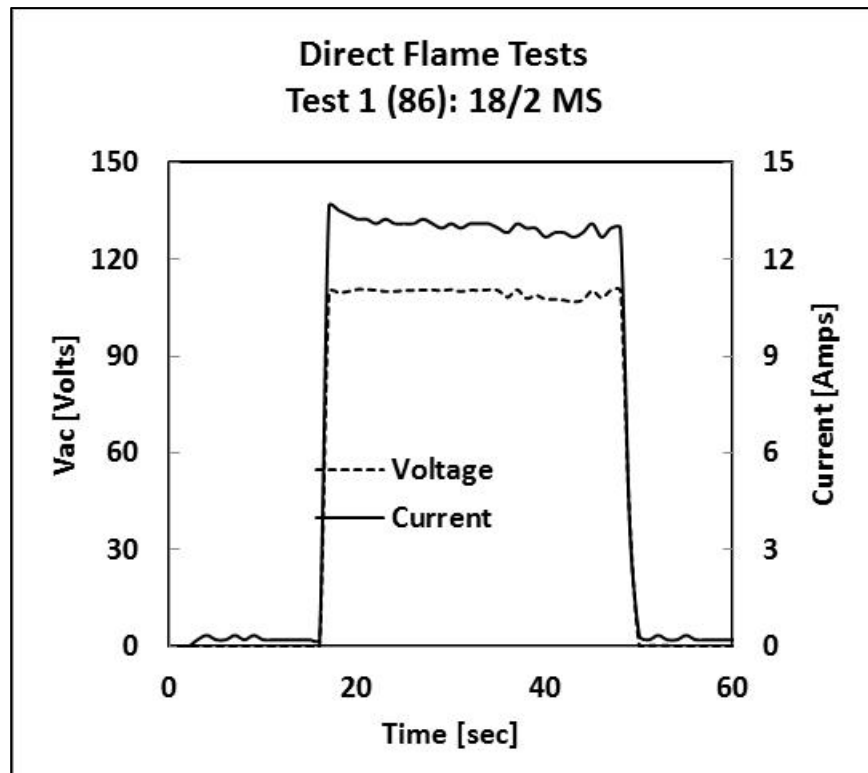


**Figure 4-3: Typical Amperage and Voltage Graph-Direct Flame Tests (Loaded Wire DF)**

In most cases, as shown in Figure 4-3, the wire broke and the current went to

zero without any registered change in the current or voltage. In some cases, however, large spikes in the current occurred before the wire was broke. The spikes, as shown in Figure 4-4, appear to be consistent with arcing through the conductive char formed between the hot, neutral, and ground conductors from the burning insulation.

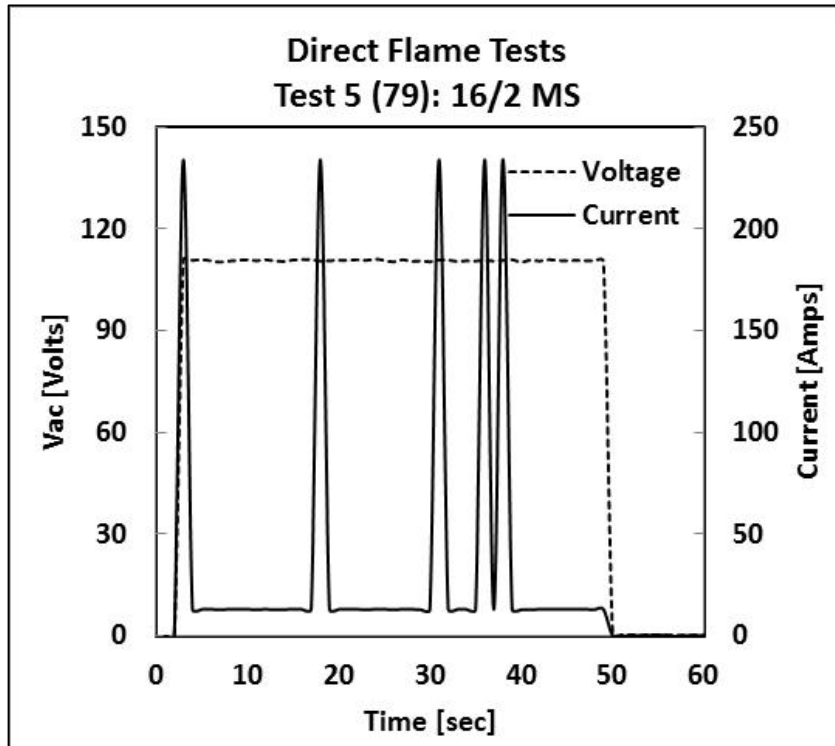


**Figure 4-4: Arcing Through Char-Direct Flame Tests (DF)**

Current spikes were observed in 9 of the 24 tests that were conducted with loaded wires. All six tests utilizing the 16-gauge, multi-stranded wires exhibited arcing through char; however, none of the 18-gauge, multi-stranded wires exhibited this effect. Only 25% (3 of 12) of the solid gauge wires exhibited arcing through char (two 14-gauge wires and one 12-gauge wire). The tendency of some wires to exhibit arcing through char is believed to be linked to the wire insulation type. Hence, the ability of the wire insulation to support charring is a significant factor in the BT. The



16-gauge wire which produced the shortest breakage time, exhibited the highest predominance of arcing through char which produced the shortest breakage time.

It should be noted that the maximum current output of the transmitter is approximately 240 amps, and there were no recorded spikes above this value. Hence, the true current spike may have been greater than the recorded value. The measured currents in this study are consistent with those found by other researchers; for example, Hagimoto et al. [25] measured currents up to 250 amps produced during arcing conditions through carbonized pathways in PVC-covered electrical cords.

#### **4.2.2 Radiant Tunnel Tests**

The breakage times and trip times for each wire type from radiant tunnel tests under all three electrical conditions: energized, loaded, and non-energized, are shown in Table 3. In some cases, the circuit tripped due to arcing prior to a breakage in the wire. In some cases, the wire broke when the circuit tripped. Under the direct flame condition, the test was discontinued when the circuit tripped or the wire broke. In the radiant tunnel condition, the tests were run until a complete severing of the wire occurred regardless of the trip time. Hence, some breakage (severing) times are longer than the trip times, and some breakage in energized wires occurred after circuit tripping when the wire was de-energized.

Out of the 24 energized wires tested (12 with load and 12 with potential only), 11 had the same breakage and trip times. Of the 11 that did have the same trip times, 8 were under load conditions. Therefore, approximately half of the energized wires that broke did so due to an arcing or shorting event that was significant enough to cause the circuit to trip. Additionally, there was a slightly higher tendency for this to

occur in loaded wires as opposed to energized wires with potential only.

**Table 4-2: Radiation Testing Results (R)**

Test No.	Romex 12-2				
	NE	E		L	
	Break	Trip	Break	Trip	Break
	[min]	[min]	[min]	[min]	[min]
1		0.67	0.67	0.45	0.45
2	1.03	0.45	1.15	0.47	1.12
3	0.95	0.47	0.50	0.42	0.42
<b>Averages</b>	<b>1.00</b>	<b>0.53</b>	<b>0.77</b>	<b>0.44</b>	<b>0.66</b>
Test No.	Romex 14-2				
1	1.07	0.58	0.67	0.37	0.75
2	1.03	0.45	0.50	0.42	0.78
3	0.92	0.32	0.45	0.47	0.47
<b>Averages</b>	<b>1.01</b>	<b>0.45</b>	<b>0.54</b>	<b>0.42</b>	<b>0.67</b>
Test No.	Multi-Stranded 16-2				
1	1.05	0.25	0.48	0.22	0.22
2	0.70	0.23	0.82	0.32	0.50
3	0.97	0.30	0.92	0.28	0.28
<b>Averages</b>	<b>0.91</b>	<b>0.26</b>	<b>0.74</b>	<b>0.27</b>	<b>0.33</b>
Test No.	Multi-Stranded 18-2				
1	0.53	0.20	0.20	0.20	0.20
2	0.58	0.18	0.58	0.22	0.22
3	0.55	0.18	0.18	0.20	0.20
<b>Averages</b>	<b>0.56</b>	<b>0.19</b>	<b>0.32</b>	<b>0.21</b>	<b>0.21</b>

The charts below represent the average break time and trip time for each wire under different electrical conditions. Figure 4-5 includes the average break times for all three electrical conditions separated by wire type, while Figure 4-6 includes average trip times for the energized wires separated by wire type.

A significant difference in the BT was present between the non-energized and energized, loaded wires. The loaded wires had quicker break time (BT) than the non-energized wires. This phenomenon is related to the tendency of the energized, loaded

wires to break and trip the circuit at the same time. Hence, arcing of the wires played a large role in the shorter BT times for the energized wires. This trend was also seen in the direct flame tests.

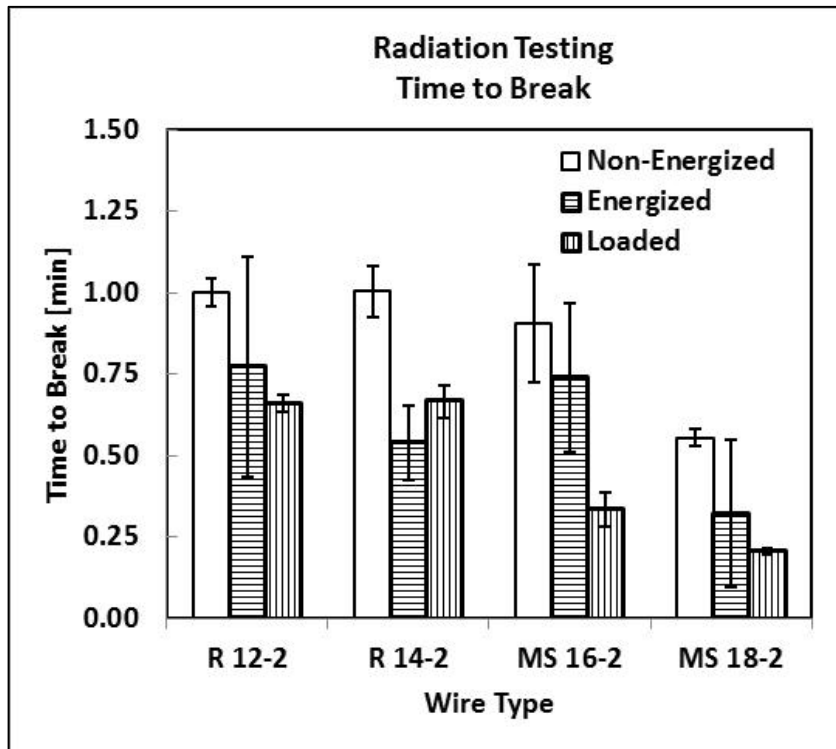


**Figure 4-5: Average Break Time-Radiation Tunnel Tests (R-All)**

There was not a significant difference in the BT for the energized, loaded and non-loaded wires with the exception of the 16-gauge stranded wires. Wire gauge did play some role in the BT for energized and loaded wires: the smaller the wire gauge the faster the BT with the exception of the 12-gauge and 14-gauge wires, which had approximately the same BTs. Additionally, the stranded wires had quicker break times than the solid gauge wires. This trend was also similar to that found in the direct flame studies.

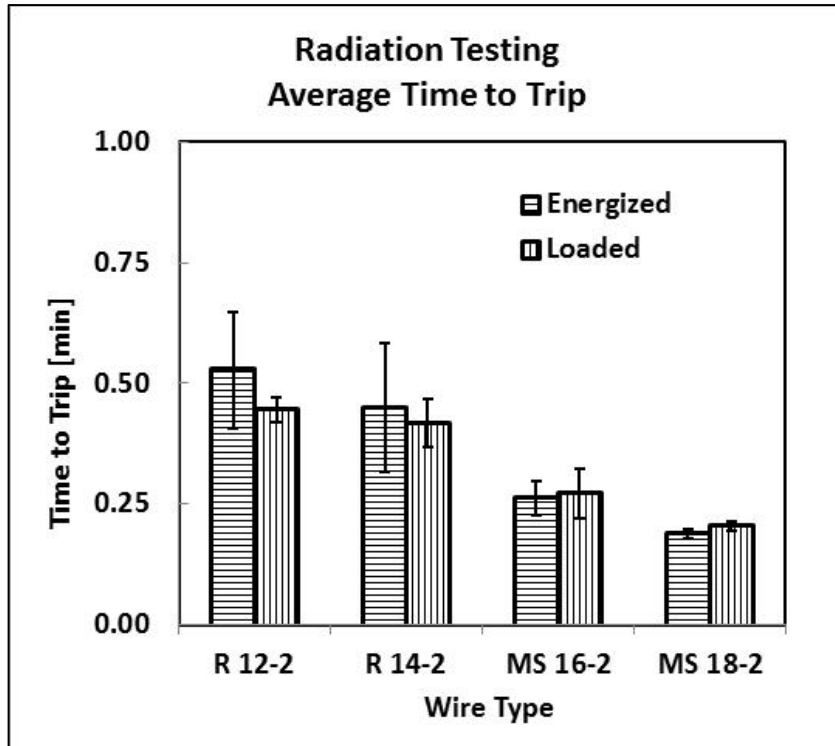


**Figure 4-6: Average Trip Time-Radiation Tunnel Tests (E and L-R)**

The trip times (TT) for the energized and loaded wires did not vary significantly within wire types; however, the TT did trend downward with decreasing wire gauge. Therefore, the TT does show some dependence on wire size. The average TT for the radiation testing is slightly lower than for the direct flame testing. In the direct flame tests, the wire insulation melted, charred, and then arced, which resulted in BT or TT. In the tunnel tests, the wire insulation was vaporized almost instantaneously due to the substantial heat flux present in the tunnel. In the tunnel tests, the copper wires were de-insulated very early in the exposure period, and a char did not form on the insulation. Without the protective insulation, it is likely that the wires would arc or short more quickly in the tunnel tests, which is consistent with the test results.

Figure 4-7 provides a comparison of the various wires types grouped by

average break times and trip times for energized loaded and non-loaded wires.

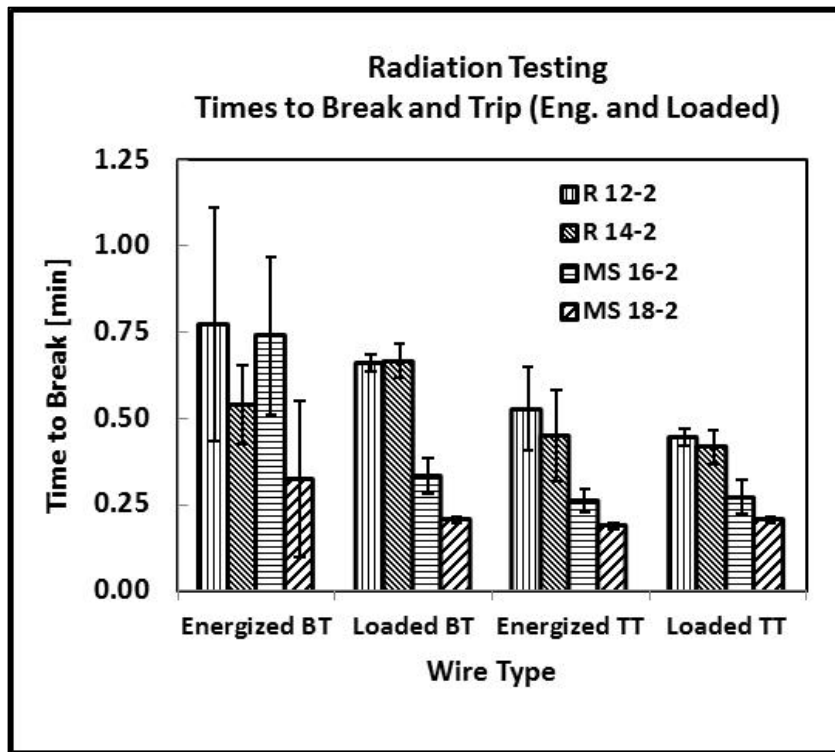


Figure 4-7: Average Break Time and Trip Time –Radiation Tunnel Tests (R)

The break times for the non-loaded wires (Energized BT) were quite variable when compared to the other three conditions (Loaded BT, Energized TT, and Loaded TT). If a break occurred in the non-loaded wires, it happened under two possible scenarios: 1) at the same time as the circuit tripped, or 2) after the breaker tripped. If the break occurred after the circuit tripped, then the wire was de-energized and the break occurred solely due to melting as opposed to arcing. Hence, the large variation in the BTs is likely due to the fact that some wires had to melt in order to break (resulting in a longer BT) while others arced and broke (resulting in a shorter BT). The presence of load on the circuit did appear to support wire failure more quickly when compared to those wires that had electric potential only. This result could be

due to the added heat generation from the presence of power ( $I^2R$ ) in the wire or due to the ability of arcing to be more easily established between wires because of the presence of an electric field.

#### **4.2.3 2/5-Scale Compartment Tests**

The maximum temperatures and heat fluxes measured in the compartment throughout the duration of the tests is shown in Table 4-3. The trip times as well as the maximum temperatures and heat fluxes at the time of tripping are also presented in the table. The total heat flux per unit area (TEA) between  $t=0$  and  $t=\text{trip}$  was calculated to establish the total energy output from the fire in the compartment. The trapezoidal method was used to derive the area under the curve to calculate the TEA.

The average maximum temperatures in the compartment ranged from 996 °C to 1149 °C. The average maximum heat fluxes in the compartment ranged from 91 kW/m<sup>2</sup> to 255 kW/m<sup>2</sup>. In the 14-gauge wire studies, the rear heat flux meter appeared to be measuring above normal heat fluxes typically given as 90-150 kW/m<sup>2</sup>. The meter was re-calibrated and measurements taken after re-calibration were within expected ranges based on the temperature profiles inside the compartment.

**Table 4-3: Scaled Compartment Testing Results (SC)**

Test	T Max		HF Max		Trip Time		T Max <sub>Trip</sub>		HF Max <sub>Trip</sub>		TEA	
	Front	Back	Front	Back	E	L	E	L	E	L	E	L
	[°C]		[kW/m <sup>2</sup> ]		[min]		[°C]		[kW/m <sup>2</sup> ]		[kJ/m <sup>2</sup> ]	
	Romex 12-2											
1	1108	1026	89.5	98.7	3.48	3.48	705	705	5.25	5.25	295	295
2	1123	1078	93.2	116	3.39	3.77	738	690	7.06	7.01	432	281
3	1119	1017	98.4	138.2	3.77	3.77	672	672	5.31	5.31	394	394
4	1190	1125	147	145.8	4.77	4.77	494	494	4.35	4.35	243	243
5	1034	1047	64.3	133.3	4.38	4.38	407	407	10.32	10.32	321	321
6	1206	1007	87.5	NA	NA	NA	605	605	3.01	3.01	208	208
7	879	675	161	97.7	3.13	3.13	611	611	4.69	4.69	448	448
<b>Ave</b>	<b>1094</b>	<b>996</b>	<b>105.8</b>	<b>121.6</b>	<b>3.82</b>	<b>3.88</b>	<b>604</b>	<b>598</b>	<b>5.71</b>	<b>5.7</b>	<b>334</b>	<b>313</b>
Test	Romex 14-2											
1	1117	1098	75.1	273.4	3.92	3.92	466	466	5.15	5.15	455	455
2	1150	1020	89.3	241	4.42	4.42	472	472	3.81	3.81	311	311
3	1154	1071	89.4	245.4	4.9	4.9	329	329	2.66	2.66	262	262
4	1173	1020	110.2	260.3	3.81	3.81	336	336	2.43	2.43	172	172
<b>Ave</b>	<b>1149</b>	<b>1052</b>	<b>91</b>	<b>255</b>	<b>4.26</b>	<b>4.26</b>	<b>401</b>	<b>401</b>	<b>3.51</b>	<b>3.51</b>	<b>300</b>	<b>300</b>
Test	Multi-Stranded 16-2											
1	1039	1150	229.9	145.9	4.24	3.34	397	261	5.33	3.28	524	282
2	1163	1047	162.3	134.1	3.61	3.51	597	592	6.08	4.72	436	400
3	1041	1148	86.4	197	No Trip	3.71	No Trip	462	No Trip	1.9	464	305
4	1050	1158	109.1	211	3.41	2.99	709	620	8.75	4.72	314	256
5	1059	1139	211.3	150.2	4.38	4.03	482	482	3.13	3.13	178	168
6	1077	1143	132.7	161	2.64	2.54	781	754	10.04	9.38	518	282
<b>Ave</b>	<b>1072</b>	<b>1131</b>	<b>155.3</b>	<b>166.5</b>	<b>3.66</b>	<b>3.35</b>	<b>593</b>	<b>528</b>	<b>6.66</b>	<b>4.52</b>	<b>405</b>	<b>282</b>
Test	Multi-Stranded 18-2											
1	967	1256	176.6	135.8	5.31	4.31	638	536	5.85	2.69	931	300
2	1033	1047	155.6	151.8	No Trip	3.96	715	501	12.8	4.2	No Trip	NA
3	1051	1085	147.4	133.9	5.53	5.38	613	579	5.97	4.65	484	434
4	1042	1081	155.1	119.4	5.28	4.48	449	405	5.04	3.01	438	251
5	1001	1179	NA	NA	3.31	2.66	704	569	12.8	5.81	786	346
<b>Ave</b>	<b>1019</b>	<b>1130</b>	<b>158.7</b>	<b>135.2</b>	<b>4.86</b>	<b>4.16</b>	<b>624</b>	<b>518</b>	<b>8.49</b>	<b>4.07</b>	<b>660</b>	<b>333</b>

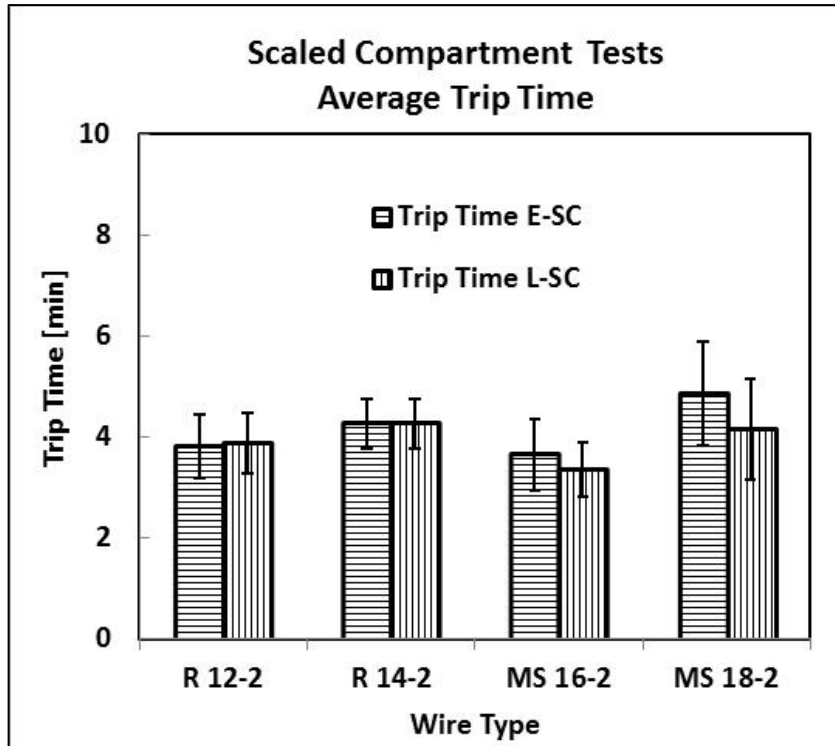


**Figure 4-8: Average Trip Time-Scaled Compartment Tests (SC)**

The average trip time ranged from 3.4 minutes to 4.9 minutes, as shown in Figure 4-8. When comparing wire types, there was no significant difference in trip times. It should be noted that the testing performed on the solid gauge, energized wires with load and without load was done at the same time in the test compartment, and both wires (loaded or un-loaded) were plugged into the same power source. Hence, when a trip occurred and the circuit was de-energized, it was not possible to identify which wire (loaded or unloaded) caused the trip. Therefore, the temperatures and heat fluxes at the time of tripping are the same for the wires energized with load and without load. In order to avoid this same issue with the stranded wire tests, separate circuits were utilized for the loaded and unloaded energized wires. There was no significant difference between the times to trip for the energized with load versus those energized without load.



Also, Table 4-3 lists the maximum heat fluxes and temperatures in the compartment at the time of circuit tripping. The heat fluxes ranged from 3.5 kW/m<sup>2</sup> to 8.5 kW/m<sup>2</sup>, and the temperatures ranged from 401 °C to 624 °C. The average maximum heat fluxes and temperatures at time of tripping are shown in Figure 4-9 and Figure 4-10, respectively.

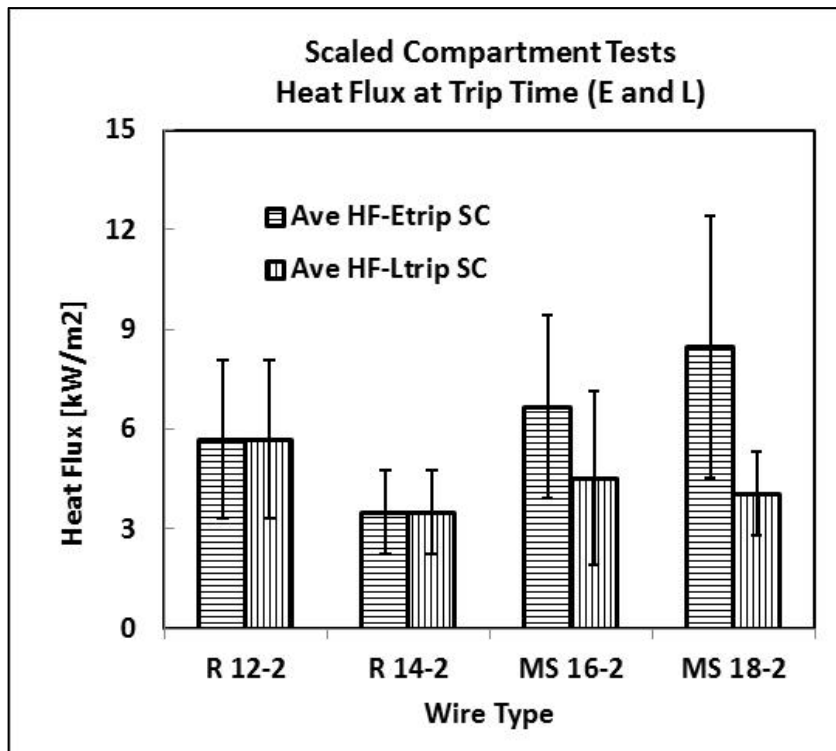


**Figure 4-9: Heat Flux at Circuit Trip Time-Scaled Compartment Tests (SC)**

When comparing wire types, there were no significant difference between the heat fluxes and temperatures at circuit trip time. The 14-gauge wires had lower average temperatures and heat fluxes at TT. The loaded stranded wires also had trip times at lower temperatures and heat fluxes. However, these differences were not highly significant based on the standard deviation in the measurement.

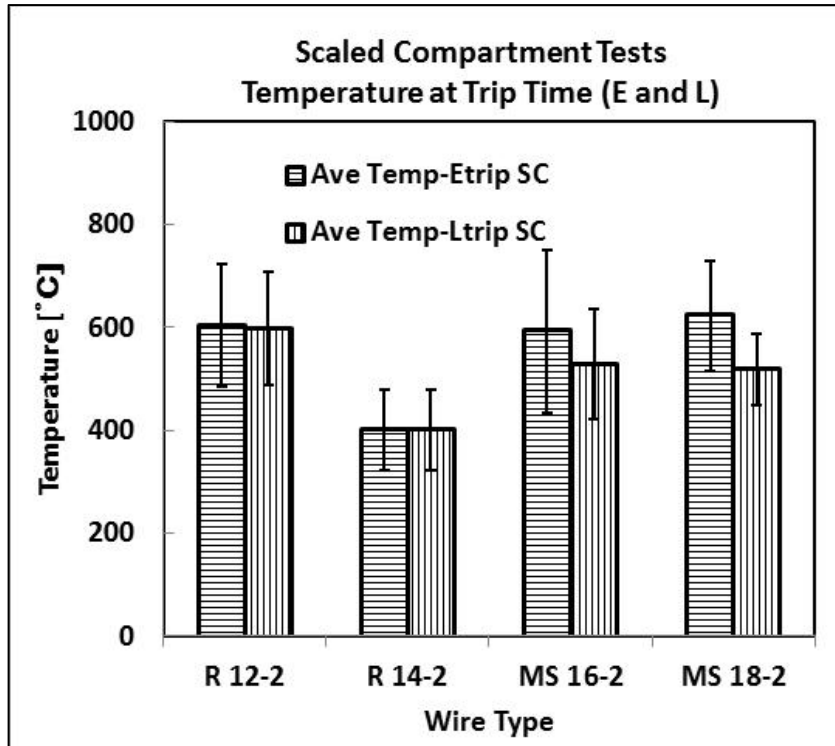


**Figure 4-10: Temperature at Circuit Trip Time-Scaled Compartment Tests (SC)**

Another method for comparison of the failure times for different wires was thorough examination of the total energy per unit area (TEA) that the wire was exposed to at the time of failure. The total energy per unit area was calculated by integrating the heat flux data as a function of time. The average TEA ranged of 282 kJ/m<sup>2</sup> to 660 kJ/m<sup>2</sup>. The TEA for the energized, non-loaded wires had a larger range of 300 kJ/m<sup>2</sup> to 660 kJ/m<sup>2</sup> when compared to the TEA for the energized, loaded wires which had a range of 282 kJ/m<sup>2</sup> to 333 kJ/m<sup>2</sup>. This finding is consistent with the direct flame and radiant tunnel tests, which shows that loaded wires tripped sooner than non-loaded wires.

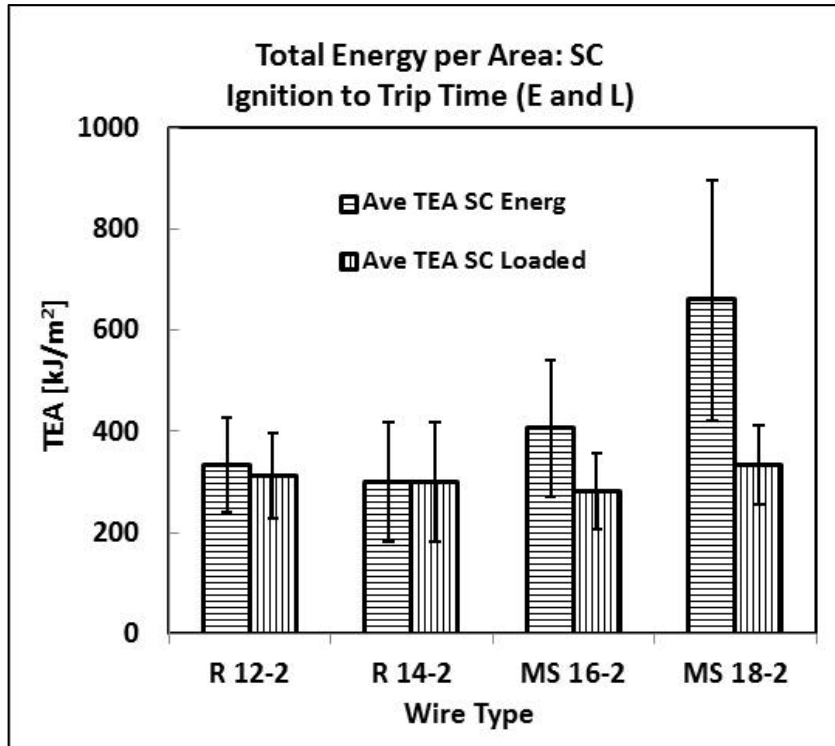


**Figure 4-11: TEA at Trip Time for the Scaled Compartment Tests (SC)**

Additionally, in some cases, the higher TEA values were due to the fact that the circuit breaker did not trip at the first sign of breakage or arcing. This condition occurred for a number of the 18-gauge wire tests, where the first breakage of the wire did not trip the circuit. Additionally, in one case the circuit breaker did not trip at all during the test. Figure 4-11 provides a graphical representation of the TEA data.

Like the temperature and heat flux data, the TEA values are also consistent throughout all wire types. The TEA for the stranded wires was less for the loaded conditions than for the non-loaded conditions, as discussed above.

#### **4.2.4 Full-Scale Compartment Tests**

The maximum temperatures and heat fluxes measured in the full-scale compartment throughout the duration of each test is shown in Table 4-4. The trip times as well as the maximum temperatures and heat fluxes at the time of tripping are

also presented in the table. The total heat flux per unit area (TEA) between  $t=0$  and  $t=$  trip was also calculated to establish the total energy output from the fire in the compartment. The trapezoidal method was used to derive the area under the curve to calculate the TEA. Due to gaps in data logging at the beginning of the 18-gauge wire tests, maximum heat flux and temperature values were recorded, but the total heat flux profile needed for TEA calculations was not recoverable.

**Table 4-4: Full-Scale Compartment Testing Results (FSC)**

Test No	T Max	HF Max	Trip Time	T Max <sub>Trip</sub>	HF Max <sub>Trip</sub>	Load	TEA
	[°C]	[kW/m <sup>2</sup> ]	[min]	[°C]	[kW/m <sup>2</sup> ]	[amps]	[kJ/m <sup>2</sup> ]
<b>Romex 12-2</b>							
1	1178	111.0	4.85	278	5.7	9.2	945
2	841	134.7	2.66	821	45.4	9.3	621
3	917	134.6	2.63	751	38.5	13.0	342
<b>Averages</b>	<b>979</b>	<b>126.8</b>	<b>3.38</b>	<b>617</b>	<b>29.9</b>	<b>10.5</b>	<b>636</b>
<b>Romex 14-2</b>							
1	910	138.5	3.05	831	42.5	13.0	270
2	848	94.7	3.02	713	15.4	9.1	624
3	1001	107.6	2.88	760	20.1	12.7	273
<b>Averages</b>	<b>920</b>	<b>113.6</b>	<b>2.98</b>	<b>768</b>	<b>26.0</b>	<b>11.6</b>	<b>389</b>
<b>Multi-Stranded 16-2</b>							
1	776	67.0	3.80	479	14.0	12.4	476
2	1000	128.0	1.55	759	23.8	12.4	103
3	930	83.8	2.79	775	65.0	12.7	270
<b>Averages</b>	<b>902</b>	<b>92.9</b>	<b>2.71</b>	<b>671</b>	<b>34.3</b>	<b>12.5</b>	<b>283</b>
<b>Multi-Stranded 18-2</b>							
1	933	115.3	3.27	342	6.7	11.7	No Data
2	846	63.9	4.88	314	14.7	12.0	No Data
3	907	109.4	3.81	209	19.5	11.6	No Data
<b>Averages</b>	<b>895</b>	<b>96.2</b>	<b>3.99</b>	<b>288</b>	<b>13.6</b>	<b>11.8</b>	<b>No Data</b>

The average maximum temperature in the compartment ranged from 895 °C to 979 °C. The average maximum heat flux ranged from 93 kW/m<sup>2</sup> to 127 kW/m<sup>2</sup>.

The range of maximum temperatures and heat fluxes achieved in the full-scale studies was slightly lower than in the scaled compartment. Since these tests were conducted in conjunction with tests at NFA which were being used for an investigations training course, there was no ability to artificially raise the temperatures within the compartment through the use of forced ventilation. Additionally, the fires were extinguished quickly after the compartment reached flashover conditions to leave some remains for the investigations class to evaluate. This quick extinguishment also limited the maximum temperatures and fluxes in the compartment.

The average trip times ranged from 2.7 minutes to 4.0 minutes, which were within the range found in the scaled compartment tests. The maximum temperatures and heat fluxes at the time of circuit tripping ranged from 288 °C to 768 °C and 14 kW/m<sup>2</sup> to 34 kW/m<sup>2</sup>, respectively. The variability in the temperature range was greater than in the scaled compartment tests; however, the scaled compartment temperature values did fall within the full-scale compartment range. The heat flux range in the full-scale compartment was approximately four (4) times higher than that found in the scaled compartment. The heat flux gauges were placed closer to the corners in the scaled compartment, whereas the heat flux gauge in the full-scale compartment was placed in the middle of the compartment but in-line with the compartment doorway. The higher heat fluxes measured in the full-scale tests are believed to be the result of better ventilation which occurred in-line with the compartment doorway.

The average trip times for four different wire types are plotted in Figure 4-12 below. The average maximum temperatures and heat fluxes at the time of tripping are

shown in Figure 4-13 and Figure 4-14, respectively. Figure 4-15 provides a graphical representation of the TEA data.

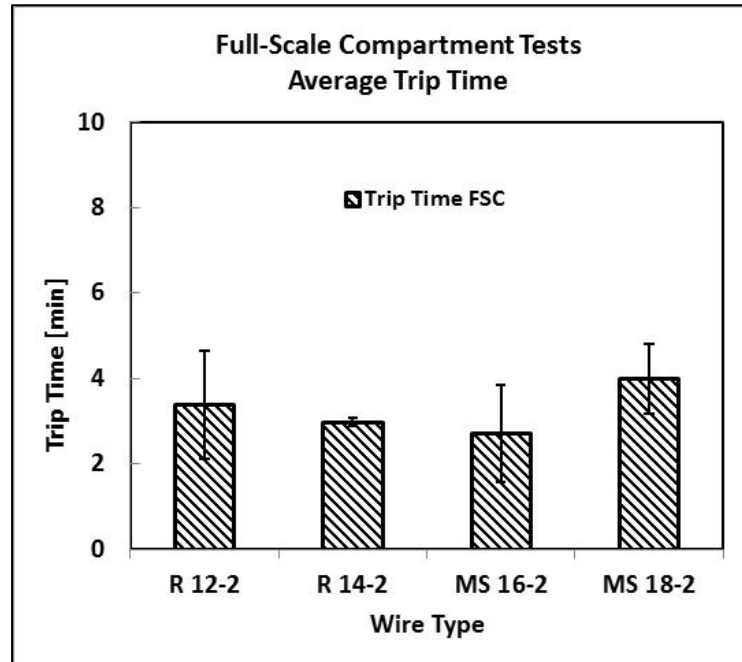


Figure 4-12: Circuit Trip Time for Full-Scale Compartment Tests (FSC)

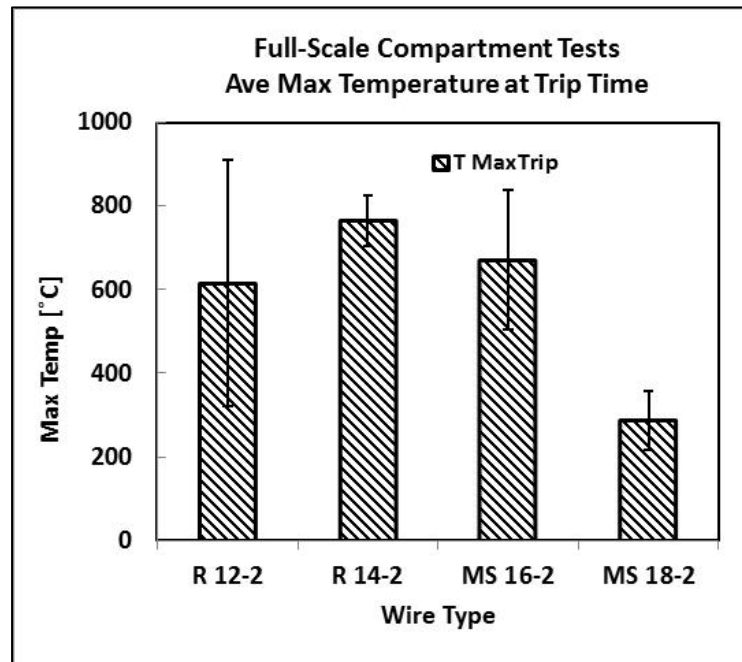


Figure 4-13: Average Temperature at Trip Time for Full-Scale Compartment Tests (FSC)

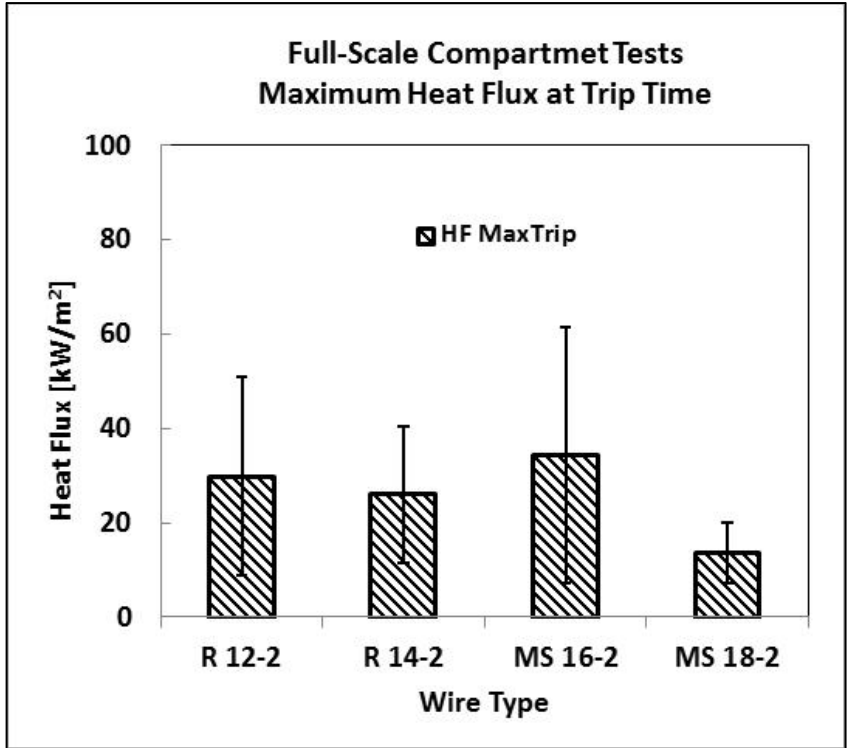


Figure 4-14: Average Heat Flux at Trip Time for Full-Scale Tests (FSC)

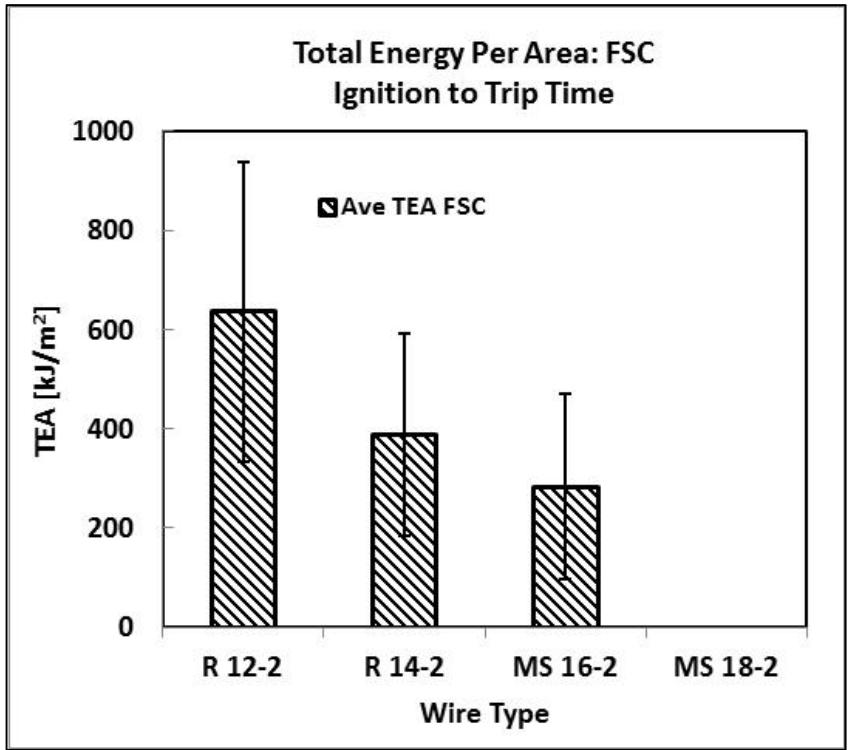


Figure 4-15: TEA for Full-Scale Compartment Tests (FSC)

The average trip times between all wire types were consistent. It should be noted that testing performed on the solid and stranded gauge, energized wires with load and without load were done at the same time in the test compartment, and both energized wires (with and without load) were plugged into the same power source. Hence, when a trip occurred and the circuit was de-energized, it was not possible to identify which wire (loaded or unloaded) caused the circuit to trip. Therefore, the temperatures and heat fluxes at the time of tripping are the same for the energized wires with load and without load.

The maximum temperatures at the time of tripping were significantly lower for the 18-gauge wires than for any of the other three wire types. The maximum heat fluxes at TT for the 18-gauge wires, while not significantly lower, were also less than the other three wire types. The cause of these differences is still being investigated, but may be related to the wire insulation type or particular dynamics of the fire. The TEA values for the wire types trended downward, according to the size of wire gauge, from larger to smaller. Hence, the amount of energy required for circuit trip time decreased as the wire diameter became smaller. While this trend was not significant based on the standard deviation in the measurement, it is logical: less energy should be required for heating of a smaller wire than a bigger wire. This same trend, however, was not seen in the scaled compartment tests.

#### **4.2.5 Stereo Microscope Results**

All test wires with thermal or electrical damage were photographed with a stereomicroscope. Specifically, each sample was analyzed for the presence of beads



and the bead diameter was measured. All of the bead pictures were organized according to test number and type of damage. These pictures are presented in Appendix 2. Figures 4-16 through 4-19 are representative images of beads formed under various thermal and electrical conditions.



**Figure 4-16: Beads Produced with Direct Flame Exposure (12-gauge: NE, E (center), and L)**

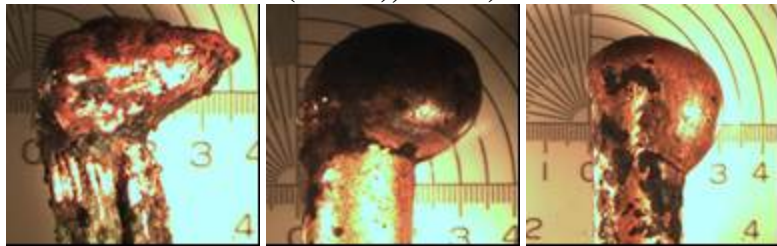


**Figure 4-17: Beads Produced with Radiant Tunnel Exposure (16-gauge: NE, 12-gauge: E (center) and L)**

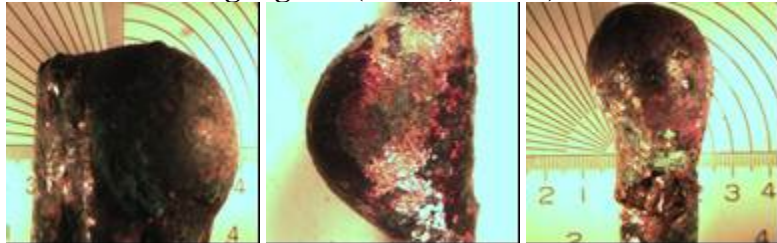


**Figure 4-18: Beads Produced with Scaled Compartment Exposure (12-gauge: NE, E (center), and L)**

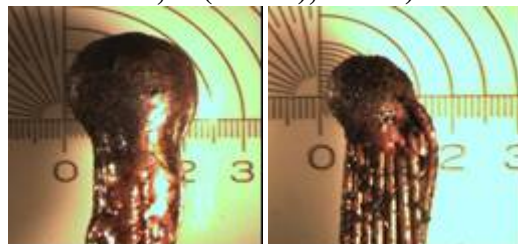


**Figure 4-19: Beads Produced with Full-Scale Compartment Exposure (16-gauge: E, 18-gauge: L)**

A total of 32 wire samples were mounted, cut, polished, and etched with  $\text{FeNO}_3$  solution to allow for microscopic surface analysis. Figure 4-20 shows two of the mounted samples.



**Figure 4-20: Mounted Samples (Cut and Etched)**

The mounted samples were photographed with a high resolution microscope at various magnifications. Figures 4-21 through 4-23 are representative images of selected loaded wires tested under different thermal exposures.

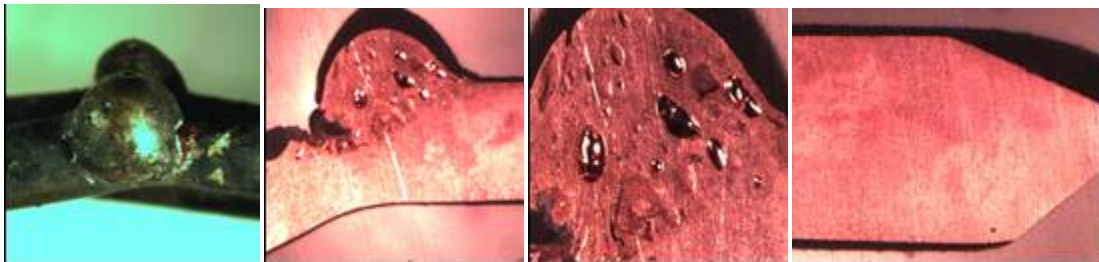


**Figure 4-21: SM Images of Loaded Wires under Direct Flame Exposure (12-gauge: L-DF)**

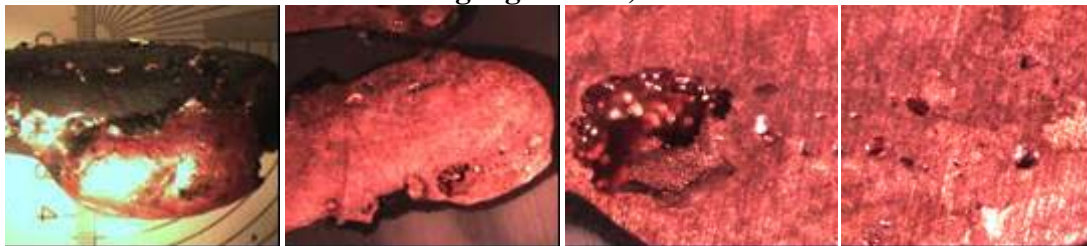


**Figure 4-22: SM Images Loaded Wire under Scaled Compartment Exposure (12-gauge: L-SC)**

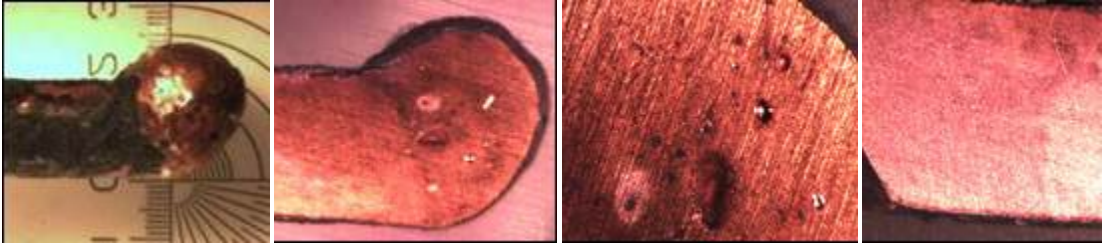


**Figure 4-23: SM Images of Loaded Wires under Radiant Tunnel Exposure (12-gauge: L-R)**

Figures 4-24 through 4-26 are representative images of selected non-energized wires tested under different thermal exposures. A full catalog of all the stereomicroscopic images is provided in Appendix 3.

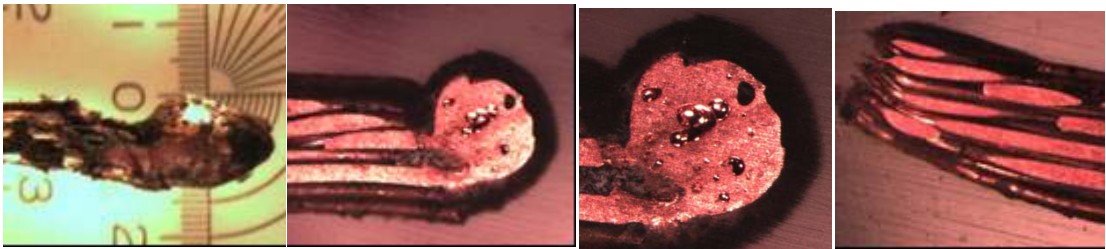


**Figure 4-24: SM Images of Non-energized Wires under Direct Flame Exposure (18-gauge: NE-DF)**

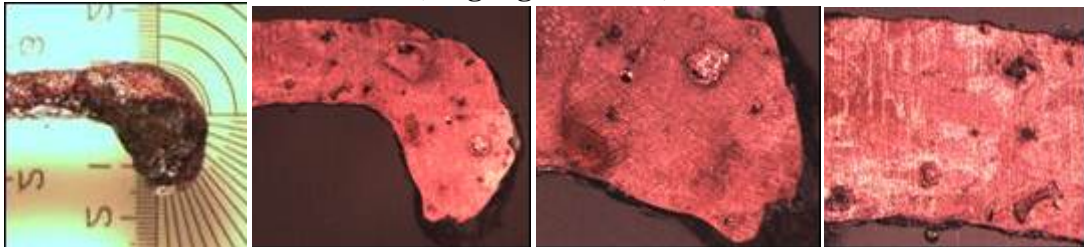


**Figure 4-25: SM Images of Non-energized Wires under Scaled Compartment Exposure (18-gauge: NE-SC)**

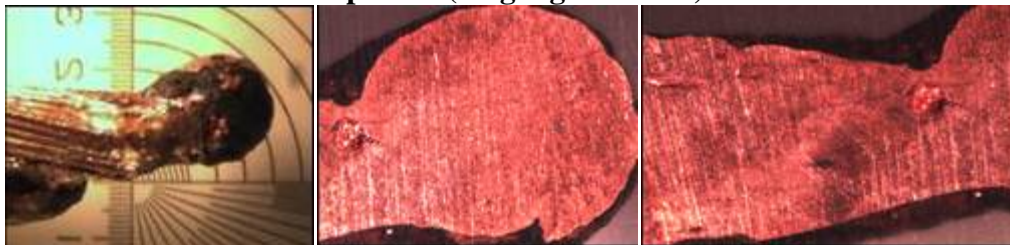


**Figure 4-26: SM Images of Non-energized Wires under Radiant Tunnel Exposure (18-gauge: NE-R)**

The mounted samples were evaluated for bead porosity, and any other characteristic trends that could be identified. In the images shown, direct flame impingement appeared to result in a more porous bead structure regardless of the energized state of the wire. However, this trend was not present in all the samples evaluated, and no consistent trends could be identified within exposure types, wire types, or energized states using a stereomicroscope. A discussion of the SEM/EDS results is given below.

#### **4.2.6 Scanning Electron Microscope and EDS**

Some samples were analyzed using SEM/EDS to determine if any differences existed between beads formed from melting versus beads formed from electrical activity. This analysis was performed by CSE staff at the University of Maryland and by Dr. Elizabeth Buc at the Fire and Materials Research Lab in Livonia Michigan. Some analyses were also performed by Dr. Lori Streit at Unified Engineering, Inc. and on-going analysis is being performed by Dr. Charles Manning of Accident Reconstruction Analysis, Inc. The main component found on the bead surface was copper, as would be expected. There was no significant difference in the chemical composition of beads from non-energized wires or energized wires or under different thermal exposures.

The stereomicroscope and SEM images from Dr. Buc's analysis are shown in Figure 4-27 where the left column shows a non-energized wire exposed to radiation and the right column shows a loaded wire exposed to direct flame.

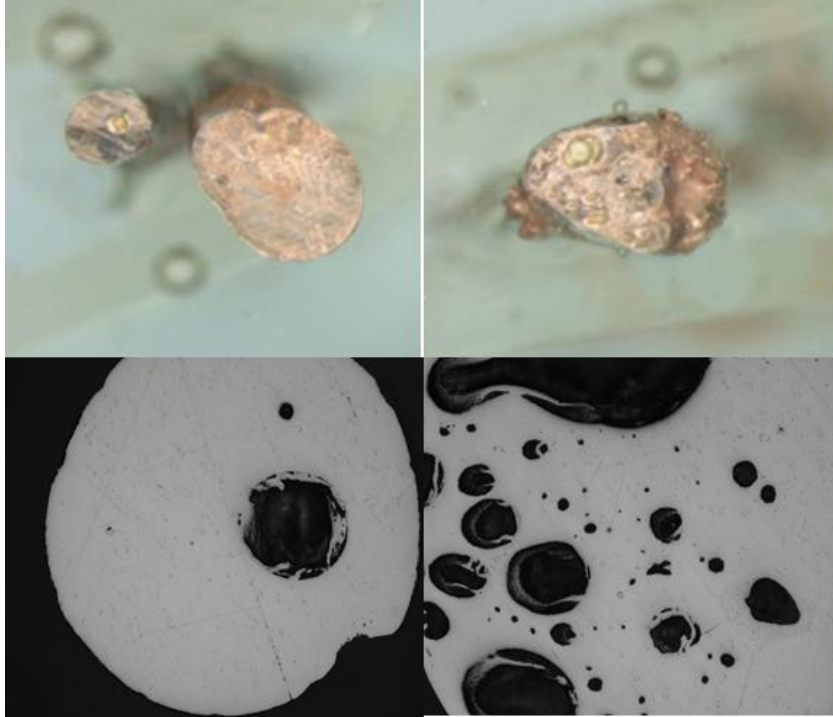


**Figure 4-27: SM and SEM Images of MS Wires under different Electrical Conditions.**

Dr. Buc did observe differences in the porosity of the beads formed on non-energized, multi-stranded wires when compared to the porosity of beads formed on energized, multi-stranded wires. These observations, however, were based on the analysis of four samples. Further analysis of the remaining bead samples has not supported the same trends.

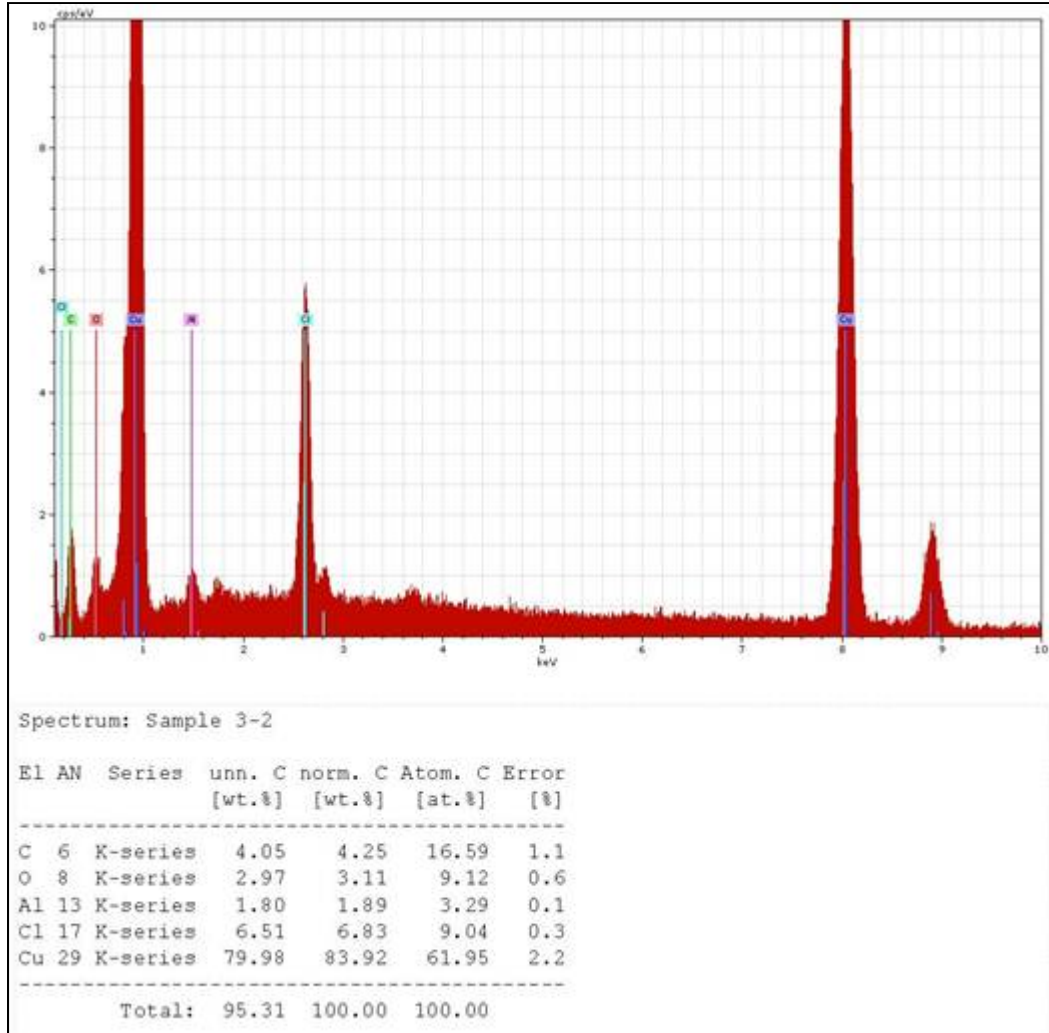


**Figure 4-28: EDS Graph for a Bead Surface formed on an Energized Wire (DF)**

Figure 4-28 and Figure 4-29 show the EDS graphs from energized and non-energized wires analyzed with the SEM at the University of Maryland. The table below each chart shows the elemental composition of the bead. Six wire samples were analyzed and no specific trends were identified in the elemental composition of the beads formed after thermal exposure under different electrical conditions. The wires contained various elements including: carbon, oxygen, chloride, aluminum, calcium, and copper. The content of the beads was not related to their exposure condition, size, energized state, etc.

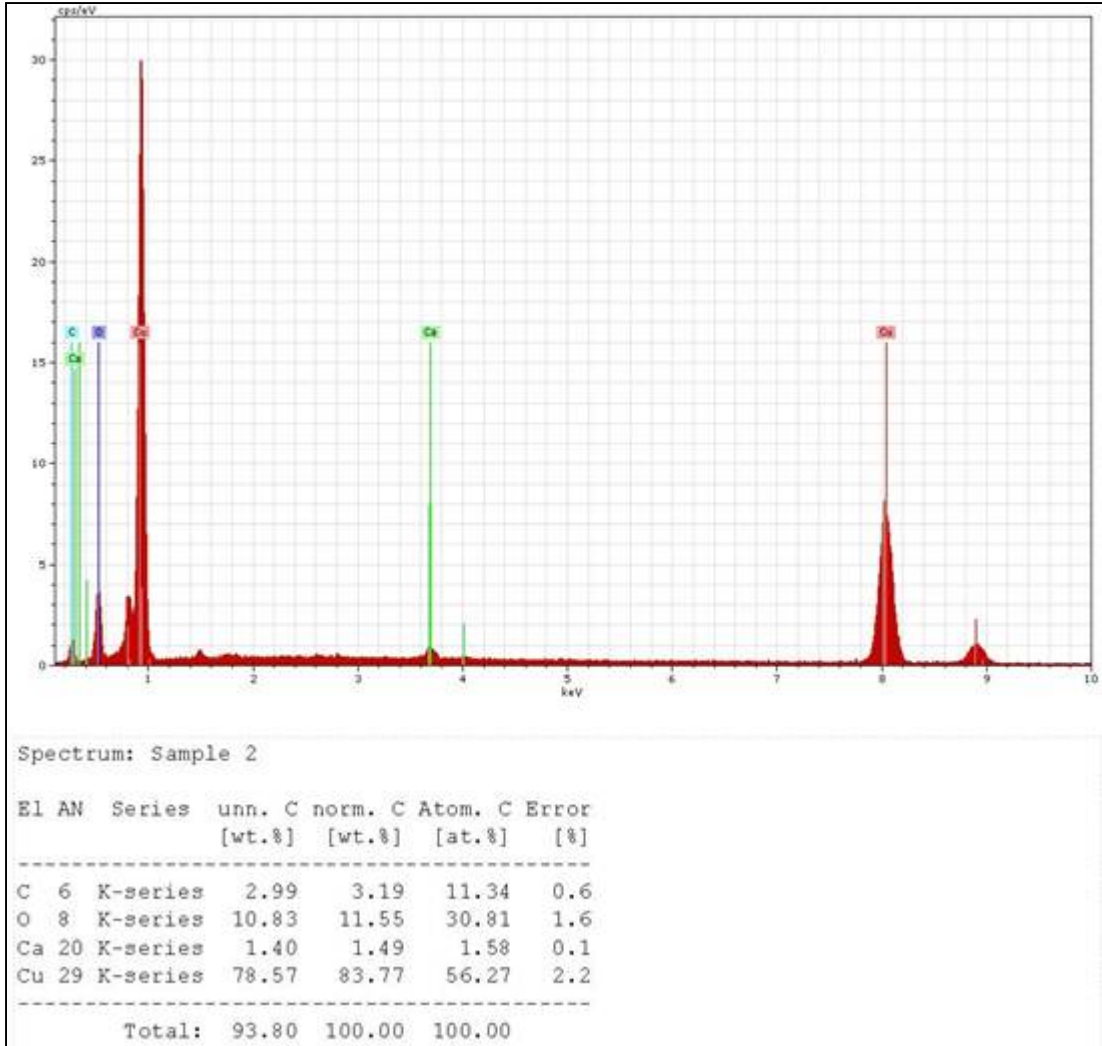


**Figure 4-29: EDS Graph for a Bead Surface formed on a Non-energized Wire (DF)**

Dr. Lori Streit performed further SEM/EDS analysis on the interior structure of the beads. Based on Dr. Streit's preliminary review of the beads, she found high concentrations of copper in both non-energized and energized beads. Dr. Streit was of the opinion that further SEM/EDS analysis would not provide useful information. Additionally, Dr. Streit felt that SEM analysis of the beads provided no more information on porosity than what could be seen utilizing a stereomicroscope, so it was decided to discontinue SEM analysis and focus on stereomicroscopic analysis.

Based on these recommendations, stereomicroscopic analysis was conducted on all of the mounted samples. Based on the limited outcomes of the SM and SEM/EDS results a further analysis of the inner grain structure of copper beads was done by ARAI as discussed in the next section.

#### **4.2.7 Analysis with Metallurgical Microscope**

Samples mounted and etched at Unified Engineering were remounted and re-etched at ARAI to be studied with an Olympus 1X70 metallurgical microscope. The etchant, known in the literature as Ammonium Hydroxide-Hydrogen Peroxide or AP etch consisted of 5 parts ammonium hydroxide ( $\text{NH}_4\text{OH}$ ), 5 parts water ( $\text{H}_2\text{O}$ ), and 4 parts hydrogen peroxide ( $\text{H}_2\text{O}_2$ ) [30, 33]. After etching, samples were analyzed and photographed with a Nikon DS-Fi1 digital camera mounted to an Olympus 1X70 metallographic microscope. Samples were photographed at a magnification range of 60X-110X. A program in Adobe Photoshop called Photomerge was utilized to combine localized, sectional images of the beads into one comprehensive image

Metallography is useful in evaluating the differences between non-energized and energized beads, because, copper undergoes grain structure changes when heated, and in some cases, these changes can be related to thermal exposure conditions [34, 39]. The grain structure begins to enlarge when temperatures reach or exceed  $260^\circ\text{C}$  [34]. Therefore, based on the size of the grain structures, it may be possible to distinguish between wires that had signs of arcing versus wires that were non-energized and only thermally heated. In some cases, the conditions of arcing are masked by continued heating of the bead. In these cases, the beads formed from arcing may look similar to beads formed from melting.



ARAI analyzed 29 wire samples of which 14 were produced while the wires were energized with load and 15 while the wires were non-energized. These samples were selected from wires exposed to direct flame, radiation, and scaled compartment fires. After examining the wire images taken with metallurgical microscope, ARAI concluded that there were several structural features present in the copper bead but none of the features were 100% consistent within the two groups analyzed (non-energized versus energized) ARAI did note that the inner structure of six of fourteen energized beads showed clear lines of demarcation, as seen in Figure 4-31 (Images A and B) and Figure 4-32 (Image C). This trend was only observed in one out of 15 non-energized samples. In the energized wire samples that did not exhibit clear lines of demarcation, ARAI concluded that further heating of the sample after arcing masked the demarcation. . Hence, on a microscopic level, clear lines of demarcation are more prevalent in beads formed under energized conditions where post-event heating is limited.

Another prevailing trend found in both energized and non-energized wires was voids of varying sizes. Voids were present in 19 of 29 samples evaluated. . Levinson [34] concluded that voids result in the copper structure due to the trapping of gaseous combustion products while the copper is molten. As is consistent with ARAI's findings, Levinson also concluded that the presence of voids was not a function of the electrical condition of the wire which is different from the conclusion of Gray et al [18] study

No distinguishing features were present within the wires that can be attributed to one thermal exposure (i.e. direct flame or radiation etc.). The full report from

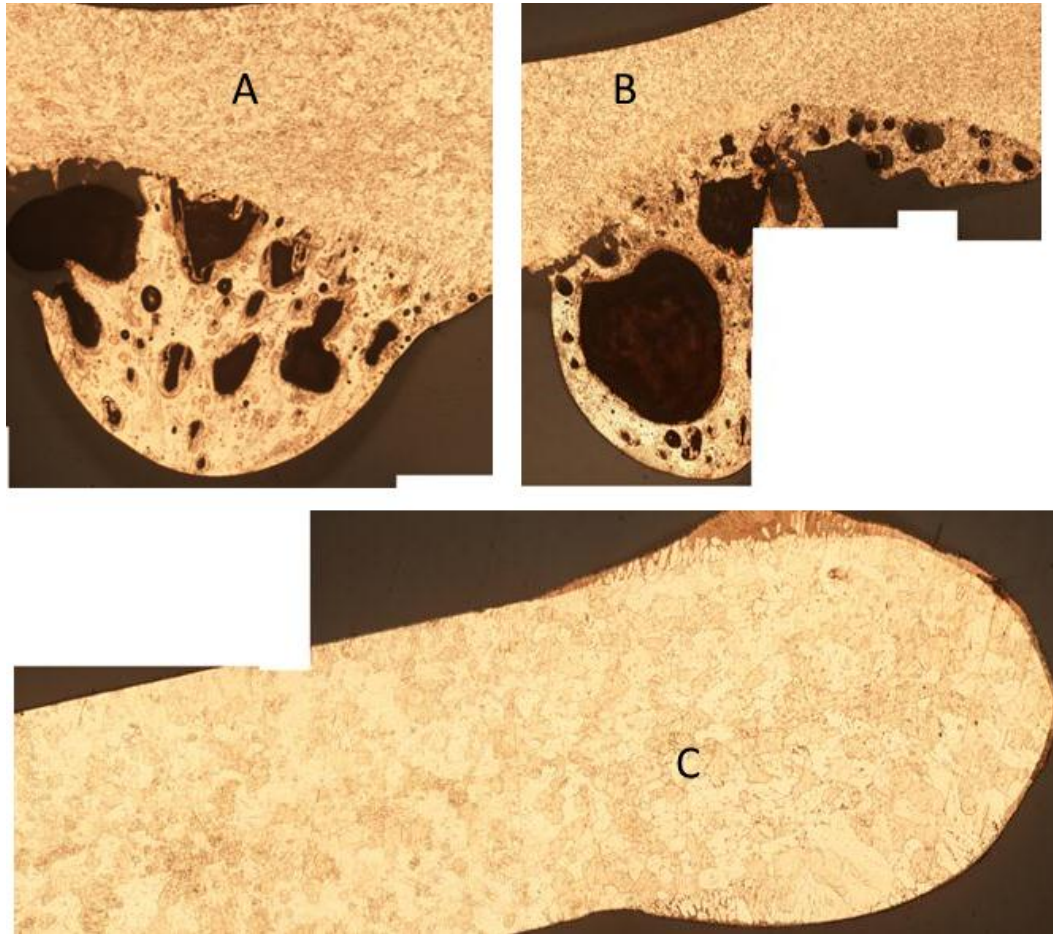
ARAI as well as images of beads is included as part of the Appendix 4 in the document, and further details this finding.



**Figure 4-30: Grain Structures of Wire Control Samples (Unexposed Wires: Solid (Top) and Stranded (Bottom))**

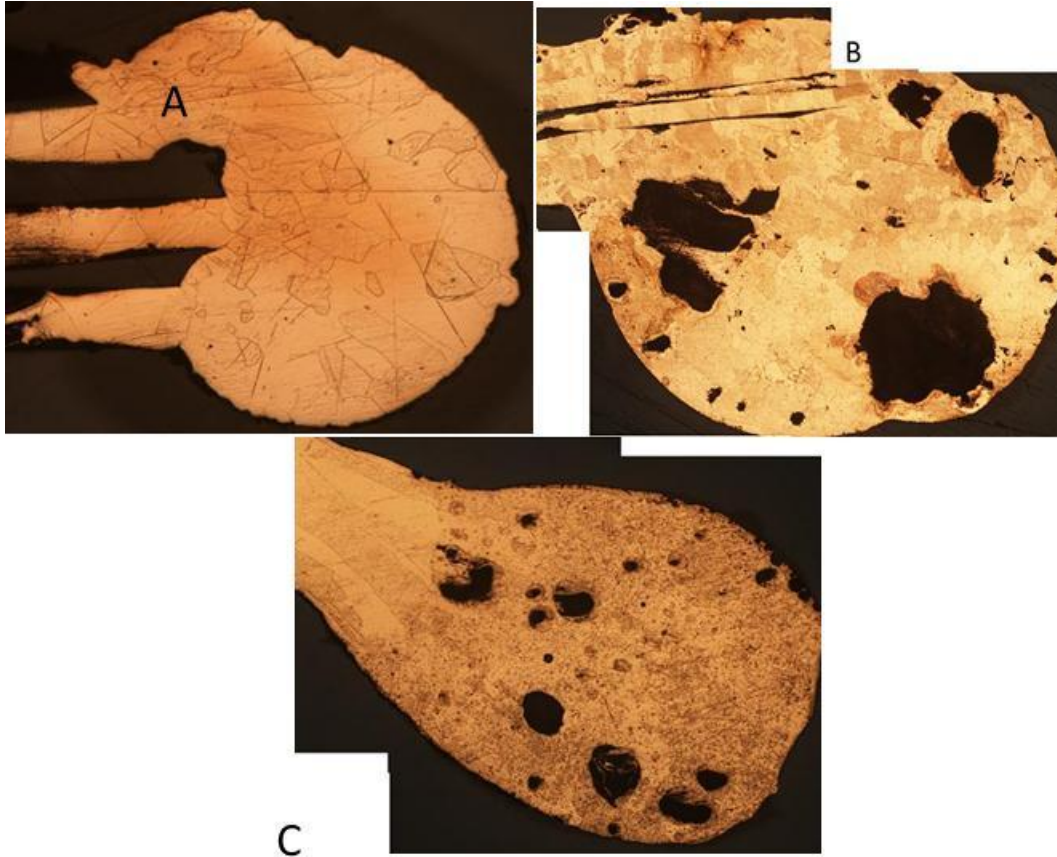
Figure 4-30 above shows images of control samples (unexposed wires) for both solid and stranded wires. These samples were used to obtain the grain structures of the wire prior to thermal exposure and served as the baseline or control samples. When copper conductors were analyzed without thermal exposure, they showed very small grain structures. These grain structures grow as copper is heated as seen in Figure 4-31 [34 and 39]. The images displayed are 12-gauge, solid, energized wires tested under direct flame exposure. All images show signs of arcing, as evident by the beads, but only the top two (A and B) show lines of demarcation and voids in

bead structures. Image C does not show any difference in grain structure when comparing the bead section to the longitudinal wire section.



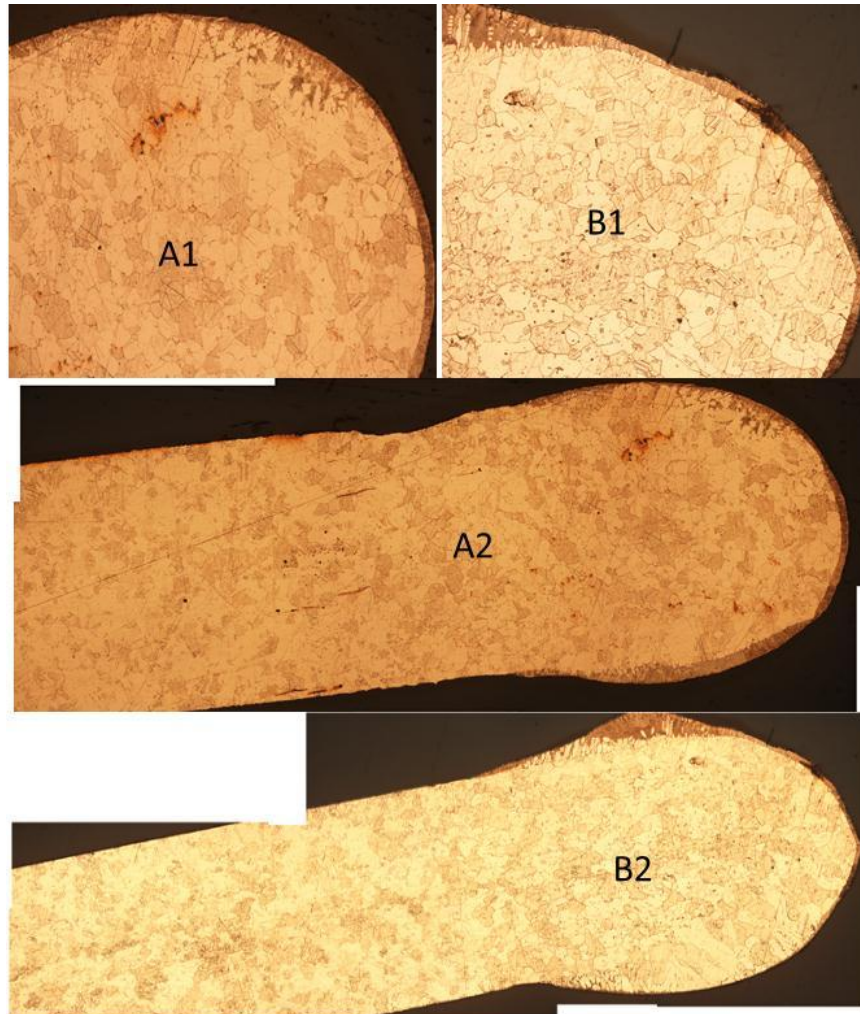
**Figure 4-31: Metallurgical Microscope Images of Beads formed under Direct Flame Exposure (All Loaded 12-R Wires)**

Figure 4-32 below shows images of 18-gauge, stranded energized wires tested in the scaled flashover compartment. Images B and C have large voids and image A has no voids. Images A and B show no lines of demarcation and enlarged grain structures whereas Image C shows a clear line of demarcation and smaller grain structures on the bead and larger grain structures on the wire portion.



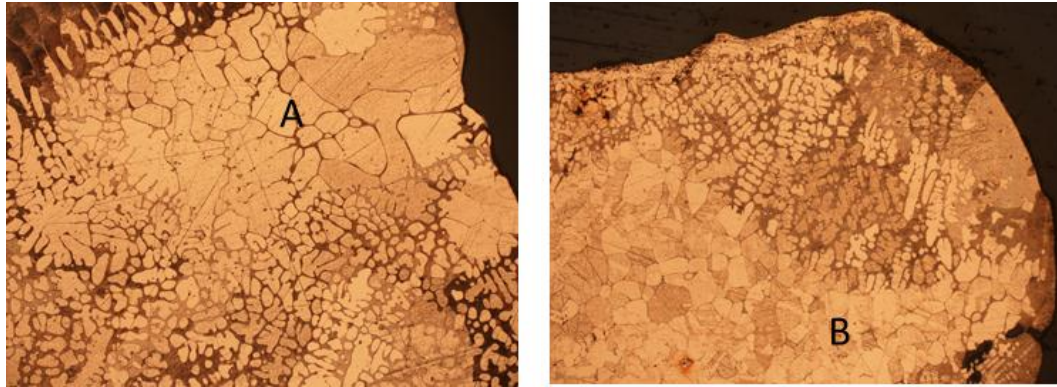
**Figure 4-32: Metallurgical Microscope Images of Beads formed under Scaled Compartment Exposure (All Loaded 18-MS Wires)**

Figure 4-33 shows beads formed on 12-gauge, solid, energized and non-energized wires exposed to direct flame impingement. The images show very similar grain structures but both wires were not held under the same electrical condition: sample A was non-energized while sample B was energized with load.



**Figure 4-33: Metallurgical Microscope Images of Beads formed under Direct Flame Exposure (12-R NE (A) and 12-R L (B))**

Figure 4-34 and Figure 4-35 also show images of grain structures that look very similar but the wires were tested under different electrical conditions. This may have been caused by continued heating of the wire after arcing, which typically occurred minutes prior to flashover. Figure 4-34 shows dendrite structures. These structures are believed to be produced when melted copper interacts with oxygen to produce  $\text{Cu}_2\text{O}$  [34]



**Figure 4-34: Metallurgical Microscope Images of Beads formed under Scaled Compartment Exposure (12-R L (A)) and Radiation (14-R NE (B))**

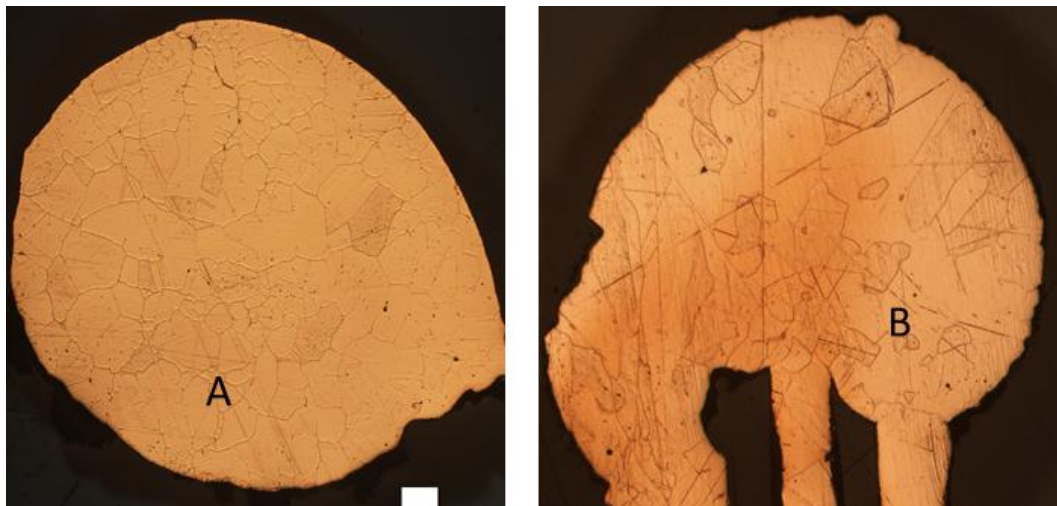


**Figure 4-35: Metallurgical Microscope Images of Beads formed under Scaled Compartment Exposure (18-MS NE (A)) and 18-MS L(B))**

#### 4.2.8 Heat Transfer Analysis

A numerical heat transfer simulation was run to better understand the results produced during testing. A one dimensional (1-D) conduction heat transfer model was developed to evaluate the axial temperature change within the heated section of the wire. Figure 4-36 shows a schematic of the simplified problem. A copper cable of diameter  $D_c$  and length  $2L$  has its axis aligned in the  $x$  direction. Only the  $x > 0$  portion of the cable is considered due to symmetry at the  $x=0$  plane. Hence property

gradients are zero at  $x=0$ . The cable is exposed to heat from a flame  $q_f$  (W/m<sup>2</sup>) in the region  $0 < x < l$  and loses heat due to free convection  $q_c$  (W/m<sup>2</sup>) in the region  $l < x < L$ . Blue dashed lines represent a control volume where conservation of energy was applied to run the 1-D conduction model.

Because of the high conductivity of copper and the small diameter of the cable, heat conduction is assumed to occur only along the axis of the cable. Therefore the conduction problem is transient and one-dimensional. It is also assumed that there is no plastic insulation in the region  $0 < x < l$  where the flame impinges on the cable. This assumption is justified because the time it takes for the insulation to melt (about 75°C) is much less than the time it takes for the copper to reach its melting temperature (about 1083°C). Ambient conditions are defined as 1 atm and 25°C. The theoretically derived time to reach the melting temperature of copper (1083°C) was compared against the experimental break/trip times.

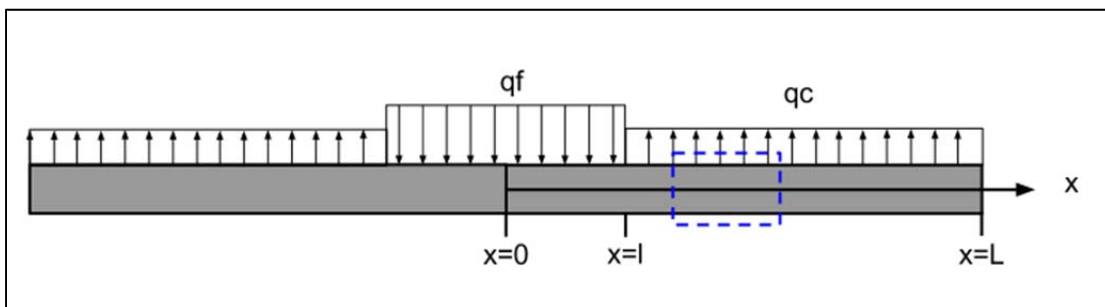


**Figure 4-36: Copper Wire Sample Setup for Heat Transfer Simulation**

The results of the numerical simulation demonstrating the effects of the cable diameter for a one meter long wire are shown in Figure 4-37. The horizontal line denotes the melting temperature of copper (1358 K or 1083°C). It should be noted in Figure 4-37B that the curves collapse when the time is scaled with the diameter of the

wire squared ( $D_c^2$ ). Thus a cable with twice the diameter of another cable will take 4 times longer to reach the melting temperature.

The melting time for the 2mm wire is about 300 seconds and for 1mm wire it is about 75 seconds as seen in Figure 4-37A.

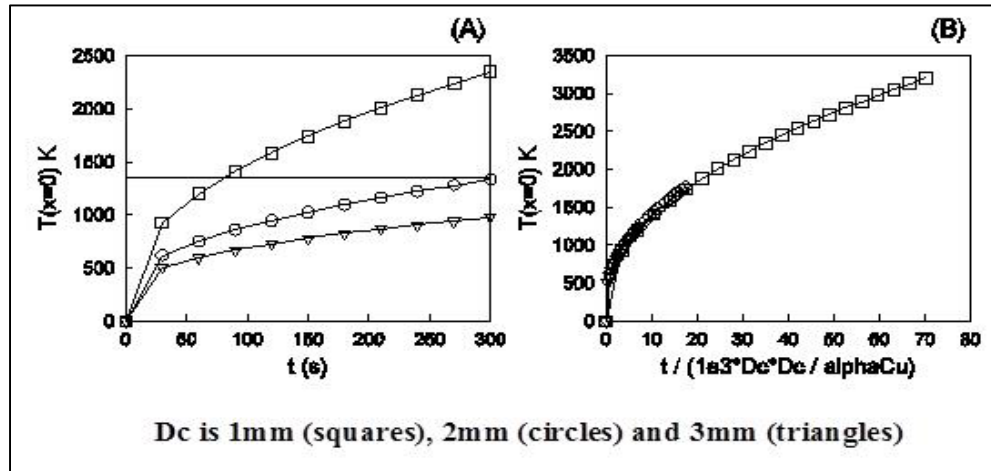
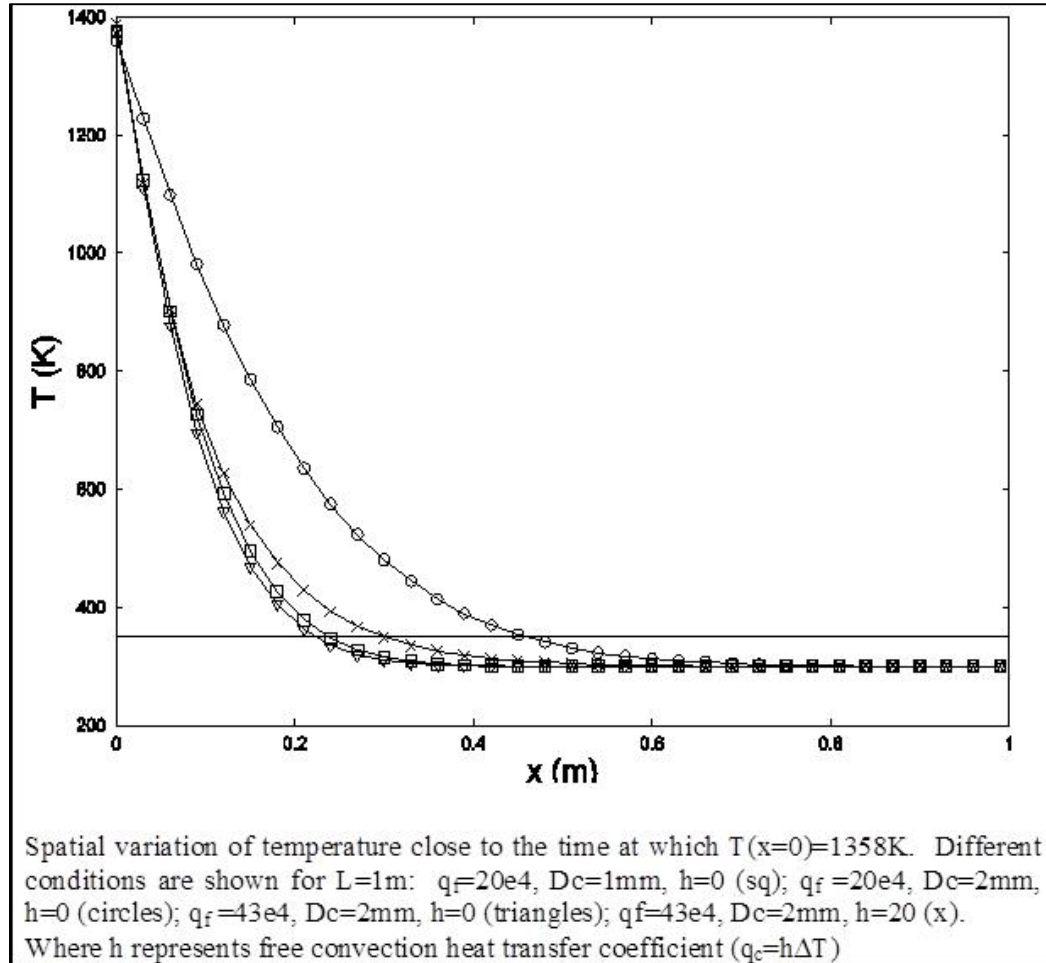


Figure 4-37: Heat Transfer Simulation Results-Temperature Change with Time

The simulation results for the axial temperature variations while the wire is being heated at the center are seen in Figure 4-38. The plot represents one axial side away from the heated section. The horizontal line on the plot is the approximate melting temperature of PVC, the insulation component on the wire. The model predicts that in most cases the wire temperature is less than the melting temperature of PVC at about 25cm away from the section exposed to flame so the wire remains insulated in this area. This shows that most of the heat input is utilized to heat the section of the wire in the flame which eventually melts and breaks. This simulation was modeled for a non-energized direct flame testing condition. An energized wire that arcs experiences temperatures in excess of 5000 K [5]. There will be even less heat transferred axially away from the arcing section due to the rapid nature of the



arcing event. Also a short duration event such as an arc will not lead to big changes in the grain structure of copper.



**Figure 4-38: Axial Temperature Change along Wire Length (Dc similar to 12-R conductors)**

## **Chapter 5: DISCUSSION**

### ***5.1 Summary***

The above section detailed the outcomes of each of the four exposure scenarios: direct flame, radiant tunnel, scaled compartment, and full-scale compartment. The outcomes of these exposures are summarized below. Additionally, the Summary section provides a comparison of results from different exposures to establish if certain trends were seen only under specific exposure conditions.

#### **5.1.1 Direct Flame Impingement Tests**

A larger portion of the energized, loaded wires tripped the circuit than did the energized, non-loaded wires with the exception of the 14-gauge wire tests where no circuits tripped. This result could be due to the presence of the electrical field in the loaded wires more easily supporting the development of an arc across the carbonized insulation. Current spikes were observed in 9 of the 24 tests that were conducted with loaded wires; hence, arcing through char was documented in the loaded wires. The greater propensity for circuit tripping may also be related to the fact that the wire is already under load. Hence, when additional load is placed on the wire due to short-circuiting or another low-resistance event, less additional current is required to overload the circuit.

When comparing the non-energized wires to the energized (loaded and non-loaded) wires, a significant difference was present between the break times and the trip times. This is a logical outcome for two reasons. Firstly, the carbonization of the

insulation in the energized wires supports arcing through char which can result in early failure. Secondly, the energized wires are at a higher internal temperature due to the resistance generated by the current traveling through the wire, hence, a smaller  $\Delta T$  is required to reach the melting temperature of the copper.

Another interesting finding was that the BT for the solid (14 and 12) gauge energized wires was longer than for the stranded (16 and 18) gauge energized wires; the same was true for the non-energized wires. Hence, overall, it took a longer period of time, regardless of the energized state, for the solid wires to break when compared to the stranded wires. One reason for this difference could be the slightly thicker insulation that is present on the solid gauge wires, which are double insulated (conductor and jacket). Additionally, since the solid wires are a larger mass of copper (12 and 14-gauge) compared to the, thermally thin stranded wires (16 and 18-gauge), it could be concluded that the longer BT was related to the difference in mass, rather than the wire geometry (stranded vs. solid).

However, when evaluating within the solid, non-energized wire group, a longer breakage time was not associated with the larger wire gauge; the same was true for the stranded wire group. The 14-gauge solid wires (smaller) had a significantly longer BT than the 12-gauge solid wires (larger), as did the 18-gauge stranded wires when compared to the 16-gauge stranded wires. Hence, the dissipation of heat in the wires does not appear to be solely based on wire diameter, but is also dependent on wire geometry (stranded versus solid). The higher surface area of the stranded wires when compared to the solid wires may play a role in the longer break times. Since one single strand is thermally thin, heat can be transferred

through the strands more quickly. Hence, heat is transferred more quickly to the surrounding copper strands, allowing for faster heat transfer radially through the diameter of the wire, as opposed to axially down the length of the wire. On the other hand, in the solid gauge wires, heat may be transferred more quickly in the radial direction resulting in longer times to melt through the conductor or arc between conductors.

Based on these findings, the fire investigator should expect to see a tripped circuit more often than not if the involved conductors on the circuit were under load or energized. Additionally, the time to failure of a non-energized wire subjected to direct flame impingement is on the order of minutes when compared to energized wires, which typically fail in less than one minute. Whether the wire is stranded or solid will dictate its placement on the failure timeline, with solid wires having a longer time to failure than stranded wires. As one example, these findings could be useful in the investigation of a potential product failure. Many products on the market are designed with flame resistant or fire retardant materials; some of these materials do not support flame spread or sustained flaming. In some cases, the flaming duration is less than one minute. Hence, the presence or absence of damage on internal electrical wires in the product may reveal information about the energized state of the product and potential exposure scenarios.

### **5.1.2 Radiant Tunnel Tests**

Out of the 24 energized wires tested (12 with load and 12 with potential only), 11 had the same breakage and trip times. Of the 11 that did have the same trip times, 8 were under load conditions. Therefore, approximately half of the energized wires

that broke did so due to an arcing or shorting event that was significant enough to cause the circuit to trip. Additionally, there was a slightly higher tendency for this to occur in loaded wires as opposed to energized wires with potential only. These findings are consistent with the direct flame test results, which showed that loaded wires had a higher tendency to trip circuits than did non-loaded wires.

A significant difference in the BT was present between the non-energized wires and the energized, loaded wires. The loaded wires had quicker BT than the non-energized wires. The stranded wires had shorter BT than the solid wires. These findings are consistent with the direct flame tests; therefore, these outcomes are not greatly affected by the exposure condition.

The average TT for the radiation testing is slightly lower than for the direct flame testing. In the direct flame tests, the wire insulation melted, charred, and then arced, resulting in BT or TT. In the tunnel tests, the wire insulation was vaporized almost instantaneously due to the substantial heat flux present in the tunnel. In the tunnel tests, the copper wires were de-insulated very early in the exposure period, and a char did not form on the insulation. Without the protective insulation, it is likely that the wires would arc or short more quickly in the tunnel tests, which is consistent with the test results.

Based on these findings, the fire investigator should expect to see a tripped circuit more often than not if the involved conductors on the circuit were under load. While the time to failure of the non-energized wires was longer than the energized wires in the tunnel exposure, the overall difference in failure times was not as large as in the direct flame testing. In all cases, regardless of the wire type or energized state,

failure occurred in one minute or less. When energized, more (but not all) solid wires failed between 0.50 to 1 minute, and more (but not all) stranded wires failed in less than 0.50 minute; however, it is likely that these failure times are too close to be resolvable for field applications.

### **5.1.3 2/5-Scaled Compartment Tests**

The average trip time in the scaled compartment tests ranged from 3 to 5 minutes. This range was higher than in the direct flame and radiant tunnel tests. This is an expected outcome, since the heat source in the compartment tests was a wood crib which required time to reach a maximum burning rate. The direct flame and radiant tunnel tests utilized a constant heat source from beginning to end, so there was no lag in wire heating.

When comparing wire types, there was no significant difference in trip times in the stranded wires. It should be noted that testing performed on the solid gauge, energized wires with load and without load was done at the same time in the test compartment, and both wires (with and without load) were powered using the same source. Hence, when a trip occurred and the circuit was de-energized, it was not possible to identify which wire (loaded or unloaded) caused the circuit to trip. Therefore, the temperatures and heat fluxes at the time of tripping are the same for the energized wires with load and without load. In order to avoid this same issue with the stranded wire tests, separate circuits were utilized for the loaded and unloaded wires. For the stranded wires, there was no significant difference between the time to trip for the energized with load wires versus the energized without load. At the time the circuit tripped, the average heat fluxes and temperatures ranged from 3 to 9 kW/m<sup>2</sup>

and 400°C to 600°C, respectively. The temperature was measured close to ceiling level. The melting temperature of PVC is between 180°C -260°C, and the melting temperature of copper is approximately 1083°C. Since failure occurs in the energized wires prior to the compartment reaching the melting temperature of copper, it is clear that insulation deformation and charring played a role in the wire failure, e.g. arcing and short-circuiting. When comparing wire types, there was no significant difference between the heat fluxes and temperatures at TT. There was no way to establish the BT of the non-energized wires during the fire; therefore, a comparison of non-energized to energized failure times could not be made.

The average total amount of energy required per unit area to achieve failure was 300 kJ/m<sup>2</sup> to 700 kJ/m<sup>2</sup>. The TEA for the energized, non-loaded wires had a larger range 300 kJ/m<sup>2</sup> to 660 kJ/m<sup>2</sup> when compared to the TEA for the energized, loaded wires which had a range of 282 kJ/m<sup>2</sup> to 333 kJ/m<sup>2</sup>. This finding is consistent with the direct flame and radiant tunnel tests, which shows that loaded wires tripped sooner than non-loaded wires.

These findings are relevant to fire investigation, because they provide a temperature and heat flux range under which the investigator would not expect to see wire damage regardless of energized state. The results also provide a failure timeline, however, it should be noted that these failure times would not be applicable for wires installed in concealed spaces, such as behind walls and ceilings, until wall or ceiling failure. Additionally, it should be noted that not all compartments that undergo flashover will reach temperatures in excess of the melting point of copper (1083°C). The thermal conditions within the compartment will be highly dependent on the

available fuel and ventilation. Even in the presence of ample fuel, ventilation will be the limiting factor in the ability of a compartment to reach temperatures capable of melting non-energized copper wires. In cases where electrical damage to wiring is present, and the electrical state of the wire is in question, the investigator may utilize various tools, such as fire modeling, to evaluate the maximum temperature achieved in the compartment based on fuel loading and ventilation conditions.

#### **5.1.4 Full-Scale Compartment Tests**

The average trip time in the full-scale compartment tests ranged from 3 to 4 minutes. This is an expected outcome, since the average trip time in the 2/5-scale compartment tests ranged from 3 to 5 minutes, and the heat source in both tests had a similar  $t^2$  growth curve. The agreement between the 2/5-scale and full-scale compartment trip times further validates the application of the 2/5-scale compartment test results to full-scale scenarios.

The average heat fluxes and temperatures ranged from 13 kW/m<sup>2</sup> to 35 kW/m<sup>2</sup> and 300°C to 770°C, respectively. This temperature range is consistent with those measured in the 2/5-scaled compartment at the time of failure. The heat fluxes, however, are higher than those measured in the scaled compartment. The difference in measurements is believed to be due to the placement of the heat flux meter in the compartment and was previously discussed in the Results Section in Chapter 4 of the report. When comparing wire types, there was no significant difference between the heat fluxes and temperatures at TT. There was no way to establish the BT of the non-energized wires during the fire, therefore, a comparison of non-energized to energized failure times could not be made. Additionally, since most tests did not reach



temperatures in excess of the melting point of copper, there were very few non-energized wires that melted.

Since the fire source (wood crib) in the scaled compartment was different from the fire sources (variable room layouts with fires starting on couches, chairs, etc.) in the full-scale compartments, the TEA is useful in comparing the two compartment types. The average total amount of energy required per unit area to achieve failure was 300 kJ/m<sup>2</sup> to 640 kJ/m<sup>2</sup>. This amount is consistent with the 2/5-scaled compartment TEA of 300 kJ/m<sup>2</sup> to 700 kJ/m<sup>2</sup>, and again, supports the use of the scaled compartment data in full-scale scenarios.

These findings are relevant to fire investigation, because they provide a temperature and heat flux range under which the investigator would not expect to see wire damage regardless of energized state. The results also provide a failure timeline; however, it should be noted that these failure times would not be applicable for wires installed in concealed spaces, such as behind walls and ceilings, until wall or ceiling failure. Additionally, it should be noted that not all compartments that undergo flashover will reach temperatures in excess of the melting point of copper (1083°C). The thermal conditions within the compartment will be highly dependent on available fuel and ventilation. Even in the presence of ample fuel, ventilation will be the limiting factor in the ability of a compartment to reach temperatures capable of melting non-energized copper wires. In cases where electrical damage to wiring is present, and the electrical state of the wire is in question, the investigator may utilize various tools, such as fire modeling, to evaluate the maximum temperature achieved in the compartment based on fuel loading and ventilation conditions.

## 5.1.5 Comparisons between Various Exposures

### 5.1.5.1 Average Failure Times

The average failure time (by wire breaking or circuit tripping) for energized wires under all thermal exposure are shown in Table 5-1 where “E” represents non-loaded wires and “L” represents loaded wires.

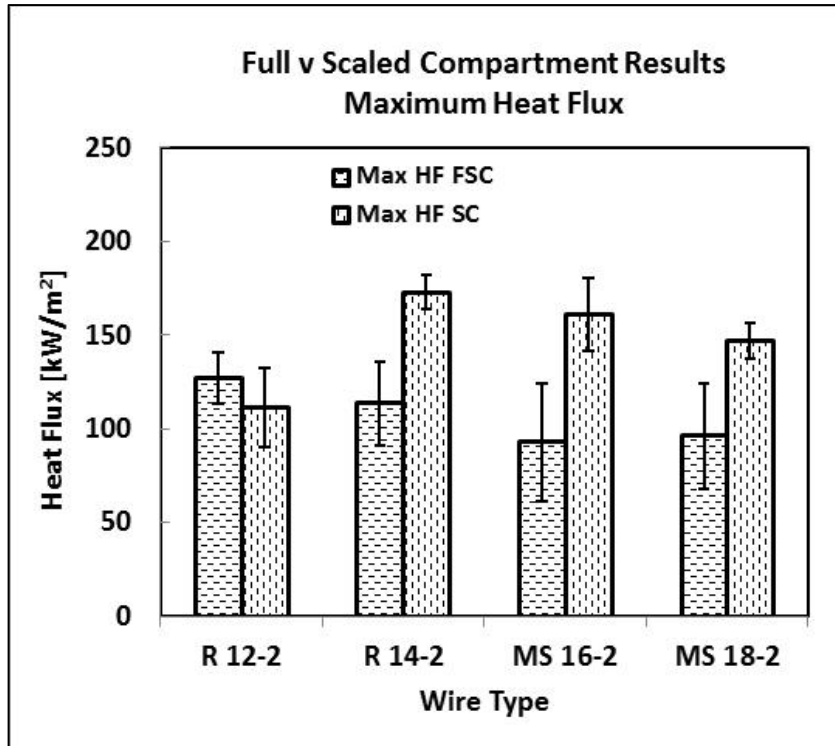
**Table 5-1 Average Failure Time-All Exposures.**

	12R		14R		16MS		18MS	
	E	L	E	L	E	L	E	L
Exposure	Wire Failure Time (Trip and/or Break)							
DF	0.78	0.62	0.67	0.72	0.33	0.33	0.28	0.28
R	0.53	0.44	0.45	0.42	0.26	0.29	0.19	0.21
C	3.82	3.88	4.26	4.26	3.66	3.35	4.86	4.16
FR	3.38	3.38	2.98	2.98	2.71	2.71	3.99	3.99

The direct flame and radiant tunnel exposures produced similar failure times. The 2/5-scale and full-scale compartment fires also produced similar failure times. These findings are expected, since the direct flame impingement and radiant tunnel tests are bench-scale, localized, and highly controlled methods, whereas the compartment fire tests (both 2/5-scale and full-scale) have a  $t^2$  growth rate. It should be additionally noted that there is good agreement between the 2/5-scale and full-scale test results. Hence, the scaled-compartment results can be applied to full-scale scenarios.

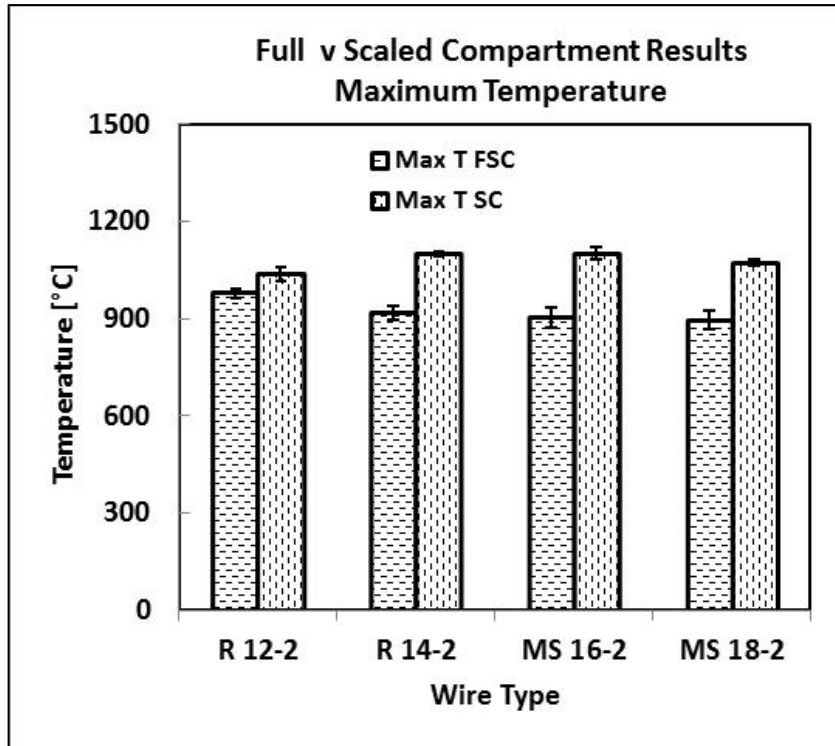
### 5.1.5.2 2/5-Scale versus Full-Scale Compartment Comparison

Figure 5-1 and Figure 5-2 provide a comparison of the temperatures and heat fluxes in the 2/5-scale and full-scale compartments.



**Figure 5-1: Maximum Heat Flux (averaged for each wire type) Measured During Testing. (FSC v SC)**

The maximum temperatures achieved in the 2/5-scaled compartment were slightly higher than those achieved in the full-scale compartment. The same was true for the heat fluxes, with the exception of the 12-gauge Romex tests. The higher temperatures and heat fluxes are consistent with the use of forced ventilation in the scaled compartment tests. Prior to the introduction of forced air, the temperatures and fluxes within the 2/5-scale compartment were more consistent with those in the full-scale compartment.



**Figure 5-2: : Maximum Temperature (averaged for each wire type) Measured During Testing. (FSC v SC)**

Regardless of the higher overall temperatures and fluxes in the 2/5-scaled compartment, the energized wires still appeared to react in a similar fashion in both compartments. Figure 5-3 shows that the wires in both the 2/5-scale compartment and the full-scale compartments had very similar average trip times.

The consistency in results between the 2/5-scale compartment and the full-scale compartment are expected, since the trip time is not related to the maximum temperature or heat flux achieved in the compartment. The trip times occurred well before the maximum temperatures were achieved in the compartment.

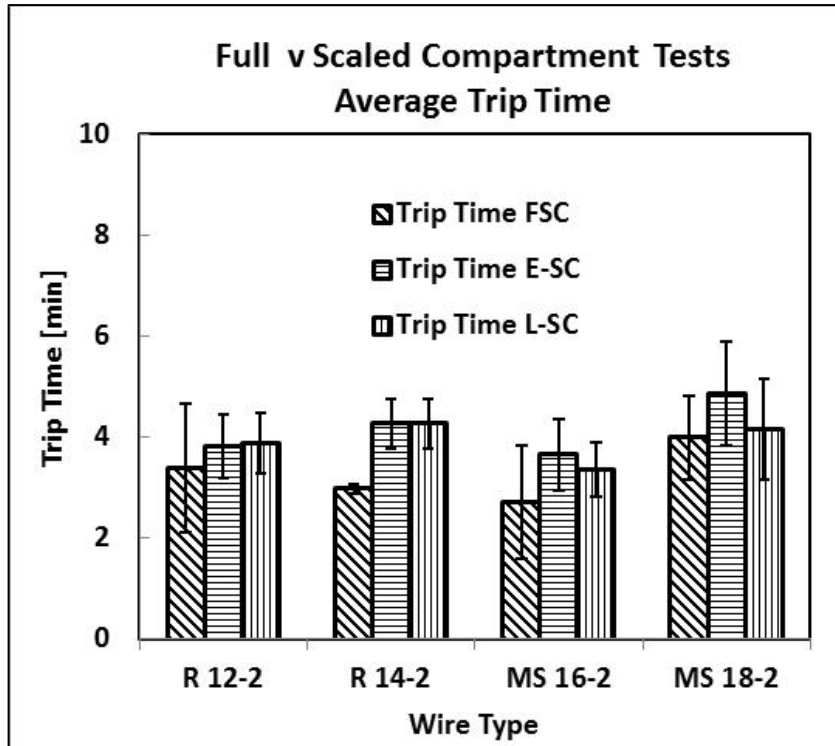


**Figure 5-3: Average Trip Times for Compartment Testing (FSC v SC)**

The trip times for both compartments were plotted against the maximum temperatures and heat fluxes at the time of tripping and are shown in Figure 5-4 and Figure 5-5. Both of the graphs show similar trends: the trip time decreases with increasing heat flux and temperature.

Additionally, the slopes and intercepts of the lines for the temperatures and heat fluxes in both compartments are similar, showing good agreement between the 2/5-scale and full-scale compartments.

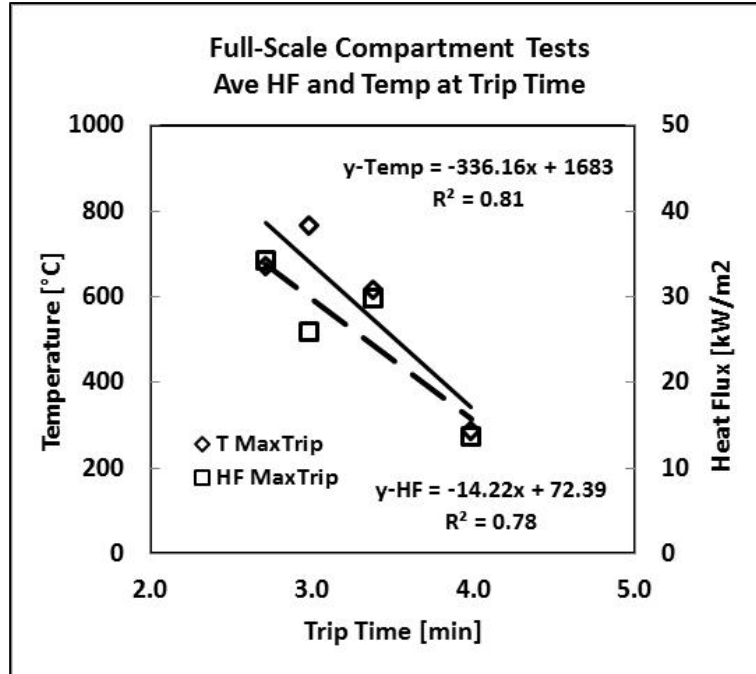


Figure 5-4: Full-Scale Compartment Trip Time Analysis (FSC)

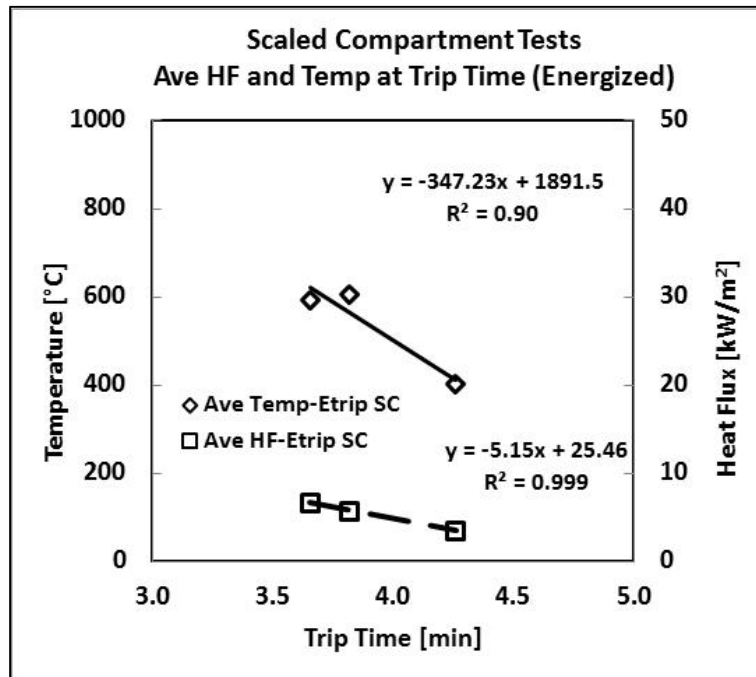


Figure 5-5: Scaled Compartment Trip Time Analysis (SC)

The TEA for the 2/5-scale and full-scale compartments was also compared. The average results are shown in Figure 5-6. In all cases, the average TEAs in both compartments was within the same range.

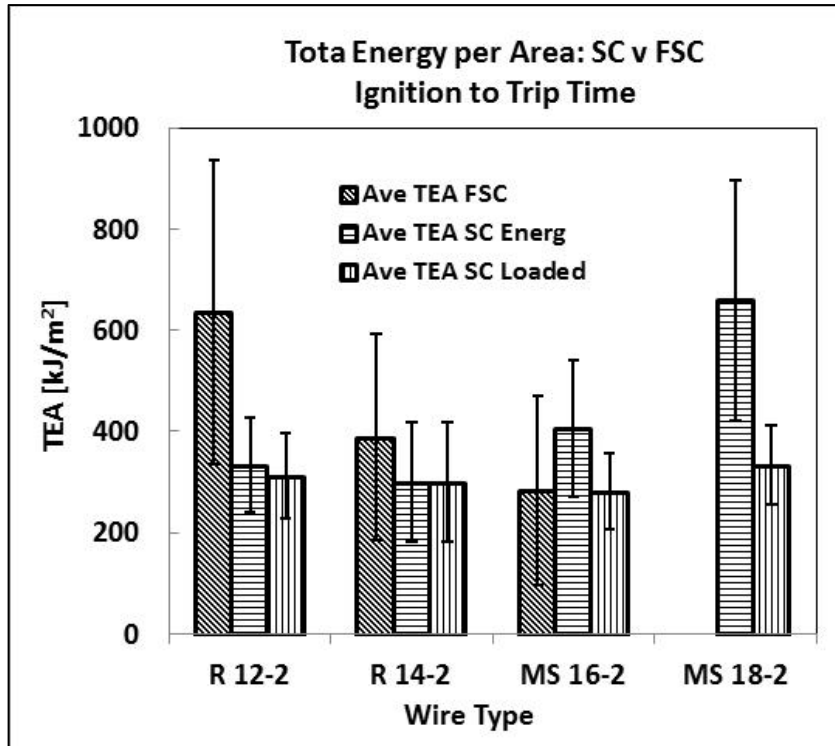


Figure 5-6: Total Energy per Area Comparison (SC and FSC)

This outcome is expected, since the total energy required to produce a failure in the wires should be the same regardless of the compartment geometry or specific fire type.

### 5.1.6 Bead Characteristics

Below, Table 5-2 shows the percentage of beads that were produced on wires based on their exposure condition, wire type, and energized state.

Table 5-2: Percentage of Samples with Bead Formation

	12R			14R			16MS			18MS		
	NE	E	L	NE	E	L	NE	E	L	NE	E	L
Exposure	Percentage of Samples with Bead Formation											
DF	67	17	83	83	83	100	67	67	67	17	83	50
R	0	33	67	67	100	67	66	100	33	33	66	100
C	80	25	50	50	50	100	100	66	66	100	71	33
FR	0	33	33	0	0	0	0	33	33	0	33	33

The production of beads on non-energized wires in the full-scale compartment was minimal. The lack of bead production occurred because on average, the compartment did not exceed 950°C. Beads were formed on non-energized wires in all scenarios except the full-scale testing and 12-gauge radiant tunnel testing. The average of the percentage of beads formed under all three exposure conditions (full-scale not included) for non-energized, energized with no load, and energized with load wire are 61%, 63%, and 68%, respectively. Therefore, when conditions are sufficient to produce temperatures within the melting range of copper, the likelihood that a bead will form on a non-energized wire (61%) is approximately the same as the likelihood that it will form on an energized wire (63%-68%).

The beads which formed on the conductors were also measured for their diameters and the average diameters are shown in Table 5-3 below. The diameters are averaged for each wire type under each electrical condition. The average bead diameter increases with increasing wire gauge, as would be expected.

An evaluation of the visual characteristics of the beads is discussed below. Both non-energized and energized wires showed similar damage as seen in Figure 5-7 below. NFPA 921 outlines methods to distinguish between the beads formed on energized and non-energized wires, namely the presence of a clear line of demarcation on beads which formed from arcing (e.g. beads formed on energized wires). As seen below, both energized and non-energized wires show beads that have clear lines of demarcation. Additionally, in some cases, beads formed on energized wires do not show clear lines of demarcation.



**Table 5-3: Average Bead Diameter**

	12R			14R			16MS			18MS		
	NE	E	L	NE	E	L	NE	E	L	NE	E	L
<b>Exposure</b>	<b>Average Bead Size [mm]</b>											
<b>DF</b>	4.0	4.0	3.1	2.7	2.2	2.6	2.7	2.7	1.3	1.5	1.8	1.5
<b>R</b>	0	3.5	3.4	2.5	2.5	3.7	2.0	1.1	2.4		0.9	1.5
<b>C</b>	4.8	5.6	4.5	4.5	0	4.6	2.6	2.3	2.4	2.8	3.1	3.1
<b>FR</b>								2.5	2.1		2.0	1.0
<b>Wire D =&gt;</b>	<b>2.16</b>			<b>1.65</b>			<b>0.76</b>			<b>0.64</b>		
Wire D given is Diameter for Single Conductor before Exposure												

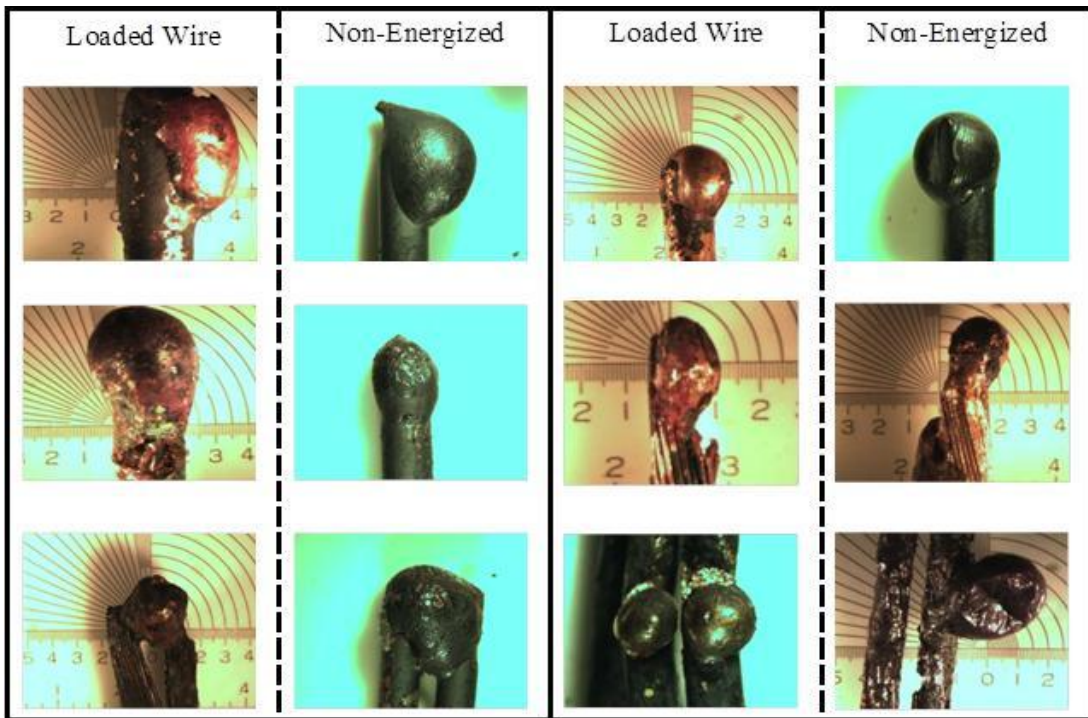


**Figure 5-7: Comparison of Loaded and Non-energized Beads for various Exposures (SM Images)**

Based on a preliminary evaluation of the exterior bead structure, there is no indication that the unloaded, energized bead was characteristically different from the loaded, energized bead. Most of the selected wires were 12-gauge solid and 18-gauge multi-stranded.

A side-by-side comparison of some of the patterns observed under the

stereomicroscope is shown in Figure 5-8. Images were paired together based on similarities in the internal bead structure. It is evident from Figure 5-8 that there are no visible patterns (at a maximum of 44 x magnification) in beads formed on loaded and non-energized samples.

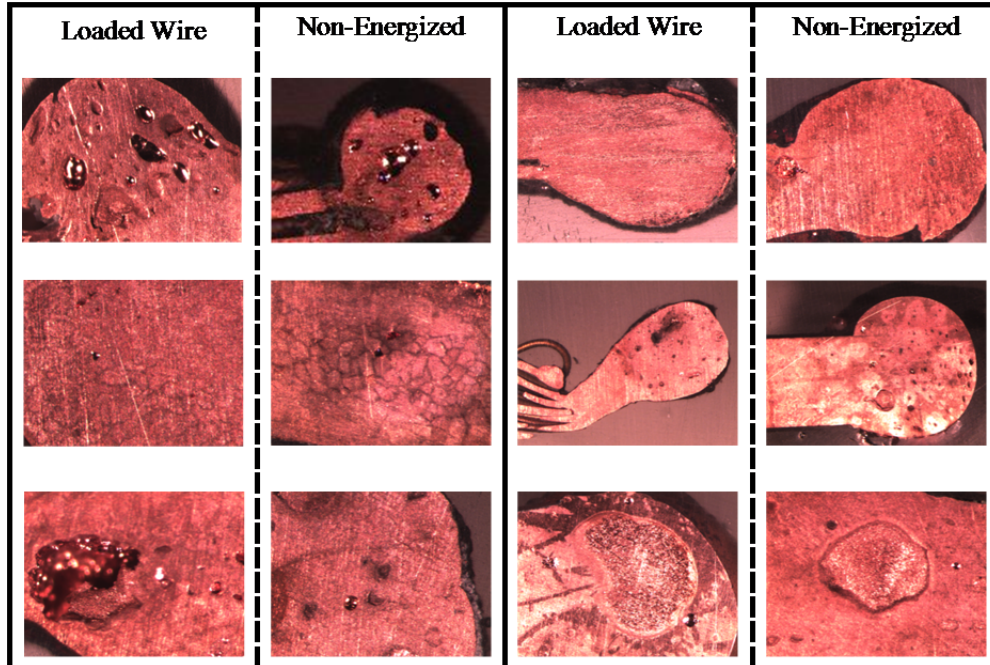


**Figure 5-8: Internal Pattern Comparison of Loaded and Non-energized Beads for various Exposures (SM Images)**

### 5.1.7 Analysis with Metallurgical Microscope

To further evaluate the grain structure of the samples, they were sent to a metallurgist, Dr. Charles Manning of ARAI in South Carolina. According to ARAI and the literature [34 and 39], copper wires will experience grain structure enlargement when exposed to elevated thermal conditions, due to the known metallurgical attributes of copper. Therefore, copper wires that experience arcing may be identifiable based upon changes in grain structure, if further heating of the beads, post-arcing, is limited. Post-arcing, heating can result in continued

enlargement of the grain structure, making it similar to the grain structures of a bead produced under non-energized conditions. . Based on ARAI's analysis, it cannot be determined with 100% accuracy that a bead was caused by thermal exposure or by electrical activity or by a combination of both events. Some of the energized wires showed clear lines of demarcation; however, some did not, as seen in Figure 4-31 and Figure 4-32 in Section 4.2.7 in Chapter 4. The six beads that displayed clear lines of demarcation are shown in Figure 5-9 and Figure 5-10 below.

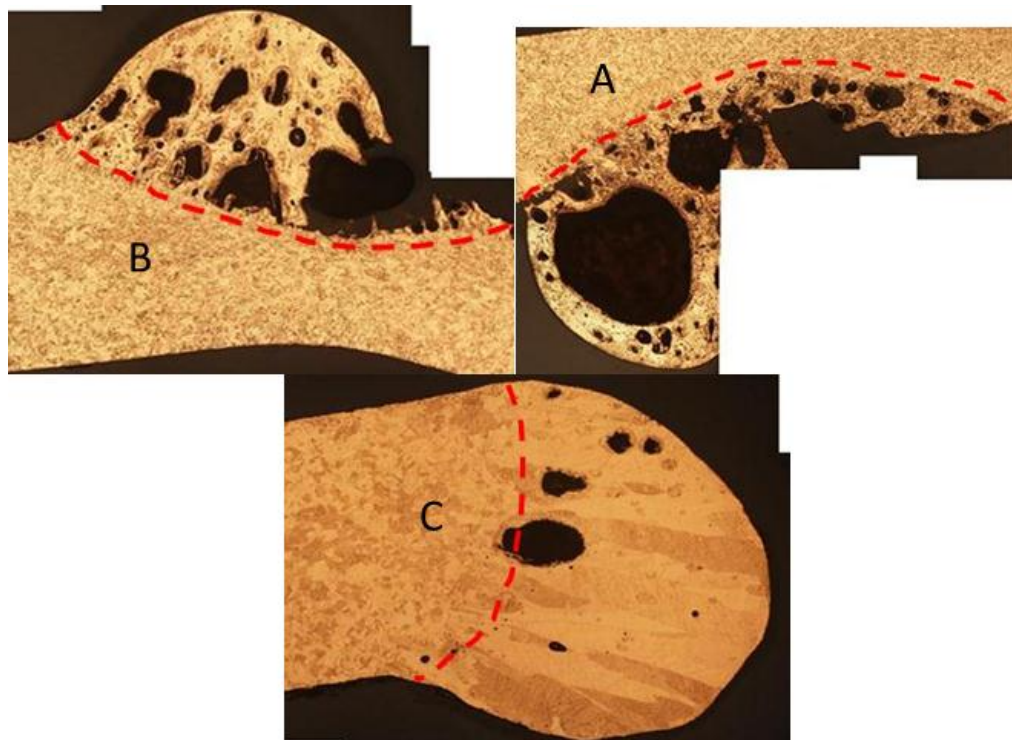


**Figure 5-9: Internal Lines of Demarcation (Direct Flame (A and B) and Radiation (C))**

There were two trends observed in the grain structure of the beads with visible lines of demarcation. The beads in Figure 5-9 showed an enlargement of the grain structure on the bead when compared to the longitudinal wire section. These beads were formed under energized, direct flame (Image A and B) and radiation (Image C)

testing conditions. The images shown in Figure 5-10 show the beads formed during energized compartment testing. The grain structure in these images is opposite; the beads show small grain structures as compared to the longitudinal section of the wire.

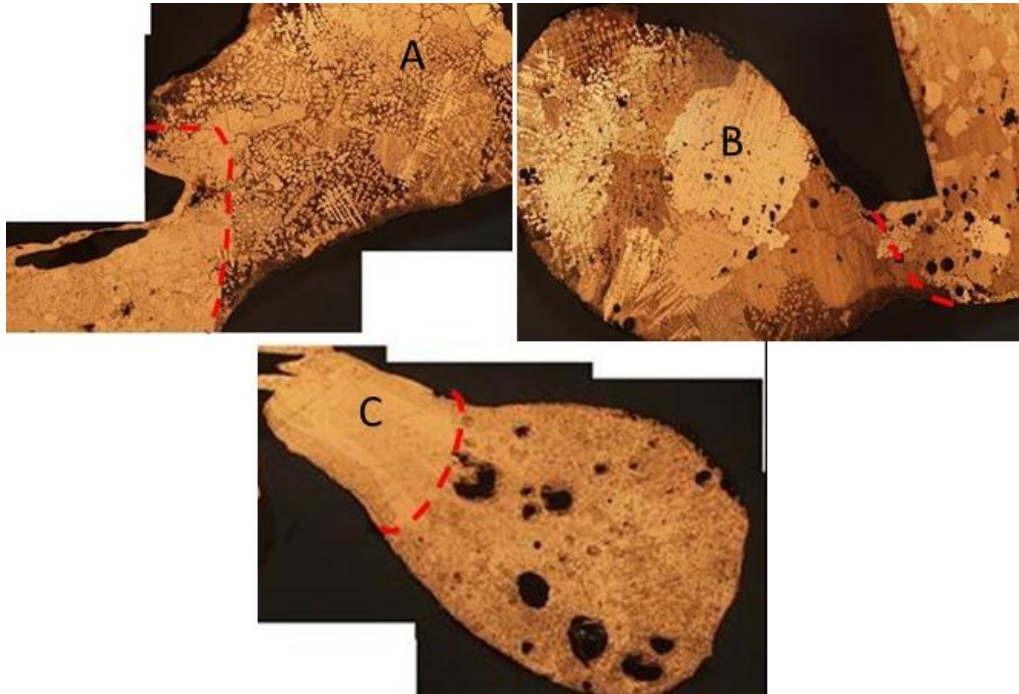


**Figure 5-10: : Internal Line of Demarcation (Scaled Compartment-All)**

### **5.1.8 Heat Transfer Analysis**

A one dimensional conduction simulation of the direct flame scenario showed that most of the heat from the flame is absorbed by the small section of the wire being heated. The axial heat transfer is small compared to the heated region as seen in Figure 4-38 in Section 4.2.8 in Chapter 4.

## **Chapter 6: CONCLUSIONS AND FUTURE WORK**

### ***6.1 Conclusions and Summary***

There are about 400,000 household fires reported per year in the United States, and the cause of more than ten percent (10%) of these fires is electrical in nature. These fires result in hundreds of injuries per year, as well as, losses of life and property. When beads are found on electrical wires during a fire scene investigation, investigators often conclude that the wire was energized at the time of bead formation. In some cases, this cases the investigator to more heavily focus on the potential for the fire to be electrical in nature. Current training suggests that beads are only produced on energized electrical wires, however, the findings of this research prove otherwise; characteristic “beads” can form on energized and non-energized wires.

The purpose of this research was to identify patterns on or inside beads that can be used to distinguish between the beads formed on non-energized wires (due to melting) and on energized wires (due to electrical activity). In order to encompass various thermal conditions found in fires, wires were tested in four different settings. These test methods covered convective, radiative, and a combination of convective/radiative exposures. After testing and analysis of all samples, it can be concluded that beads can be formed on copper wires under both non-energized and energized conditions. Moreover, the bead formation is not a function of the electrical conditions but can also be a function of the thermal conditions of the fire environment. Analysis with a stereo microscope showed that non-energized and

energized beads both possessed clear lines of demarcation. According to NFPA921 [35], clear lines of demarcation are only considered to be present on beads formed because of arcing in energized wires.

This supposition is clearly wrong and has been disproven by the research conducted in this study. These findings clearly show that more analysis and investigation is required to determine the status of an electrical circuit prior to and during a fire if a bead is uncovered during the post-fire examination. The presence of a wire bead does not mean that the circuit was necessarily energized and that an arcing event occurred. Additionally, a visual inspection of a bead is insufficient support the determination of a beads caused by arcing versus thermal heating.

Some of the wire beads were analyzed with SEM/EDS. SEM/EDS analysis was done at the University of Maryland (College Park) by CSE, at the Unified Engineering (Aurora, IL), and at the Fire and Materials Research Laboratory (Lavonia, MI). Analysis with SEM did not show any trends that could be used to distinguish between the beads formed on non-energized and energized wires. It was additionally concluded that SEM/EDS analysis of samples did not show any useful trends in the elemental composition of the beads or in structural patterns.

Another round of analysis was done with a stereo microscope to study the internal structures of the beads. To prepare the beads for this analysis, the beads were mounted in epoxy and sanded down with fine grit sanding paper to 3 micrometers depth to reveal their inner structure. These samples were then polished and etched. All of the beads were then photographed with a 40x magnification stereo microscope to study grain structure. The images of non-energized and energized beads showed

several common patterns on the beads including voids. These patterns were present in both non-energized and energized wire beads. It was concluded that although several patterns were present within the bead structures, no distinguishing patterns were found between energized and non-energized beads.

In final analysis method, these mounted samples were removed from their mounts and remounted and re-etched with a different solution for observation at ARAI with a metallurgical microscope. These beads were photographed with a high resolution Nikon camera attached to the microscope. This imaging revealed the grain structures of the copper beads. Six out of 14 (40%) beads formed on the energized wires showed a clear line of demarcation between the bead grain structures on the wire and only one of the 15 non-energized beads also showed a line of demarcation. Some of the energized beads had grain structures similar to those found on the non-energized beads.

The six samples that displayed clear lines of demarcation also had some revealing trends. Two of these were produced by direct flame exposure, three were tested in scaled compartment, and one in the radiation tunnel. The samples tested with direct flame and radiation showed larger copper microstructures on the bead than on the wire and the samples tested in compartment showed smaller microstructures on bead compared to wire.

In summary, two important conclusions that disprove previous beliefs about beads present or absent on copper wiring exposed to fire can be derived. First, the presence or absence of a bead on a wire exposed to fire does not provide a reliable indication whether the wire was energized or non-energized at the time of the fire.

Furthermore, the presence of bead cannot be used to determine whether the electrical wire failure was a cause or effect of the fire. Second, all of the bead analysis methods used during this research indicate that it is not possible to differentiate between the beads formed on energized and non-energized wires exposed to fire. These conclusions show that fire investigators cannot rely on the presence or absence of beads alone to understand the role copper wiring may have played in a fire. The fire investigators must look at other scene information, like extent of the fire, duration of the fire, and nature of the fire to reach valid conclusions about the performance of copper wiring in the fire.

Finally, it was hypothesized at the beginning of this research that beads will form on both energized and non-energized wires. It was also hypothesized that macroscopic and/or microscopic analysis of these beads would lead to indicators that could be used to differentiate between beads formed on energized and non-energized wires. Based on this work, it can be concluded that beads can form on wires regardless of electrical condition, and that it is not possible to differentiate between the beads formed on energized and non-energized wires using the macroscopic and microscopic analysis techniques used in this research.

## ***6.2 Future Work***

There is a general lack of reproducible, consistent techniques available for the analysis of beads formed on electrical wires. When this research proposal was first developed, it was assumed that the material science and metallurgical communities had some type of established, uniform techniques to analyze copper beads developed



under fire conditions. While the material science and metallurgical communities have available techniques for the analysis of copper beads, there appears to be a general disagreement as to which technique is valid and appropriate.

The three main issues in bead analysis which require further research are establishing the appropriate etch and preparation techniques, the appropriate analysis technique (SM, SEM, EDS, Auger, etc.), and the appropriate location on the bead. Since different etches reveal different grain structures, the first issue is establishing which grain structure is most important for the specific condition of interest. Since fire is a dynamic thermal process, it is probably necessary to select multiple etches and to re-etch and re-evaluate the samples accordingly. As for the analysis equipment, some researchers suggest that stereomicroscopic analysis is sufficient, while others suggest that SEM/EDS, or various other combinations of metallurgical and material analysis should be used. Furthermore, when analyzing a bead using EDS, the following questions arise: 1) should the surface of the bead be analyzed, and if so, should it be cleaned first and how should it be cleaned? 2) What location on the surface of the bead should be analyzed, and if multiple locations are recommended for analysis, how many are enough? 3) When analyzing interior of a bead, what depth is appropriate, what surface area is appropriate, and how many locations are appropriate? 4) Can a technique which is developed based on the size and shape of one bead be equally applied to another bead of a different size or shape, and if so, will the results be truly comparable? A full study is needed to address these questions.

## **APPENDIX 1**

### **Stereo Microscope Images of all Beads**

**Note:**  
**NE – Non Energized**  
**EN – Energized**  
**L – Loaded**

**SCALED COMPARTMENT TEST; 16-2 MULTISTRAND WIRE**

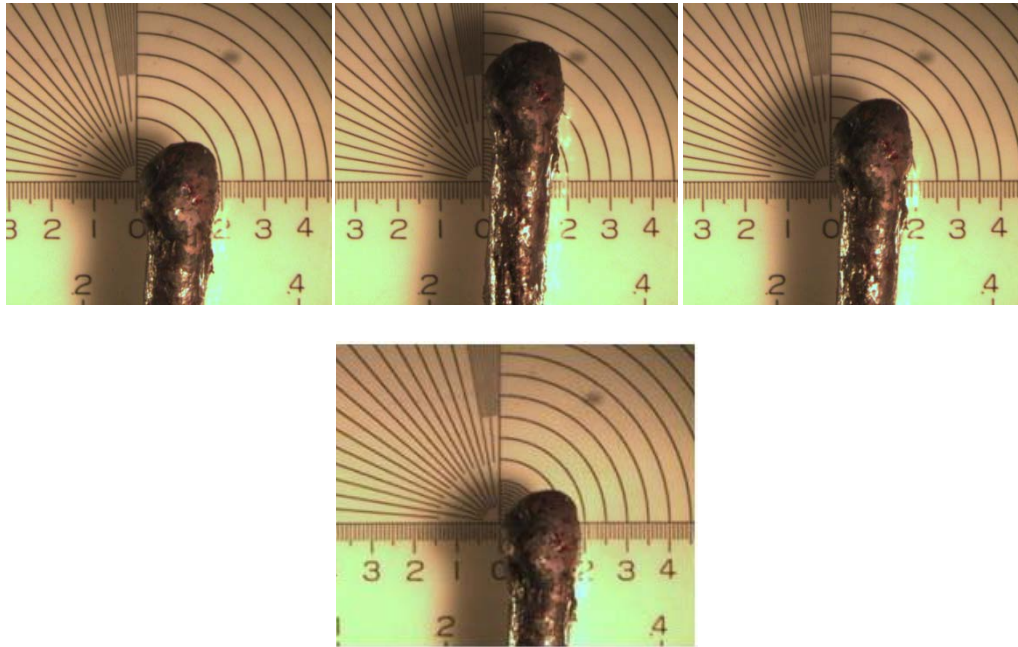


Figure 1: Compartment Tests, MS 16-2, Energized (Test No. 30)

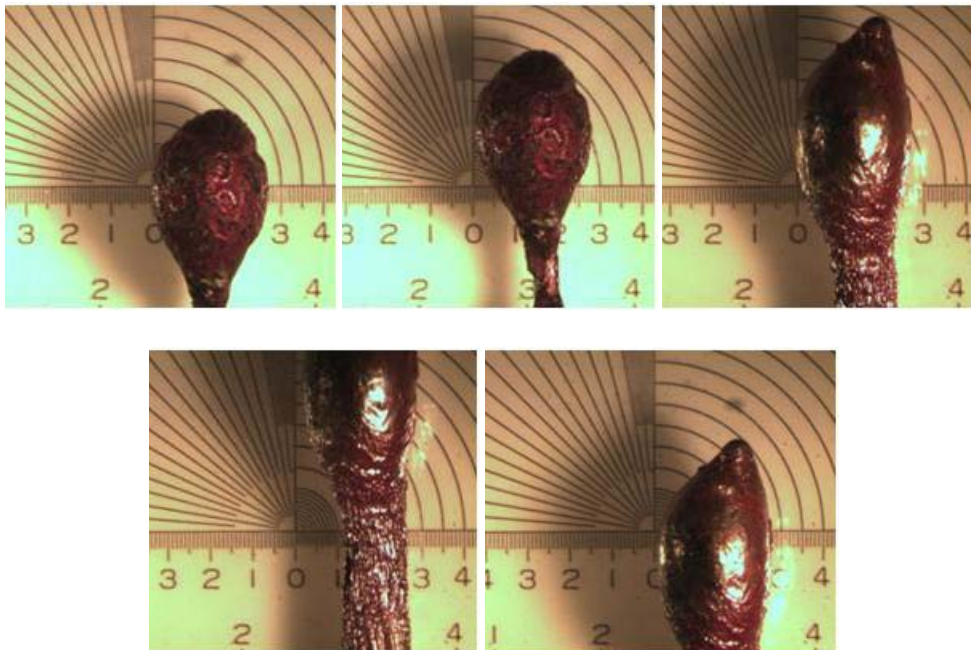


Figure 2: Compartment Tests, MS 16-2, Non Energized (Test No. 36)

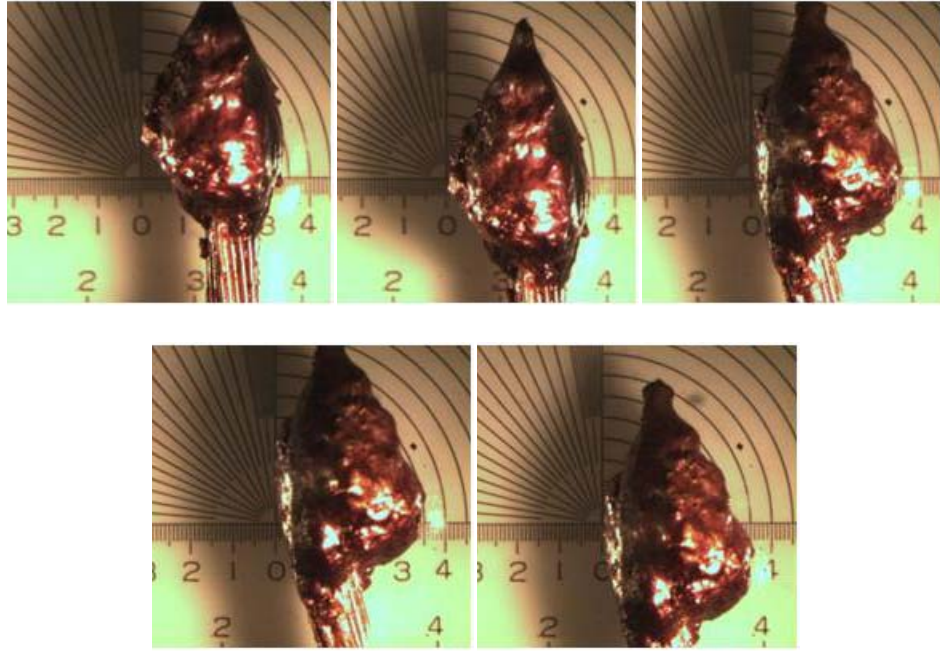


Figure 3: Compartment Tests, MS 16-2, Energized (Test No. 37)

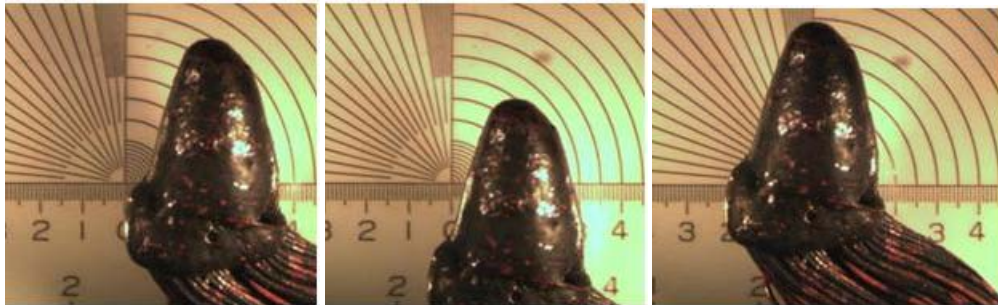


Figure 4: Compartment Tests, MS 16-2, Loaded (Test No. 37)



Figure 5: Compartment Tests, MS 16-2, Energized (Test No. 38)

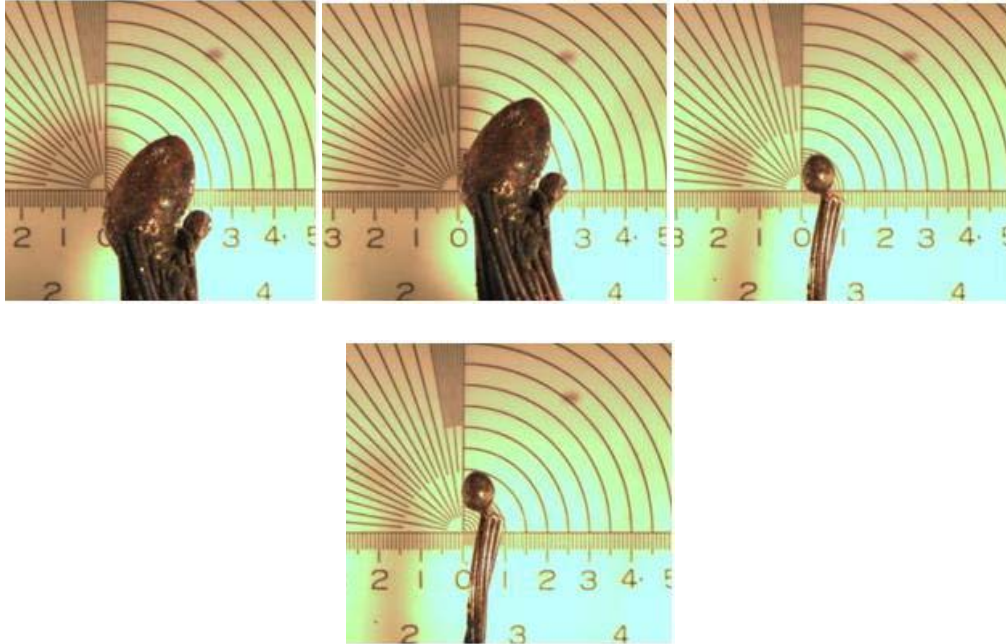


Figure 6: Compartment Tests, MS 16-2, Energized (Test No. 39)

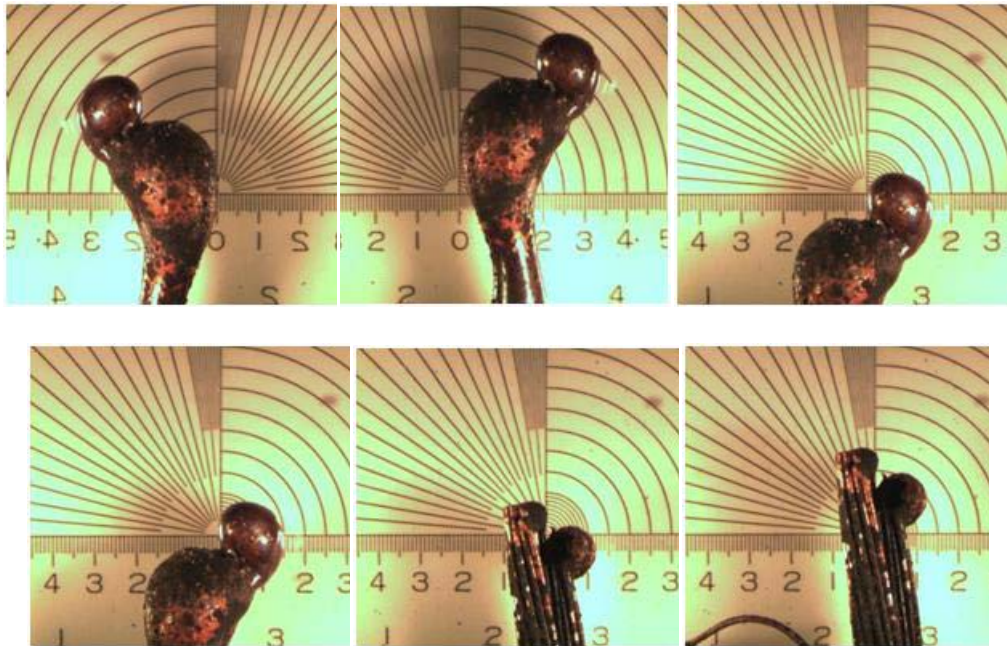


Figure 7: Compartment Tests, MS 16-2, Loaded (Test No. 39)

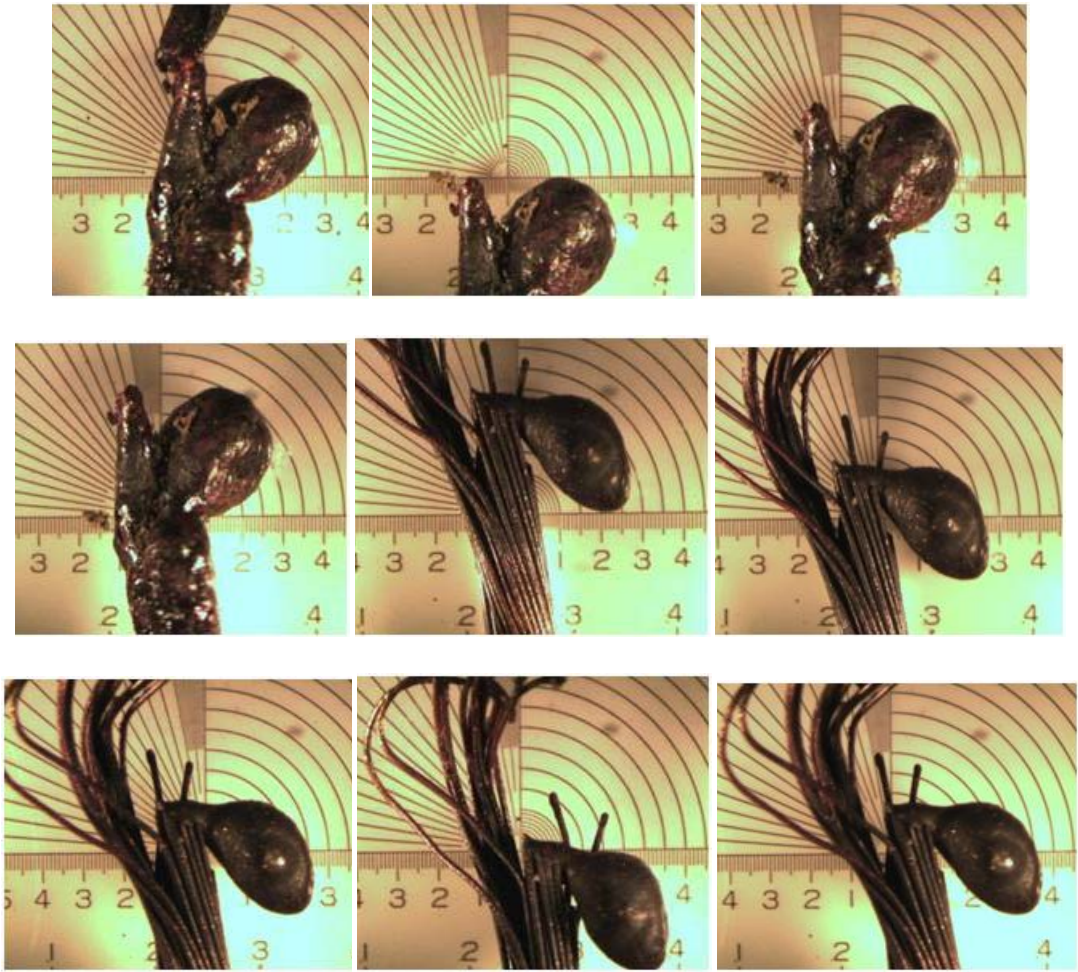


Figure 8: Compartment Tests, MS 16-2, Energized (Test No. 40)

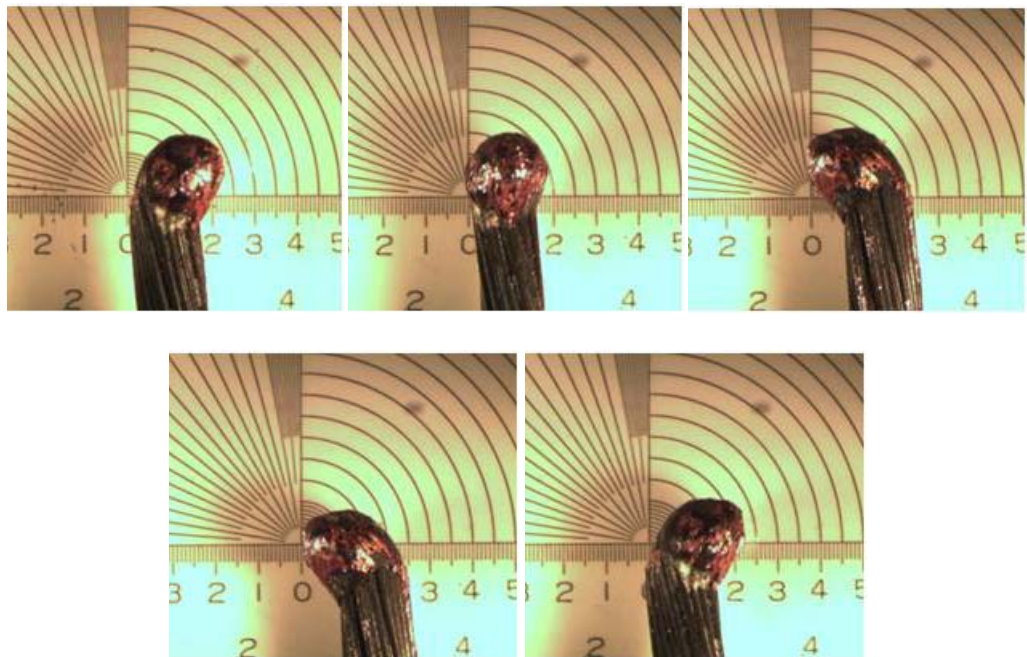


Figure 9: Compartment Tests, MS 16-2, Loaded (Test No. 41)

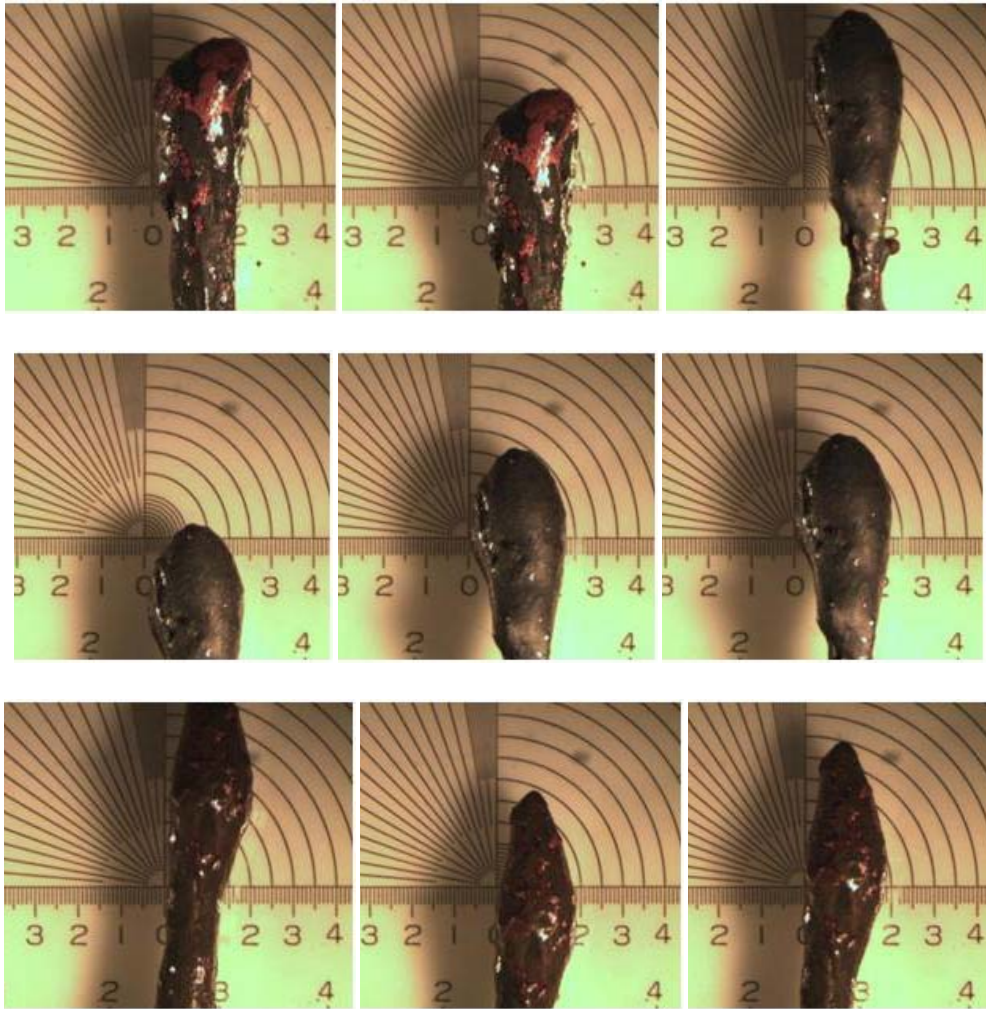


Figure 10: Compartment Tests, MS 16-2, Non Energized (Test No. 42)

**SCALED COMPARTMENT TEST; 18-2 MULTISTRAND WIRE**

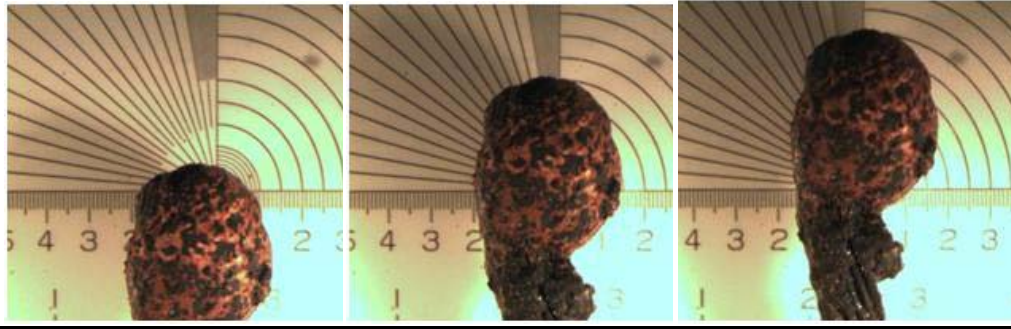


Figure 11: Compartment Tests, MS 18-2, Non Energized (Test No. 27)

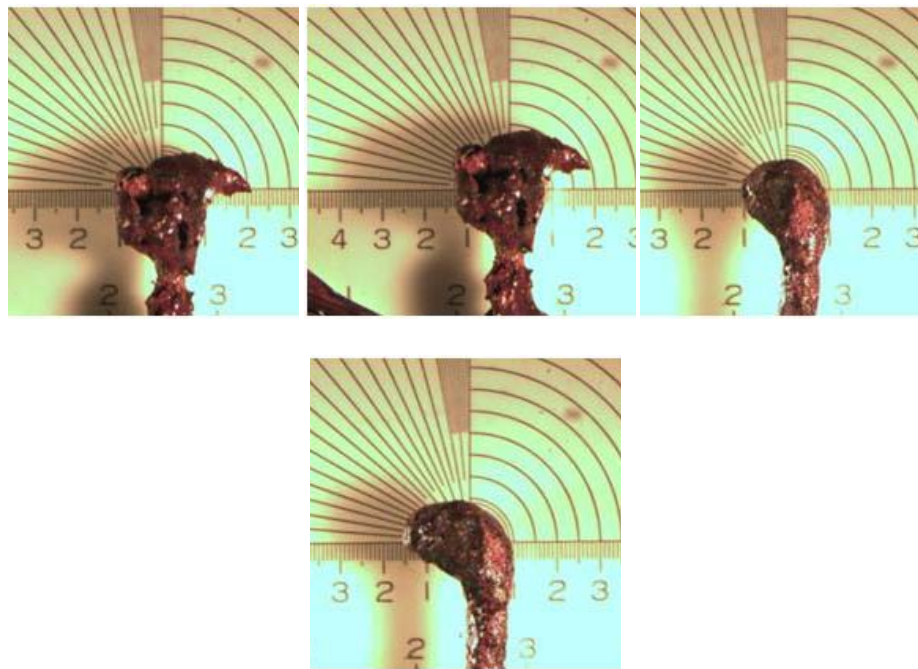


Figure 12: Compartment Tests, MS 18-2, Loaded (Test No. 27)





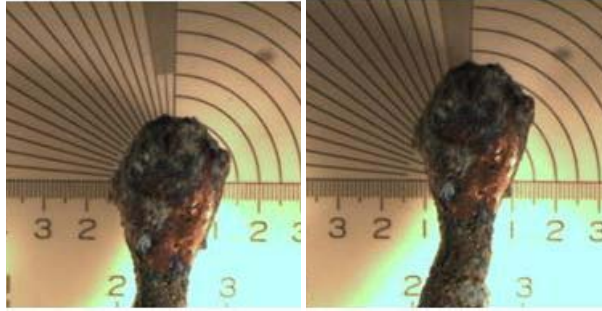


Figure 13: Compartment Tests, MS 18-2, Non Energized (Test No. 28)

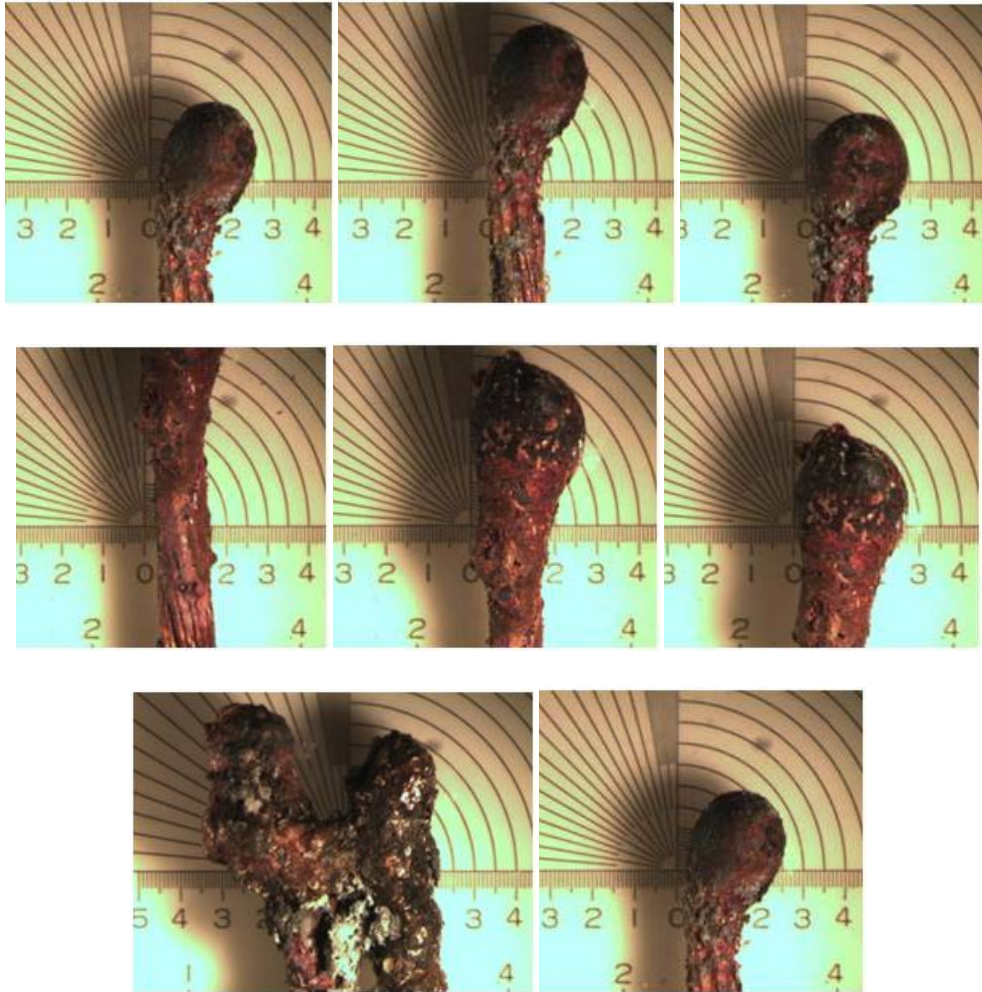


Figure 14: Compartment Tests, MS 18-2, Energized (Test No. 31)

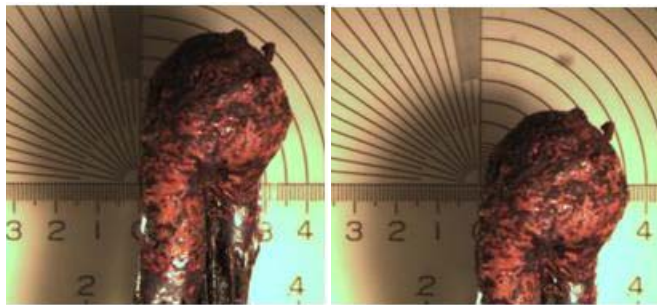
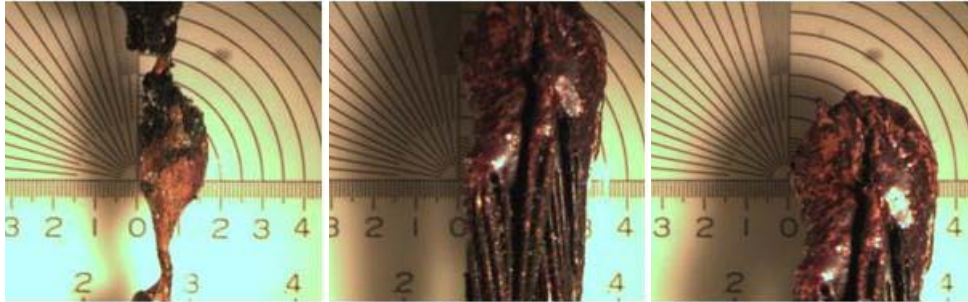
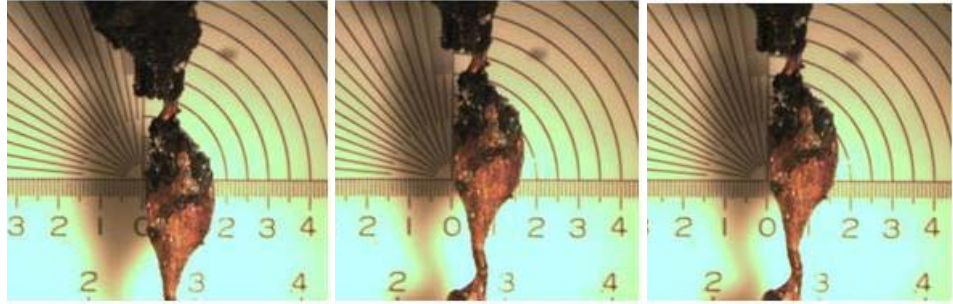


Figure 15: Compartment Tests, MS 18-2, Loaded (Test No. 31)

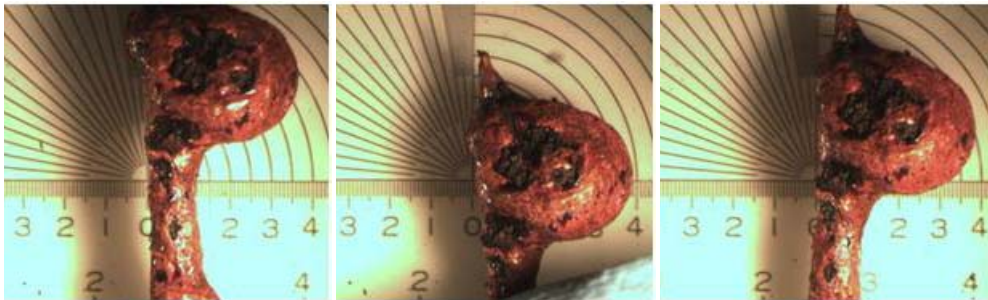


Figure 16: Compartment Tests, MS 18-2, Energized (Test No. 32)

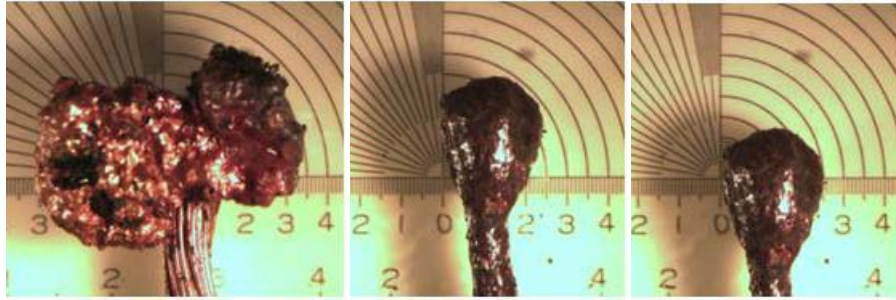
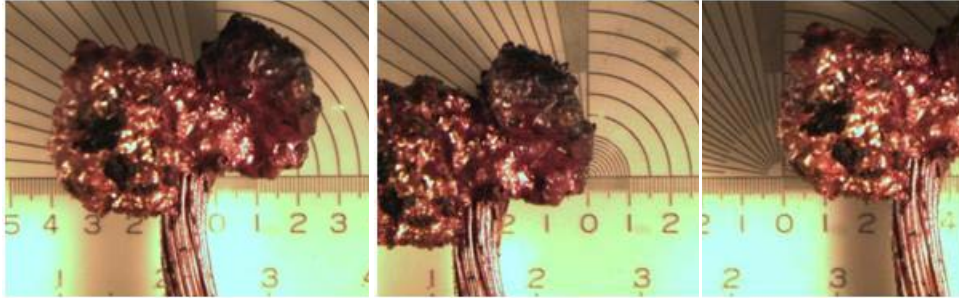


Figure 17: Compartment Tests, MS 18-2, Loaded (Test No. 32)

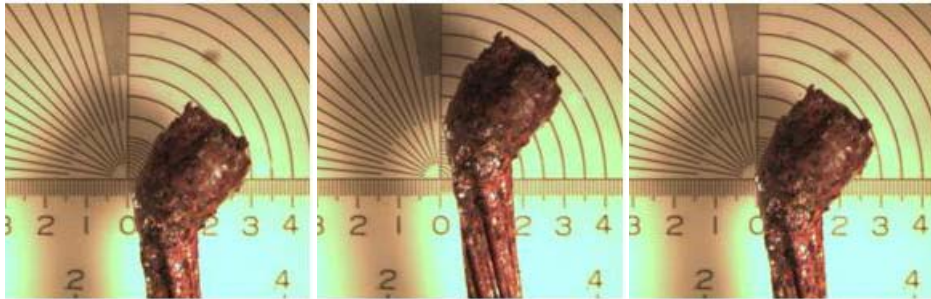


Figure 18: Compartment Tests, MS 18-2, Energized (Test No. 33)

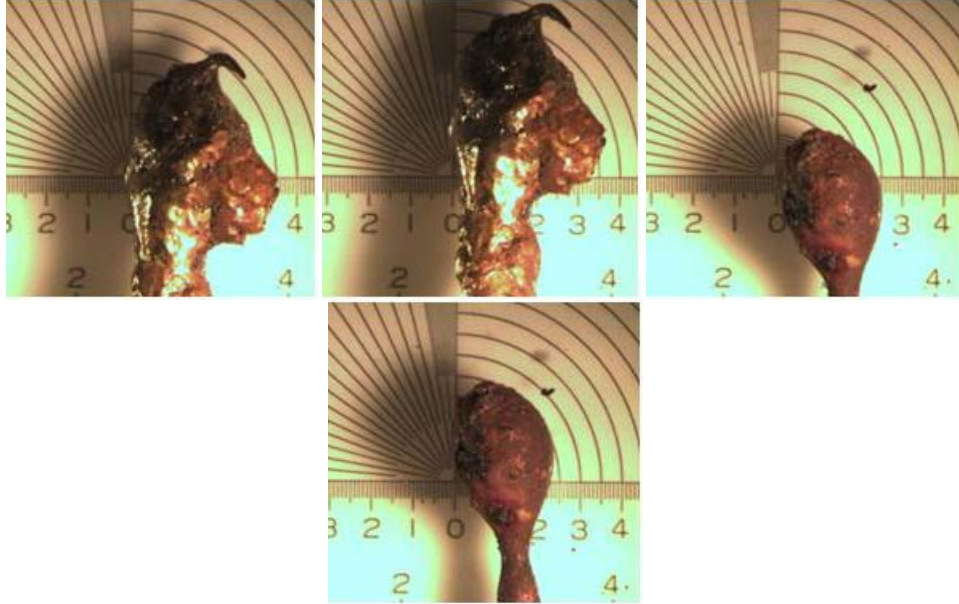


Figure 19: Compartment Tests, MS 18-2, Energized (Test No. 34)

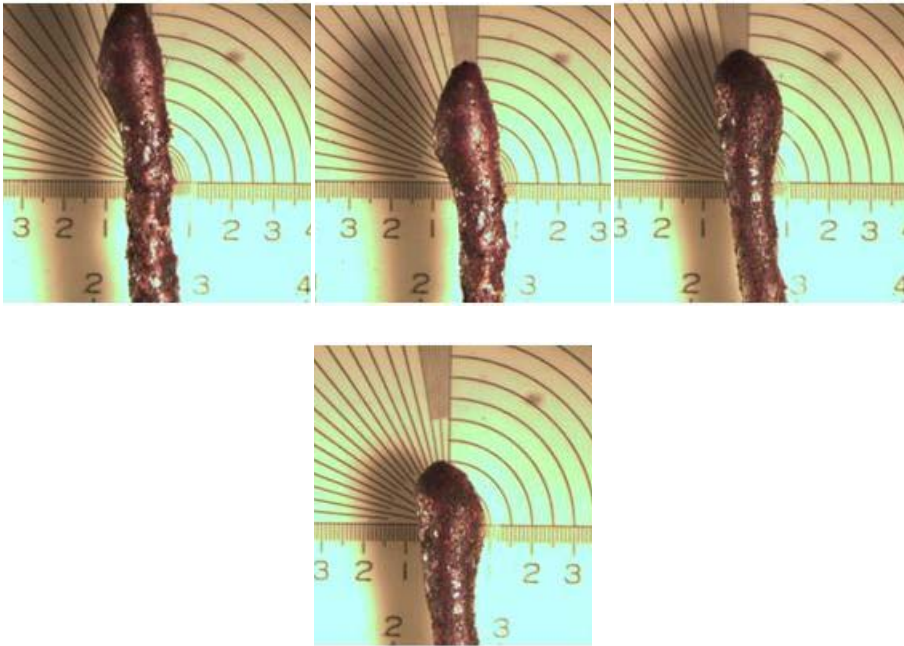


Figure 20: Compartment Tests, MS 18-2, Loaded (Test No. 34)

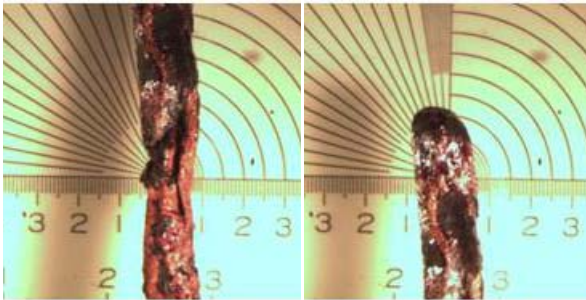


Figure 21: Compartment Tests, MS 18-2, Energized (Test No. 35)

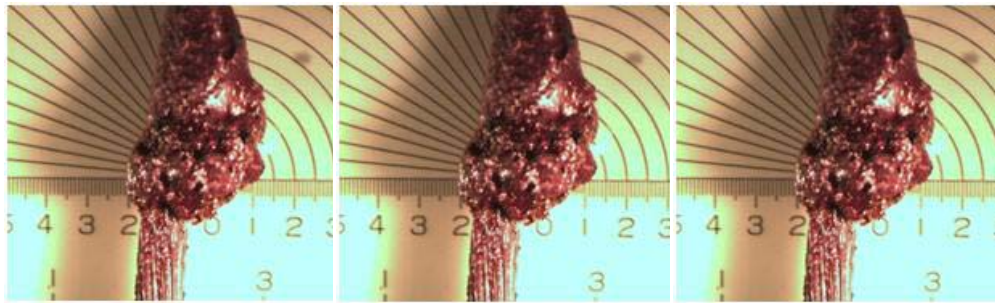


Figure 22: Compartment Tests, MS 18-2, Loaded (Test No. 35)

**SCALED COMPARTMENT TEST; 12-2 ROMEX WIRE**

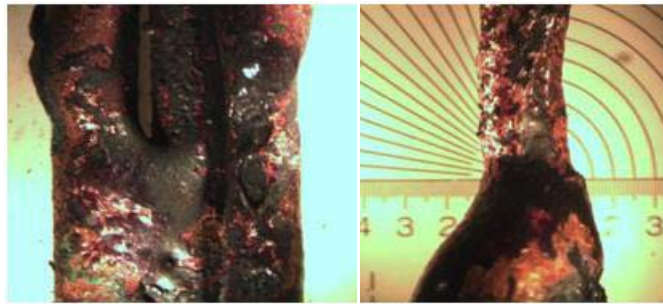
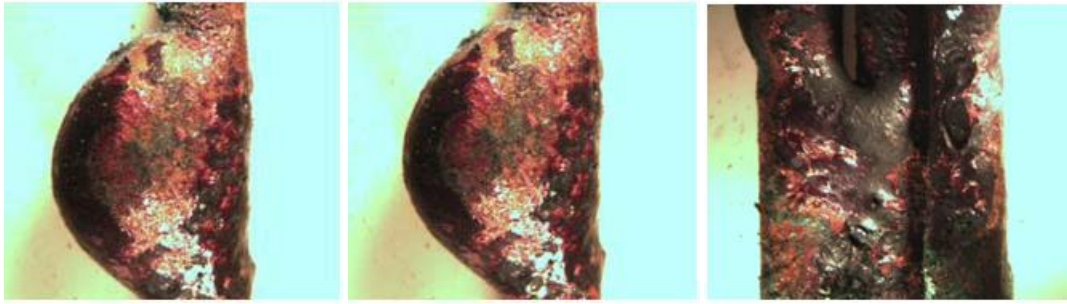


Figure 23: Compartment Tests, ROMEX 12-2, Energized (Test No. 12)

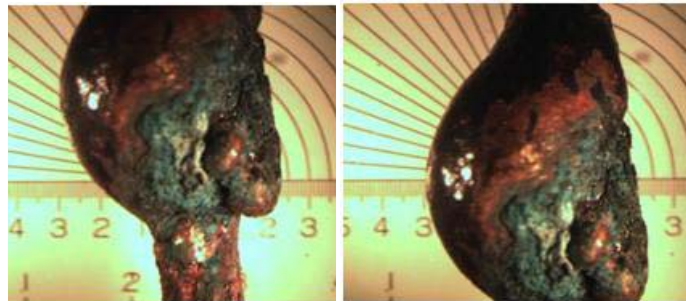


Figure 24: Compartment Tests, ROMEX 12-2, Loaded (Test No. 12)

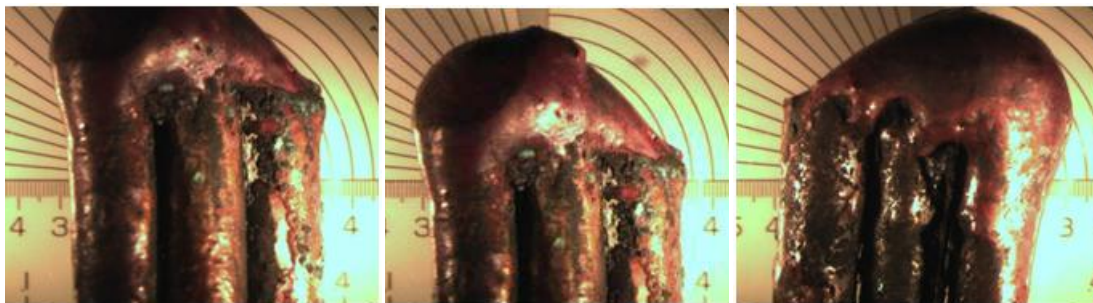


Figure 25: Compartment Tests, ROMEX 12-2, Energized (Test No. 14)

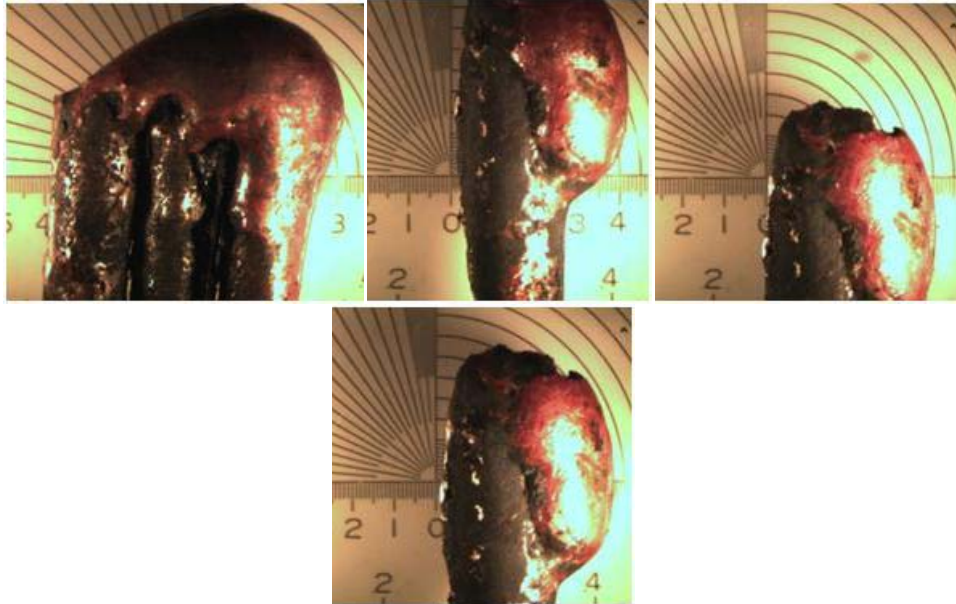


Figure 26: Compartment Tests, ROMEX 12-2, Loaded (Test No. 15)

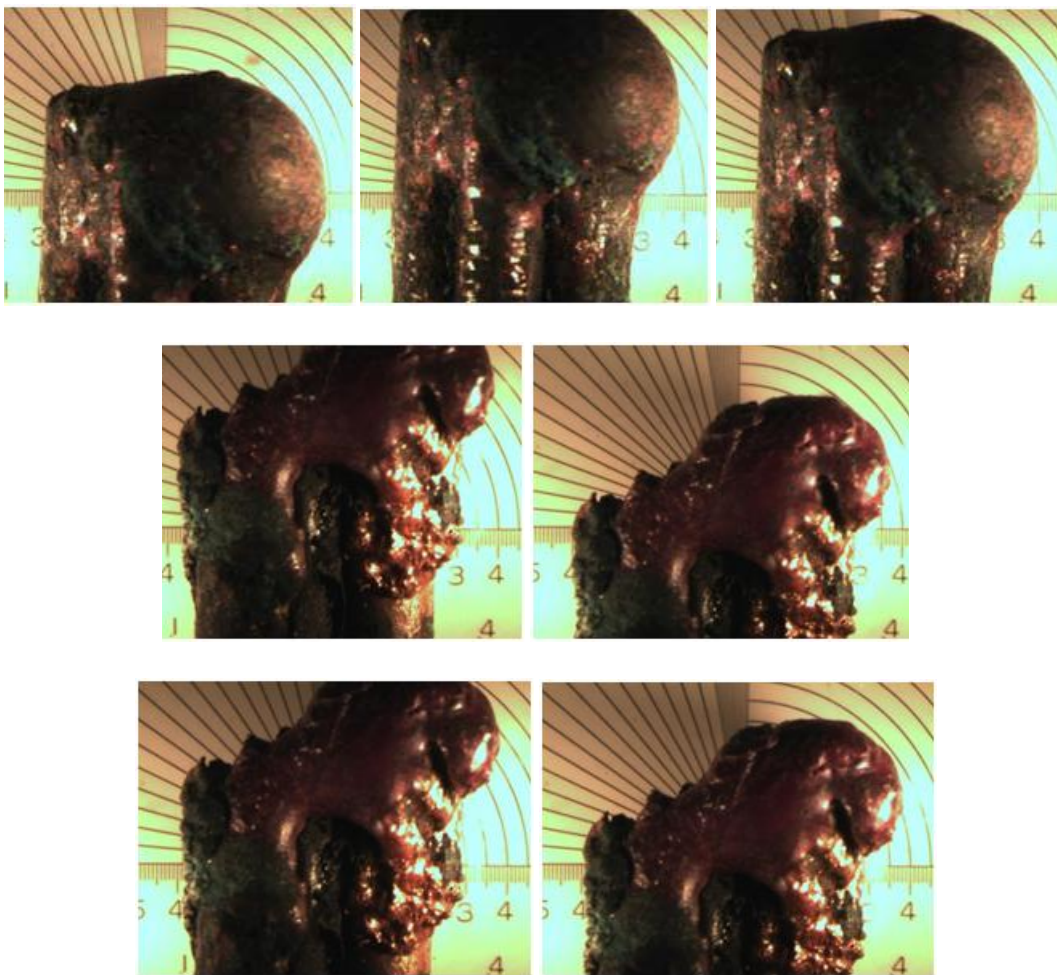


Figure 27: Compartment Tests, ROMEX 12-2, Non Energized (Test No. 14)

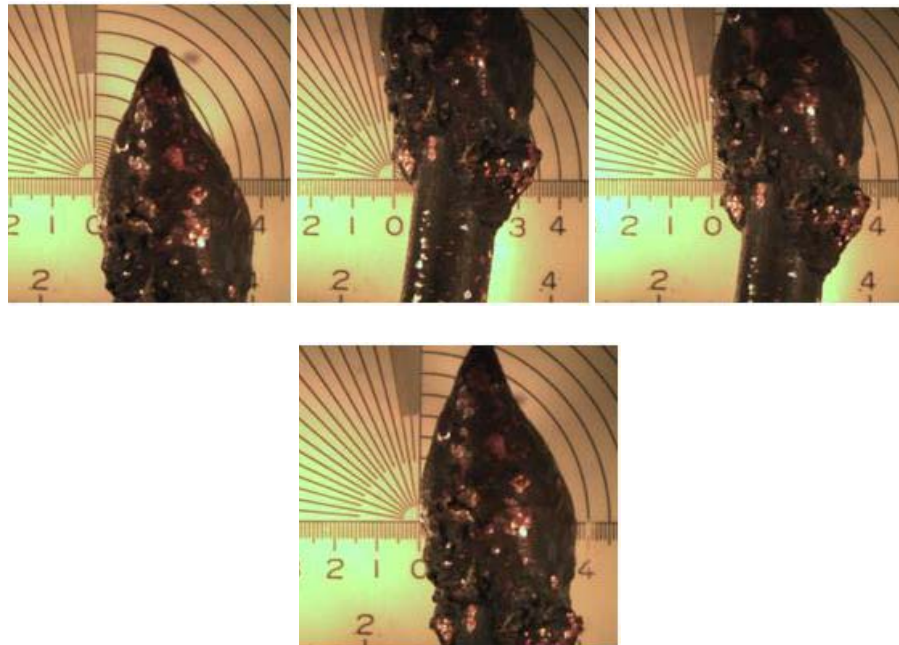


Figure 28: Compartment Tests, ROMEX 12-2, Loaded (Test No. 15)

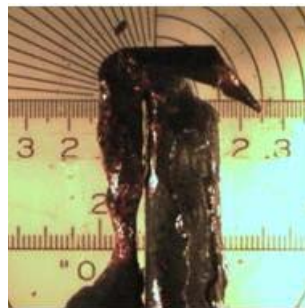
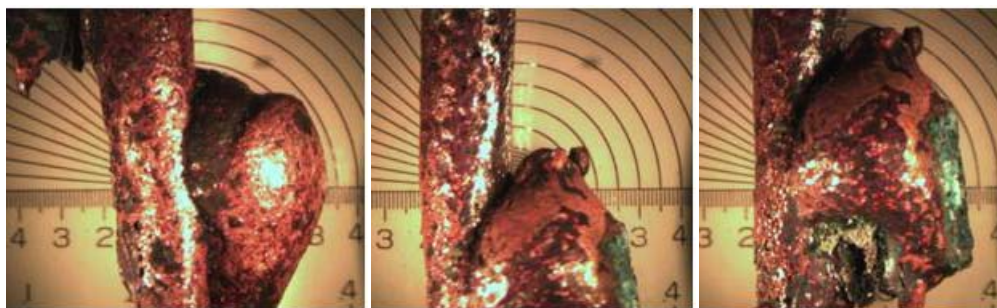


Figure 29: Compartment Tests, ROMEX 12-2, Non Energized (Test No. 15)





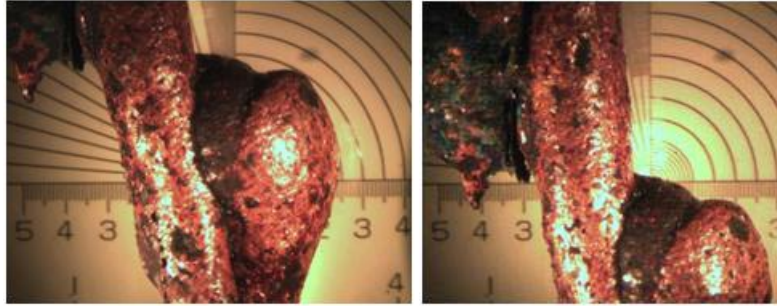


Figure 30: Compartment Tests, ROMEX 12-2, Energized (Test No. 21)

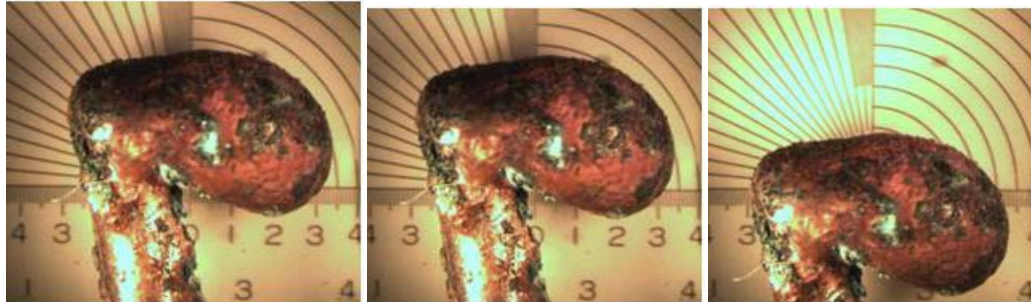
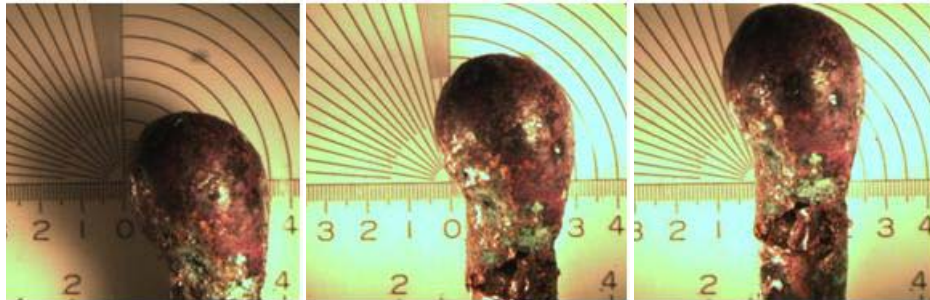


Figure 31: Compartment Tests, ROMEX 12-2, Loaded (Test No. 21)

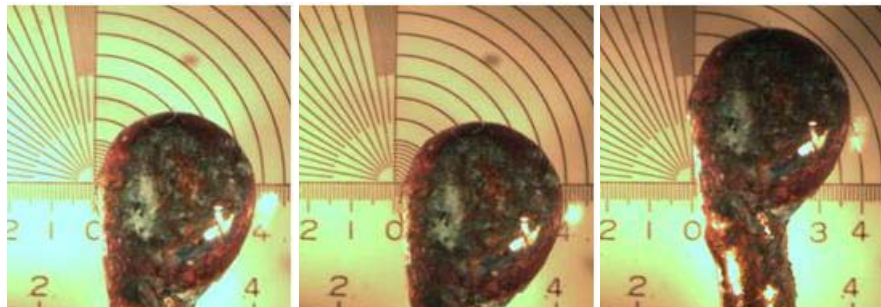


Figure 32: Compartment Tests, ROMEX 12-2, Non Energized (Test No. 25)

**SCALED COMPARTMENT TEST; 14-2 ROMEX WIRE**

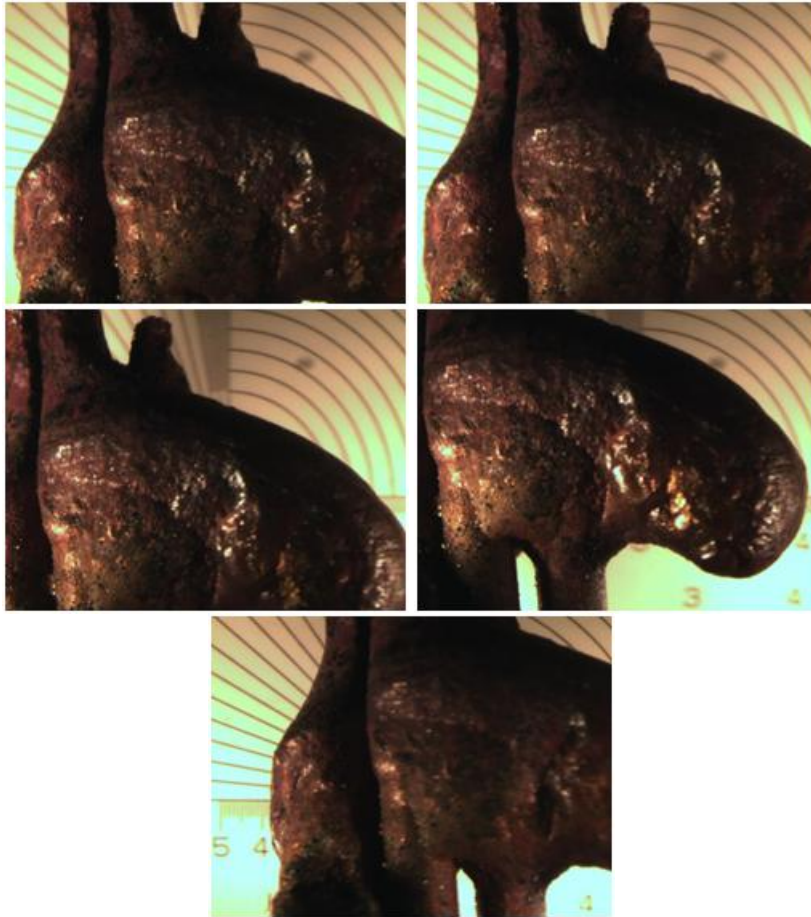
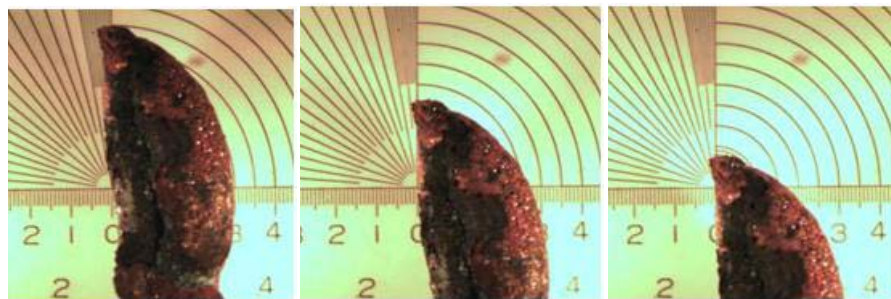


Figure 33: Compartment Tests, ROMEX 14-2, Energized (Test No. 16)



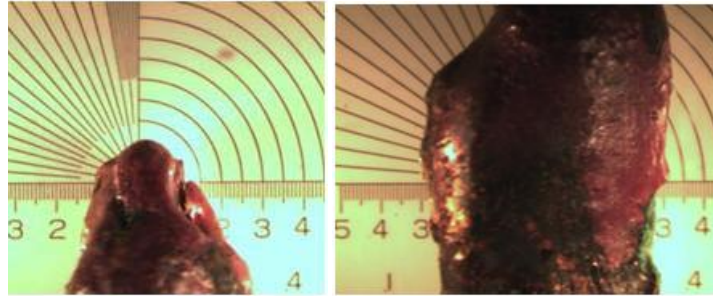
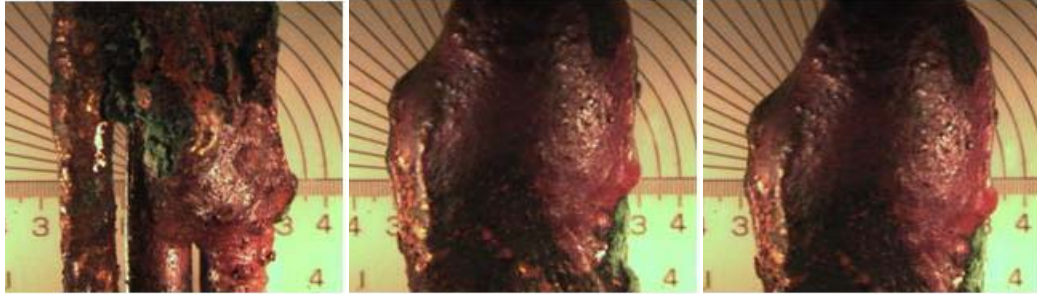


Figure 34: Compartment Tests, ROMEX 14-2, Energized (Test No. 16)

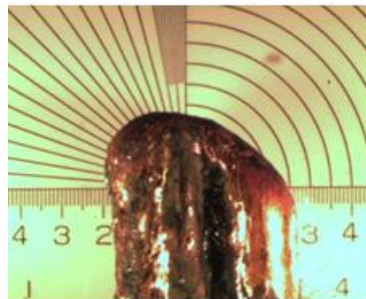
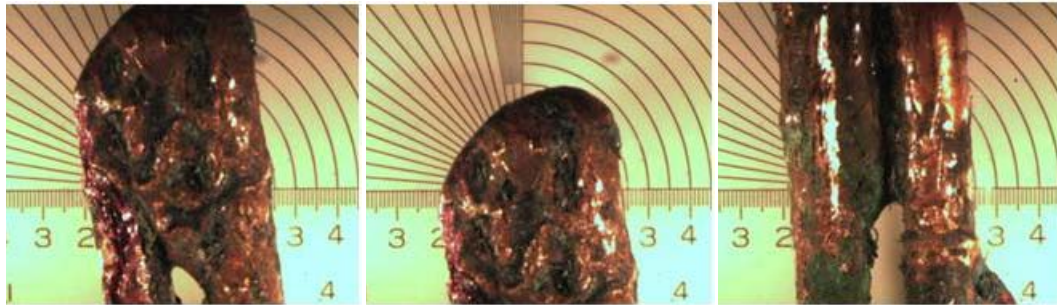


Figure 35: Compartment Tests, ROMEX 14-2, Non Energized (Test No. 16)

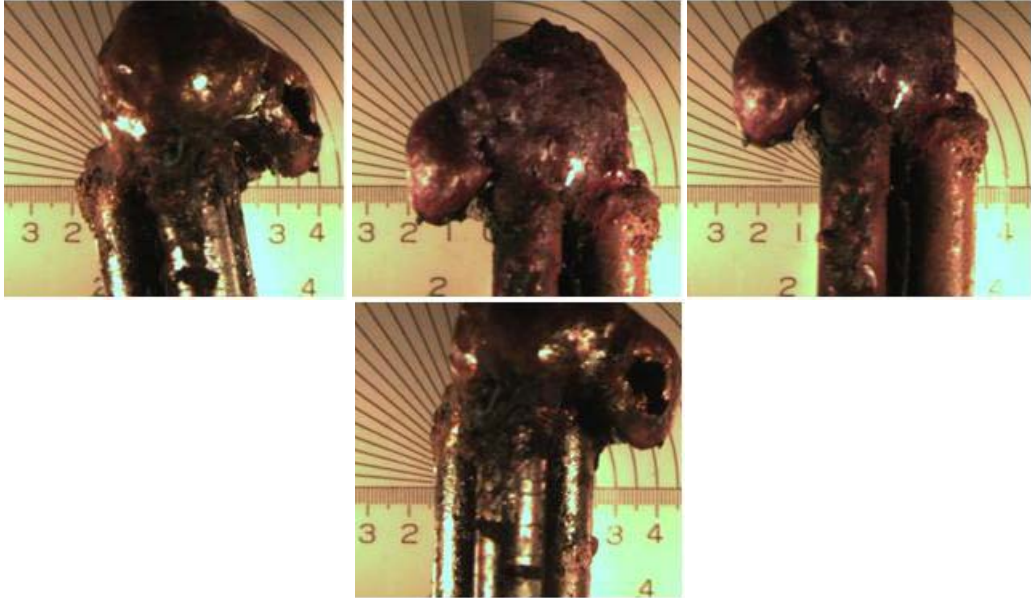


Figure 36: Compartment Tests, ROMEX 14-2, Energized (Test No. 17)

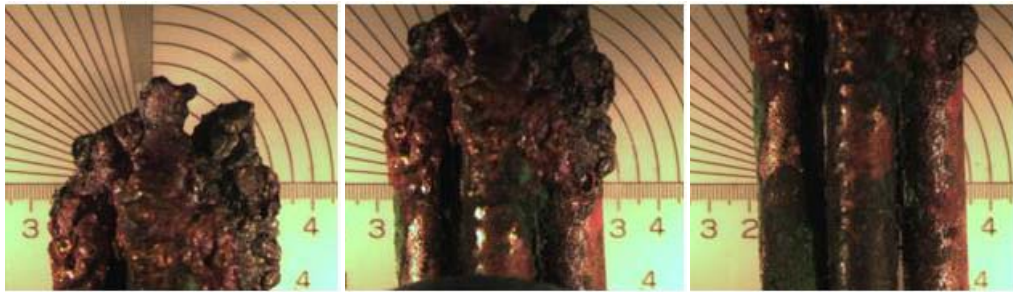
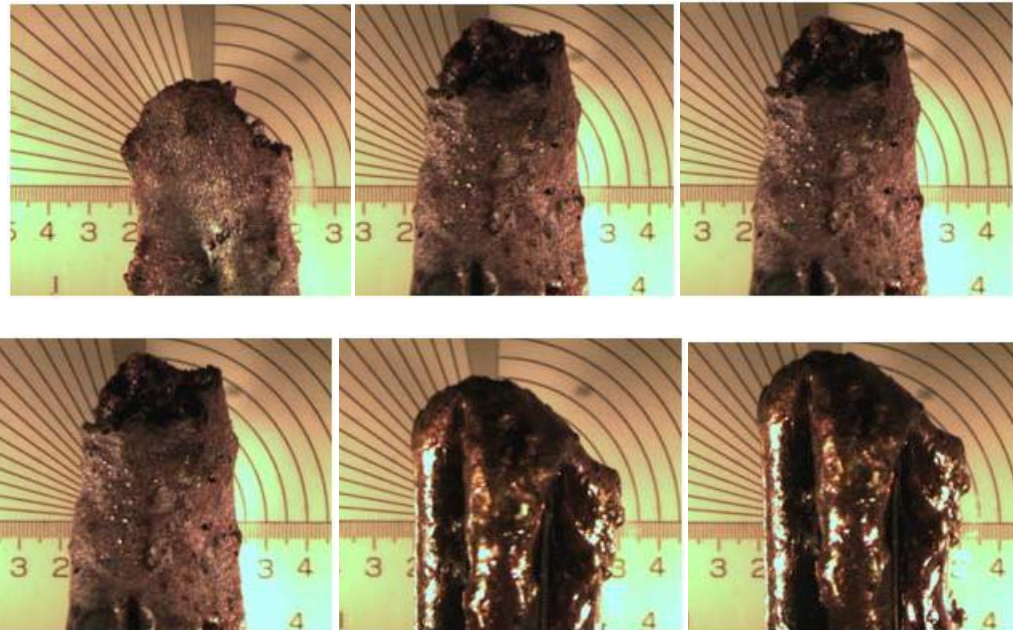


Figure 37: Compartment Tests, ROMEX 14-2, Energized (Test No. 18)



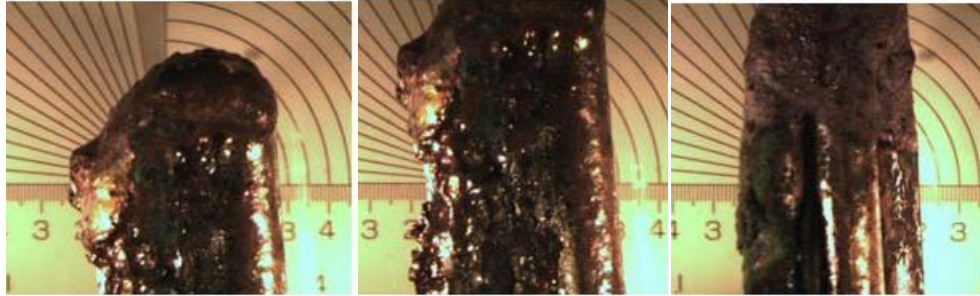


Figure 38: Compartment Tests, ROMEX 14-2, Loaded (Test No. 18)

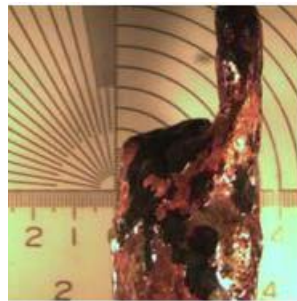
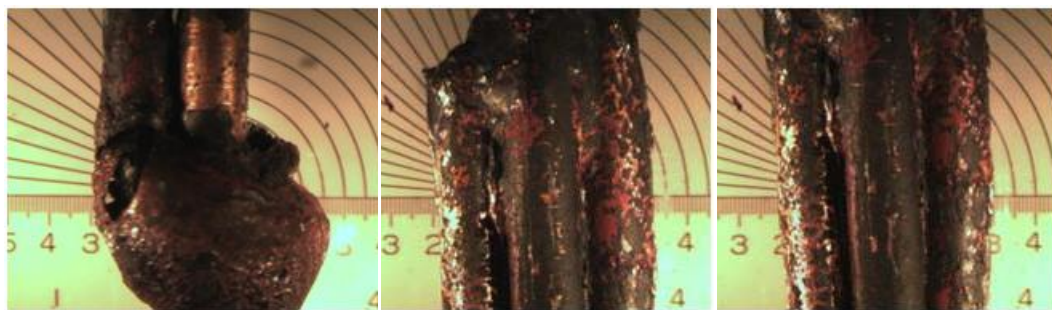


Figure 39: Compartment Tests, ROMEX 14-2, Energized (Test No. 19)



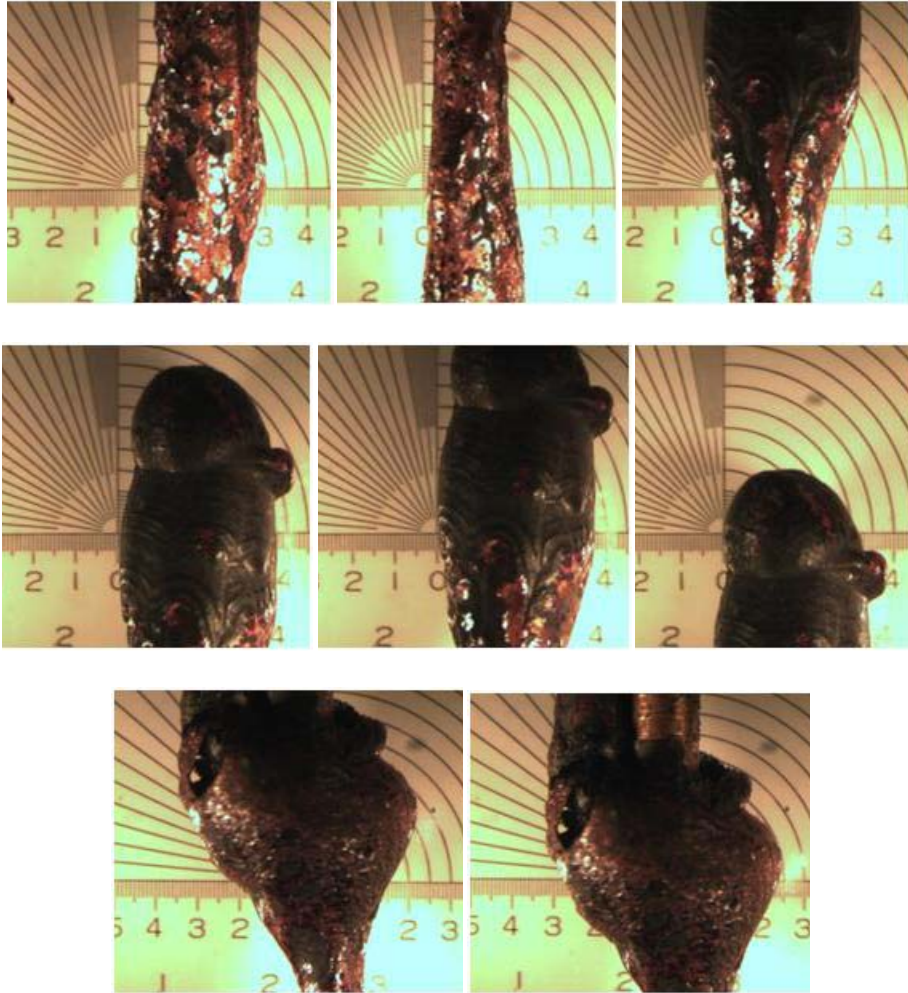


Figure 40: Compartment Tests, ROMEX 14-2, Loaded (Test No. 19)

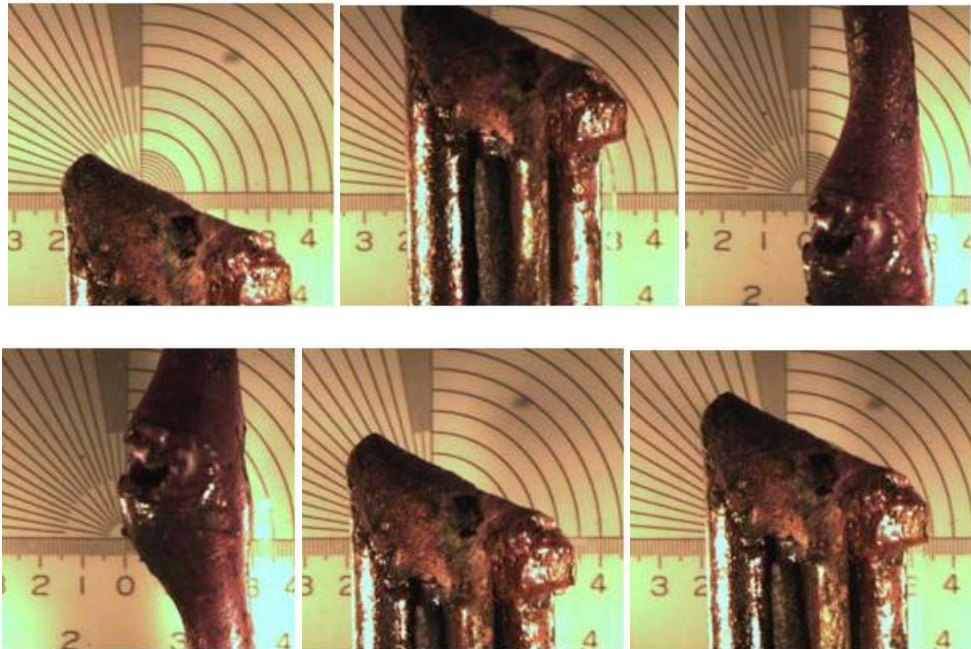


Figure 41: Compartment Tests, ROMEX 14-2, Non Energized (Test No. 19)

**DIRECT FLAME TEST; 12-2 ROMEX WIRE**

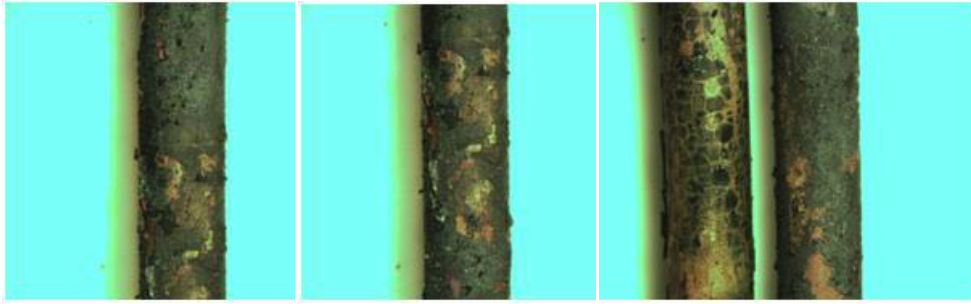


Figure 42: Direct Flame, ROMEX 12-2, Non Energized (Test No. 1)

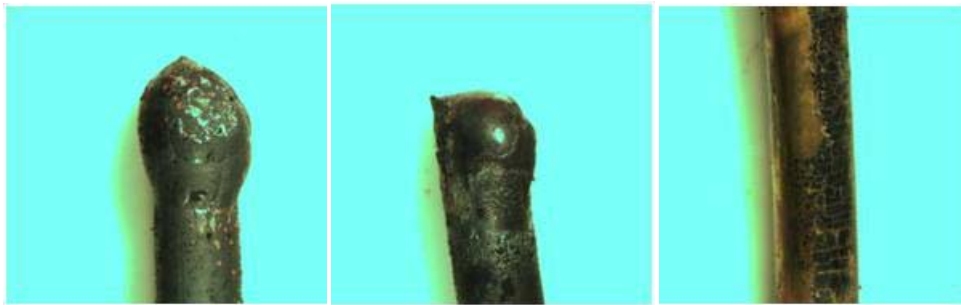


Figure 43: Direct Flame, ROMEX 12-2, Non Energized (Test No. 2)

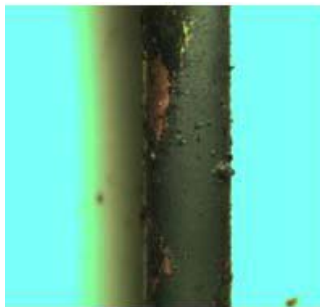


Figure 44: Direct Flame, ROMEX 12-2, Non Energized (Test No. 3)

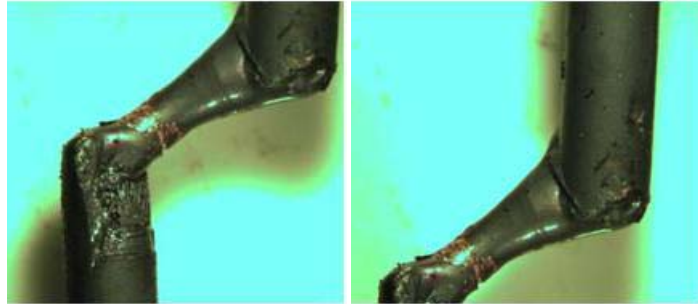
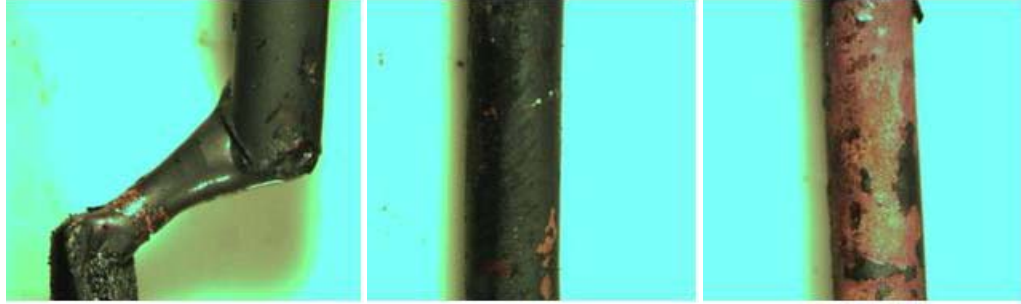
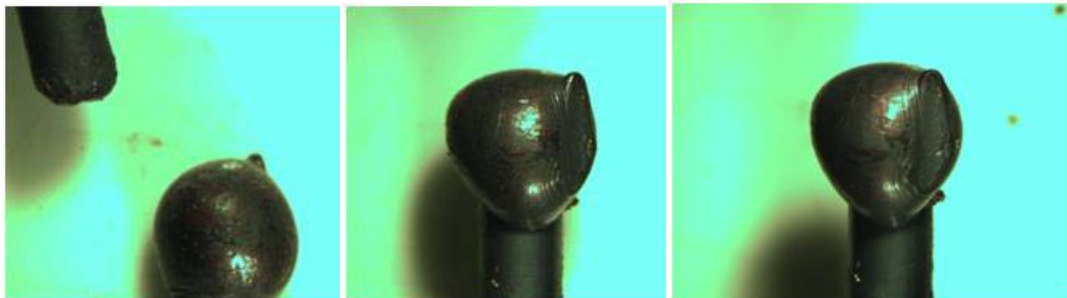
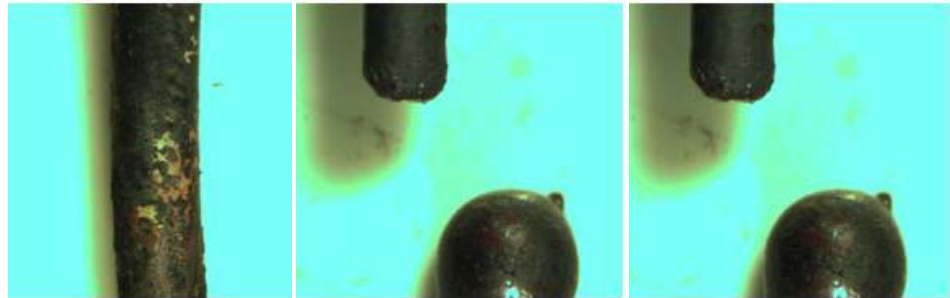
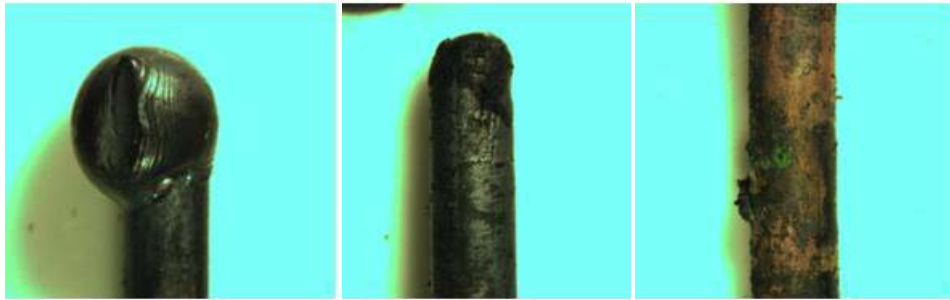


Figure 45: Direct Flame, ROMEX 12-2, Non Energized (Test No. 4)





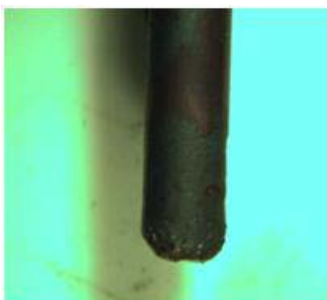


Figure 46: Direct Flame, ROMEX 12-2, Non Energized (Test No. 5)

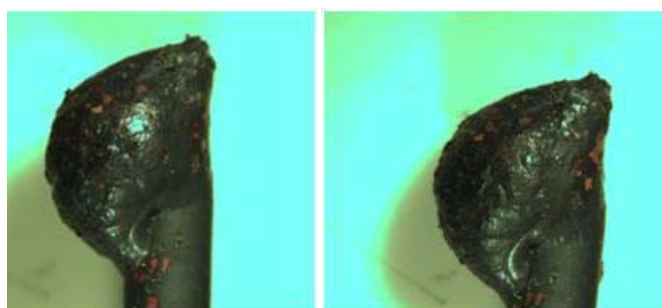
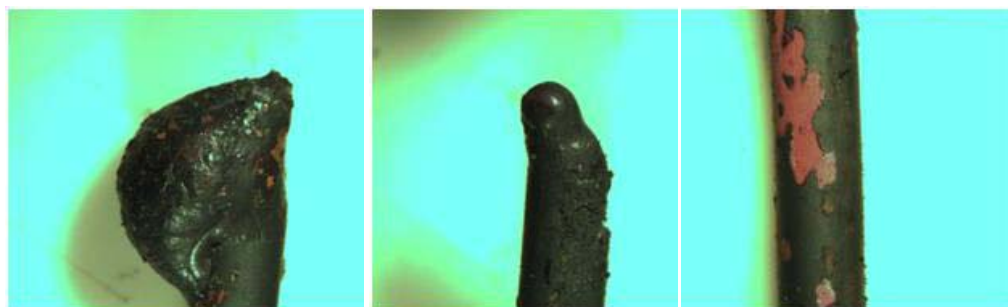


Figure 47: Direct Flame, ROMEX 12-2, Non Energized (Test No. 6)

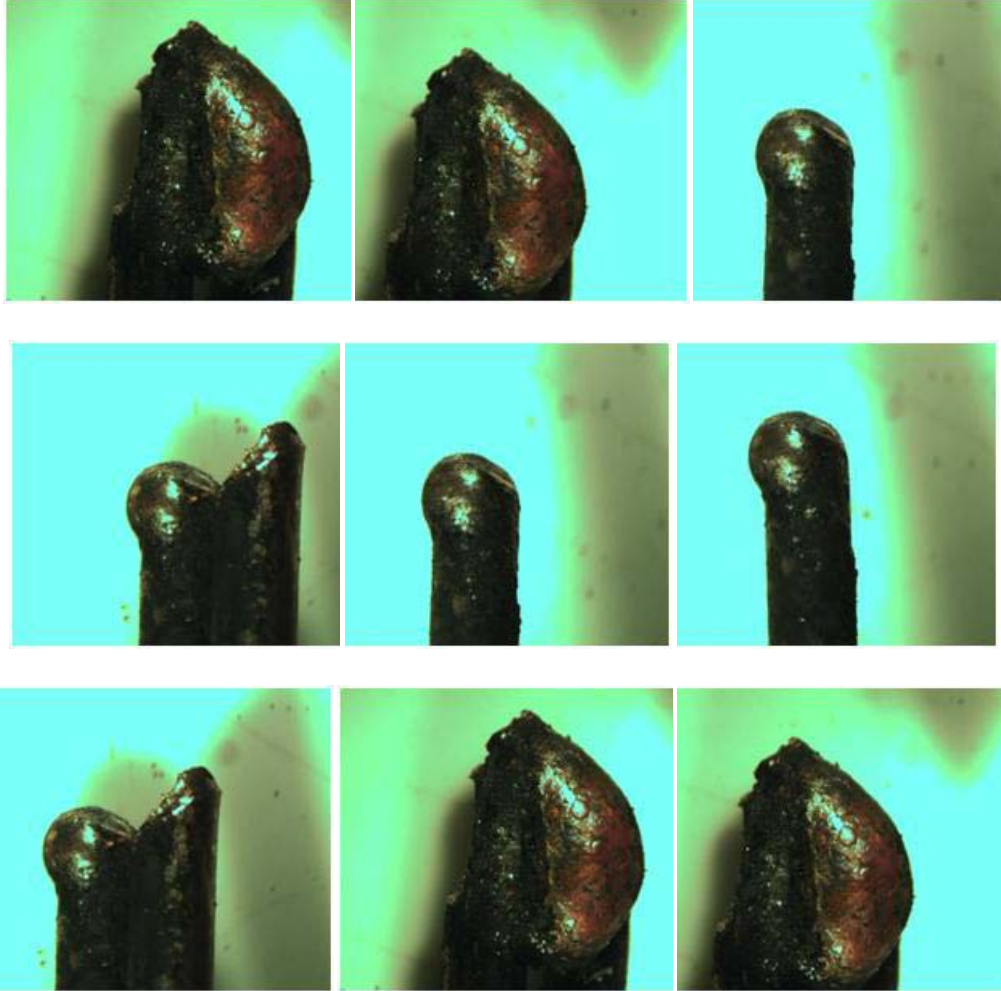


Figure 48: Direct Flame, ROMEX 12-2, Energized (Test No. 7)

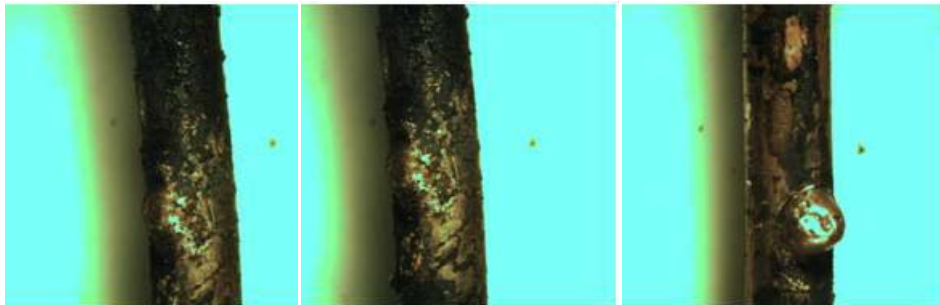


Figure 49: Direct Flame, ROMEX 12-2, Energized (Test No. 8)

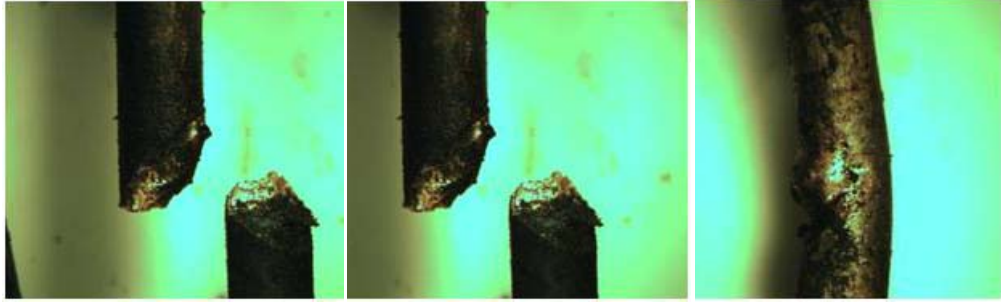


Figure 50: Direct Flame, ROMEX 12-2, Energized (Test No. 9)

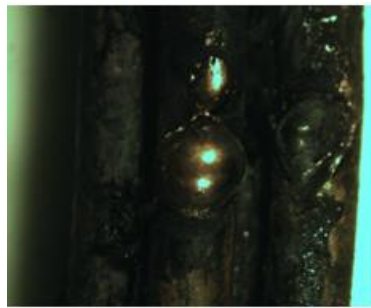
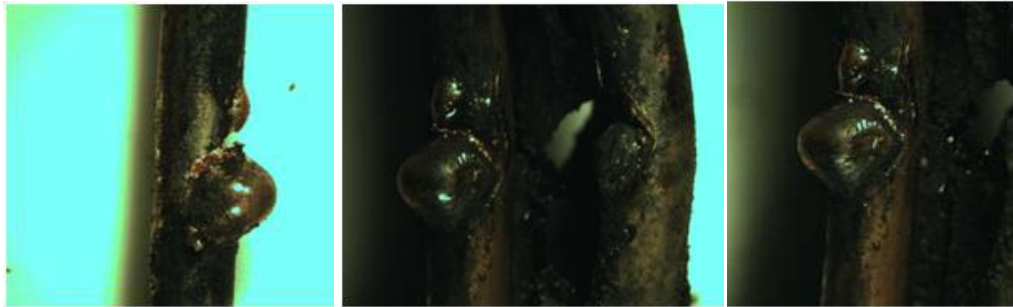
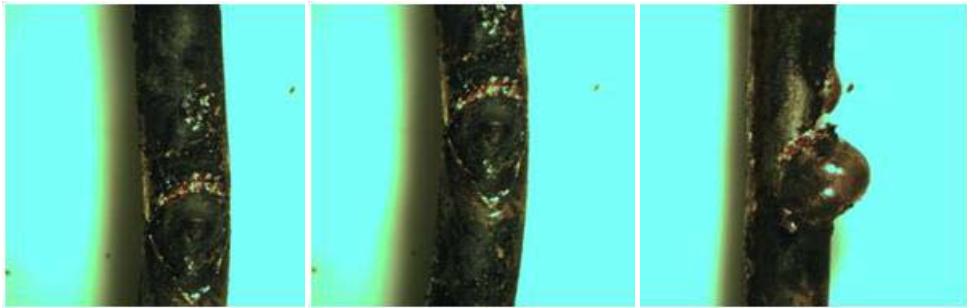


Figure 51: Direct Flame, ROMEX 12-2, Energized (Test No. 10)

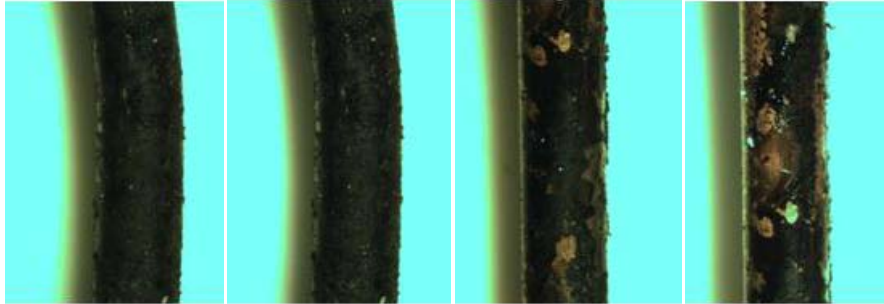


Figure 52: Direct Flame, ROMEX 12-2, Energized (Test No. 11)

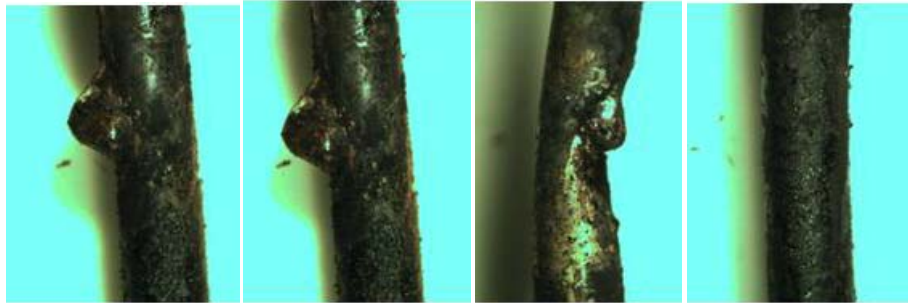


Figure 53: Direct Flame, ROMEX 12-2, Energized (Test No. 12)

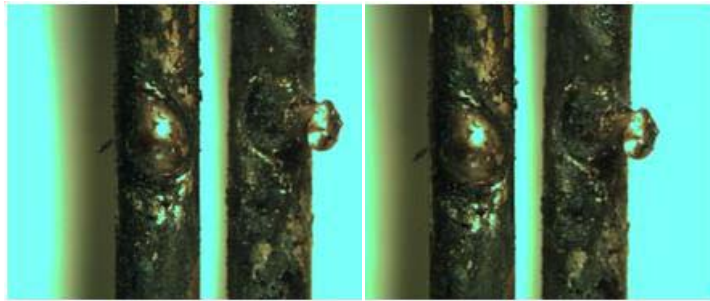


Figure 54: Direct Flame, ROMEX 12-2, Loaded (Test No. 13)





Figure 55: Direct Flame, ROMEX 12-2, Loaded (Test No. 14)

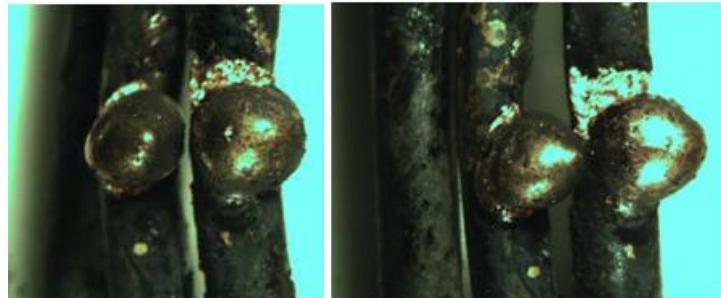
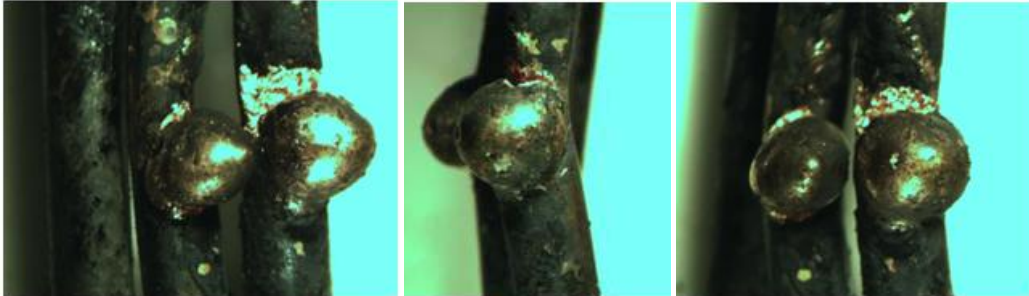


Figure 56: Direct Flame, ROMEX 12-2, Loaded (Test No. 15)

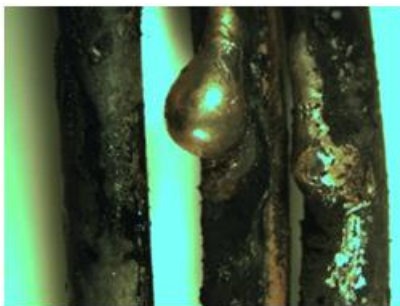


Figure 57: Direct Flame, ROMEX 12-2, Loaded (Test No. 16)

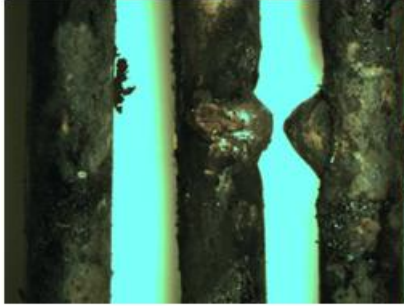


Figure 58: Direct Flame, ROMEX 12-2, Loaded (Test No. 17)

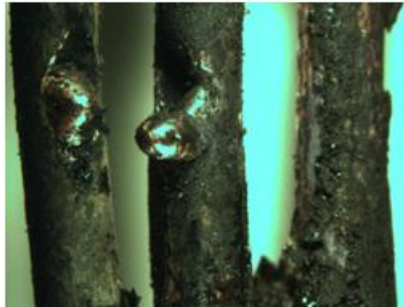


Figure 59: Direct Flame, ROMEX 12-2, Loaded (Test No. 18)

**DIRECT FLAME TEST; 14-2 ROMEX WIRE**

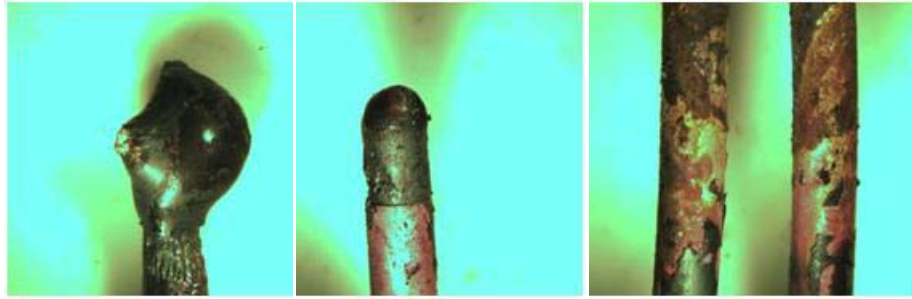


Figure 60: Direct Flame, ROMEX 14-2, Non Energized (Test No. 56)



Figure 61: Direct Flame, ROMEX 14-2, Non Energized (Test No. 57)

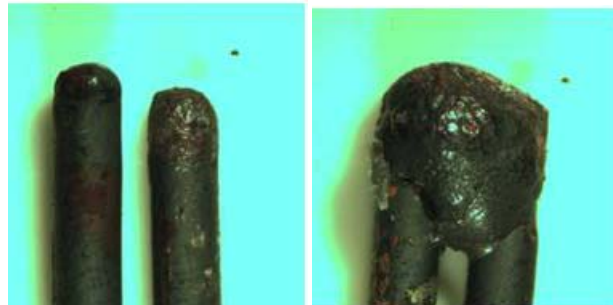


Figure 62: Direct Flame, ROMEX 14-2, Non Energized (Test No. 58)

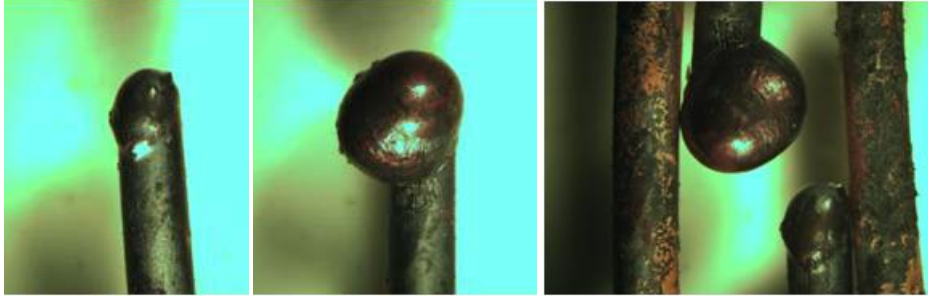


Figure 63: Direct Flame, ROMEX 14-2, Non Energized (Test No. 59)

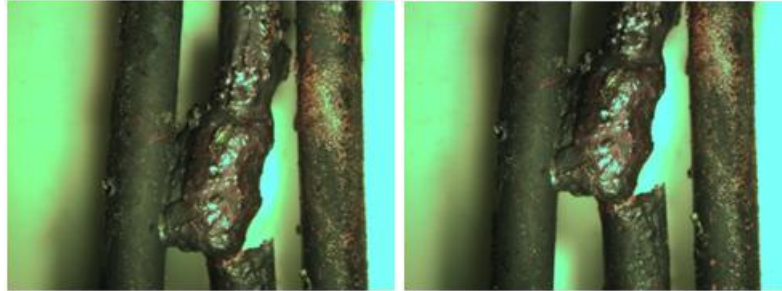
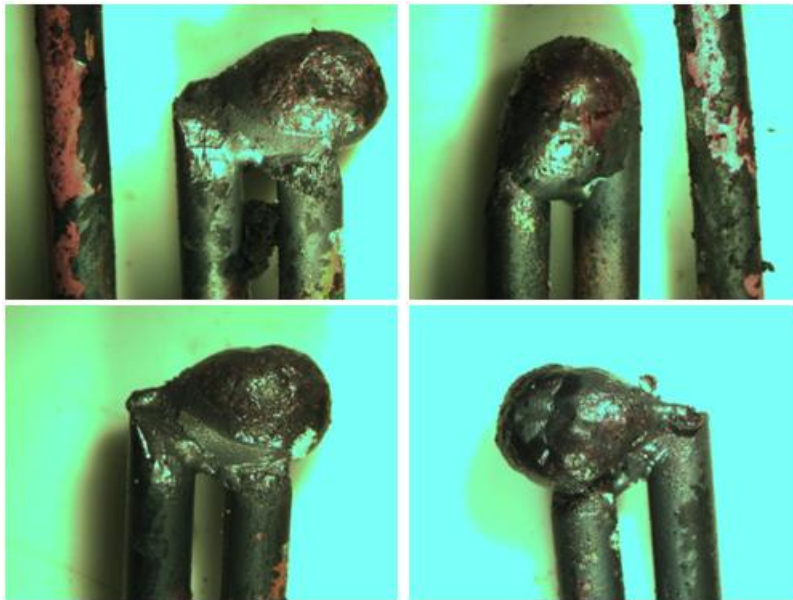


Figure 64: Direct Flame, ROMEX 14-2, Non Energized (Test No. 60)





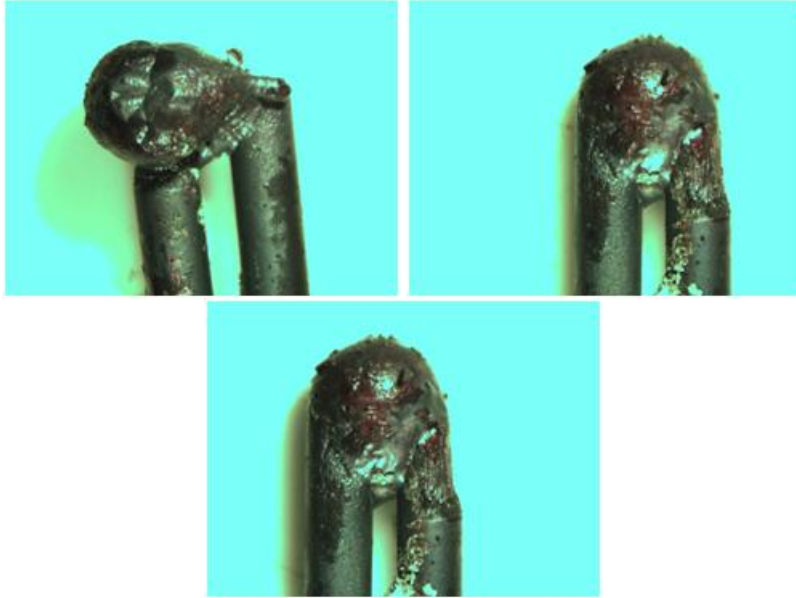


Figure 65: Direct Flame, ROMEX 14-2, Energized (Test No. 61)

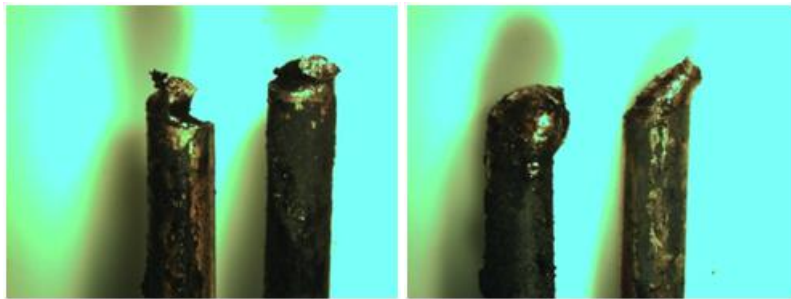


Figure 66: Direct Flame, ROMEX 14-2, Energized (Test No. 64)



Figure 67: Direct Flame, ROMEX 14-2, Energized (Test No. 65)

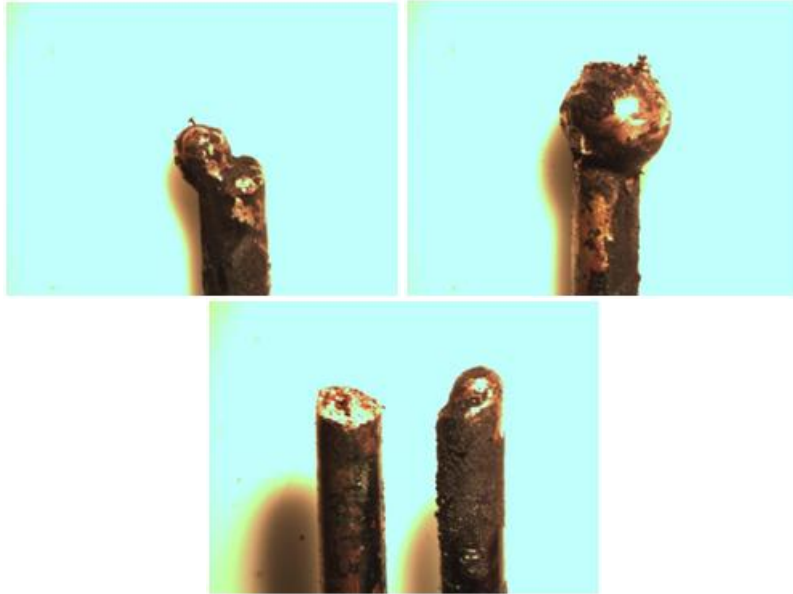


Figure 68: Direct Flame, ROMEX 14-2, Energized (Test No. 66)

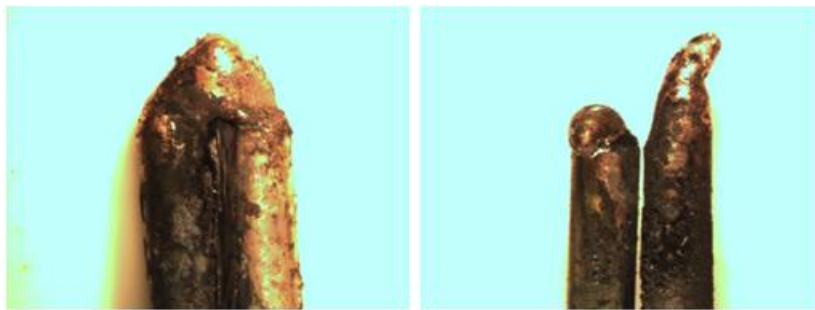
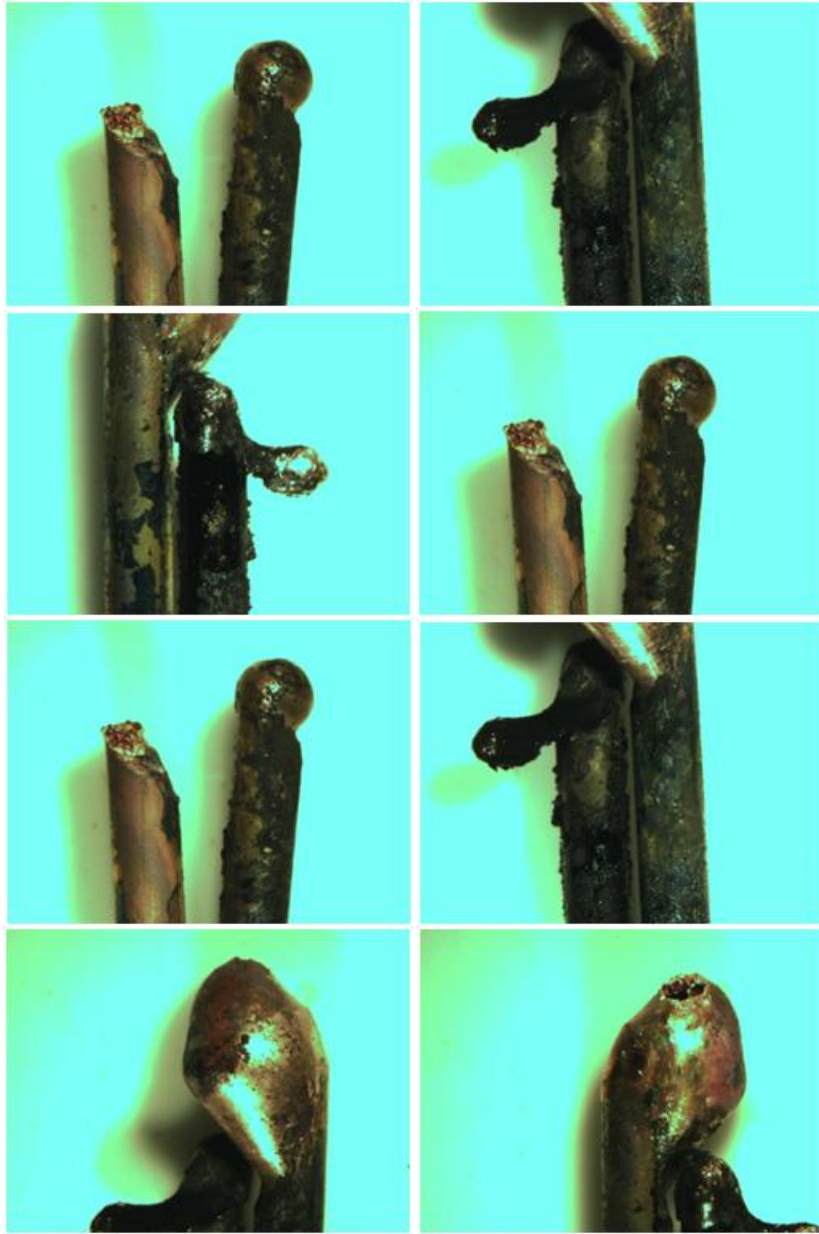


Figure 69: Direct Flame, ROMEX 14-2, Loaded (Test No. 67)



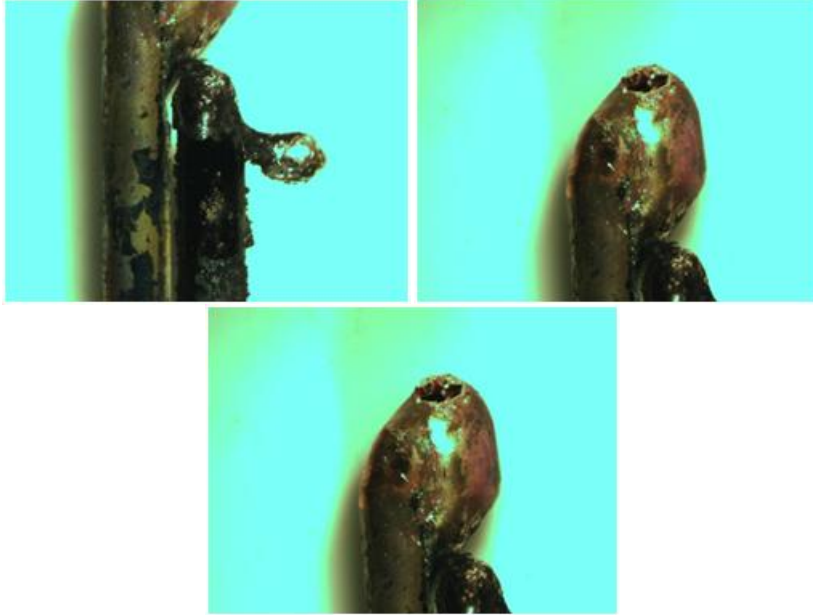


Figure 70: Direct Flame, ROMEX 14-2, Loaded (Test No. 68)

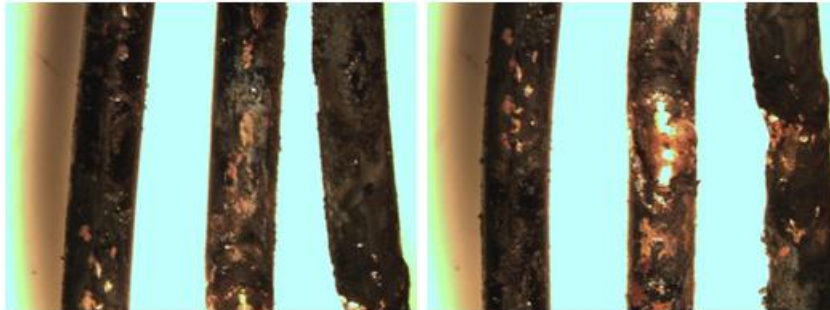


Figure 71: Direct Flame, ROMEX 14-2, Loaded (Test No. 69)

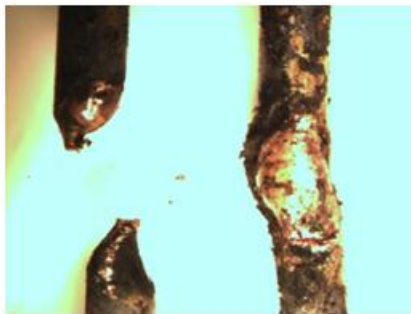


Figure 72: Direct Flame, ROMEX 14-2, Loaded (Test No. 70)

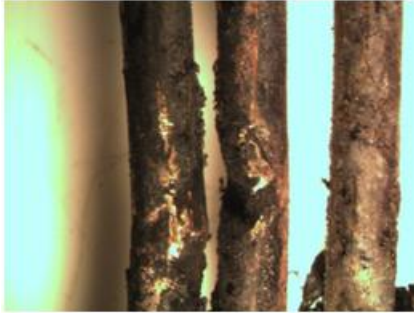


Figure 73: Direct Flame, ROMEX 14-2, Loaded (Test No. 71)



Figure 74: Direct Flame, ROMEX 14-2, Loaded (Test No. 72)

**DIRECT FLAME TEST; 16-2 MULTISTRAND WIRE**



Figure 75: Direct Flame, Multi-strand 16-2, Non Energized (Test No. 19)

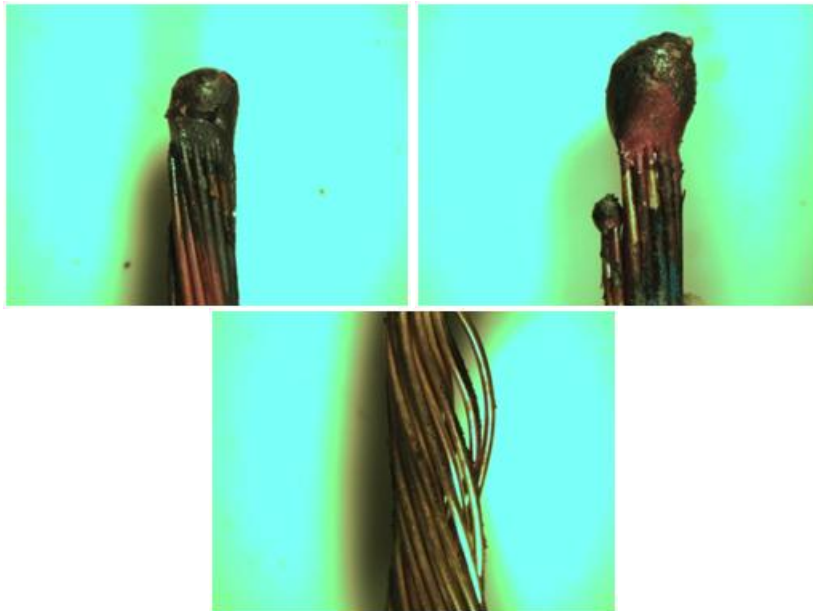


Figure 76: Direct Flame, Multi-strand 16-2, Non Energized (Test No. 20)

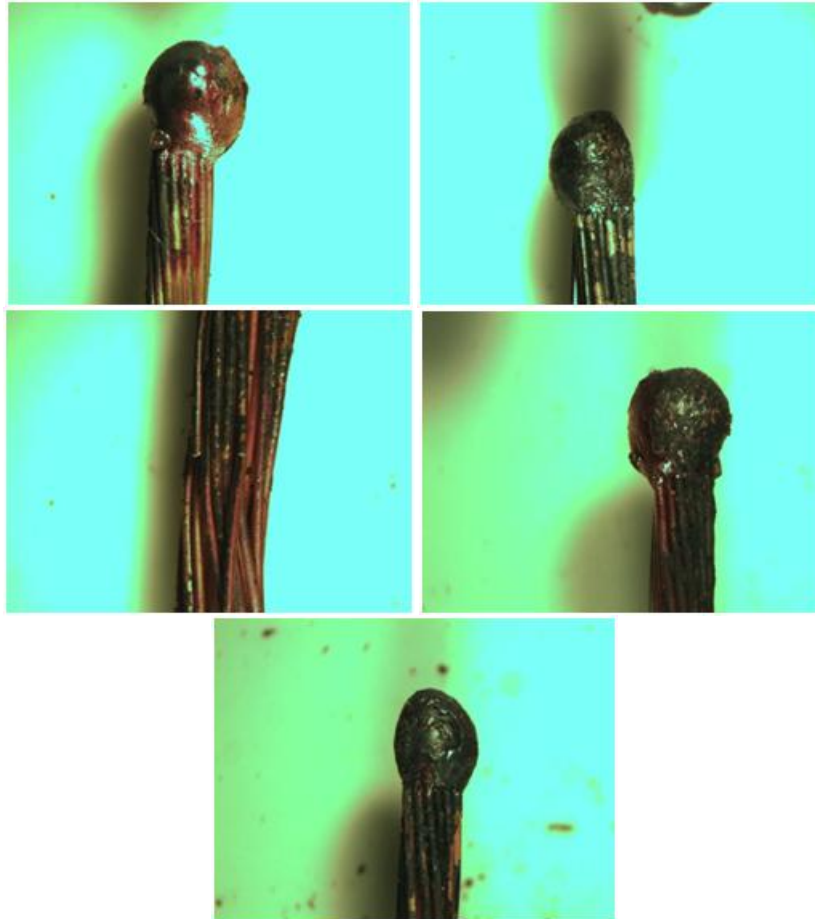


Figure 77: Direct Flame, Multi-strand 16-2, Non Energized (Test No. 21)

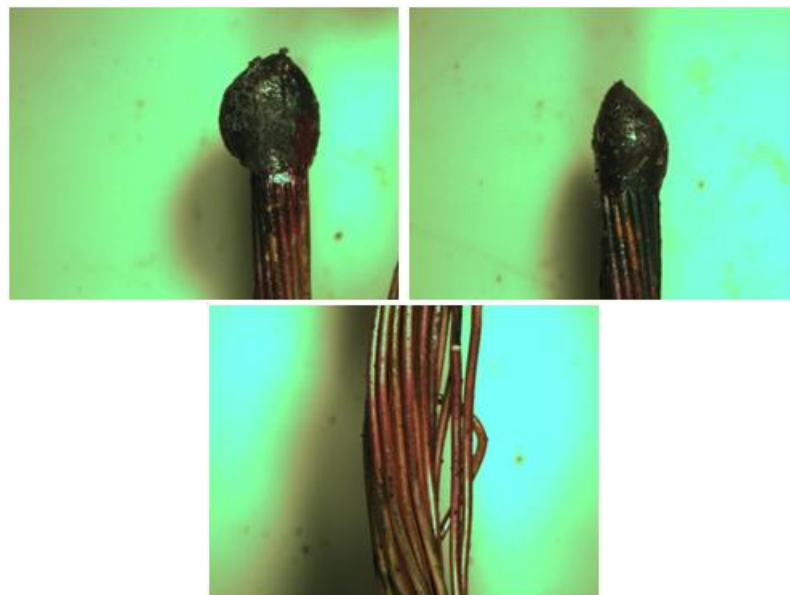


Figure 78: Direct Flame, Multi-strand 16-2, Non Energized (Test No. 22)



Figure 79: Direct Flame, Multi-strand 16-2, Non Energized (Test No. 23)

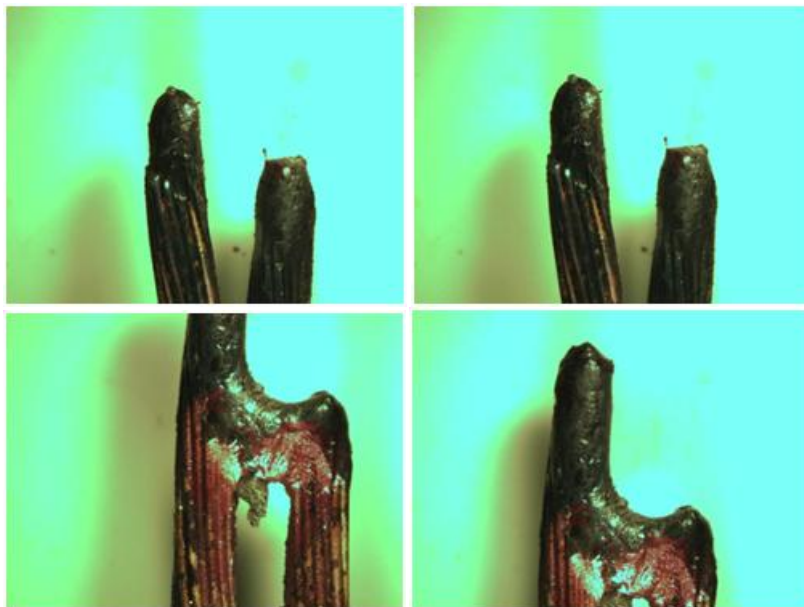
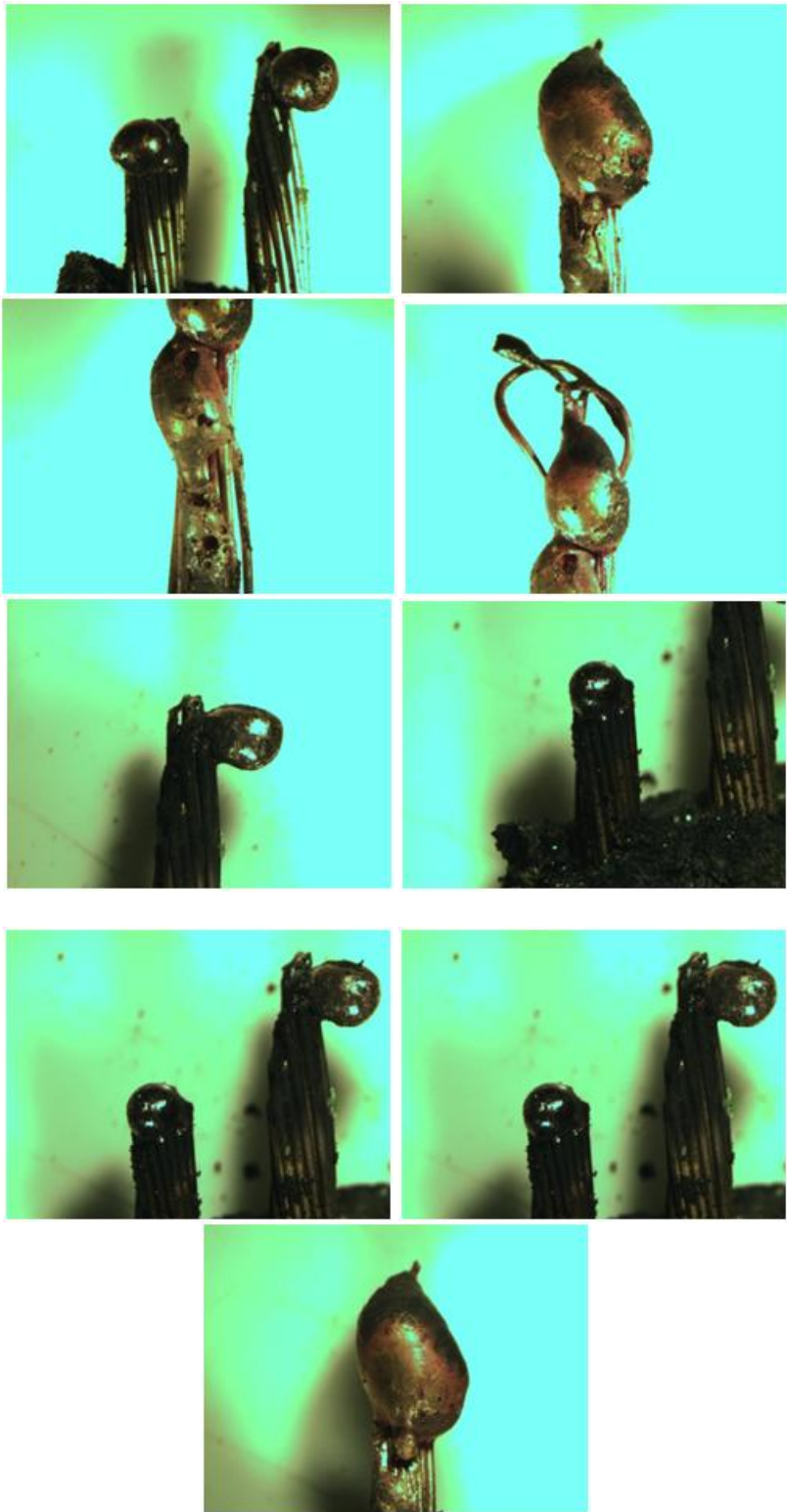


Figure 80: Direct Flame, Multi-strand 16-2, Non Energized (Test No. 24)



Figure 81: Direct Flame, Multi-strand 16-2, Energized (Test No. 25)





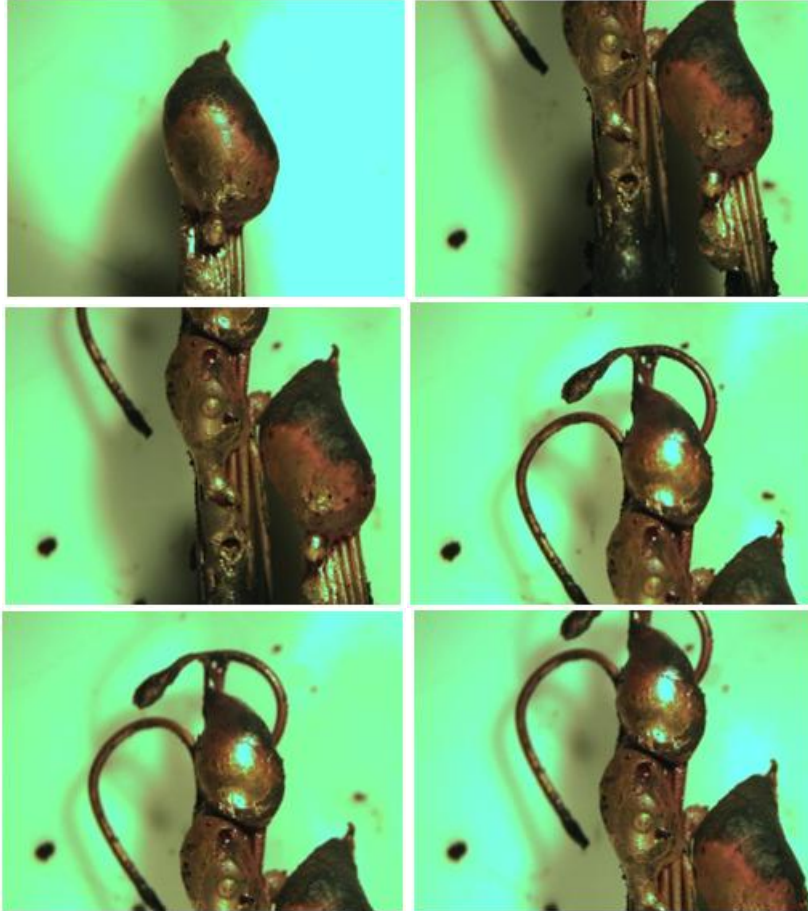


Figure 82: Direct Flame, Multi-strand 16-2, Energized (Test No. 26)

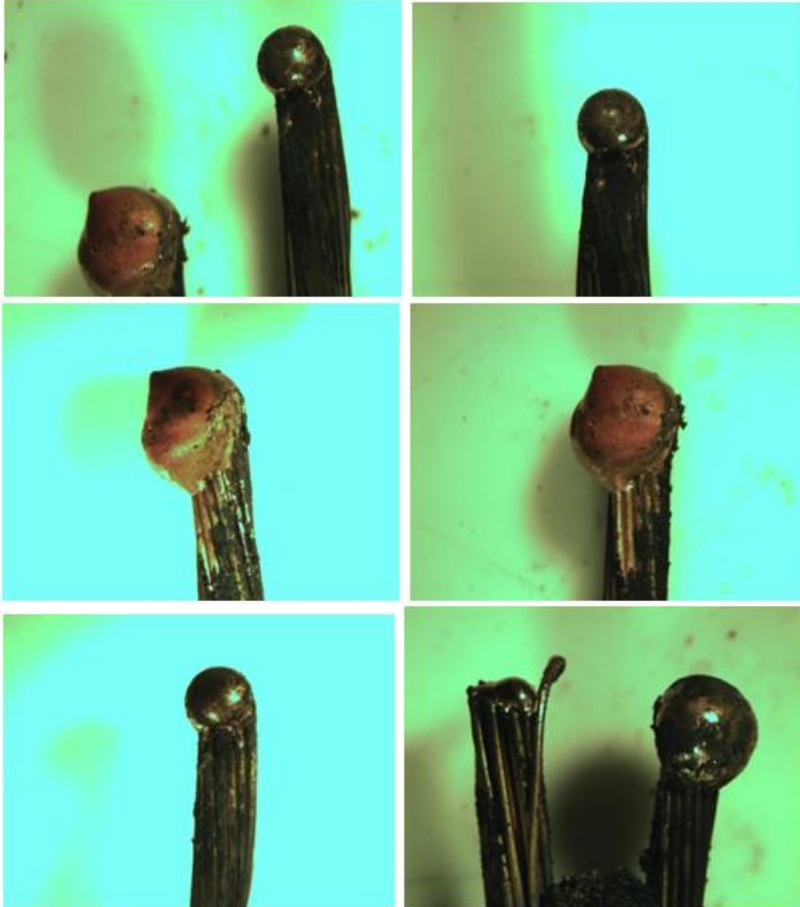


Figure 83: Direct Flame, Multi-strand 16-2, Energized (Test No. 27)

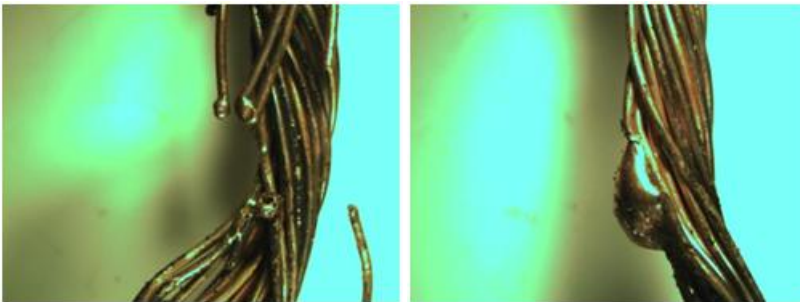


Figure 84: Direct Flame, Multi-strand 16-2, Energized (Test No. 29)

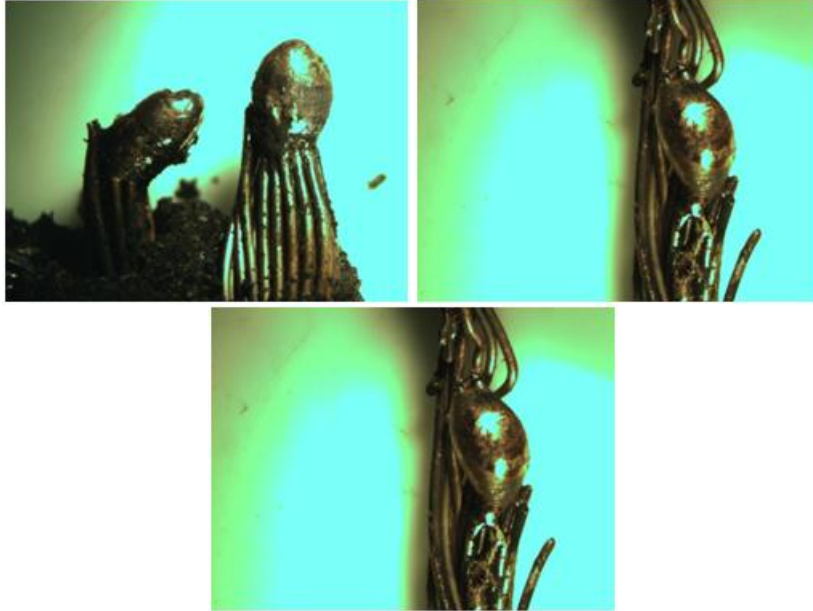


Figure 85: Direct Flame, Multi-strand 16-2, Energized (Test No. 30)

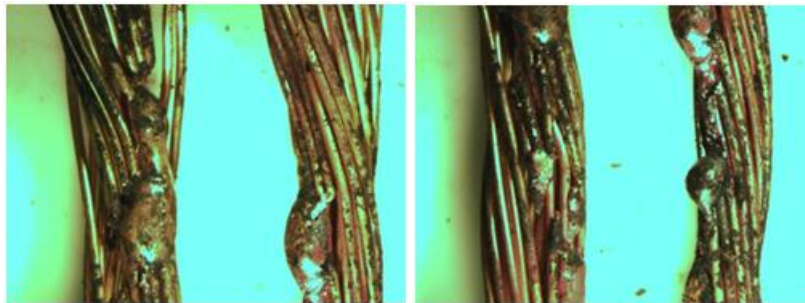


Figure 86: Direct Flame, Multi-strand 16-2, Loaded (Test No. 31)

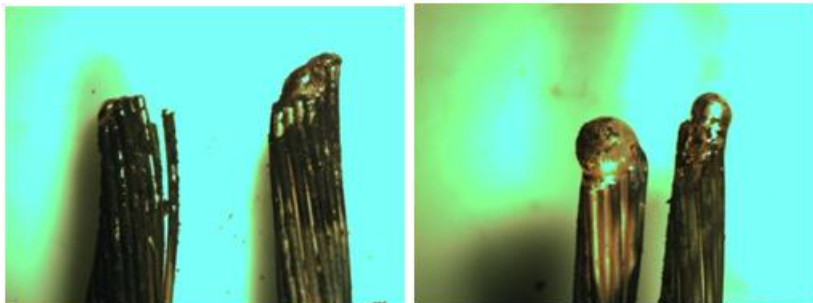


Figure 87: Direct Flame, Multi-strand 16-2, Loaded (Test No. 32)

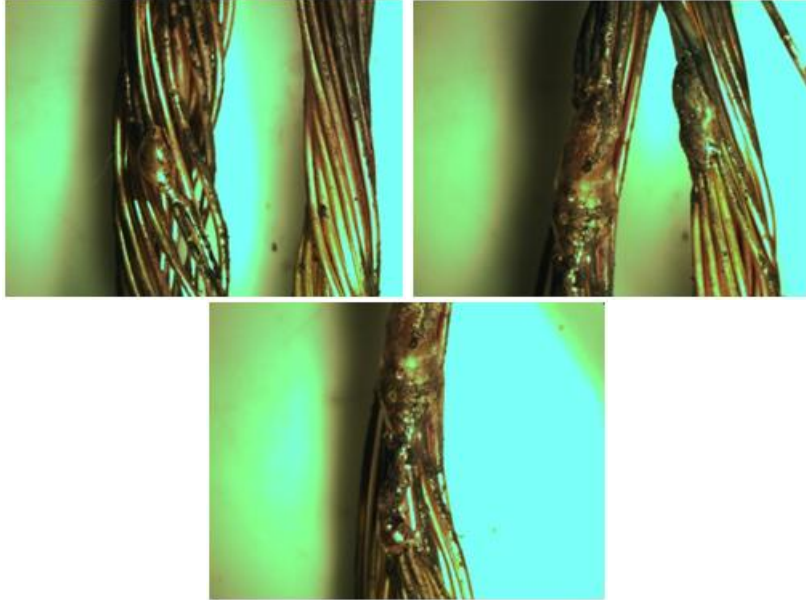
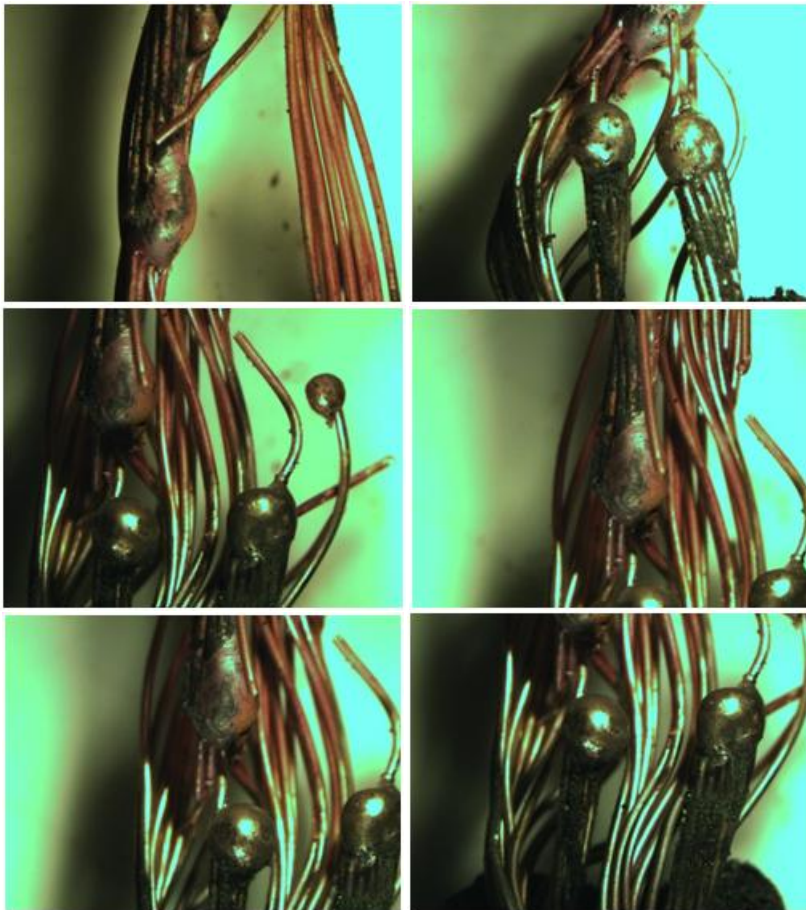


Figure 88: Direct Flame, Multi-strand 16-2, Loaded (Test No. 33)



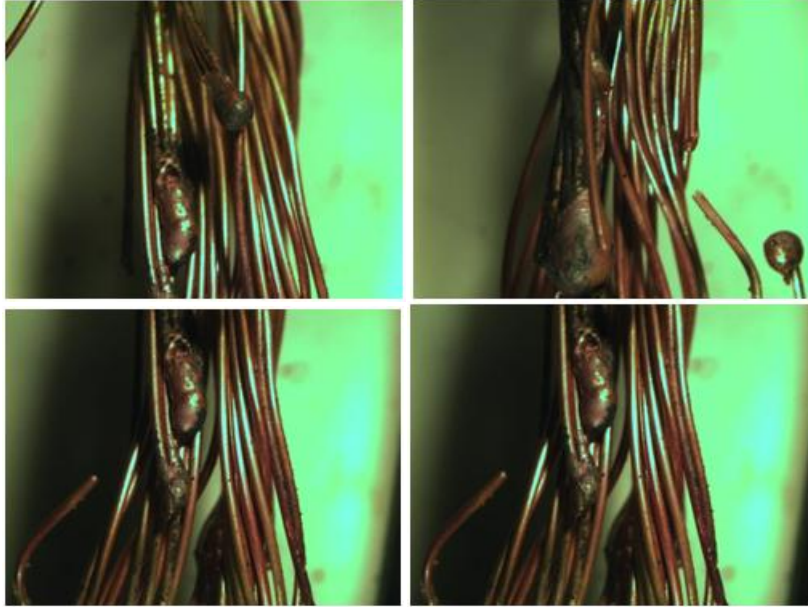


Figure 89: Direct Flame, Multi-strand 16-2, Loaded (Test No. 34)

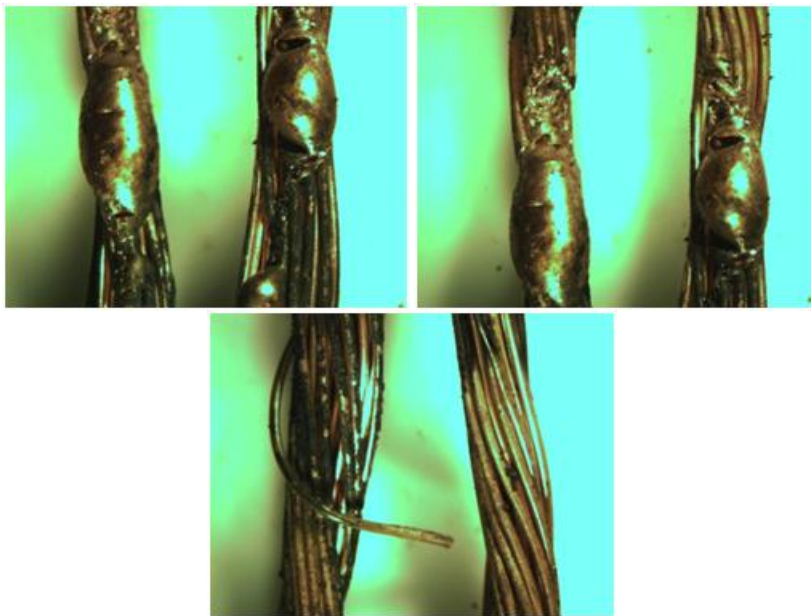


Figure 90: Direct Flame, Multi-strand 16-2, Loaded (Test No. 35)

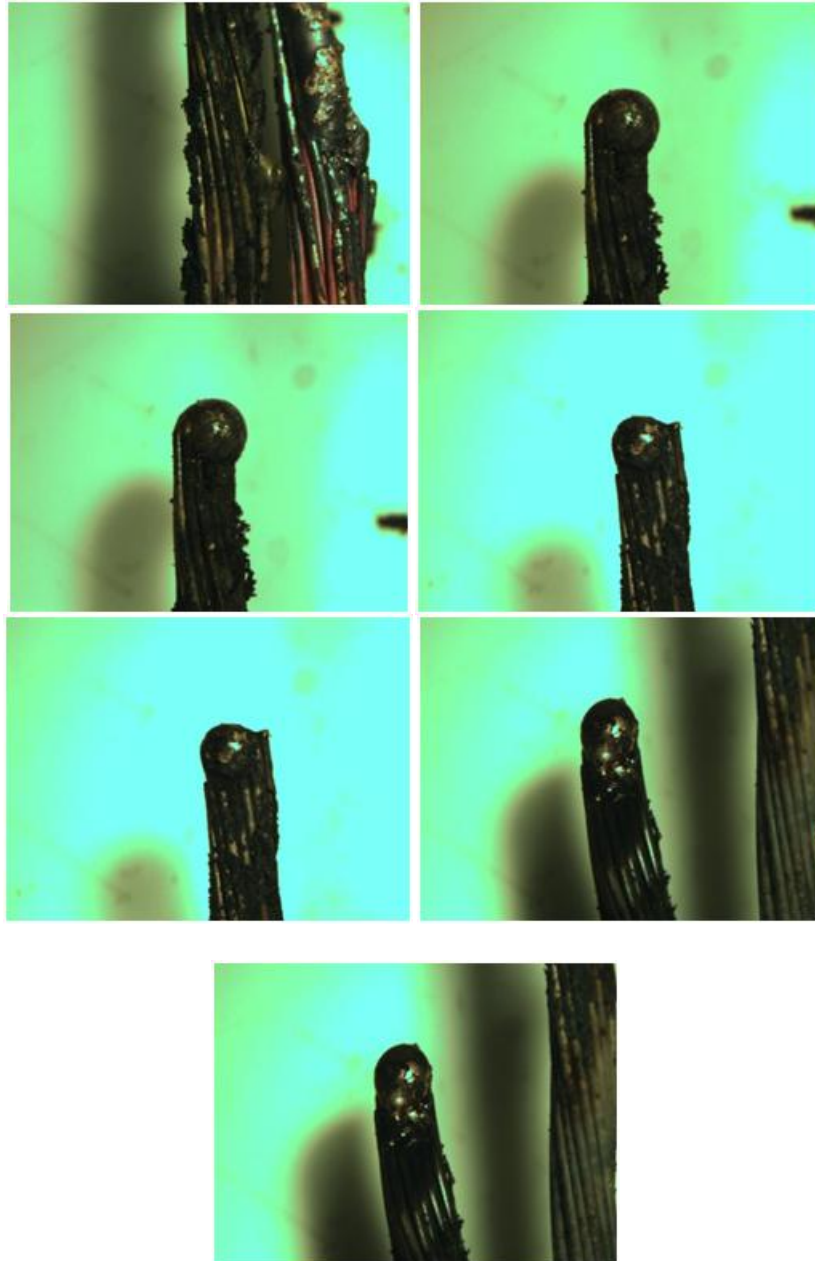


Figure 91: Direct Flame, Multi-strand 16-2, Loaded (Test No. 36)

**DIRECT FLAME TEST; 18-2 MULTISTRAND WIRE**



Figure 92: Direct Flame, Multi-strand 18-2, Non Energized (Test No. 37)

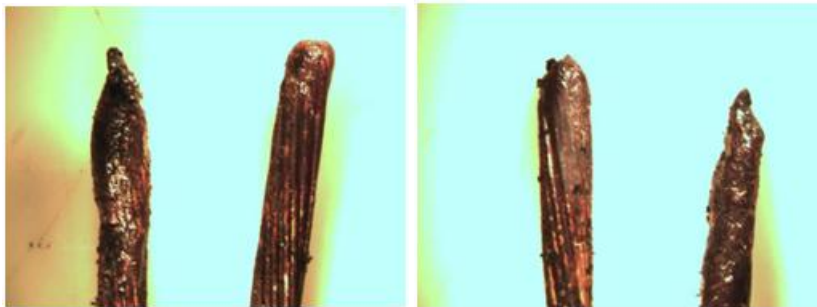
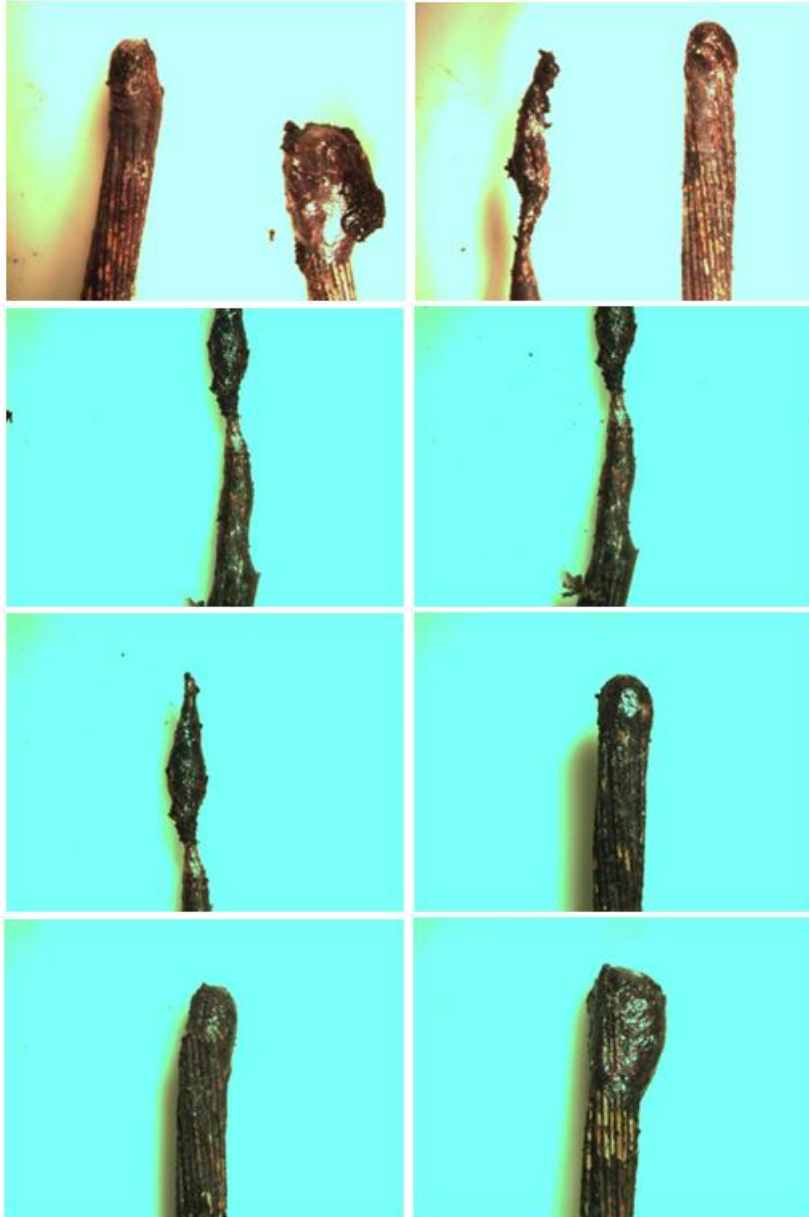


Figure 93: Direct Flame, Multi-strand 18-2, Non Energized (Test No. 38)



Figure 94: Direct Flame, Multi-strand 18-2, Non Energized (Test No. 39)





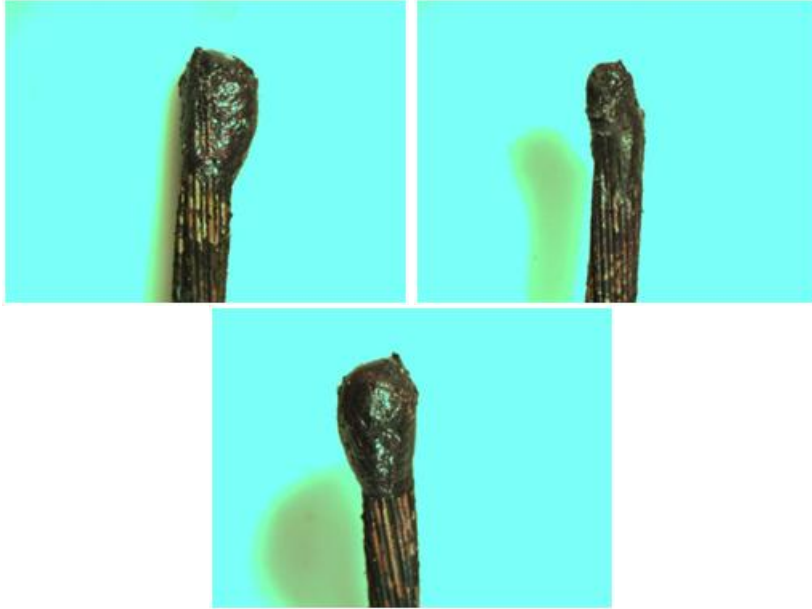


Figure 95: Direct Flame, Multi-strand 18-2, Non Energized (Test No. 40)

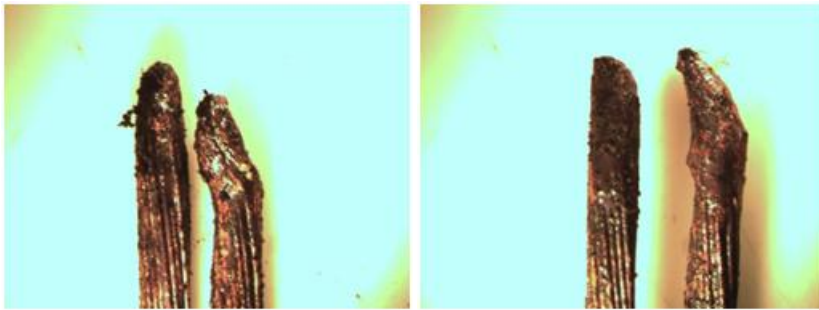


Figure 96: Direct Flame, Multi-strand 18-2, Non Energized (Test No. 41)



Figure 97: Direct Flame, Multi-strand 18-2, Non Energized (Test No. 42)

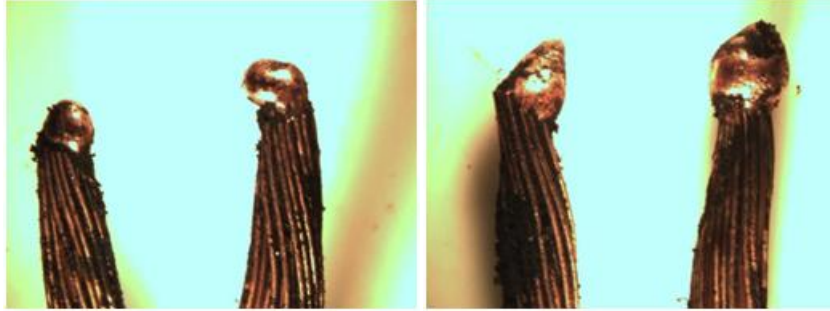


Figure 98: Direct Flame, Multi-strand 18-2, Energized (Test No. 43)

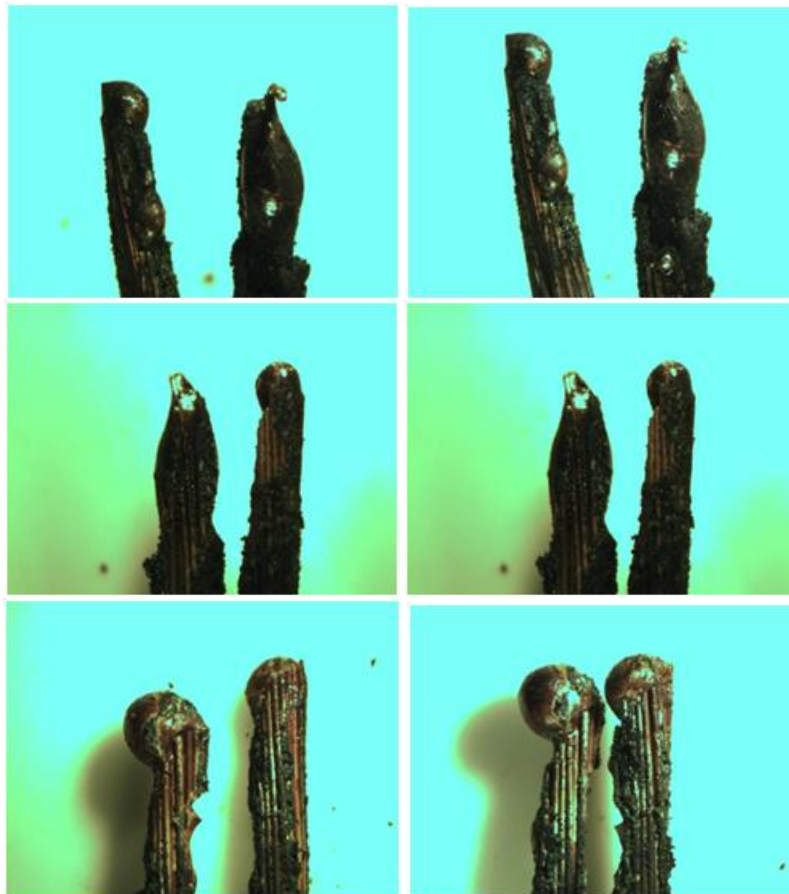


Figure 99: Direct Flame, Multi-strand 18-2, Energized (Test No. 44)

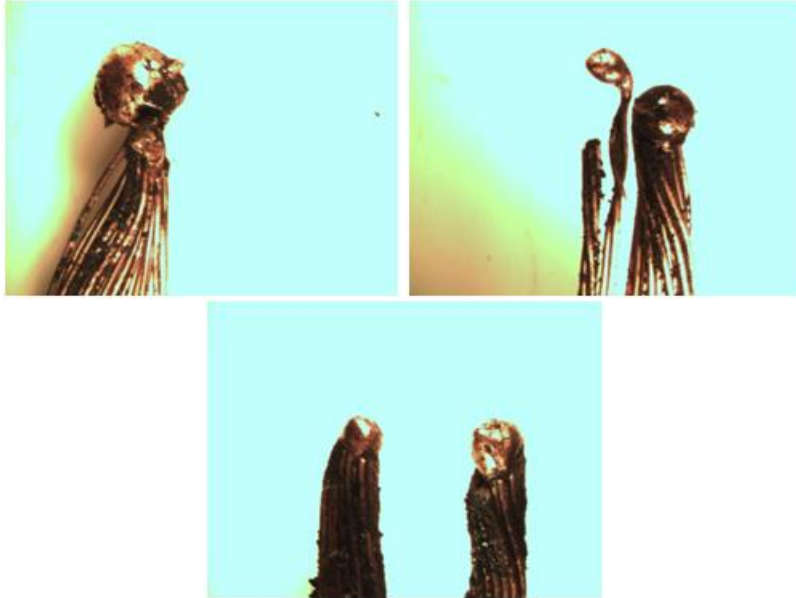


Figure 100: Direct Flame, Multi-strand 18-2, Energized (Test No. 46)

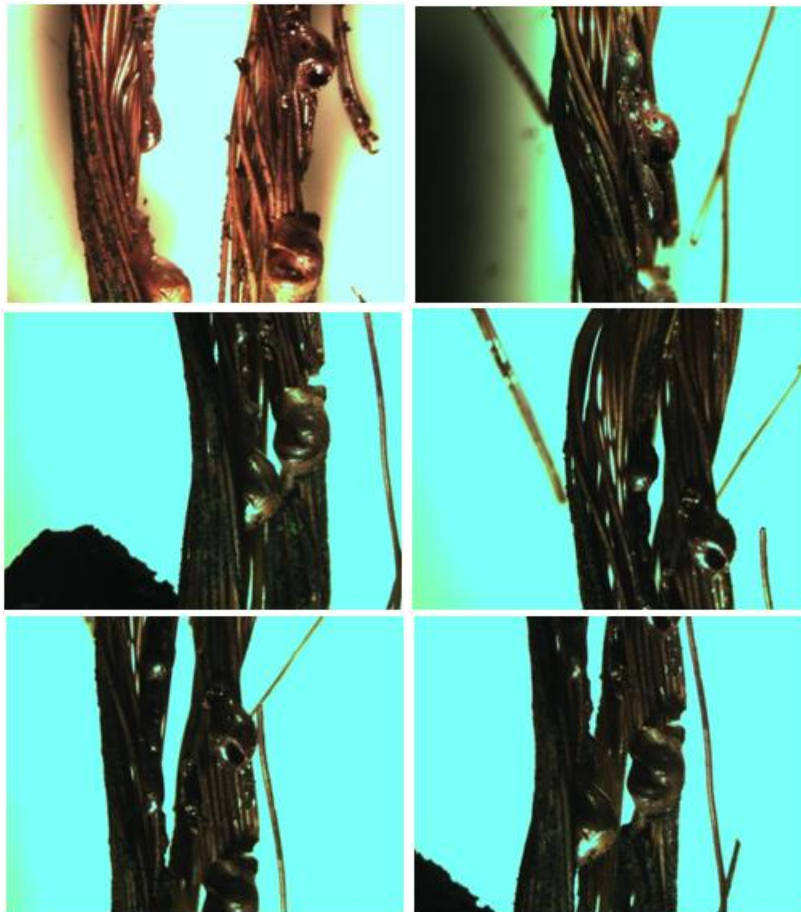


Figure 101: Direct Flame, Multi-strand 18-2, Energized (Test No. 47)

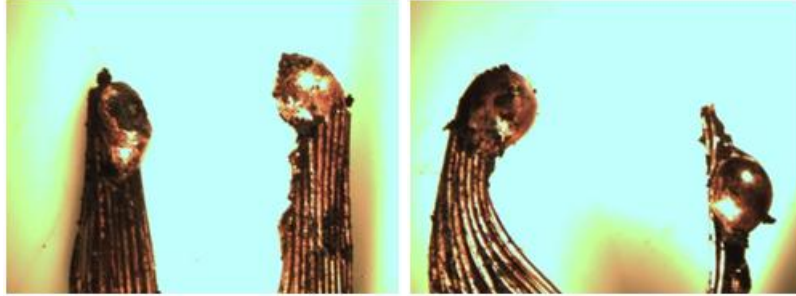


Figure 102: Direct Flame, Multi-strand 18-2, Energized (Test No. 48)

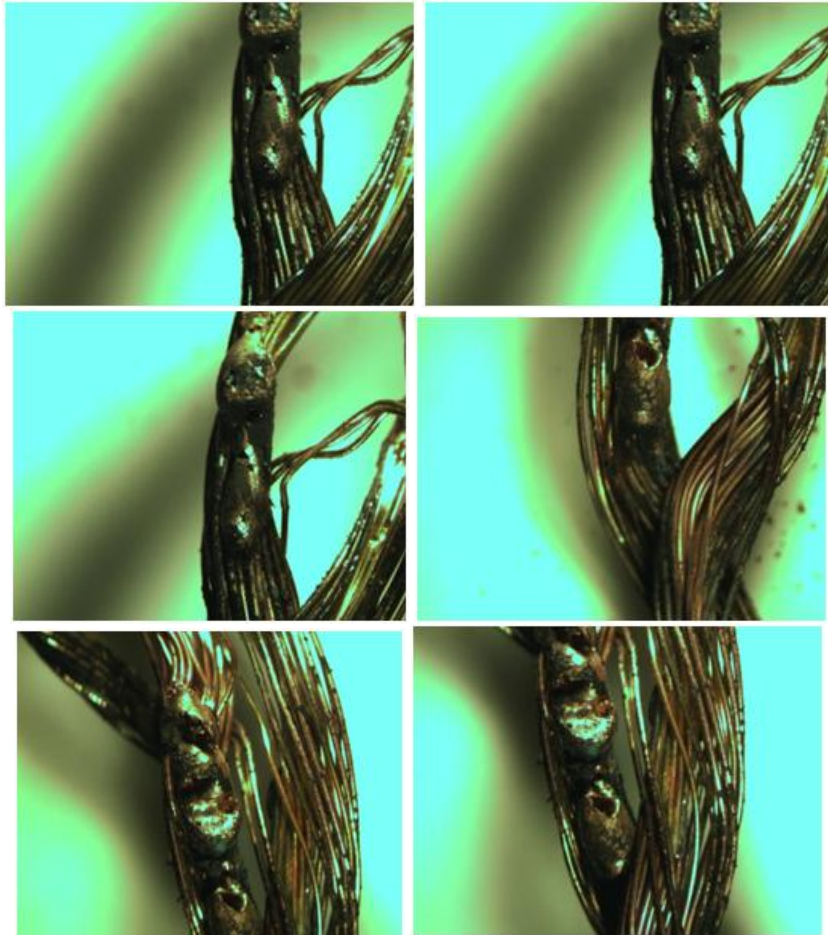


Figure 103: Direct Flame, Multi-strand 18-2, Loaded (Test No. 50)

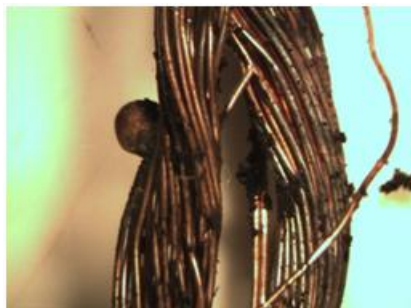


Figure 104: Direct Flame, Multi-strand 18-2, Loaded (Test No. 51)

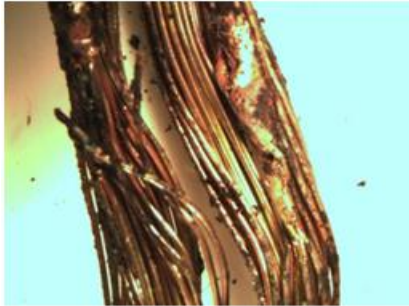


Figure 105: Direct Flame, Multi-strand 18-2, Loaded (Test No. 52)

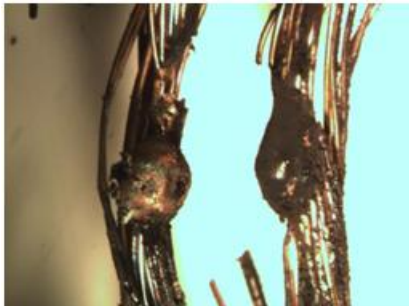


Figure 106: Direct Flame, Multi-strand 18-2, Loaded (Test No. 53)



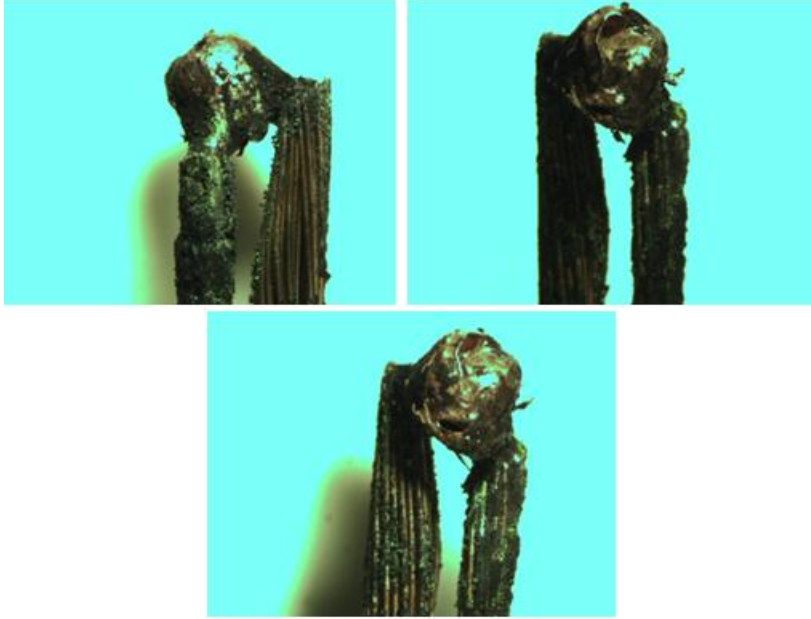
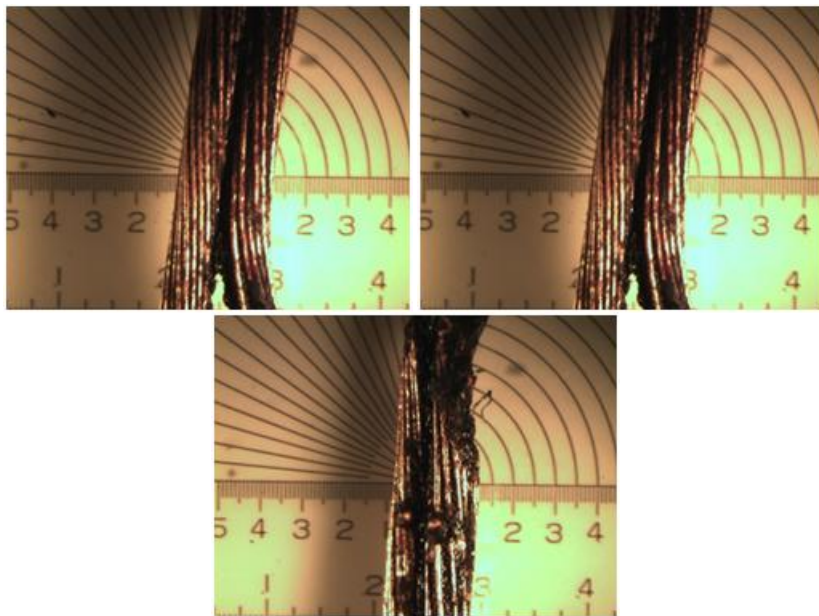


Figure 107: Direct Flame, Multi-strand 18-2, Loaded (Test No. 54)

**RADIATION TEST; 18-2 MULTISTRAND WIRE**



Figure 108: Radiation, Multi-strand 18-2, Energized (Test No. 1)





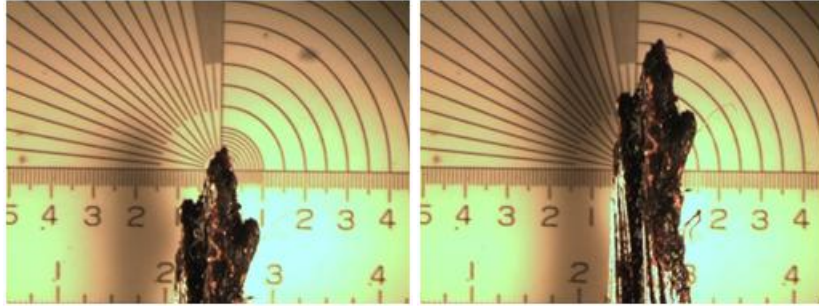


Figure 109: Radiation, Multi-strand 18-2, Energized (Test No. 2)

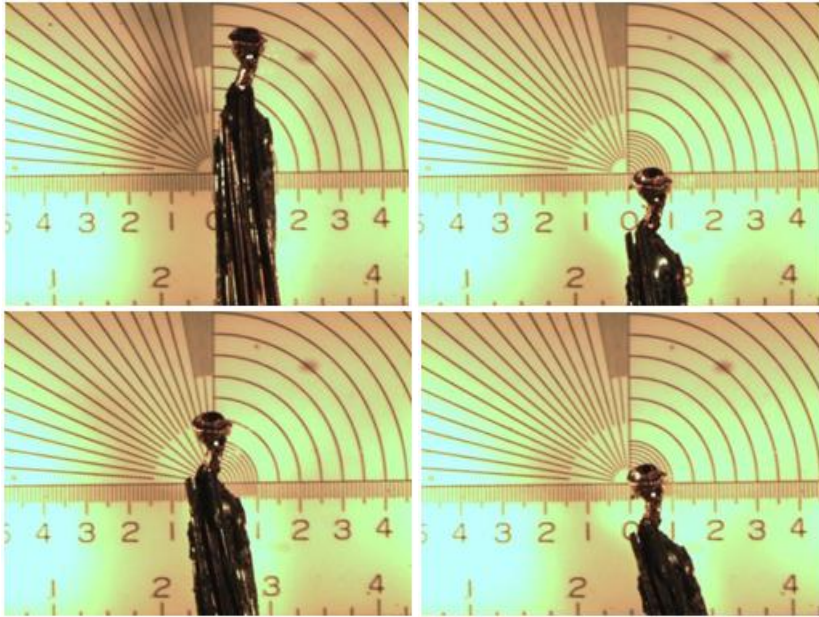


Figure 110: Radiation, Multi-strand 18-2, Energized (Test No. 3)

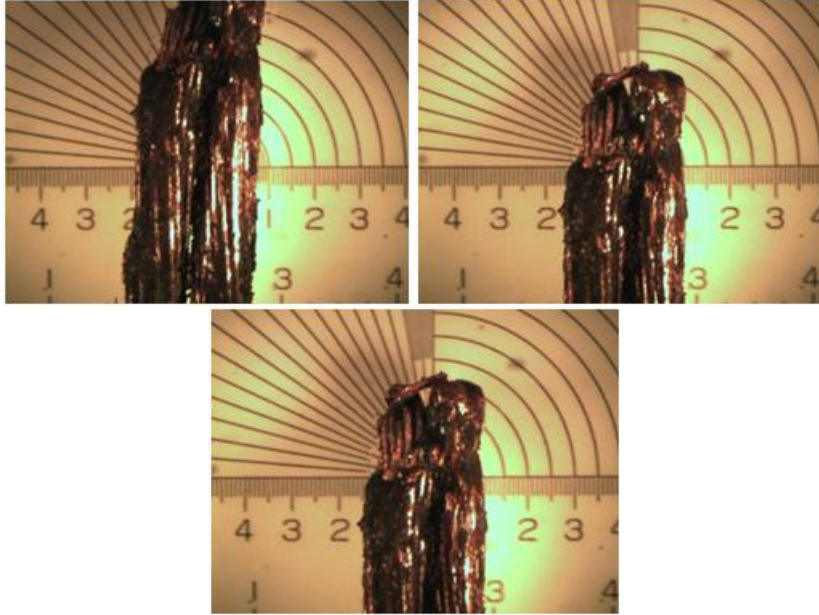


Figure 111: Radiation, Multi-strand 18-2, Non Energized (Test No. 1)

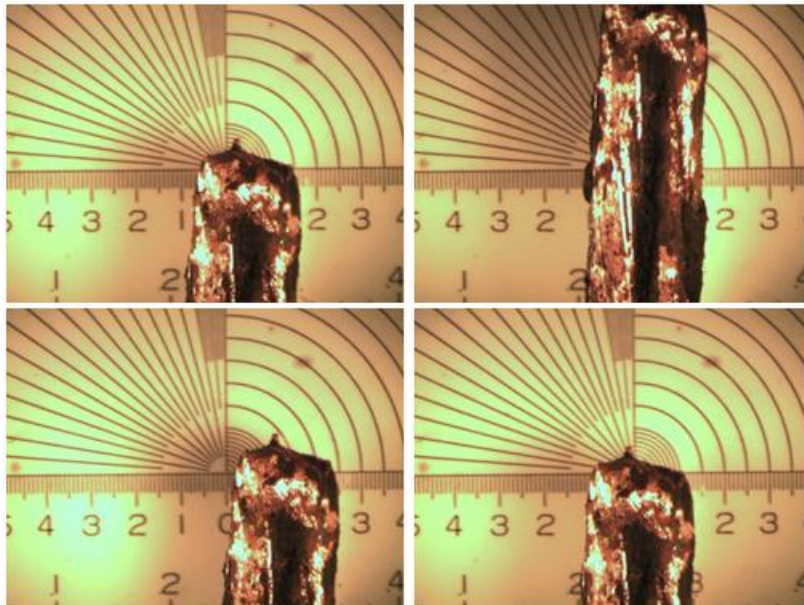


Figure 112: Radiation, Multi-strand 18-2, Non Energized (Test No. 2)

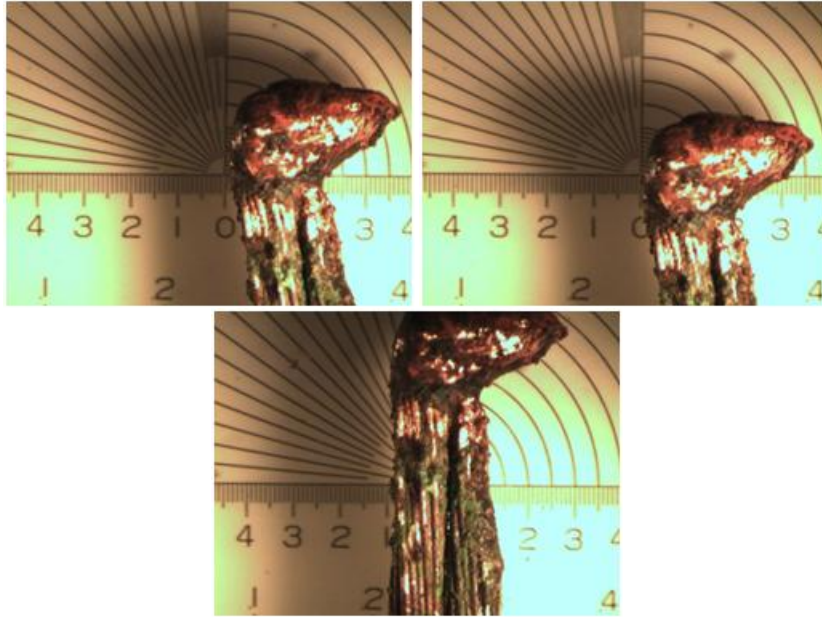


Figure 113: Radiation, Multi-strand 18-2, Non Energized (Test No. 3)



Figure 114: Radiation, Multi-strand 18-2, Loaded (Test No. 1)

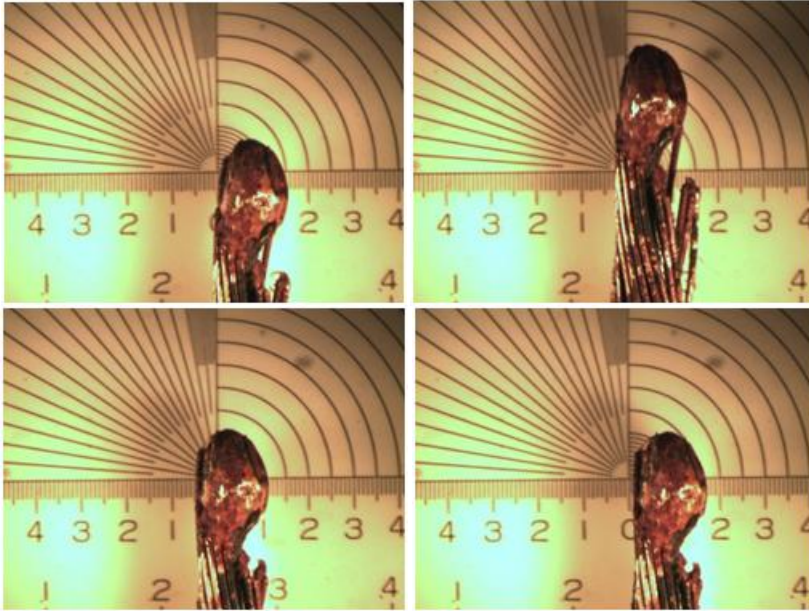


Figure 115: Radiation, Multi-strand 18-2, Loaded (Test No. 2)

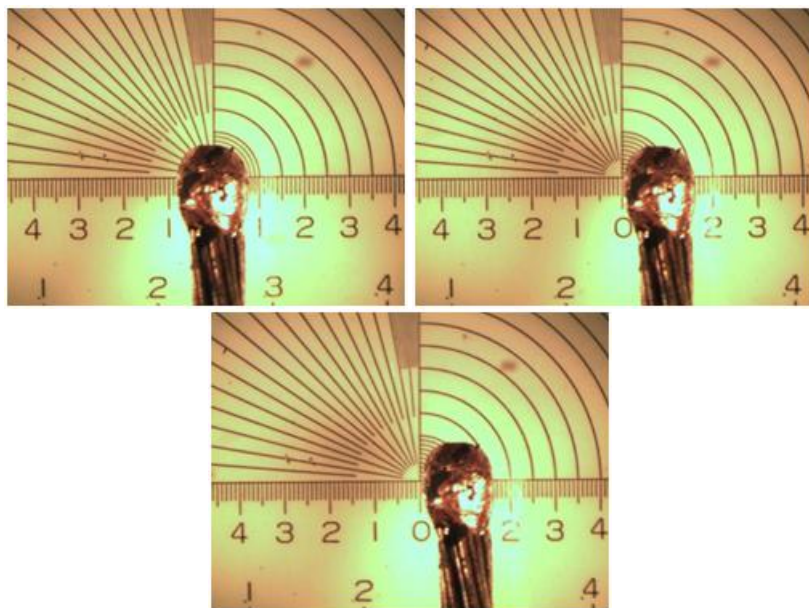


Figure 116: Radiation, Multi-strand 18-2, Loaded (Test No. 3)

**RADIATION TEST; 16-2 MULTISTRAND WIRE**

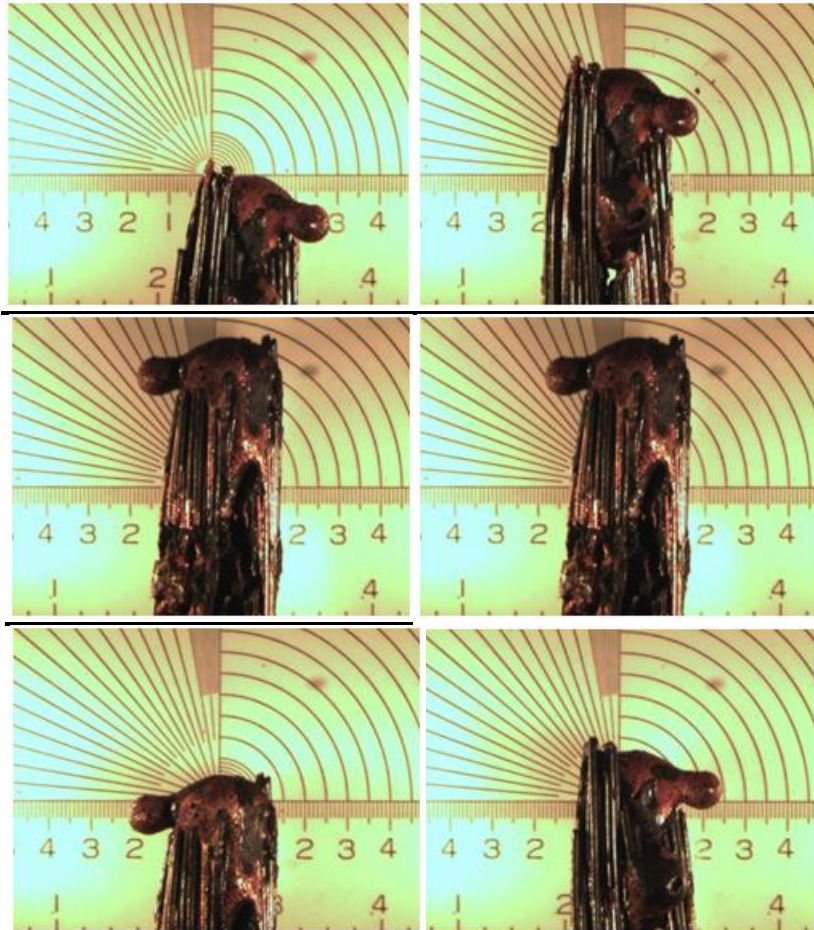


Figure 117: Radiation, Multi-strand 16-2, Energized (Test No. 1)

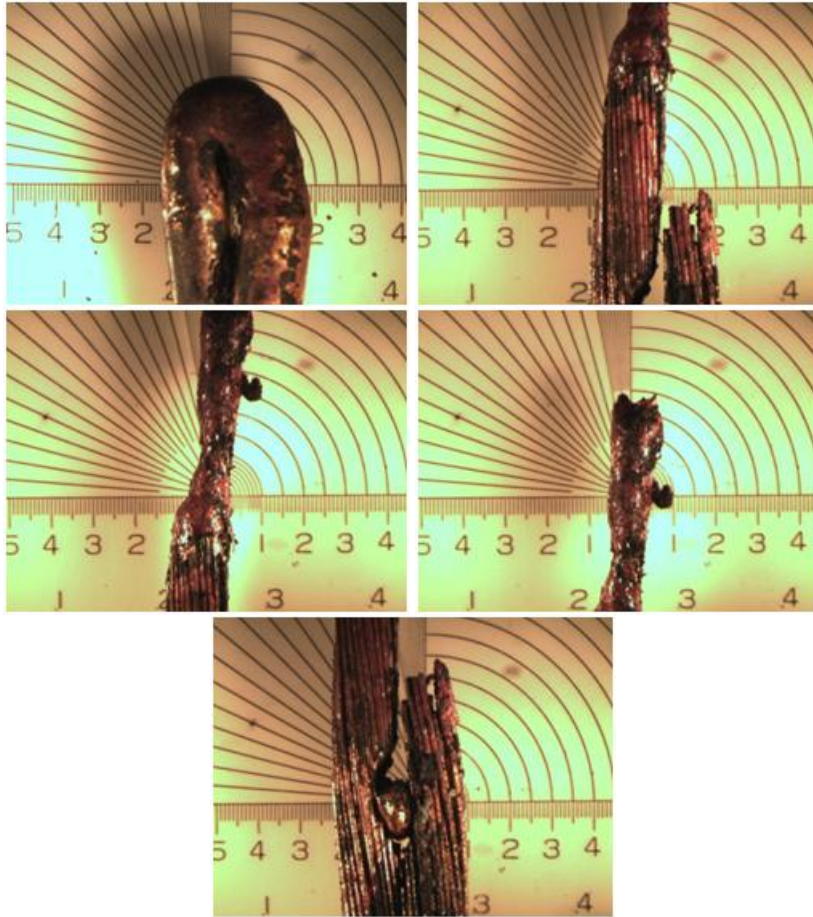


Figure 118: Radiation, Multi-strand 16-2, Energized (Test No. 2)

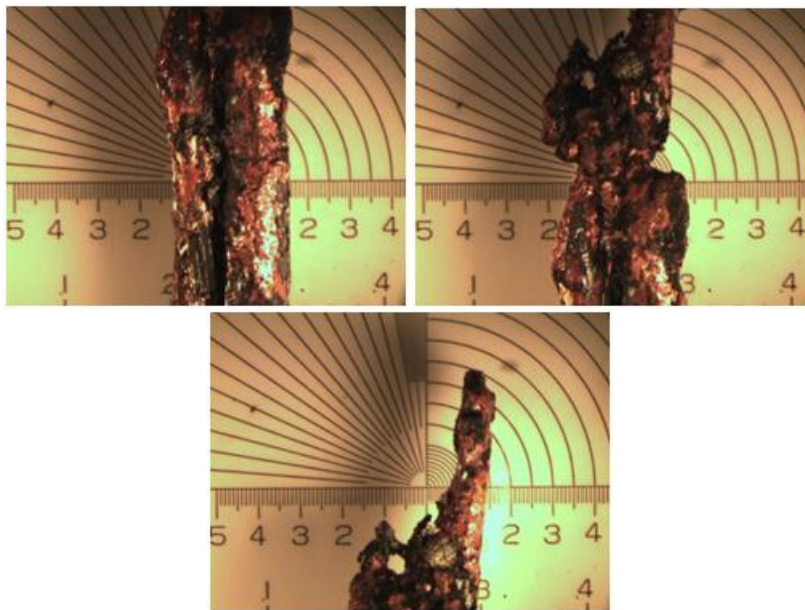


Figure 119: Radiation, Multi-strand 16-2, Energized (Test No. 3)



Figure 120: Radiation, Multi-strand 16-2, Non Energized (Test No. 1)



Figure 121: Radiation, Multi-strand 16-2, Non Energized (Test No. 2)

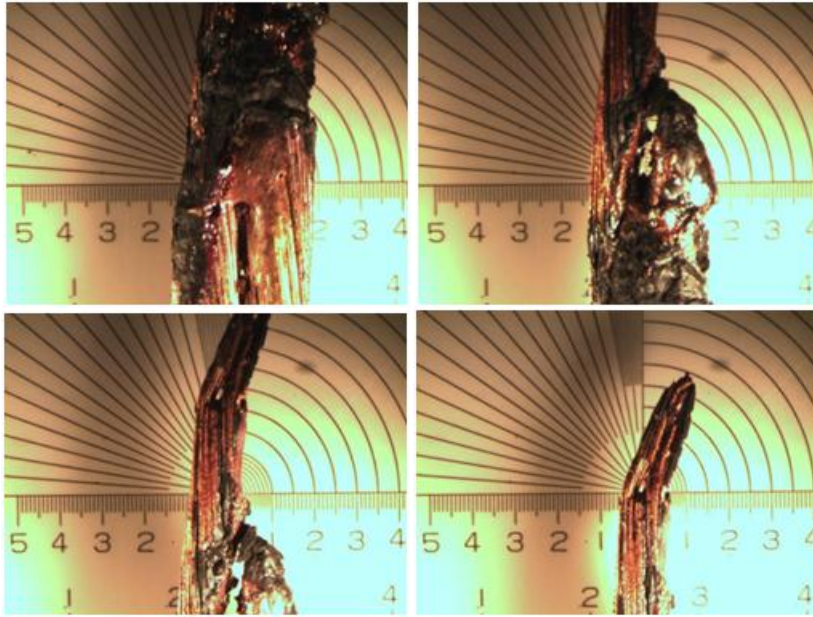


Figure 122: Radiation, Multi-strand 16-2, Non Energized (Test No. 3)

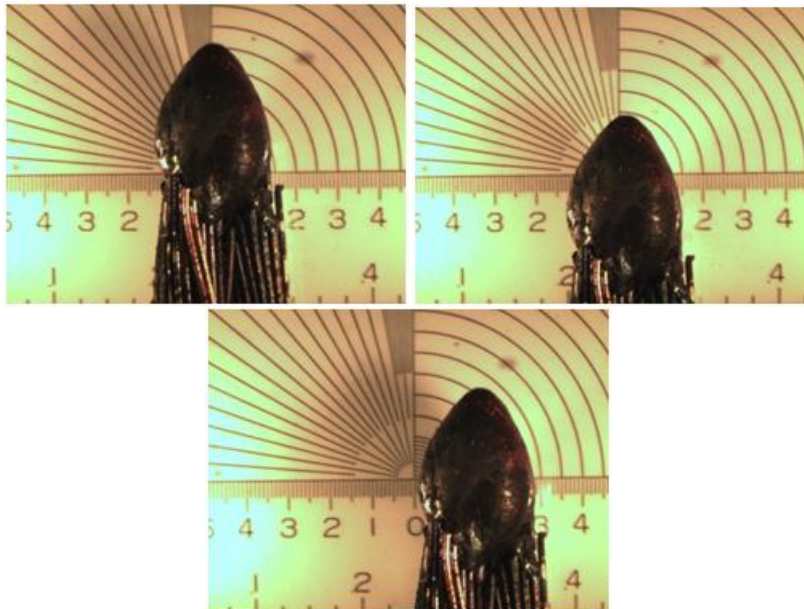


Figure 123: Radiation, Multi-strand 16-2, Loaded (Test No. 1)



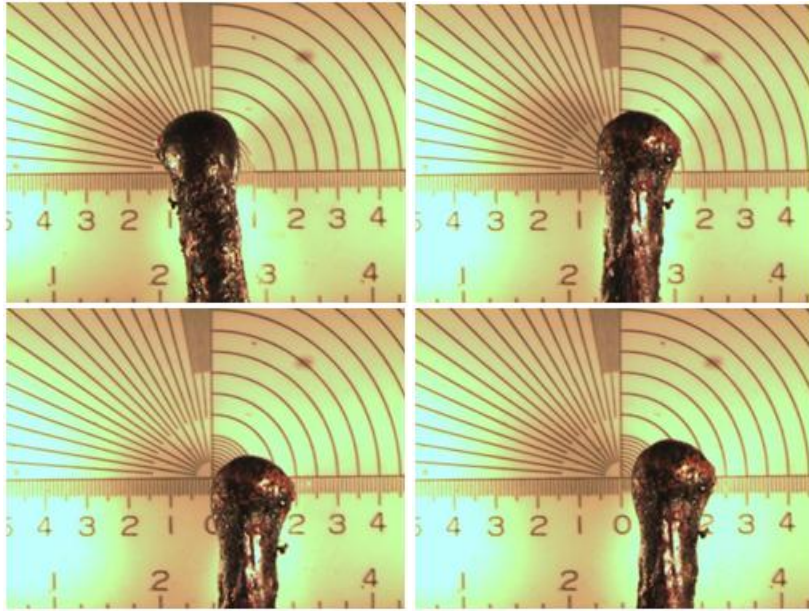


Figure 124: Radiation, Multi-strand 16-2, Loaded (Test No. 2)



Figure 125: Radiation, Multi-strand 16-2, Loaded (Test No. 3)

**RADIATION TEST; 14-2 ROMEX WIRE**

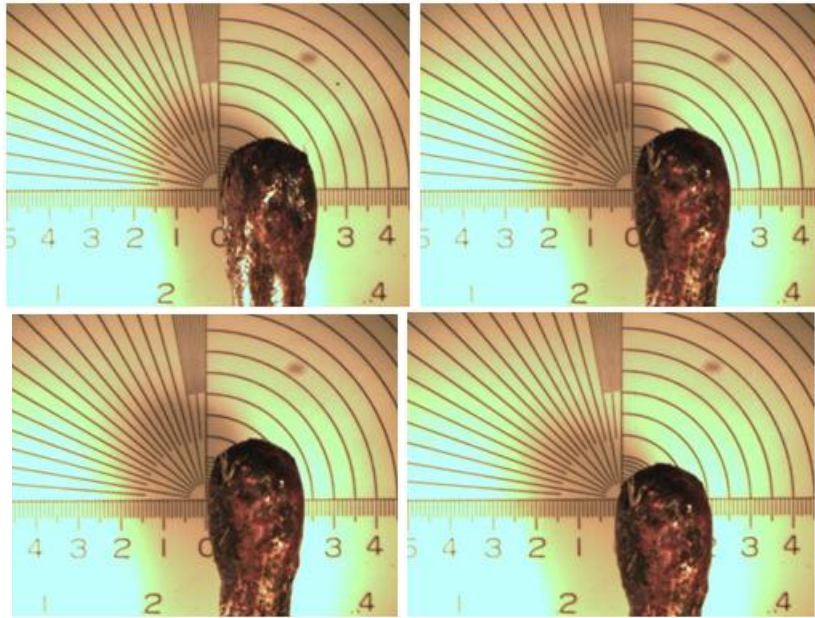


Figure 126: Radiation, Romex 14-2, Non Energized (Test No. 1)

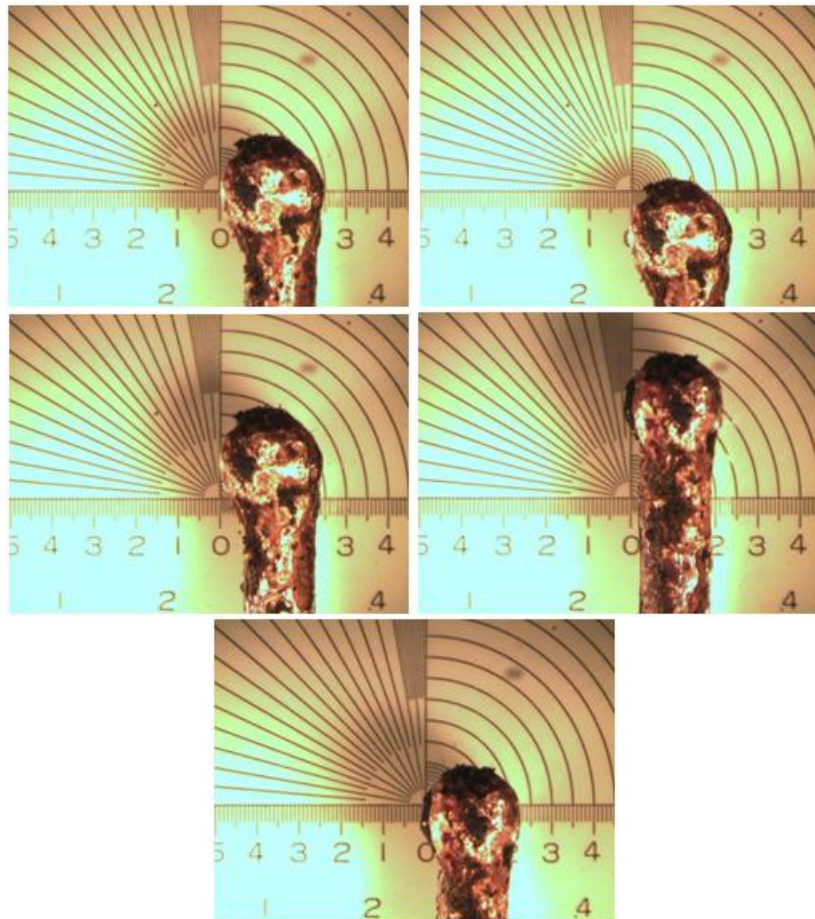


Figure 127: Radiation, Romex 14-2, Non Energized (Test No. 2)

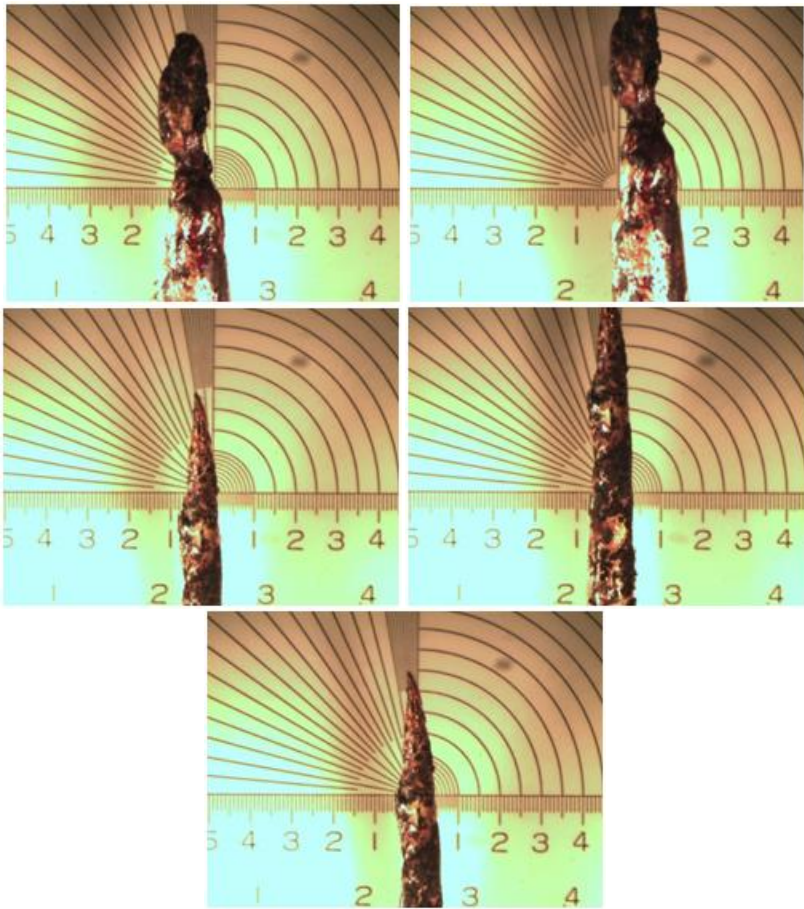


Figure 128: Radiation, Romex 14-2, Non Energized (Test No. 3)

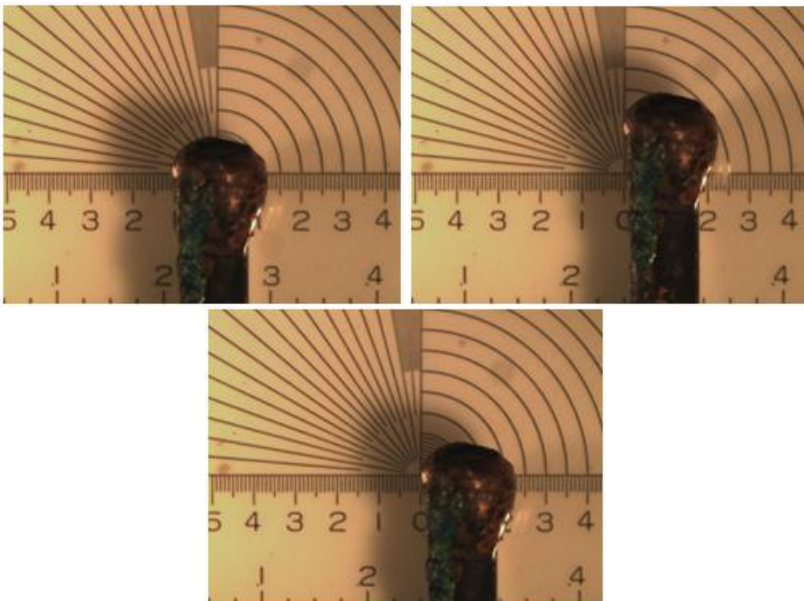


Figure 129: Radiation, Romex 14-2, Energized (Test No. 1)

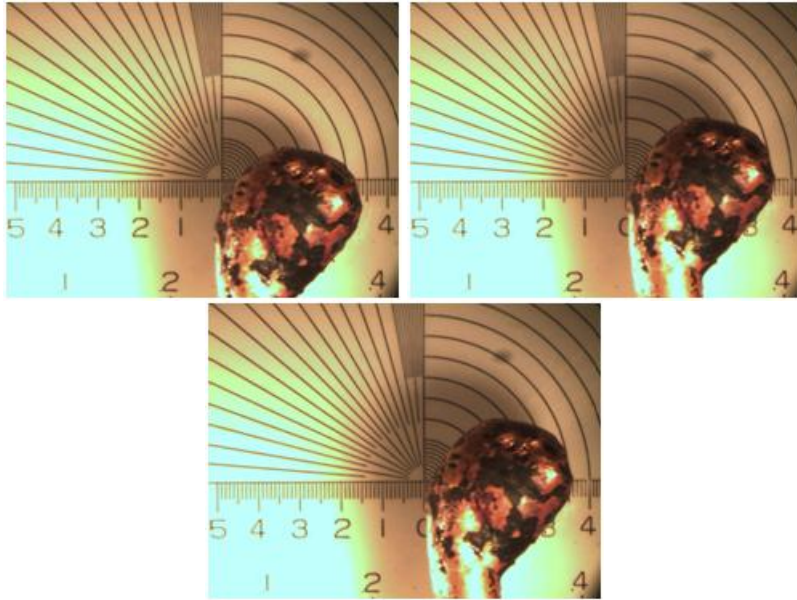


Figure 130: Radiation, Romex 14-2, Energized (Test No. 2)

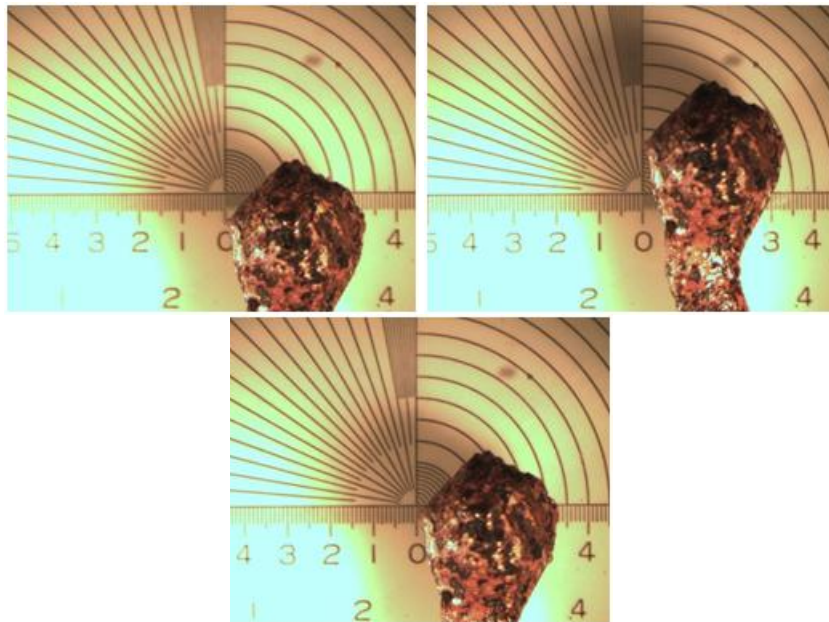


Figure 131: Radiation, Romex 14-2, Energized (Test No. 3)

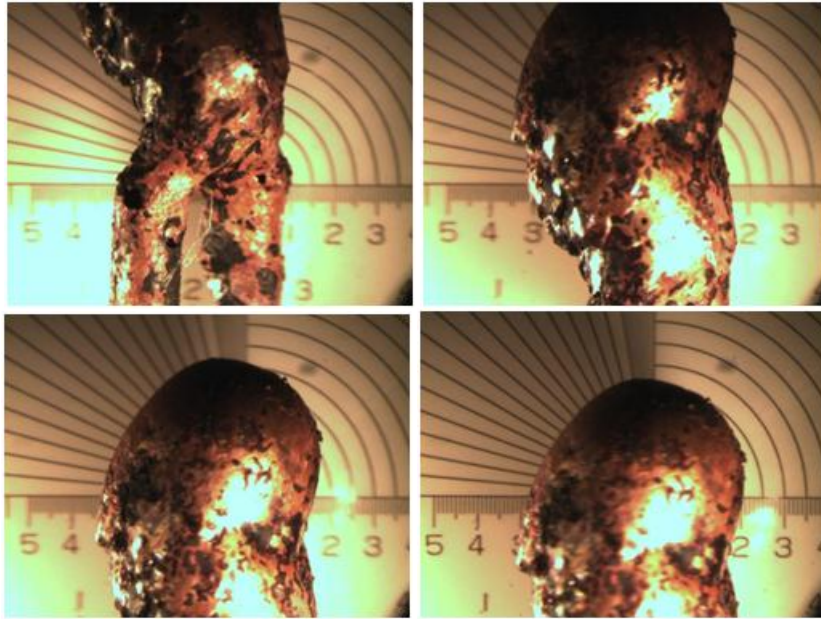


Figure 132: Radiation, Romex 14-2, Loaded (Test No. 1)

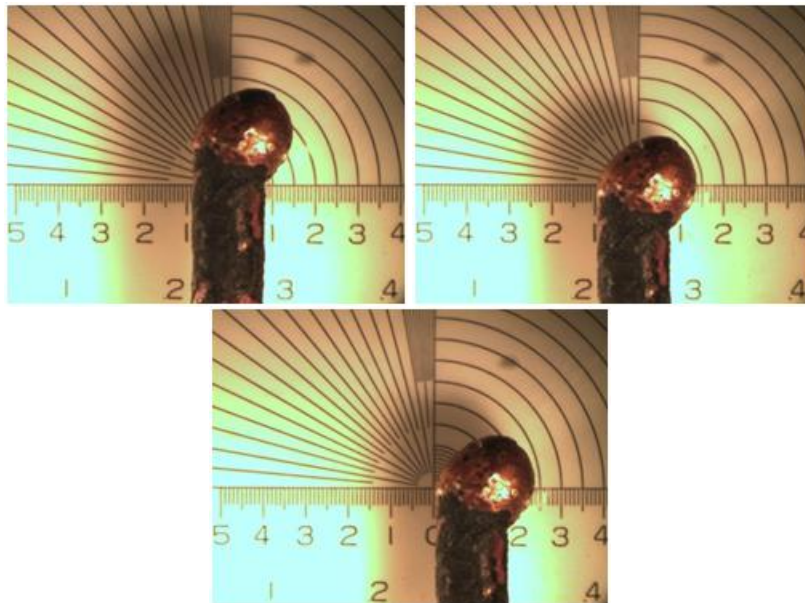


Figure 133: Radiation, Romex 14-2, Loaded (Test No. 2)

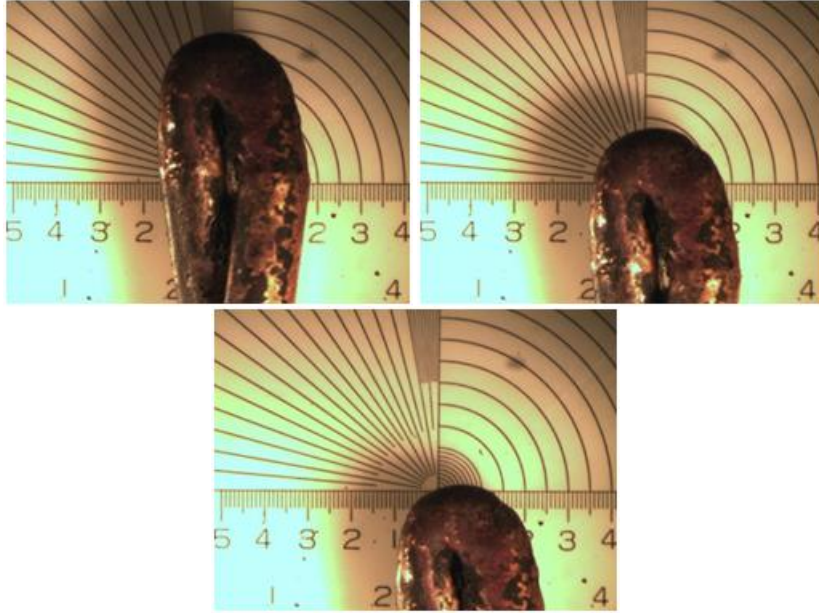


Figure 134: Radiation, Romex 14-2, Loaded (Test No. 3)

**RADIATION TEST; 12-2 ROMEX WIRE**

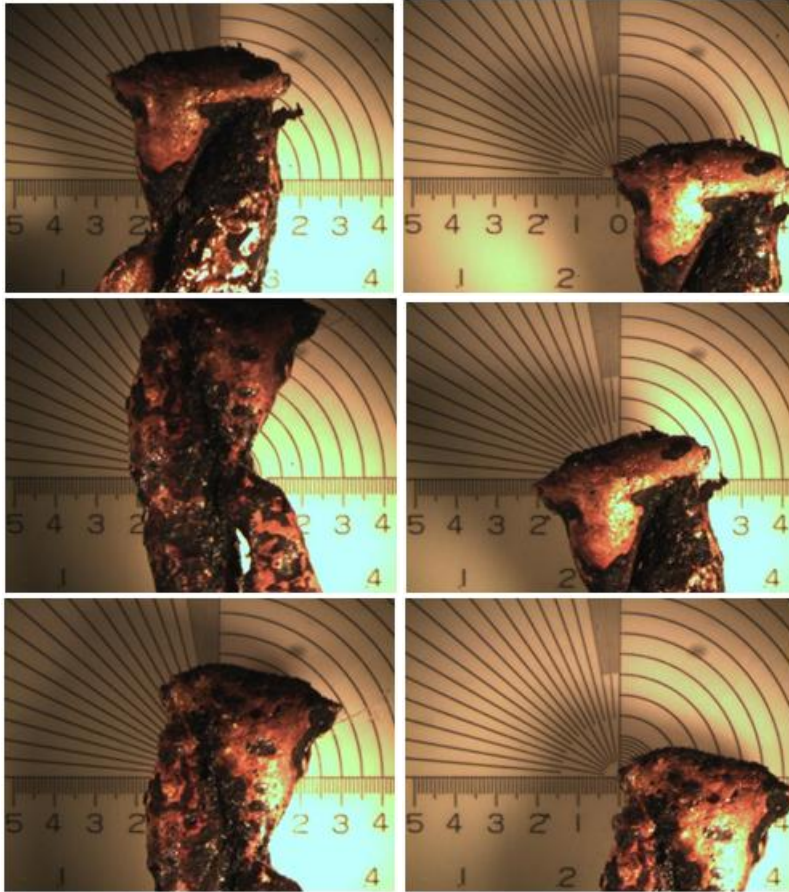


Figure 135: Radiation, Romex 12-2, Non Energized (Test No. 1)



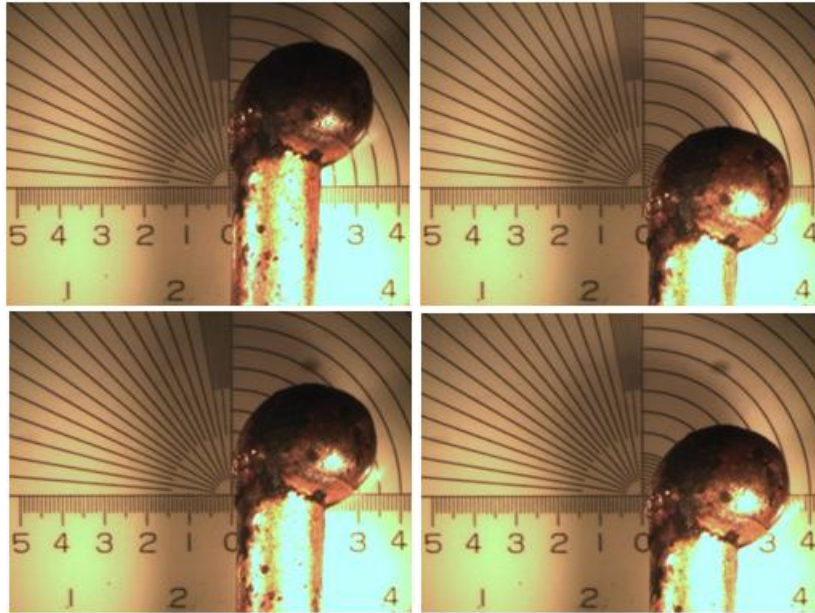


Figure 136: Radiation, Romex 12-2, Non Energized (Test No. 2)

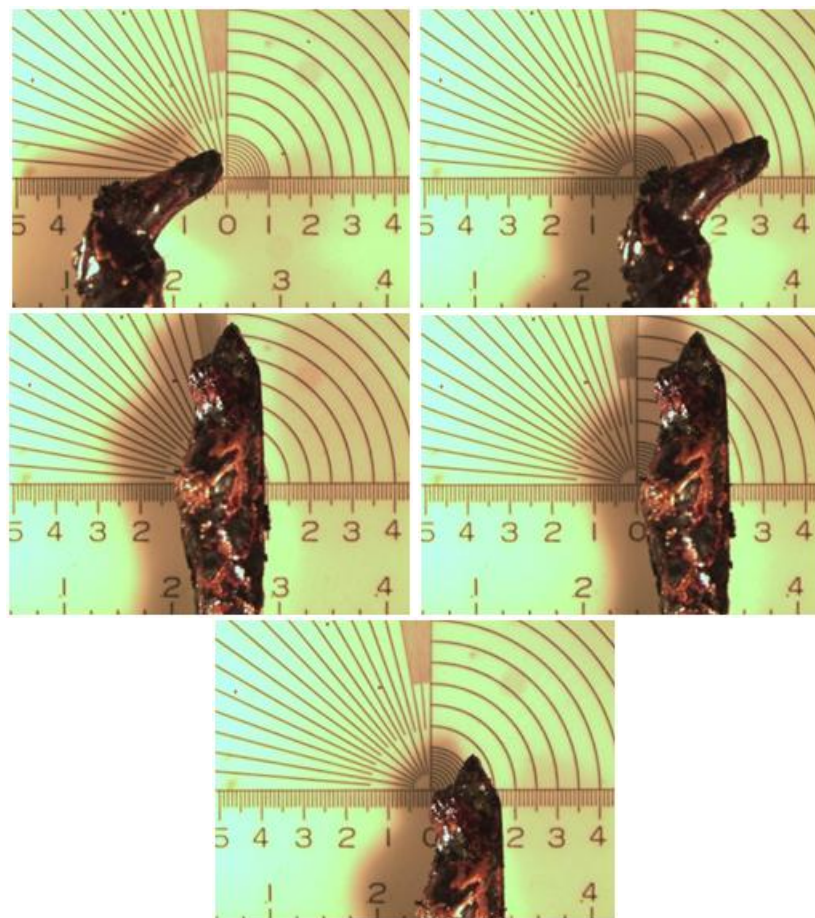


Figure 137: Radiation, Romex 12-2, Non Energized (Test No. 3)



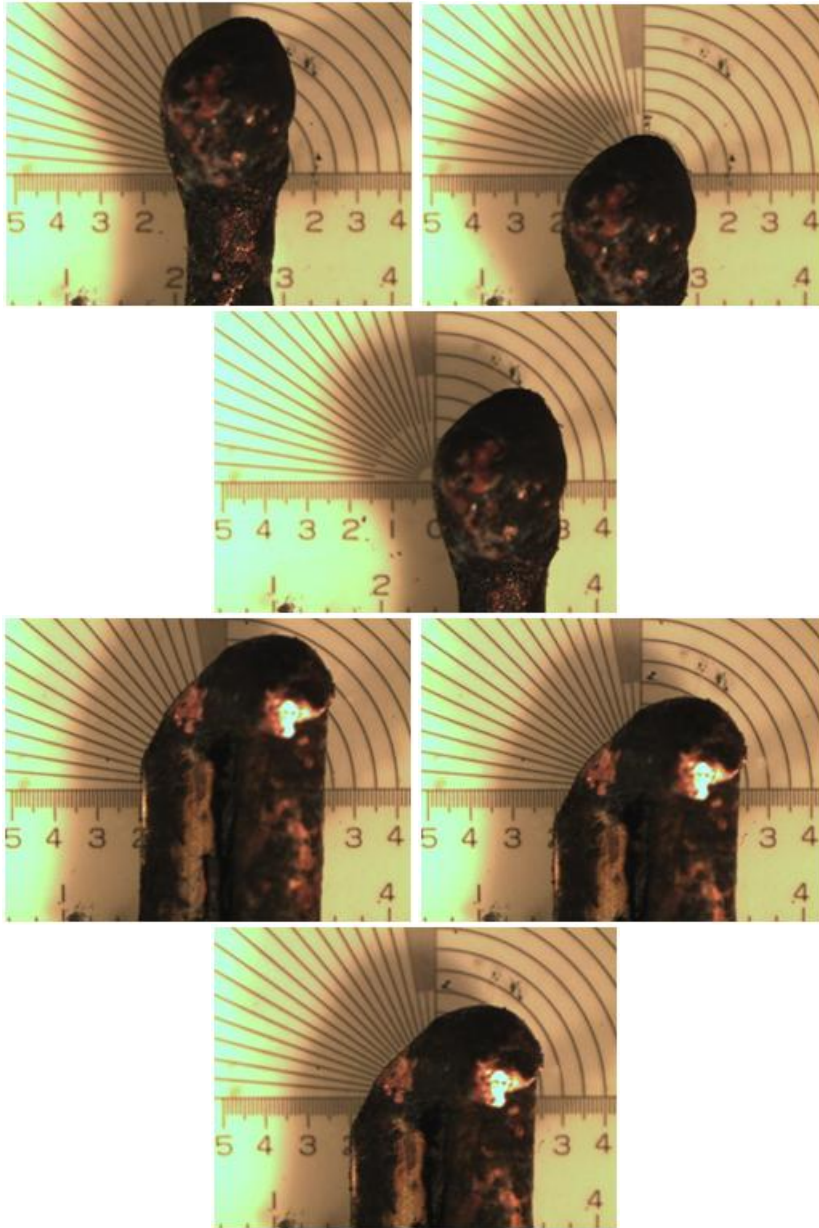


Figure 138: Radiation, Romex 12-2, Energized (Test No. 1)

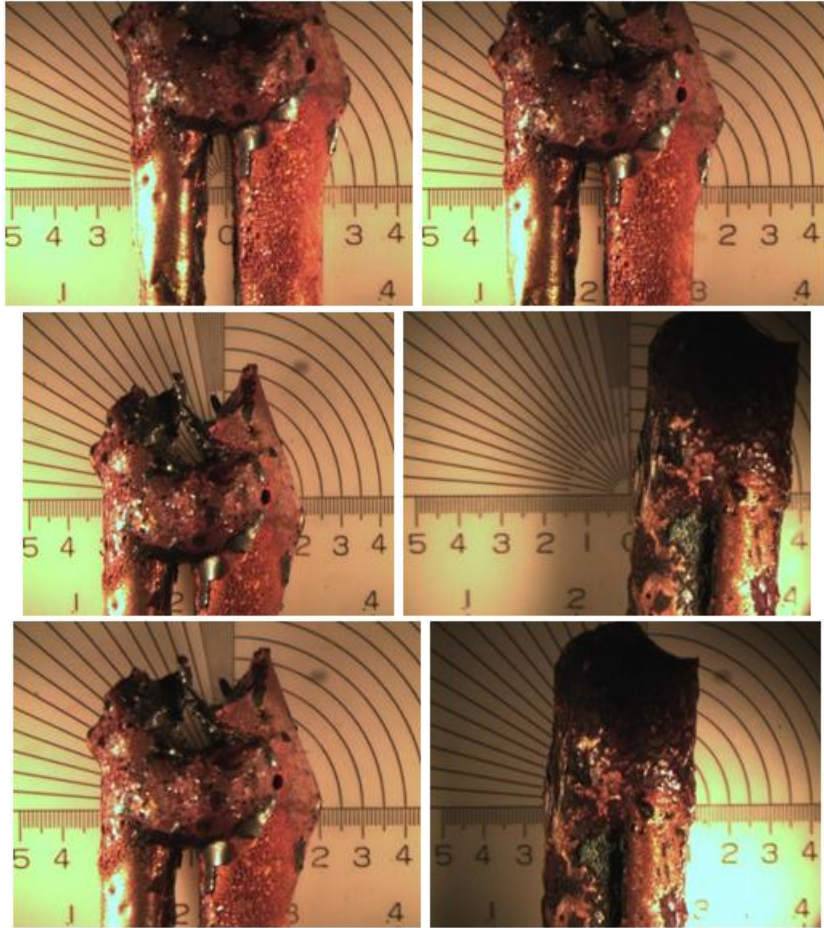
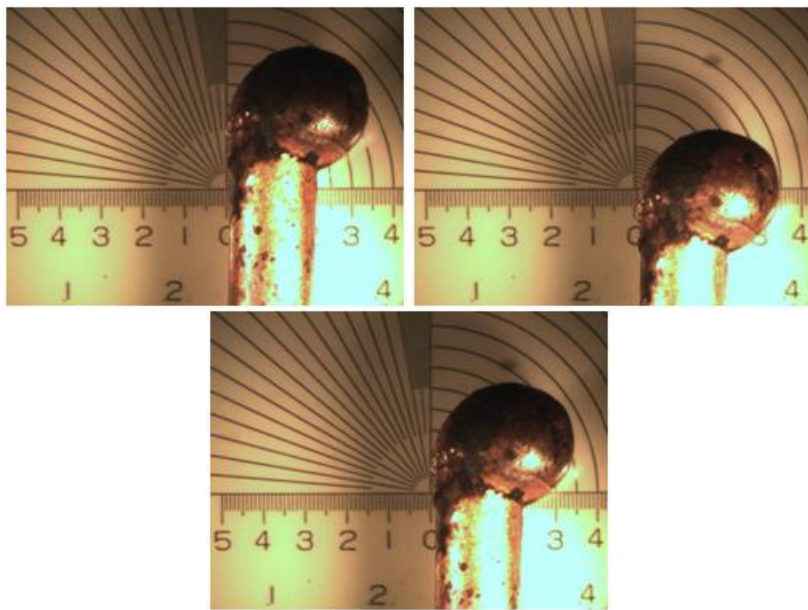


Figure 139: Radiation, Romex 12-2, Energized (Test No. 2)



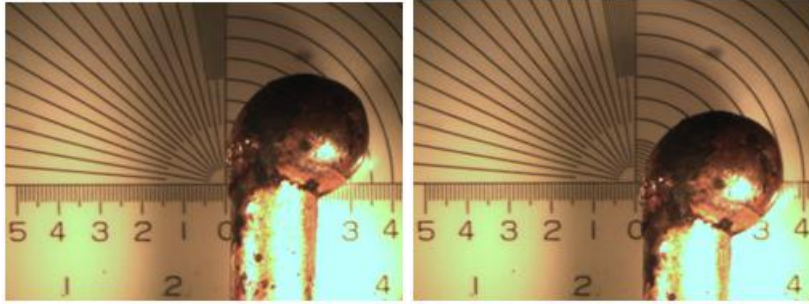
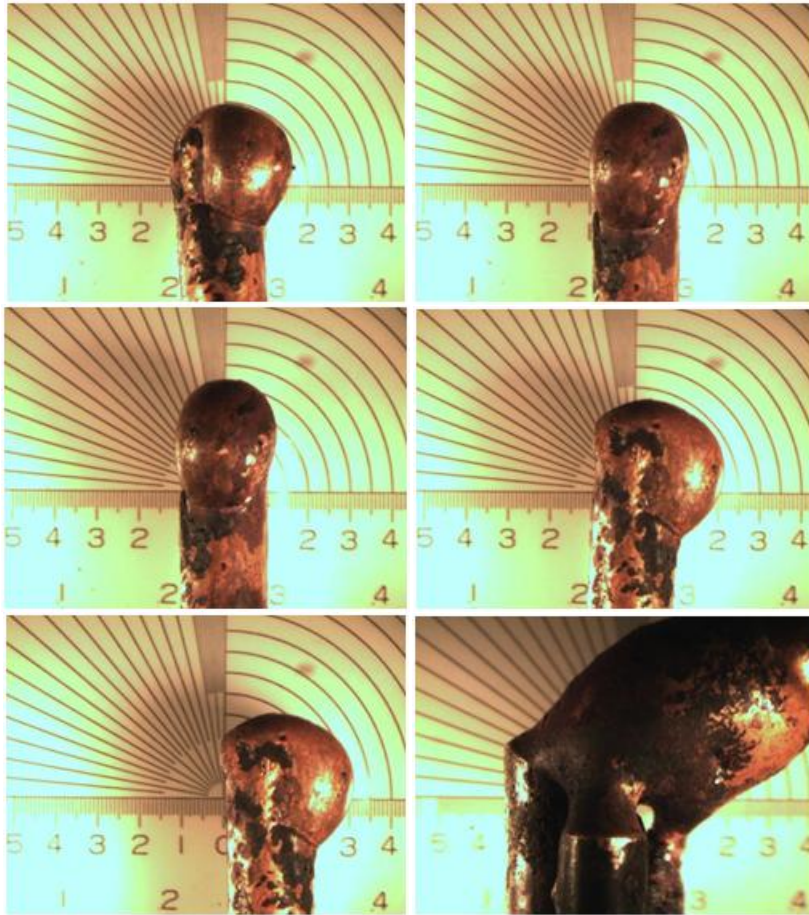


Figure 140: Radiation, Romex 12-2, Energized (Test No. 3)



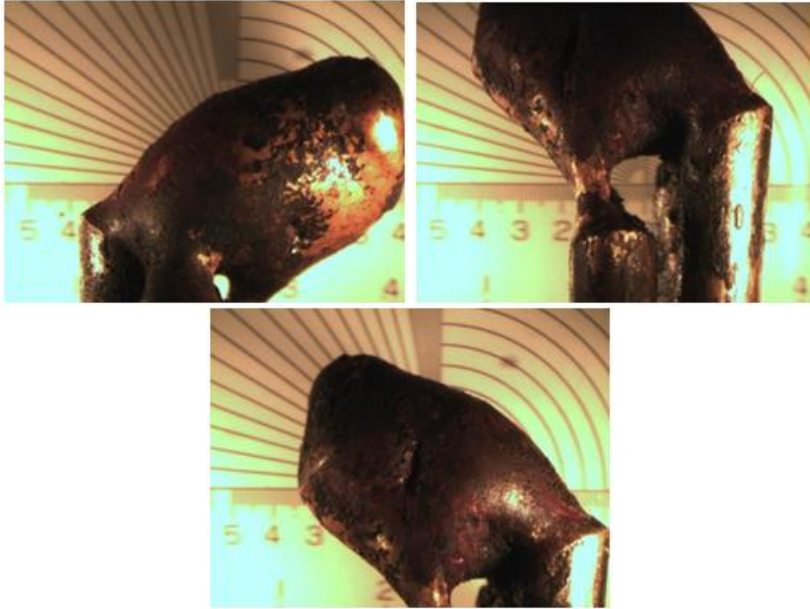


Figure 141: Radiation, Romex 12-2, Loaded (Test No. 1)

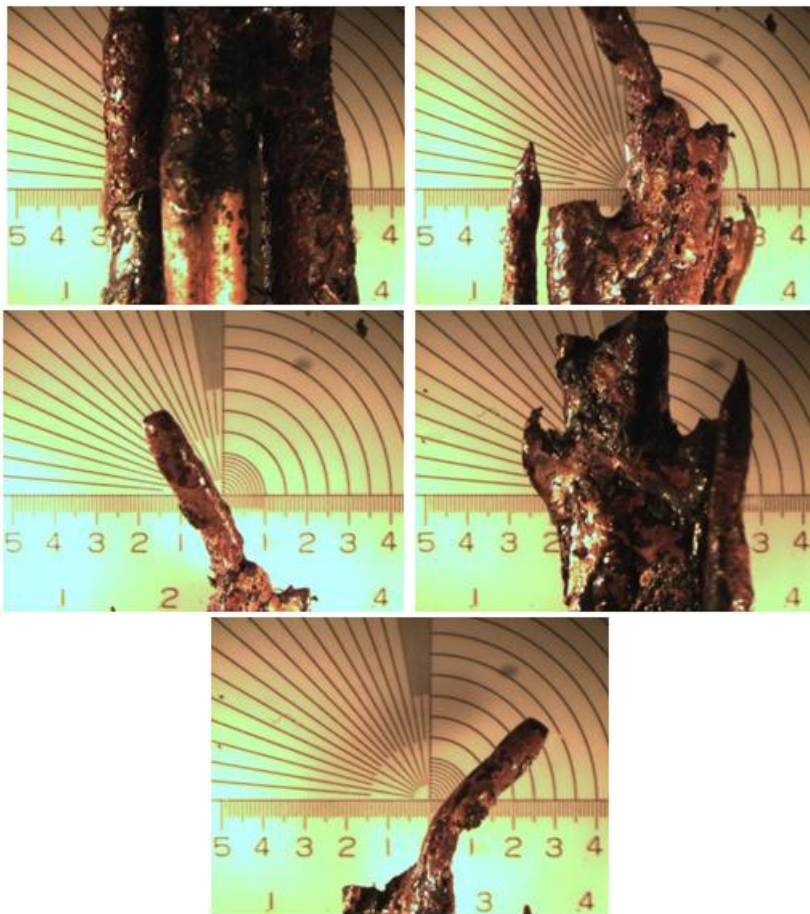


Figure 142: Radiation, Romex 12-2, Loaded (Test No. 2)

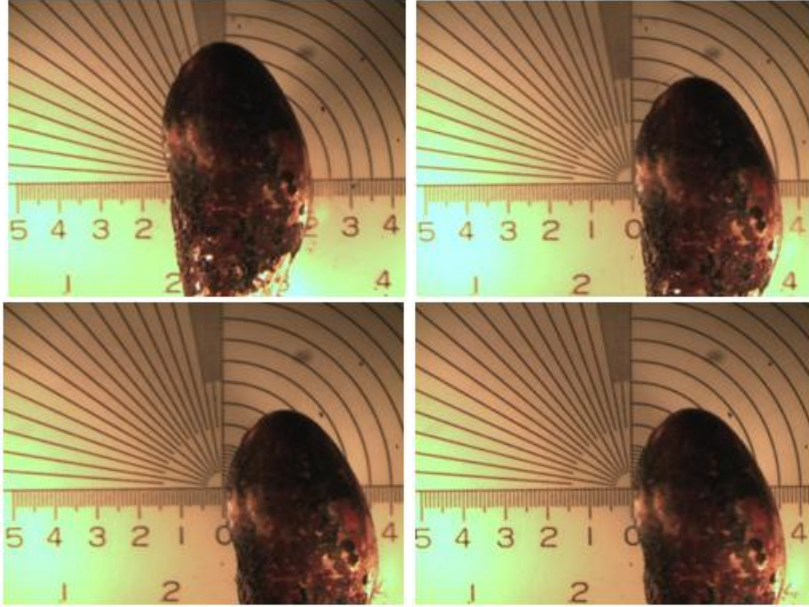


Figure 143: Radiation, Romex 12-2, Loaded (Test No. 3)

**FULL-SCALE COMPARTMENT TEST; 12-2 ROMEX WIRE**

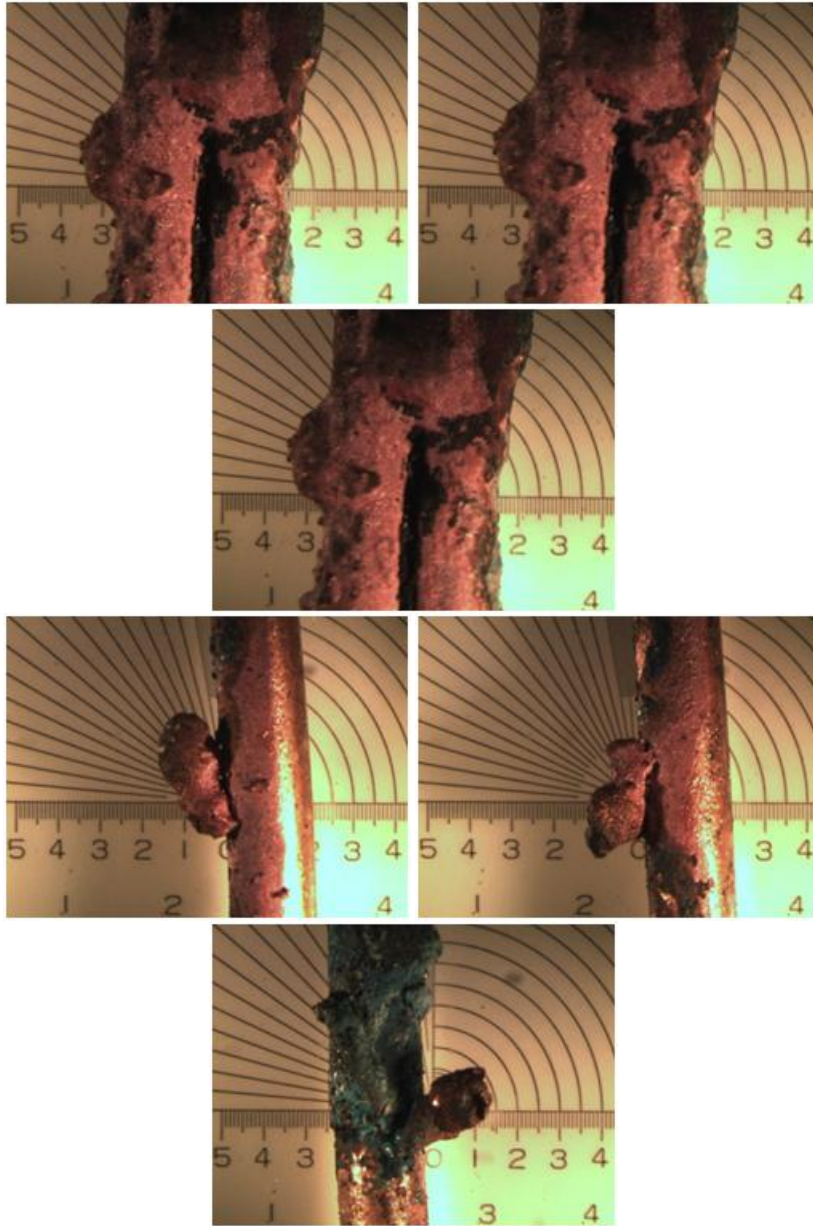


Figure 144: Full Scale, Romex 12-2, Energized (Room No. 6)

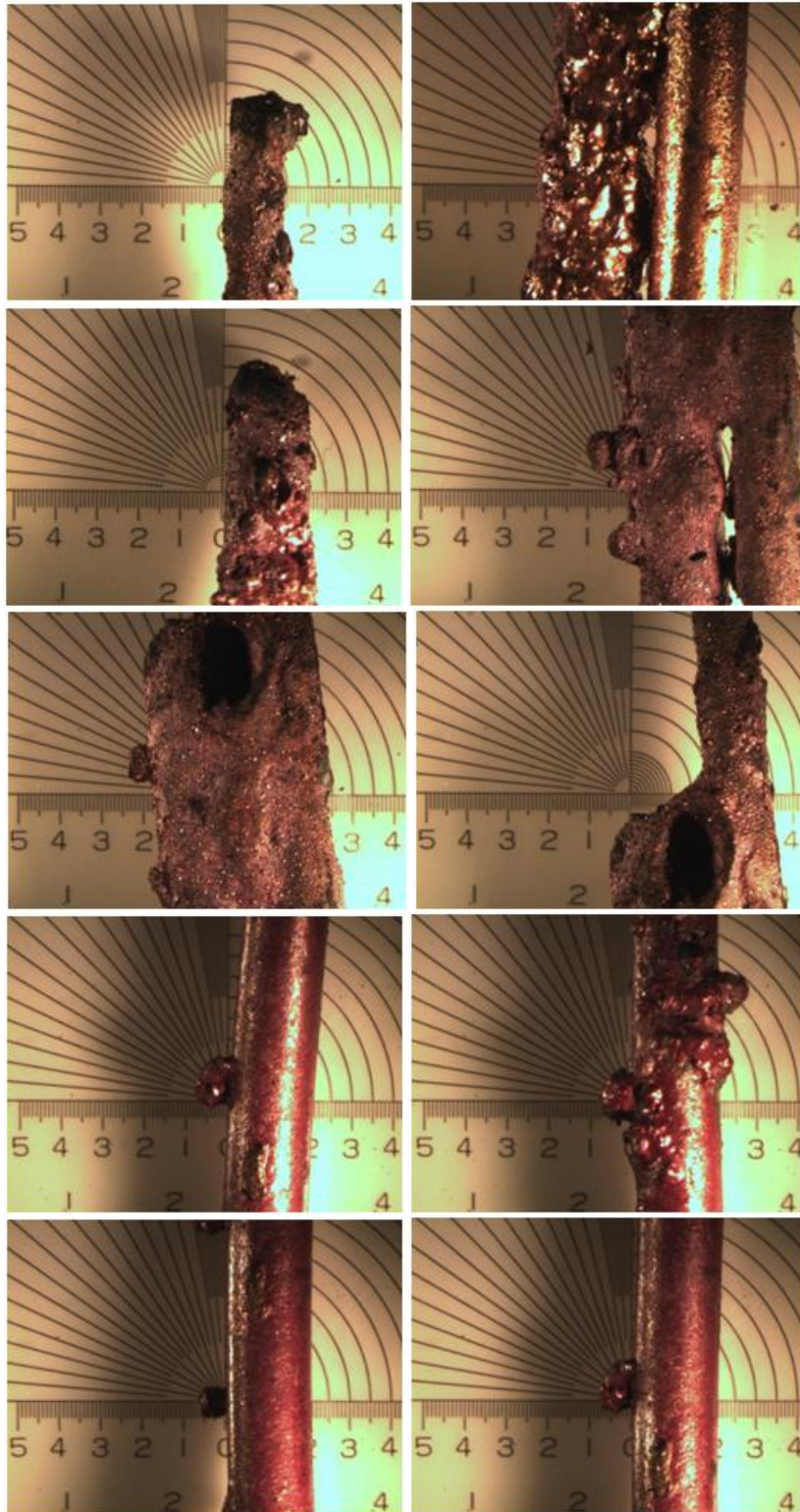


Figure 145: Full Scale, Romex 12-2, Loaded (Room No. 6)

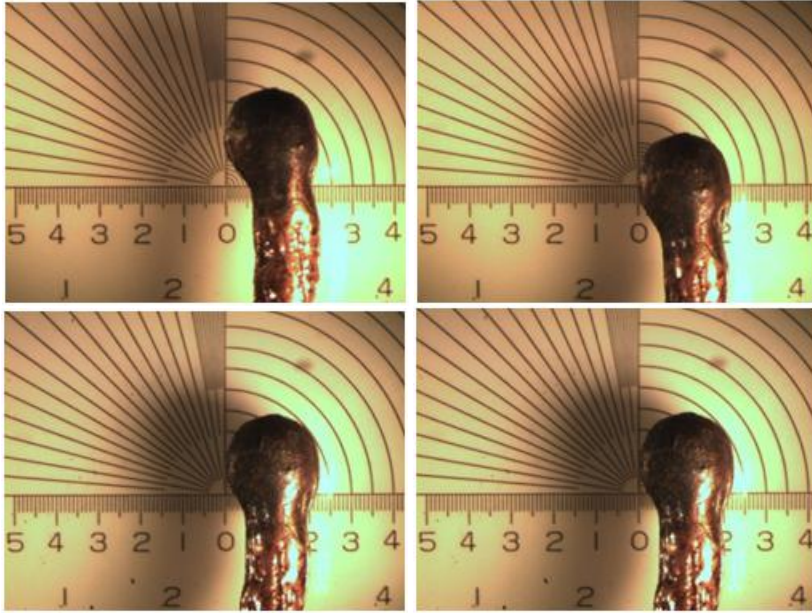


Figure 146: Full Scale, Romex 12-2, Loaded (Room No. 6)



**FULL SCALE COMPARTMENT TEST; MULTISTRAND 16-2 WIRE**

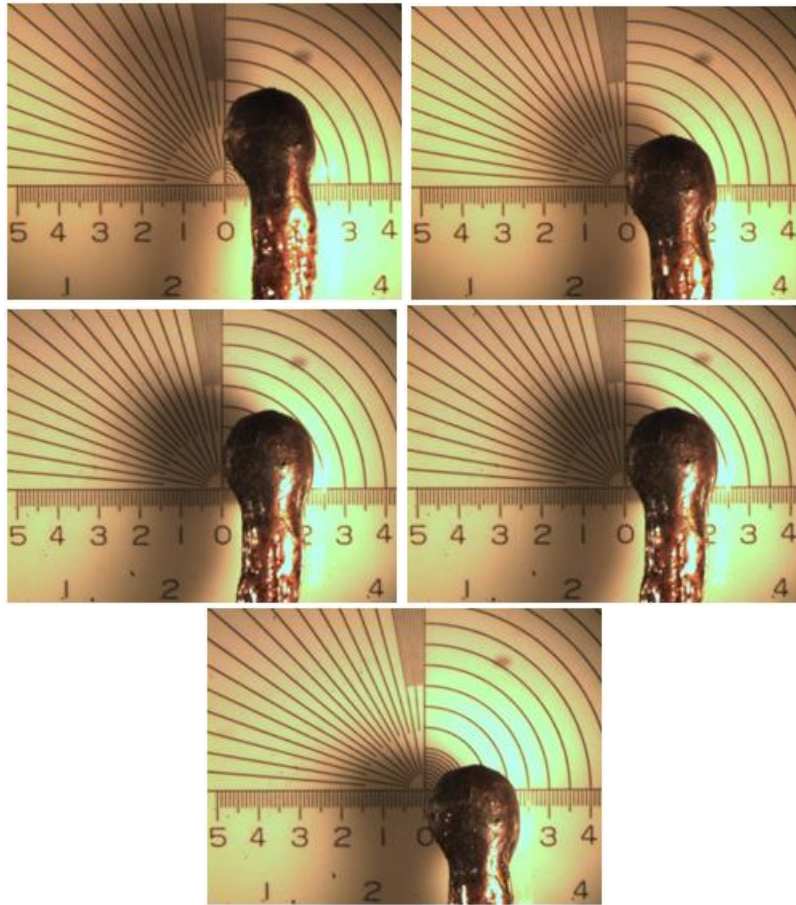


Figure 147: Full Scale, Multi-strand 16-2, Energized (Room No. 3)

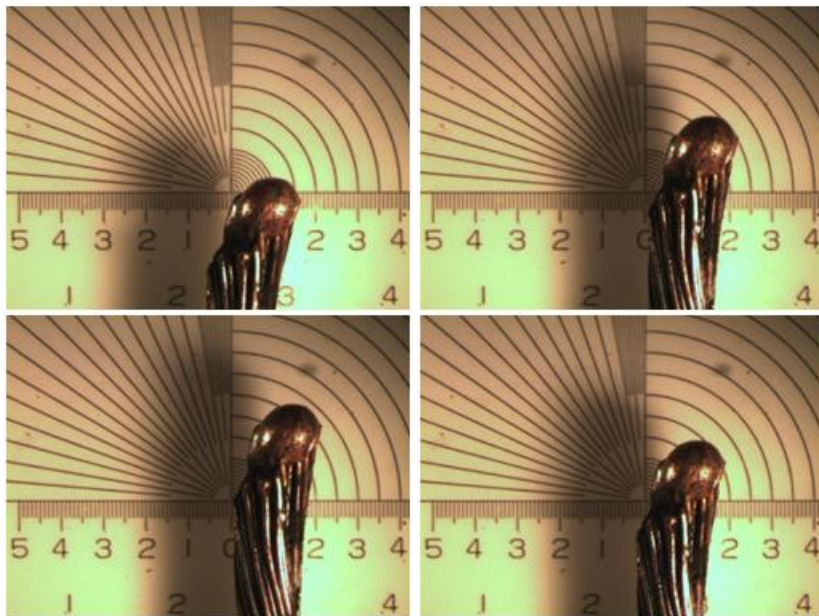


Figure 148: Full Scale, Multi-strand 16-2, Loaded (Room No. 3)

**FULL SCALE COMPARTMENT TEST; MULTISTRAND 18-2 WIRE**

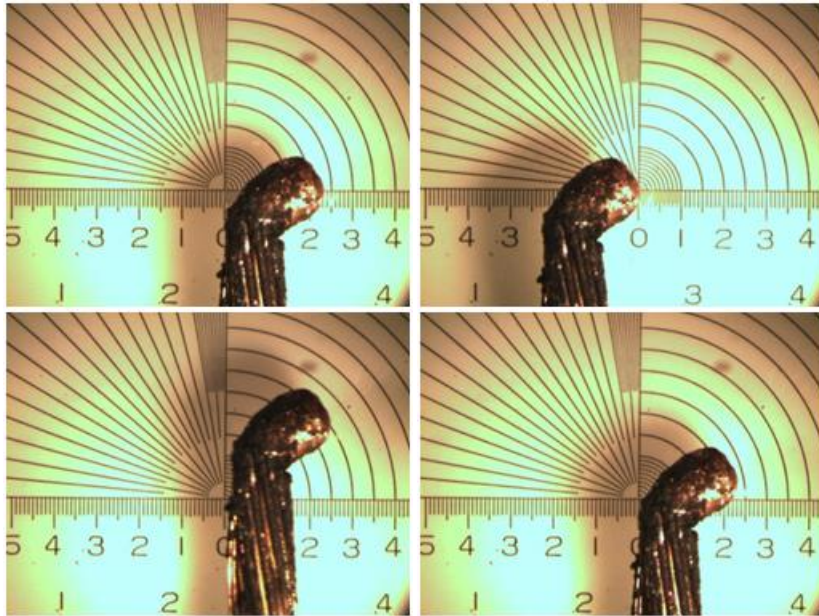


Figure 149: Full Scale, Multi-strand 18-2, Energized (Room No. 3)



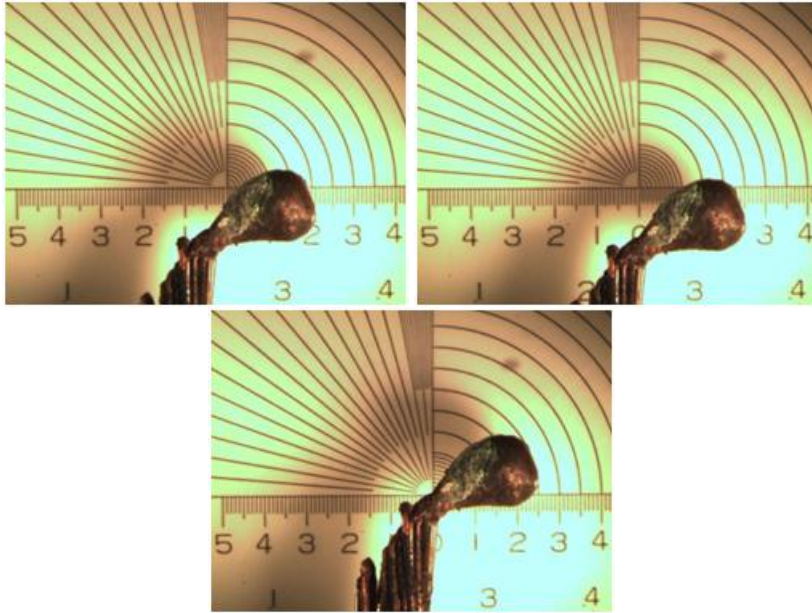


Figure 150: Full Scale, Multi-strand 18-2, Loaded (Room No. 5)

## **APPENDIX 2**

### **All Graphs of Testing Results**

<b>DF</b>	<b>Direct Flame</b>
<b>SC</b>	<b>Scaled Compartment</b>
<b>R</b>	<b>Radiation</b>
<b>FSC</b>	<b>Full-Scale Compartment</b>
<b>L</b>	<b>Energized with Load</b>
<b>E</b>	<b>Energized no-load</b>
<b>NE</b>	<b>Non-energized</b>

## 2A: Direct Flame Testing

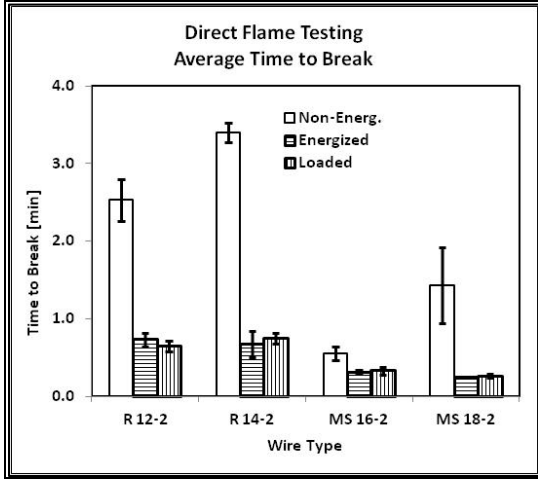


Figure A1: Average Time to Break (DF)

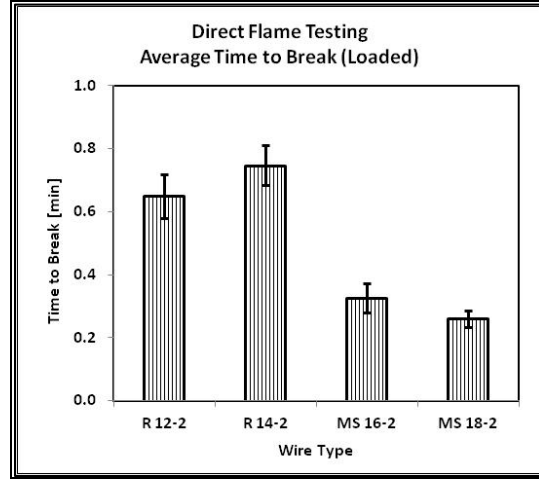


Figure A4: Average Time to Break Loaded (DF)

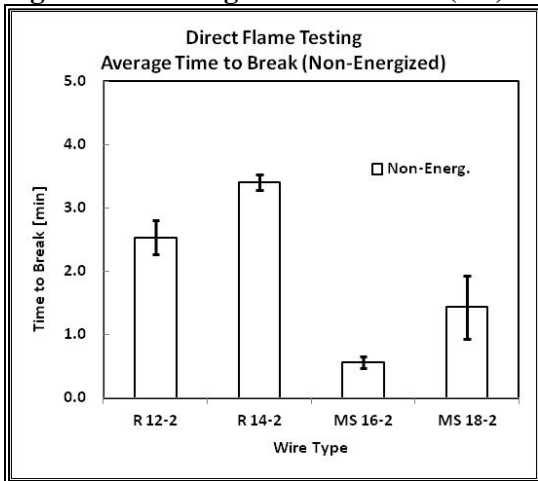


Figure A2: Average Time to Break Non-Energized (DF)

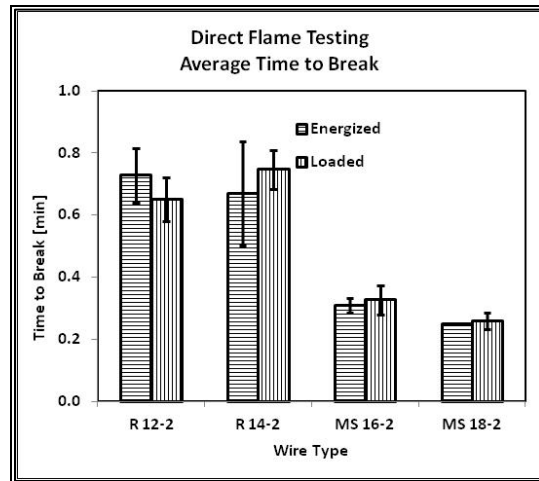


Figure A5: Average Time to Break Loaded vs Energized (DF)

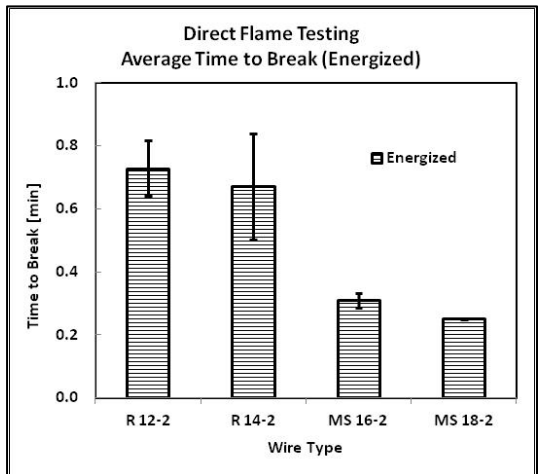
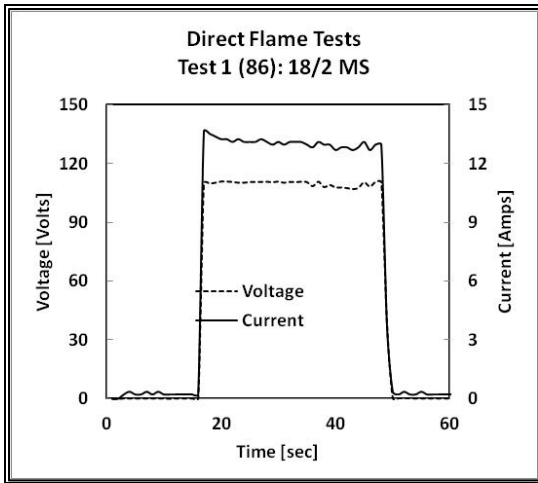
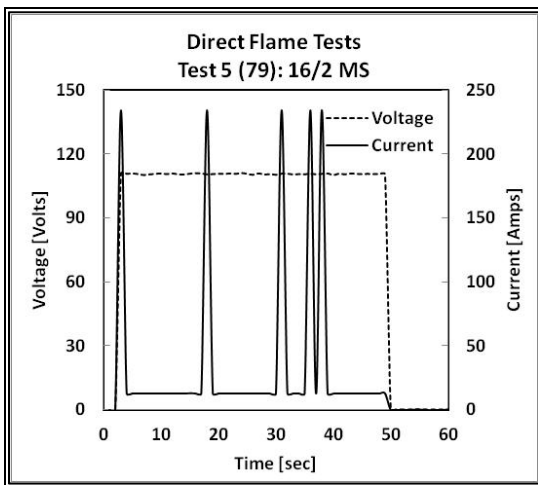


Figure A3: Average Time to Break Energized (DF)



**Figure A6: Test 1 (86): 18/2 MS (DF)**



**Figure A7: Test 5 (79): 16/2 MS (DF)**

## 2B: Radiation Tunnel Testing

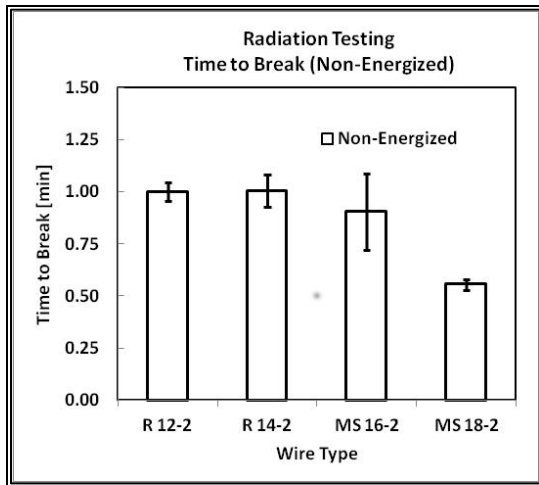


Figure B1: Time to Break Non Energized (R)

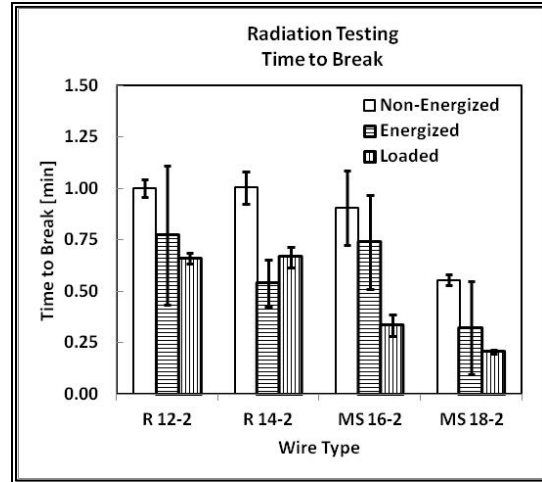


Figure B4: Time to Break Comparison (R)

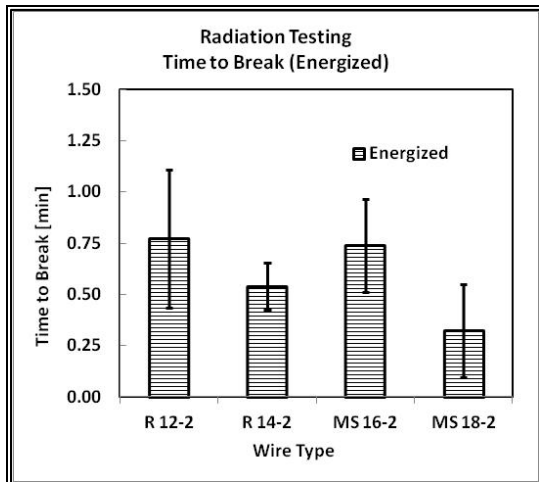


Figure B2: Time to Break Energized (R)

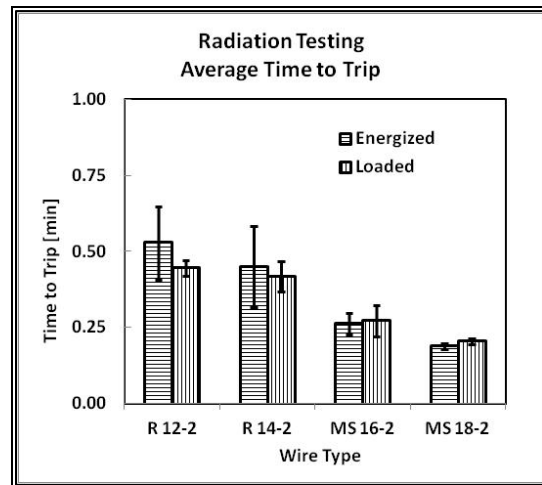


Figure B5: Average Time to Trip Loaded vs Energized (R)

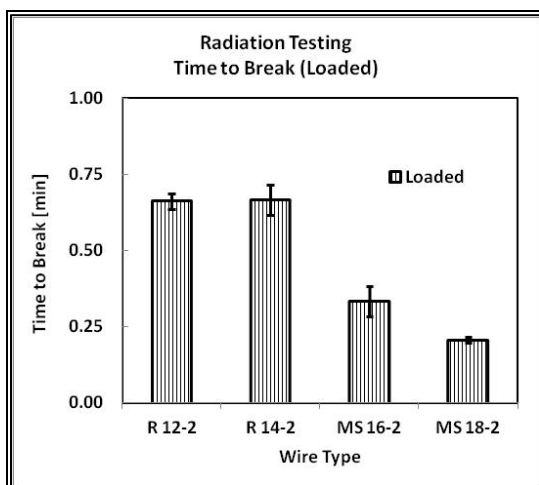


Figure B3: Time to Break Loaded (R)

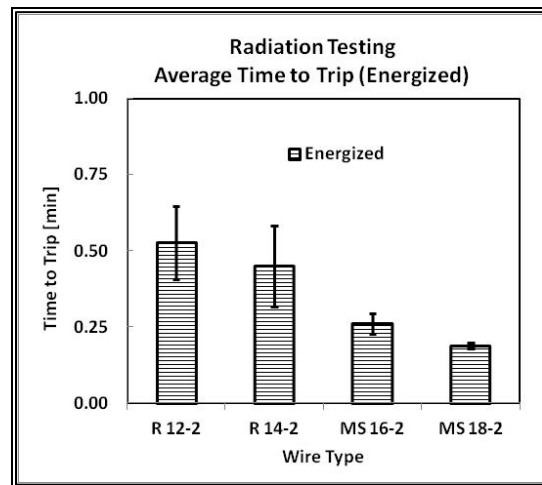


Figure B6: Average Time to Trip Energized (R)

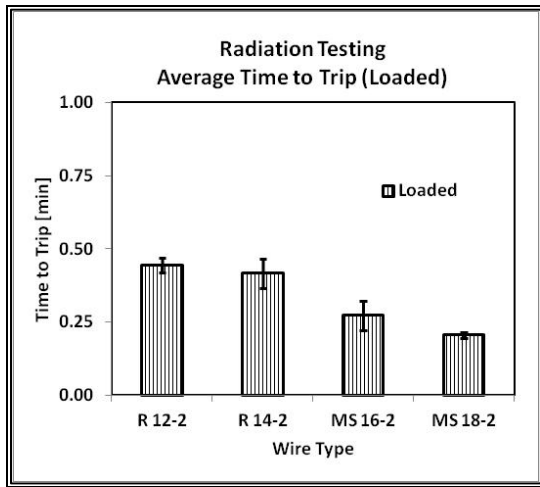


Figure B7: Average Time to Trip Loaded (R)

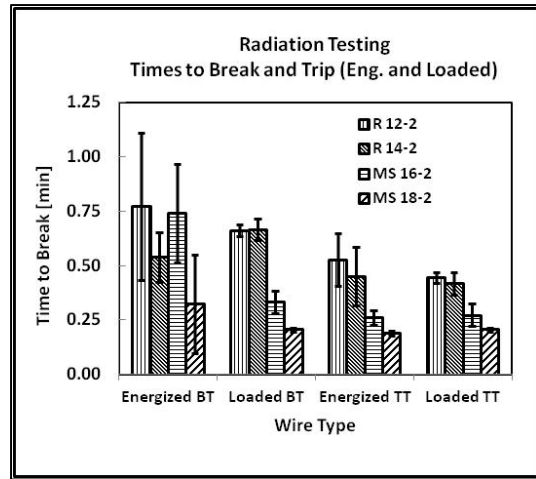


Figure B8: Times to Break and Trip Energ. and Loaded (R)



## 2C: Scaled Compartment Testing

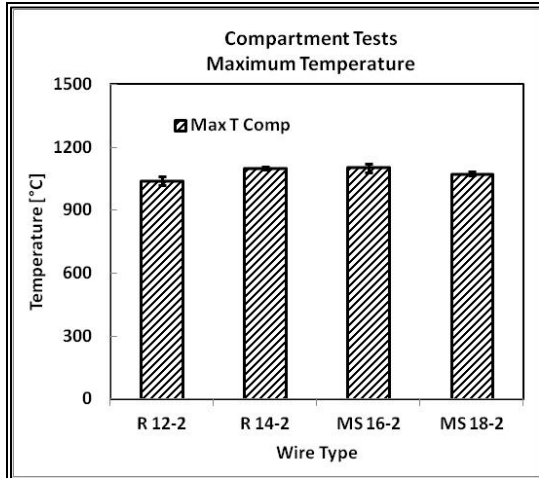


Figure C1: Maximum Temperature (SC)

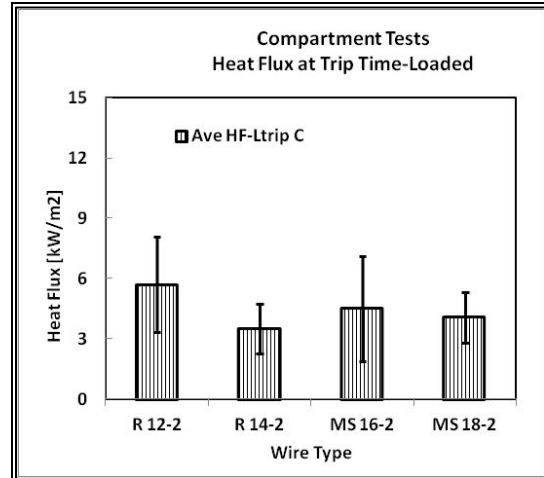


Figure C4: Heat Flux at Trip Time Loaded (SC)

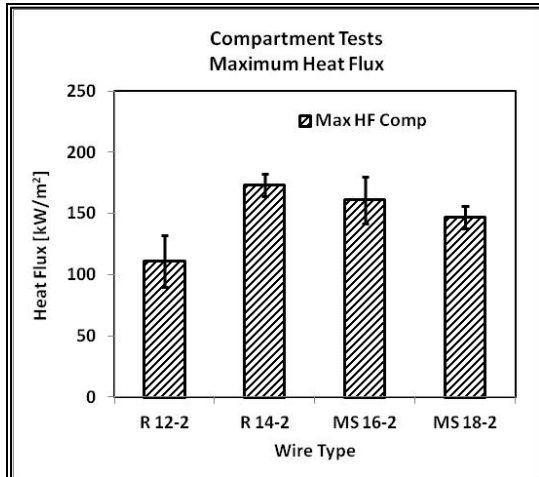


Figure C.2: Maximum Heat Flux (SC)

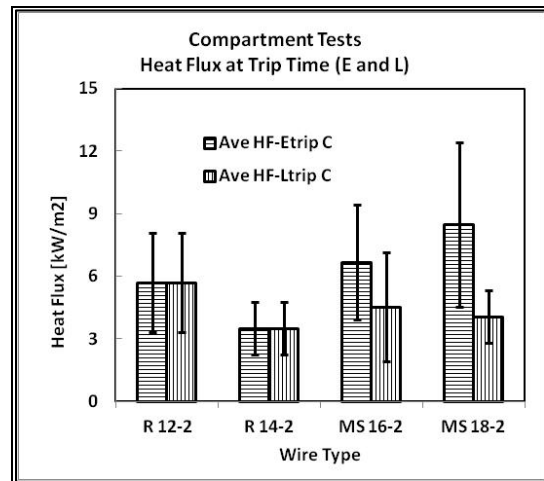


Figure C5: Heat Flux at Trip Time (SC)

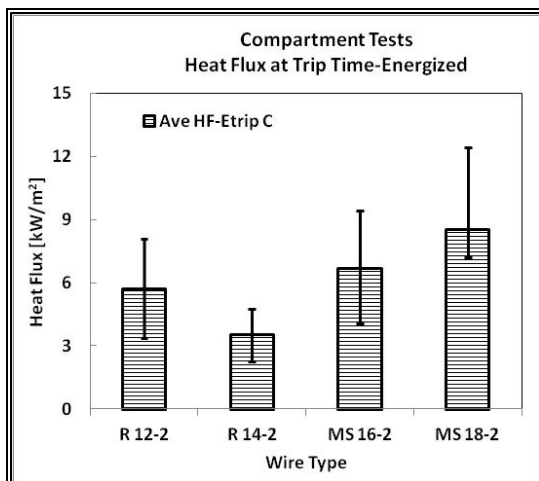


Figure C3: Heat Flux at Trip Time Energized (SC)

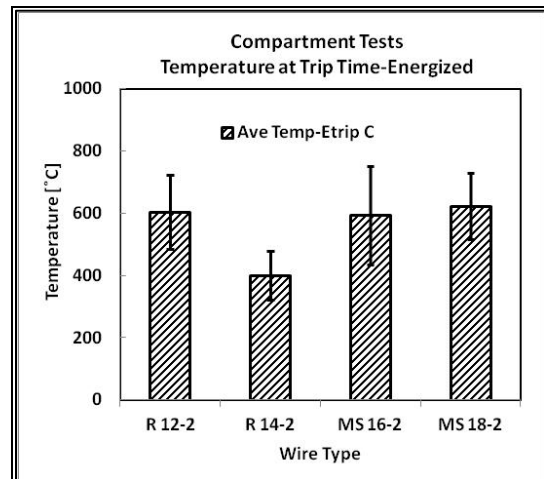


Figure C6: Temperature at Trip Time Energized (SC)

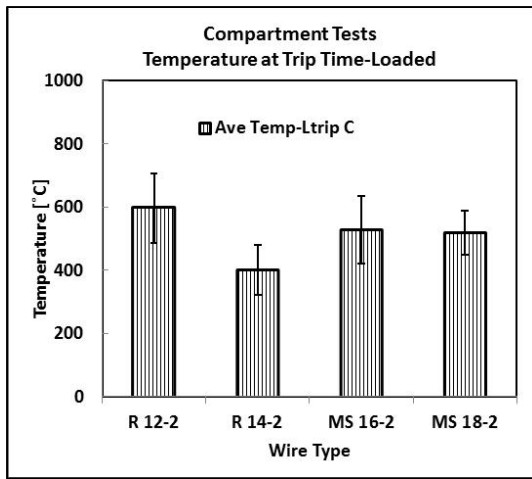


Figure C7: Temperature at Trip Time Loaded (SC)

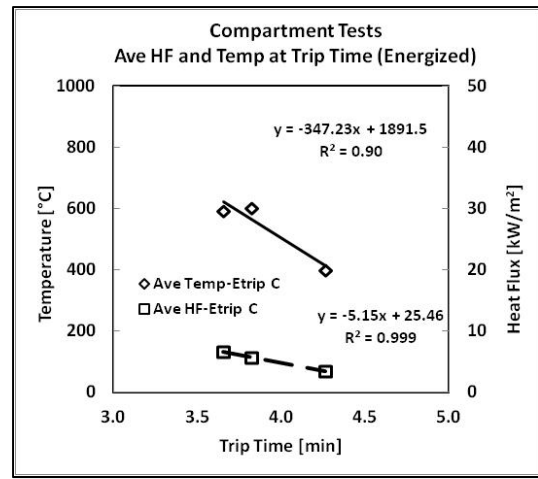


Figure C10: Avg HF and Temp at Trip Time Energized (SC)

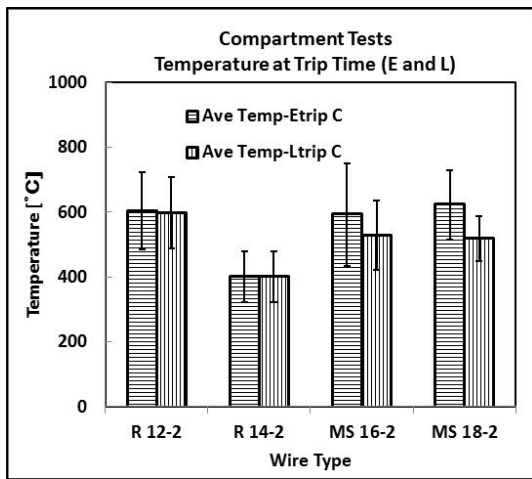


Figure C8: Avg Temperature at Trip Time Load/Ener (SC)

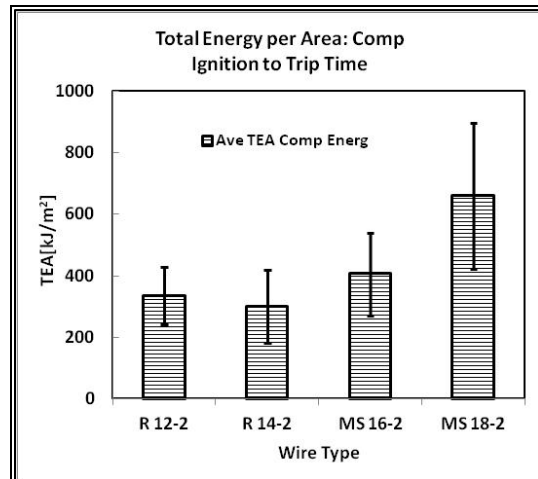


Figure C11: Total Energy per Area (SC)

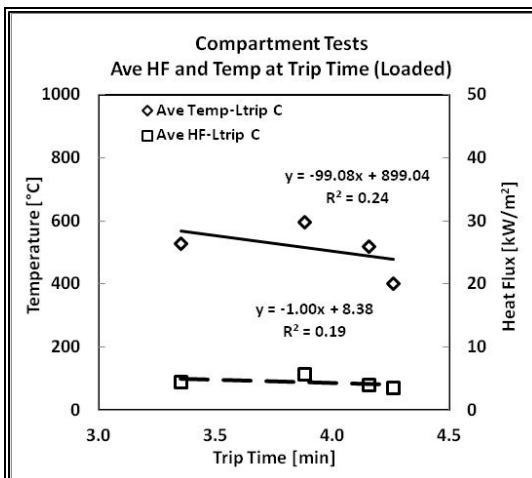


Figure C9: Avg HF and Temp at Trip Time Loaded (SC)

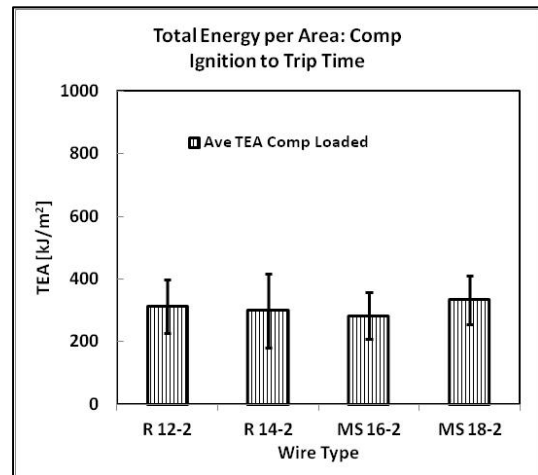


Figure C12: Total Energy per Area (SC)

## 2D: Full-Scale Compartment Testing

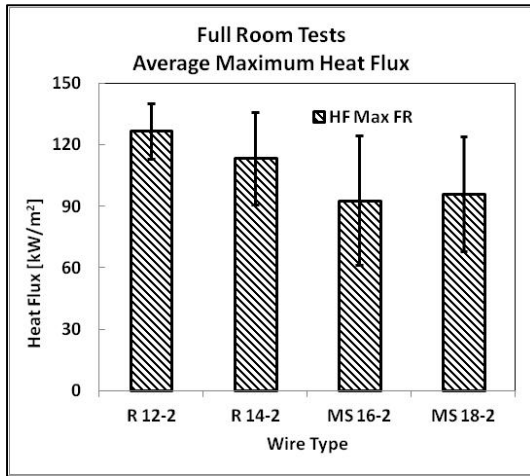


Figure D1: Average Maximum Heat Flux (FSC)

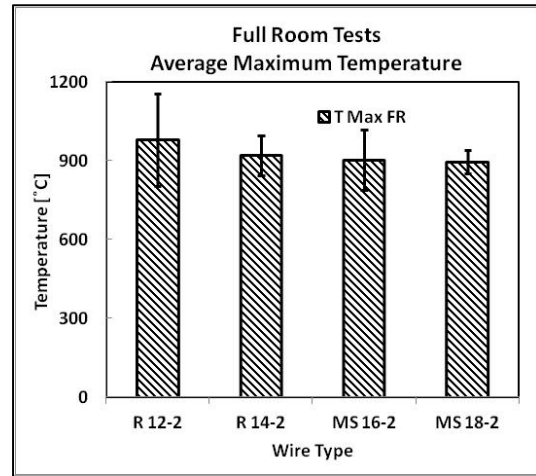


Figure D4: Average Maximum Temperature (FSC)

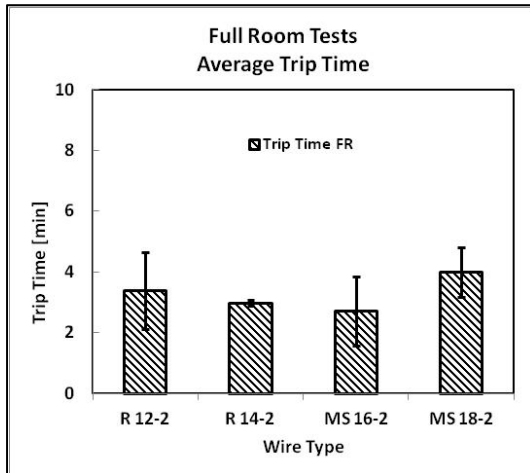


Figure D2: Average Trip Time (FSC)

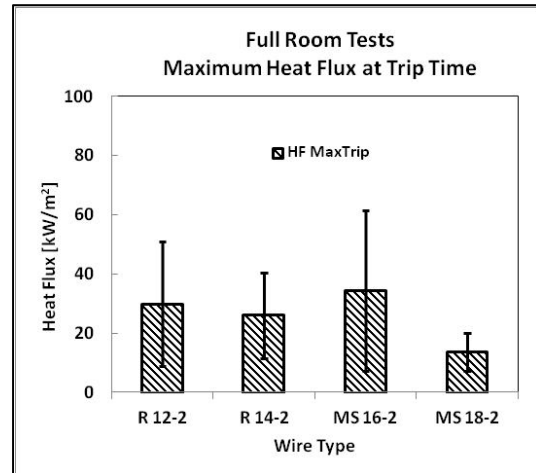


Figure D5: Maximum Heat Flux at Trip Time (FSC)

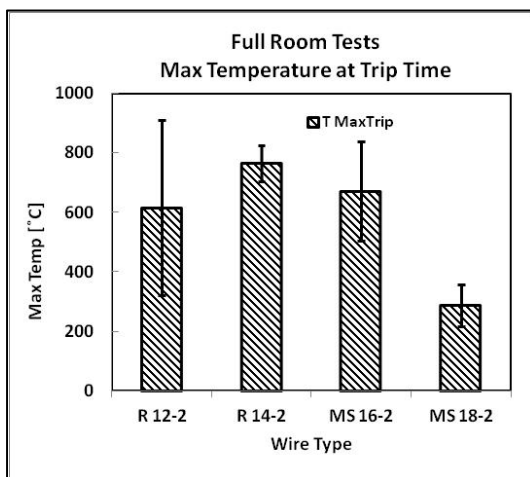


Figure D3: Maximum Temperature at Trip Time (FSC)

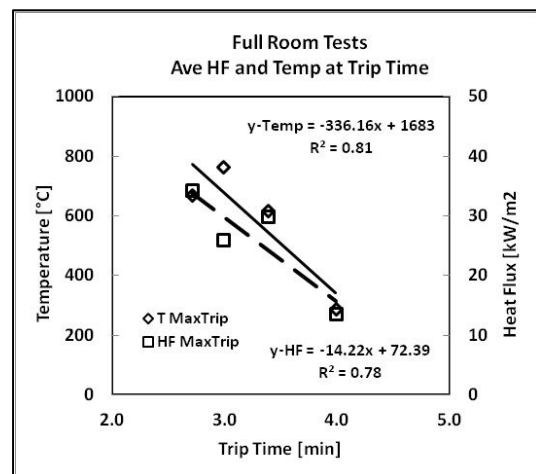
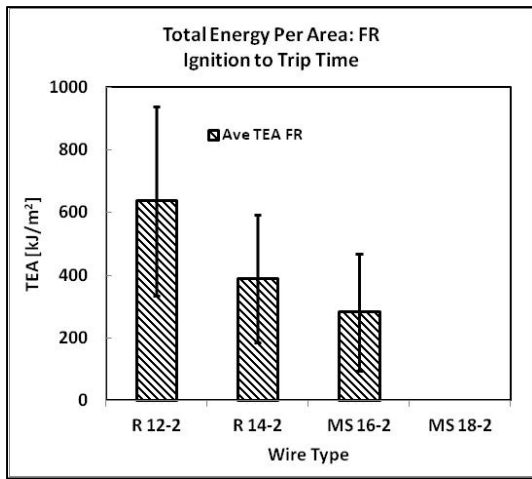


Figure D6: Avg HF and Temp at Trip Time Loaded (FSC)



**Figure D7: Total Energy per Area (FSC)**

## II-E: Full Room and Compartment Compare

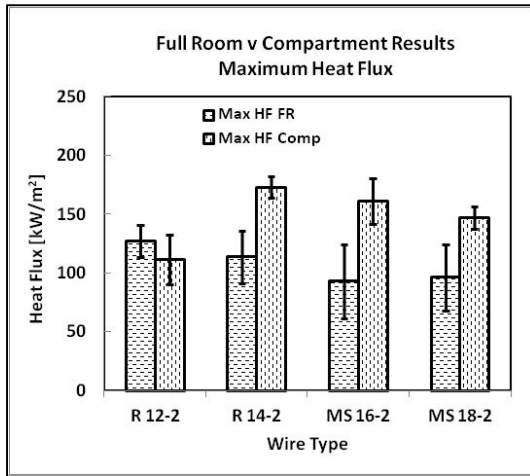


Figure E1: Maximum Temperature (FSC vs SC)

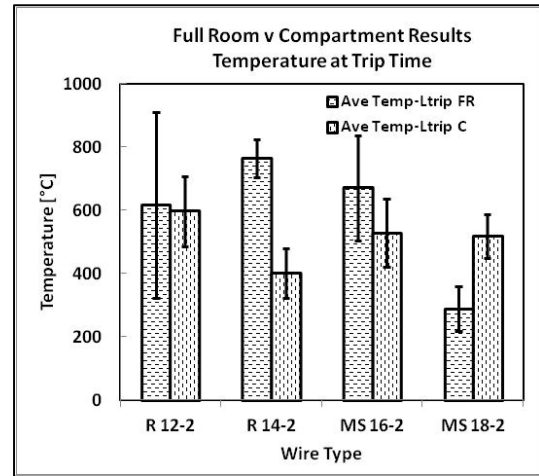


Figure E4: Temperature at Trip Time (FSC vs SC)

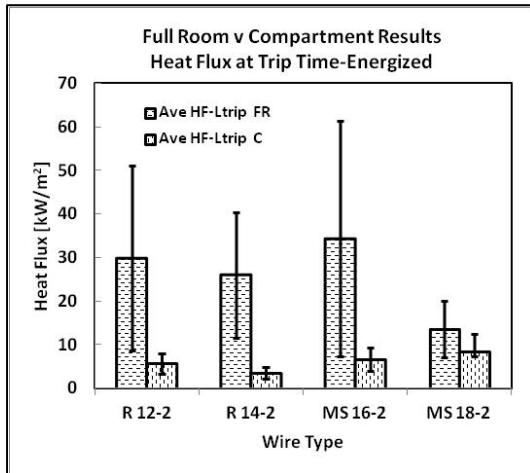


Figure E2: Heat Flux at Trip Time-Energized (FSC vs SC)

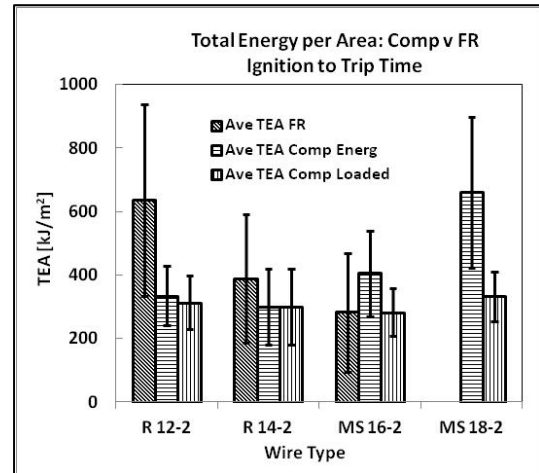


Figure E5: Total Energy per Area (FSC v SC)

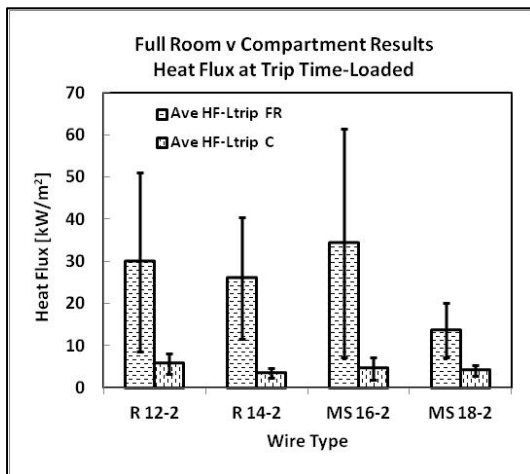


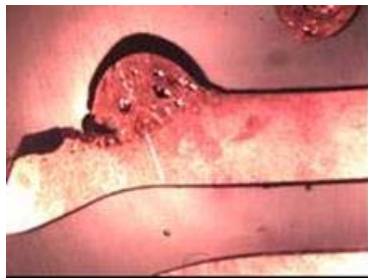
Figure E3: Heat Flux at Trip Time-Loaded (FSC vs SC)

## **APPENDIX 3**

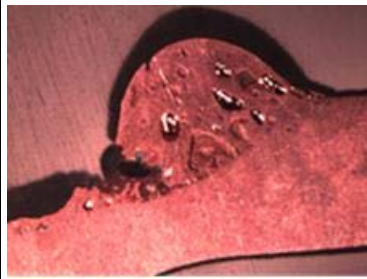
### **Stereo Microscope of Internal Structures of Beads**

<b>DF</b>	<b>Direct Flame</b>
<b>SC</b>	<b>Scaled Compartment</b>
<b>R</b>	<b>Radiation</b>
<b>FSC</b>	<b>Full-Scale Compartment</b>
<b>L</b>	<b>Energized with Load</b>
<b>E</b>	<b>Energized no-load</b>
<b>NE</b>	<b>Non-energized</b>

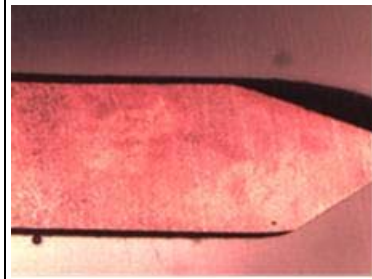
12R-L-DF (S32)



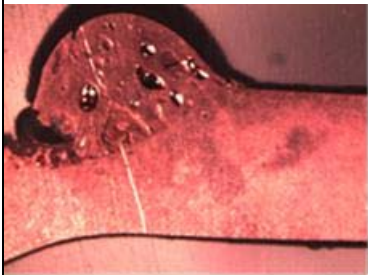
7X



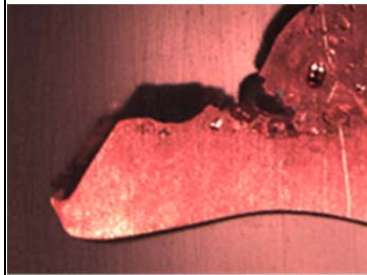
14X



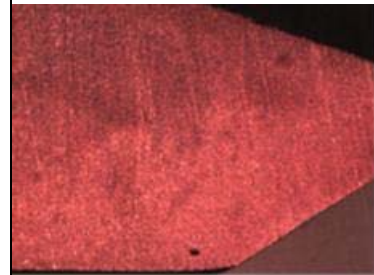
14X-1



14X-2



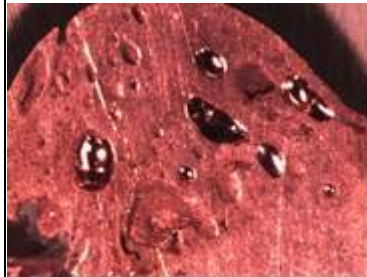
14X-3



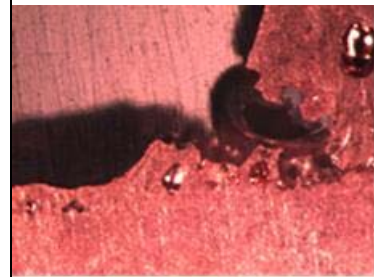
28X-1



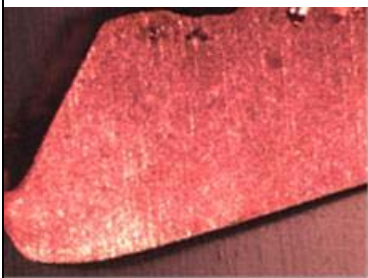
28X-2



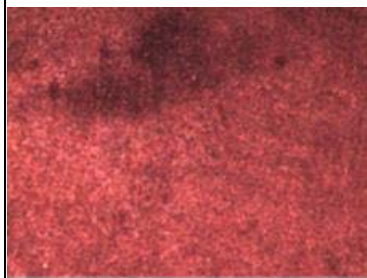
28X-3



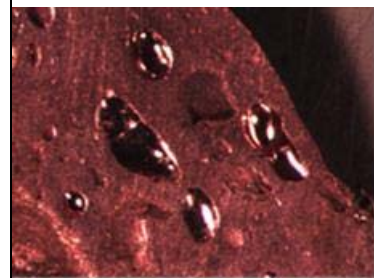
28X-4



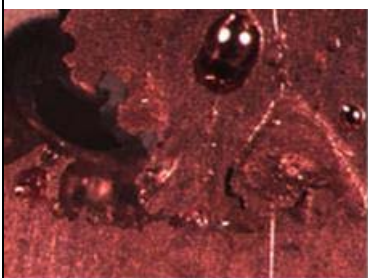
28X-5



44X-1



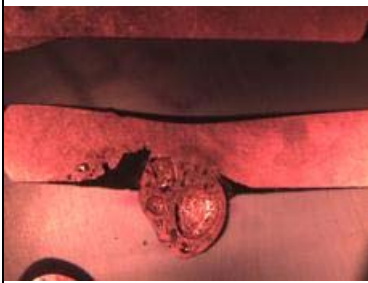
44X-2



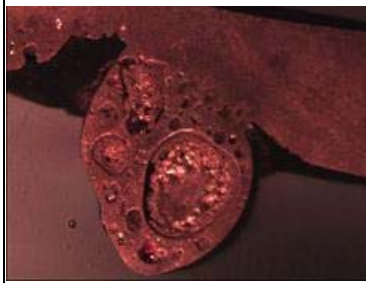
44X-3



12R-L-DF (S33)



7X



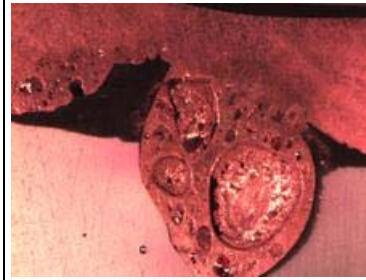
14X



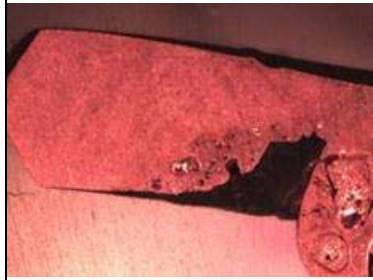
14X-1



14X-2



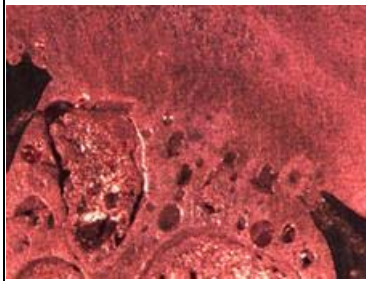
14X-3



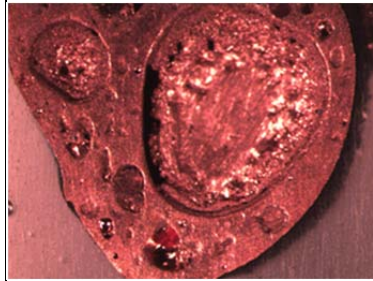
14X-4



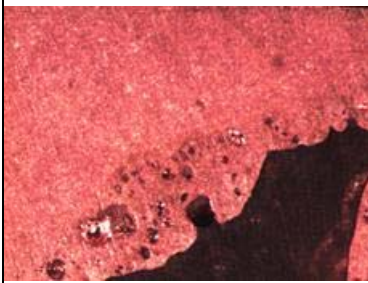
28X-1



28X-2



28X-3



28X-4



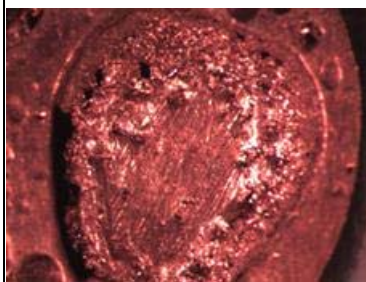
28X-5



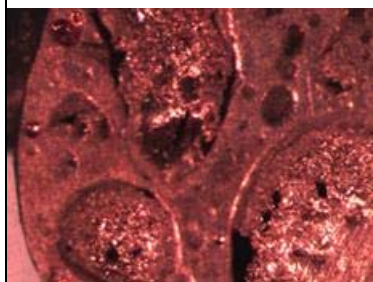
28X-6



44X-1



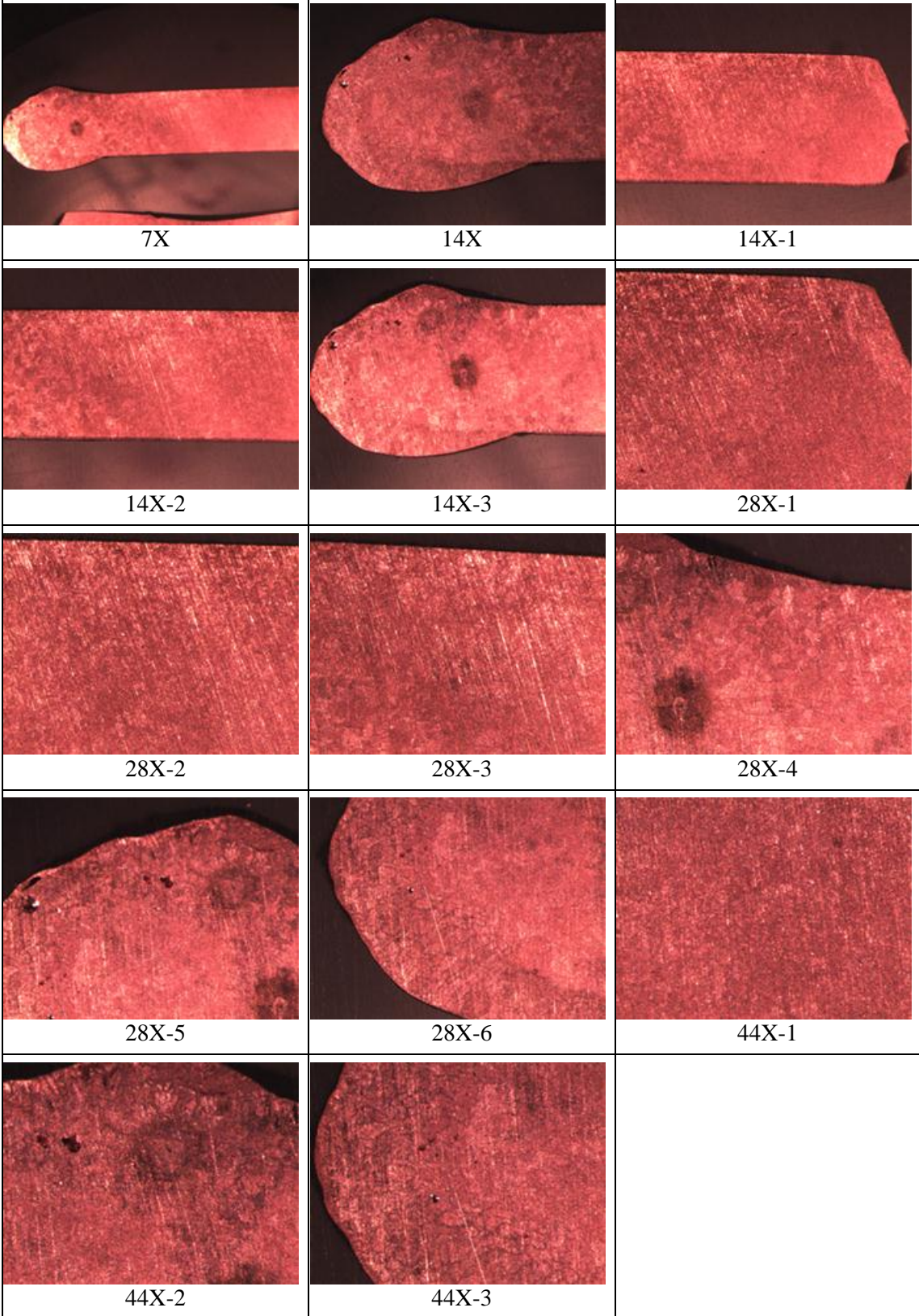
44X-2



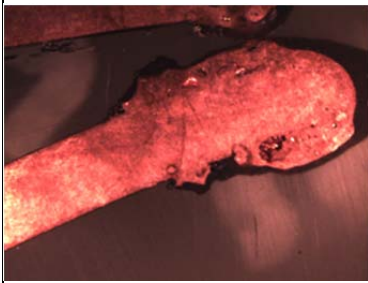
44X-3



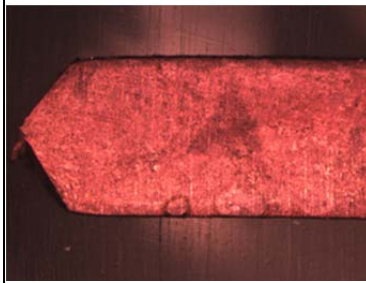
12R-L-DF (S34)



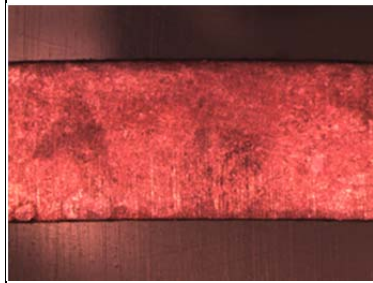
12R-L-SC (S41)



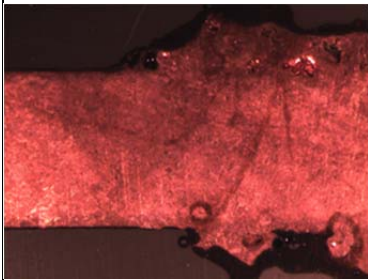
7X



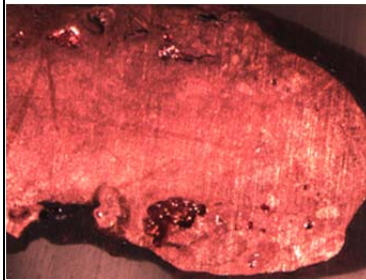
14X-1



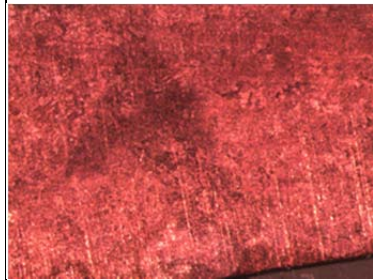
14X-2



14X-3



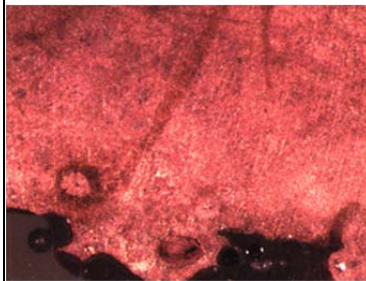
14X-4



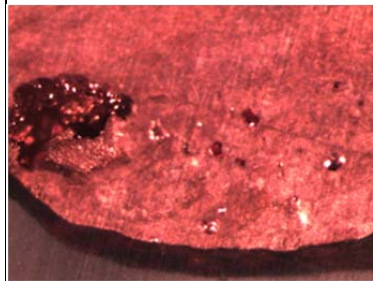
28X-1



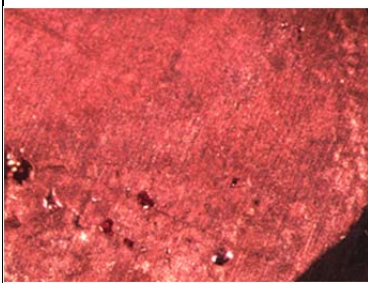
28X-2



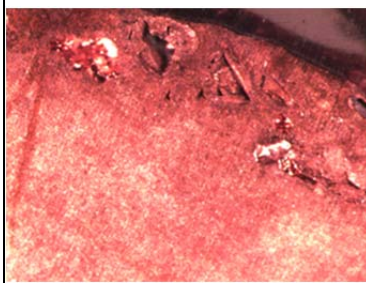
28X-3



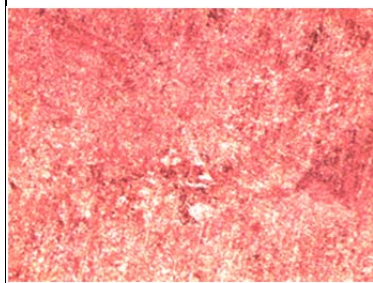
28X-4



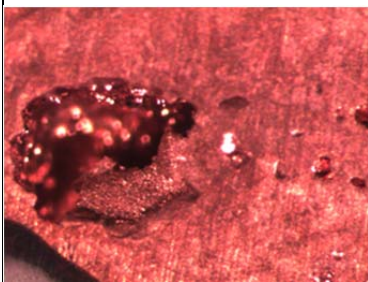
28X-5



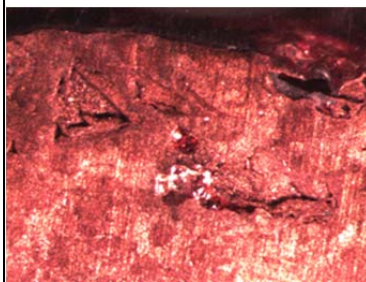
28X-6



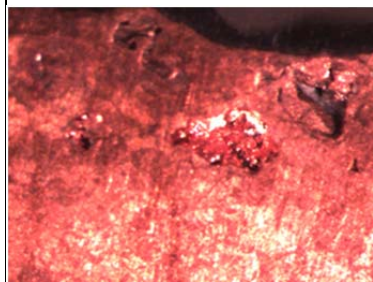
44X-1



44X-2

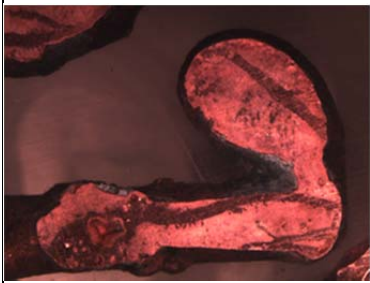


44X-3

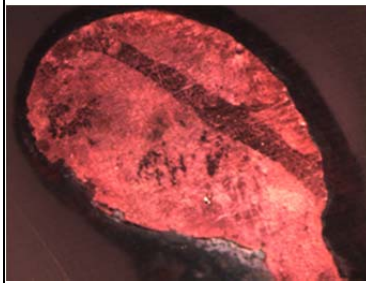


44X-4

12R-L-SC (S42)



7X



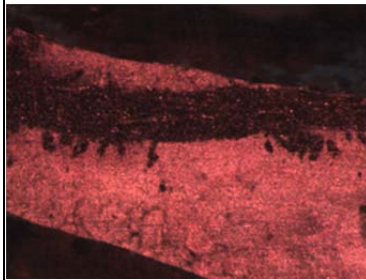
14X-1



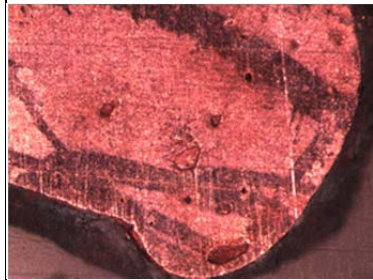
14X-2



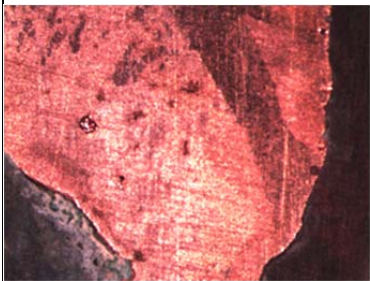
28X-1



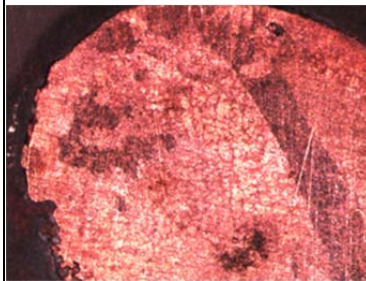
28X-2



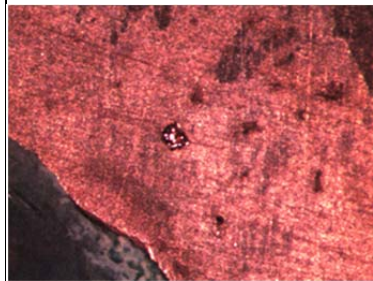
28X-3



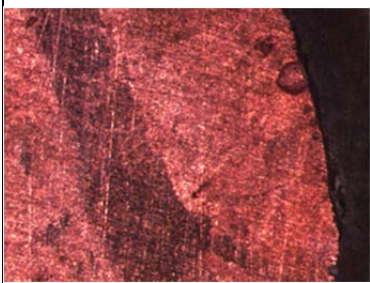
28X-4



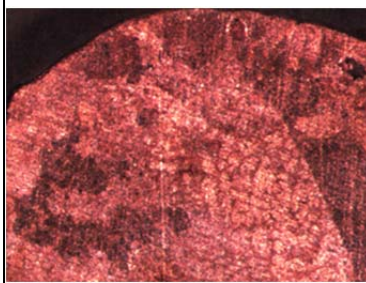
28X-5



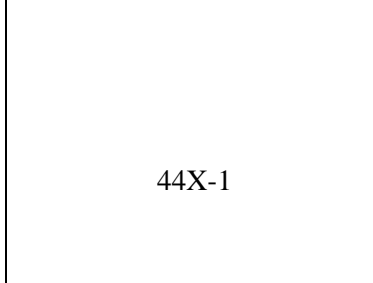
44X-1



44X-2

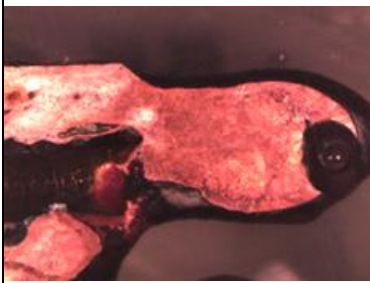


44X-3

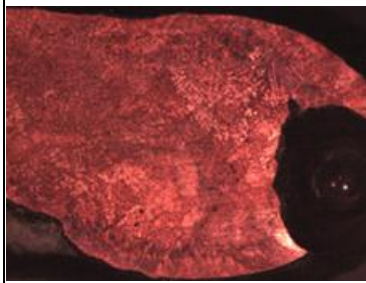


44X-1

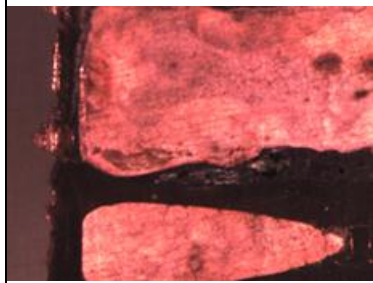
12R-L-SC (S43)



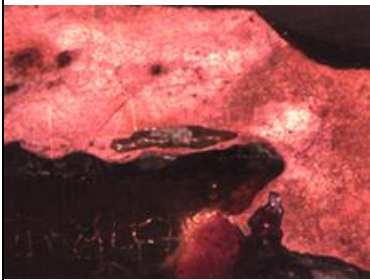
7X



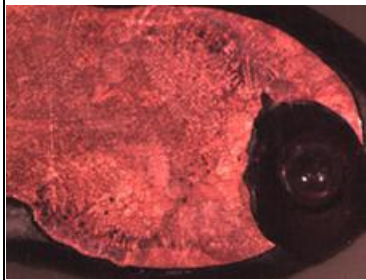
14X-1



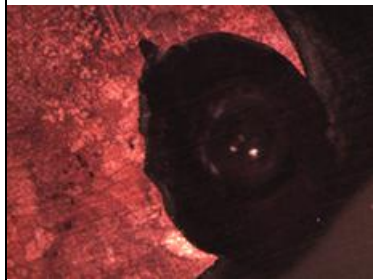
14X-2



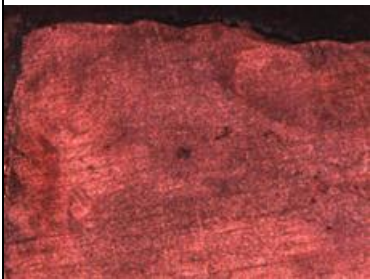
14X-3



14X-4



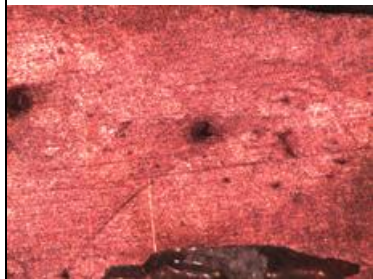
21X-1



28X-1



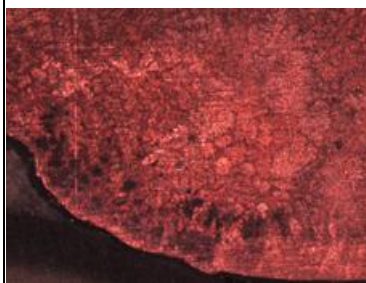
28X-2



28X-3



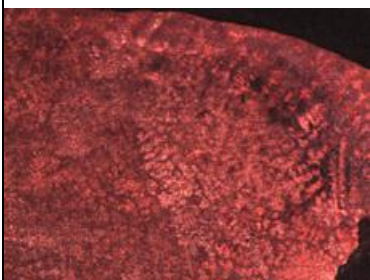
28X-4



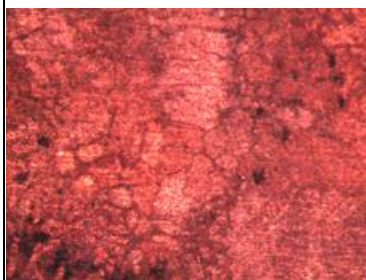
28X-5



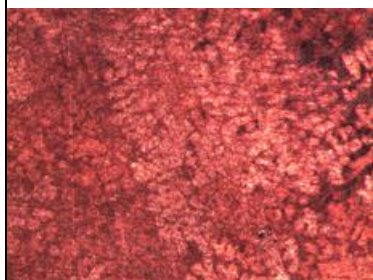
28X-6



28X-7

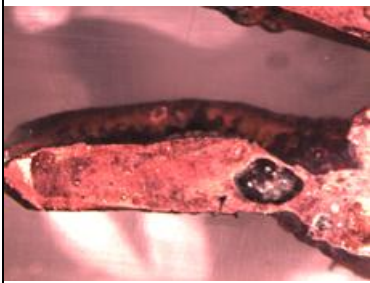


44X-1

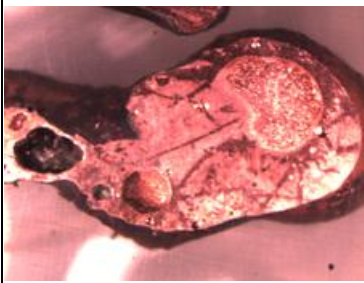


44X-2

12R-L-R (S50)



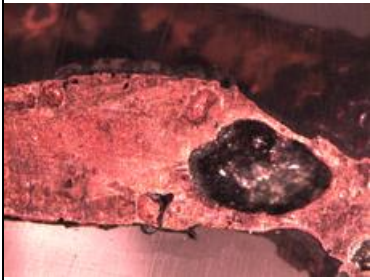
7X-1



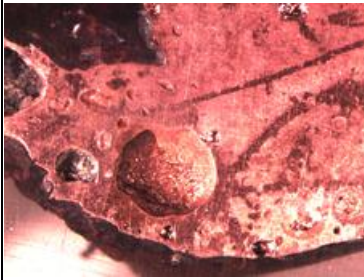
7X-2



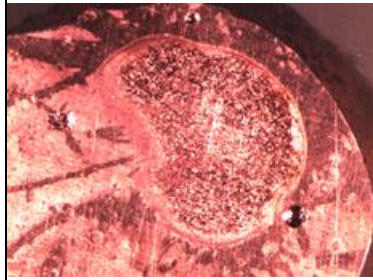
14X-1



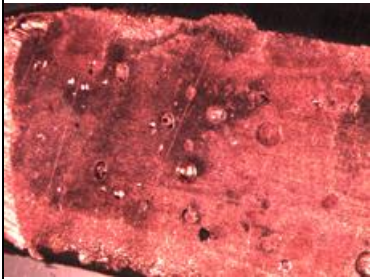
14X-2



14X-3



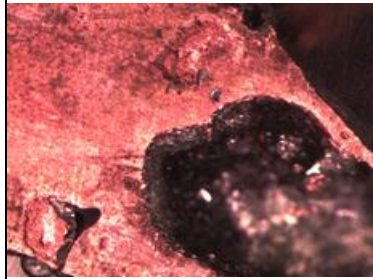
14X-4



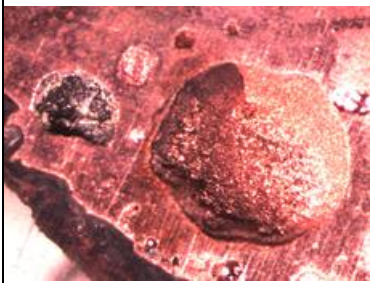
28X-1



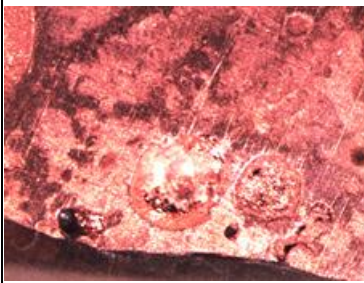
28X-2



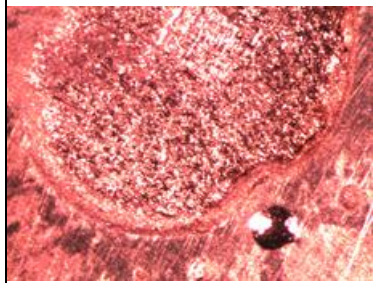
28X-3



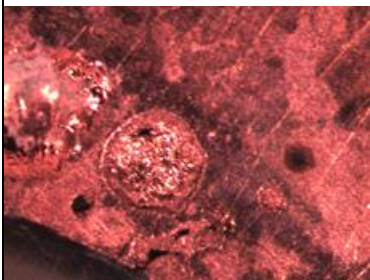
28X-4



28X-5



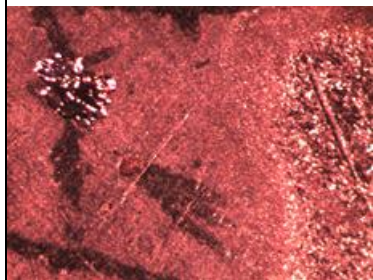
28X-7



44X-2

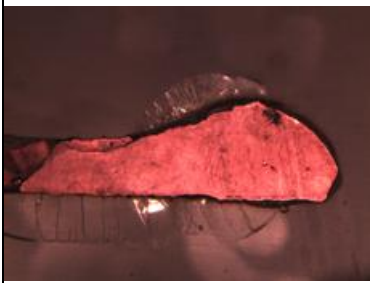


44X-3

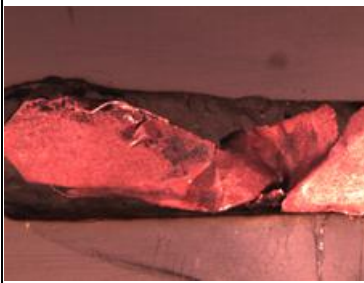


44X-4

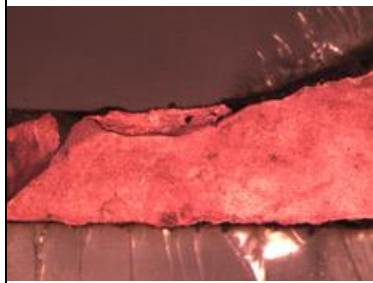
12R-L-R (S51)



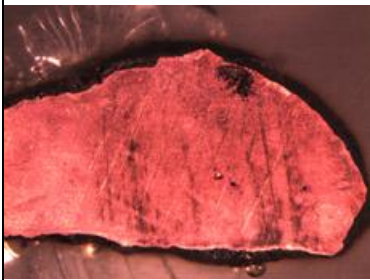
7X-1



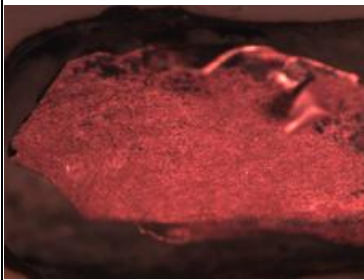
14X-1



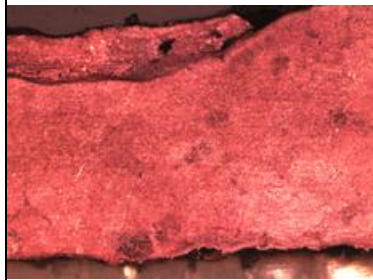
14X-2



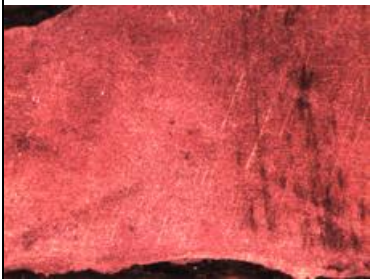
14X-3



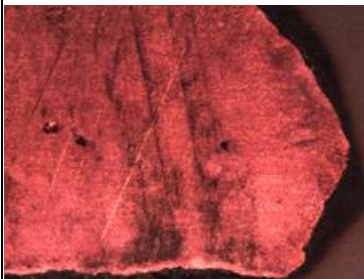
28X-1



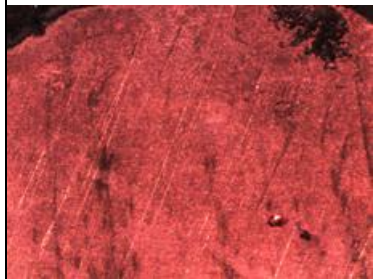
28X-2



28X-3



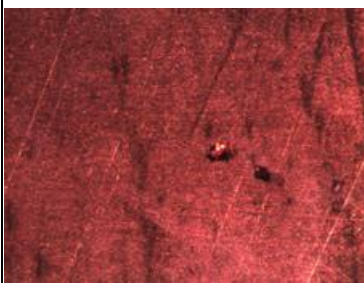
28X-4



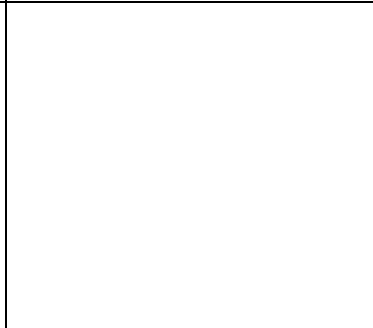
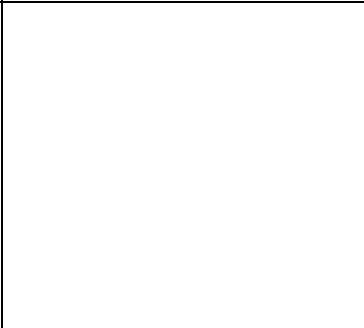
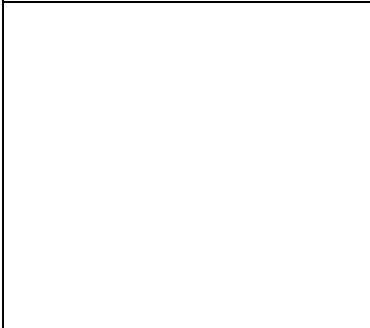
28X-5



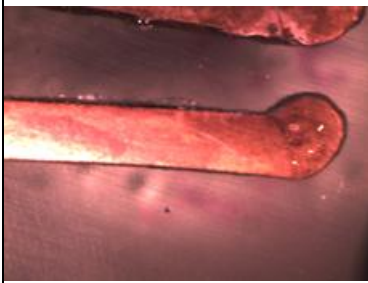
44X-1



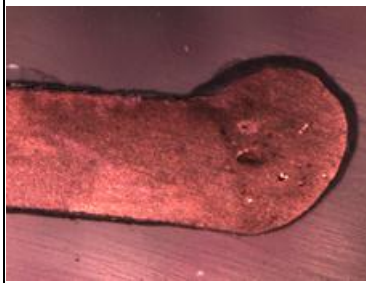
44X-2



12R-L-R (S52)



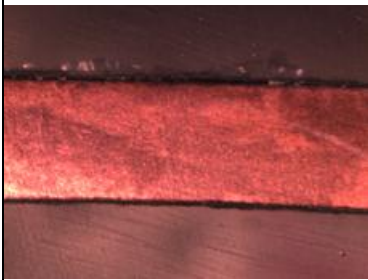
7X



14X



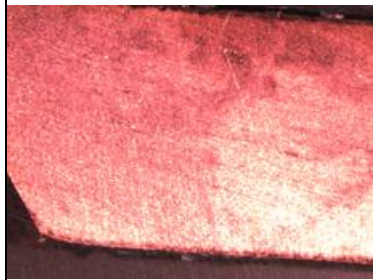
14X-1



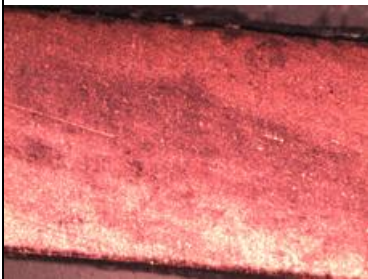
14X-2



14X-3



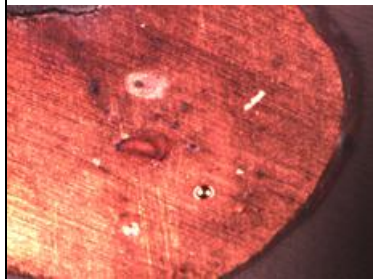
28X-1



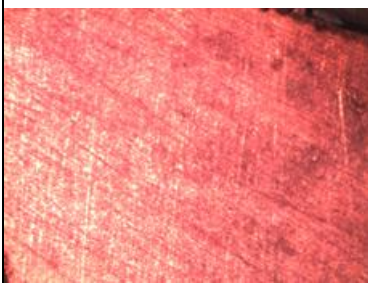
28X-2



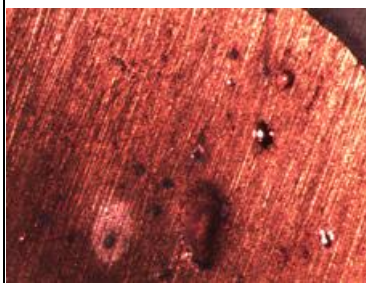
28X-3



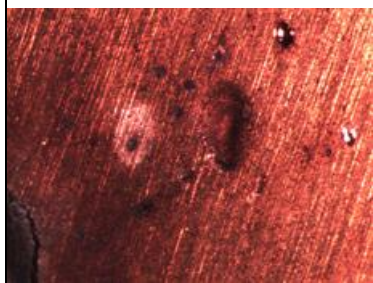
28X-4



44X-1

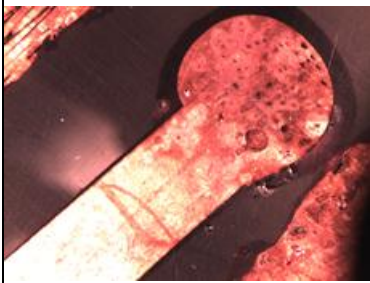


44X-2

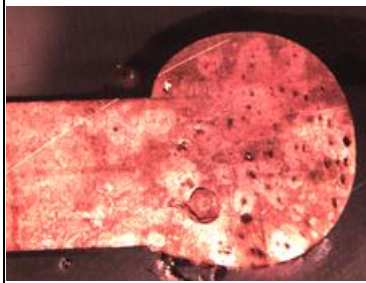


44X-3

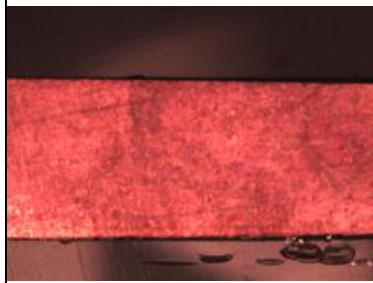
12R-NE-DF (S29)



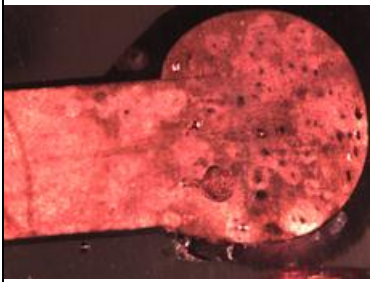
7X



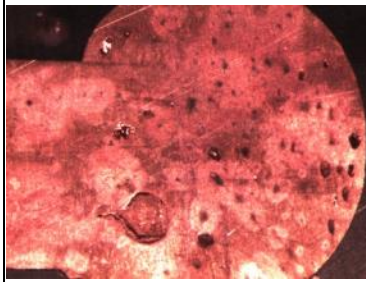
14X



14X-1



14X-2



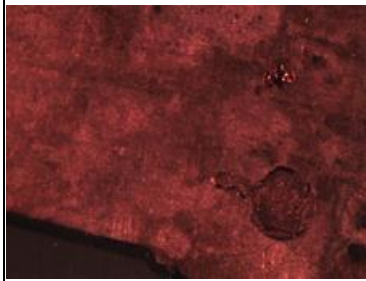
21X-1



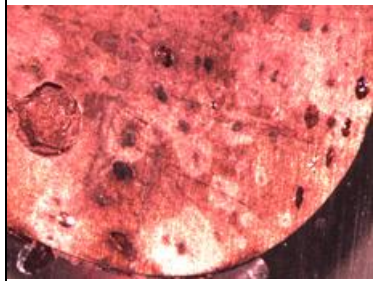
28X-1



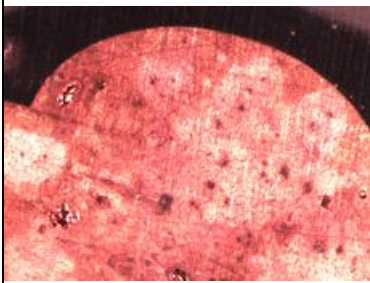
28X-2



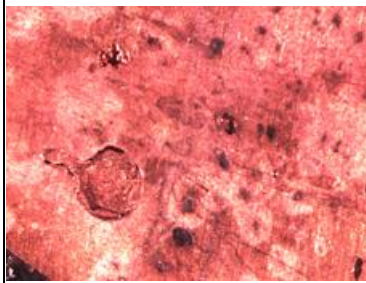
28X-3



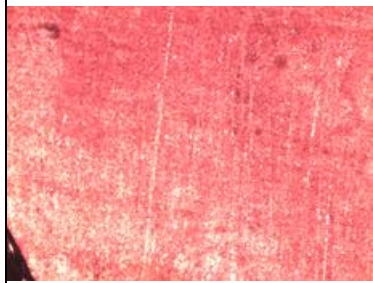
28X-4



28X-5



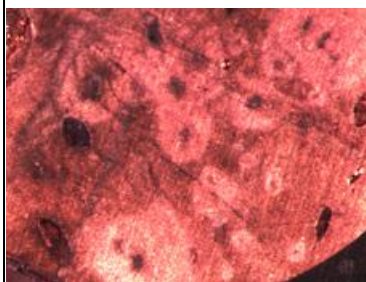
28X-6



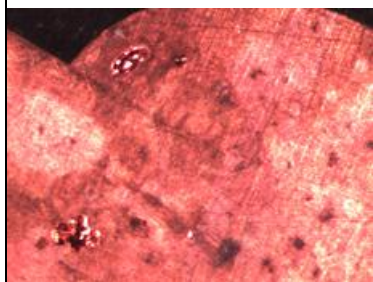
44X-1



44X-2





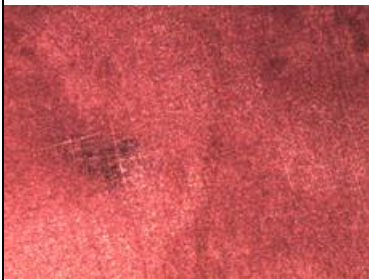
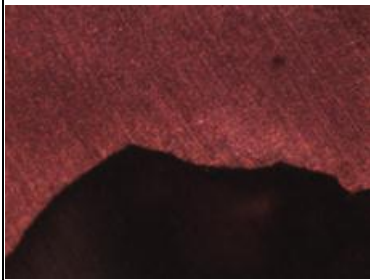
44X-3



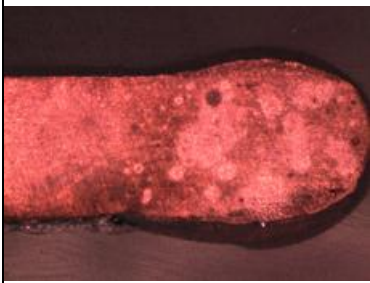
44X-4



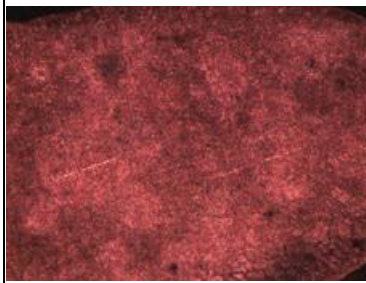
**12R-NE-DF (S30) (BEAD wasn't cut Properly)**

		
14X	28X-1	28X-2
		
28X-3	28X-4	

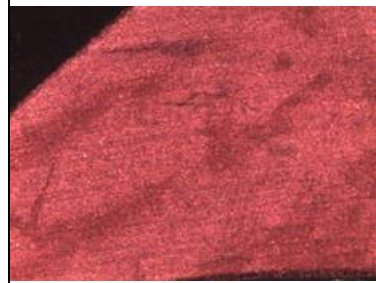
**12R-NE-DF (S31)**



14X



28X



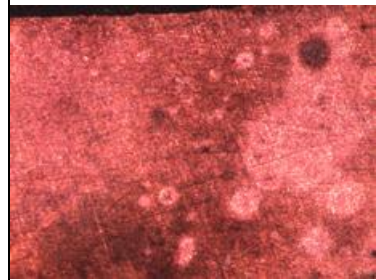
28X-1



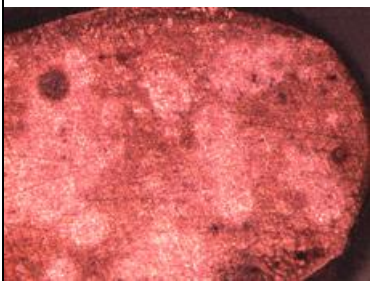
28X-2



28X-3



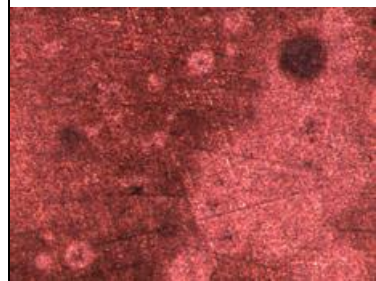
28X-4



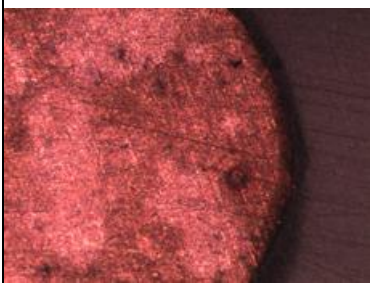
28X-5



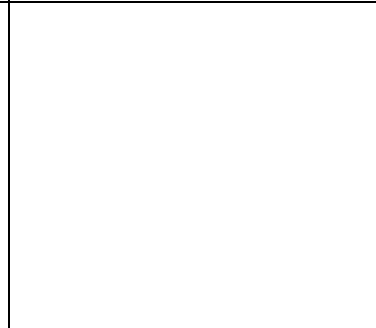
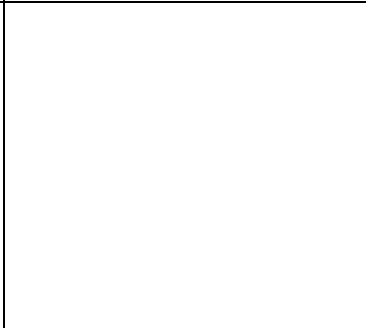
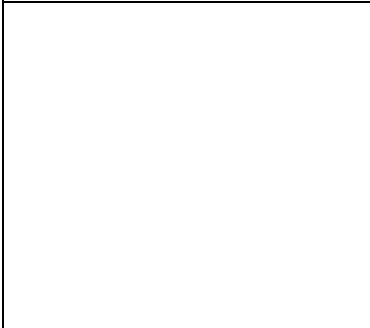
44X-1



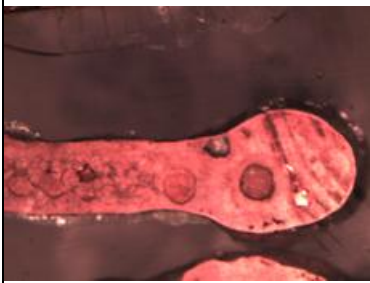
44X-2



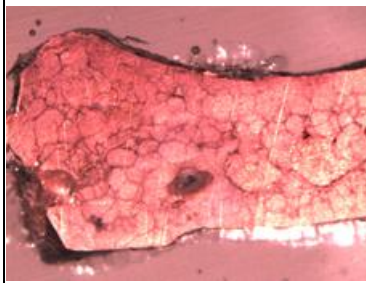
44X-3



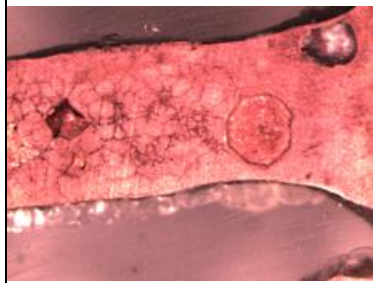
12R-NE-SC (S38)



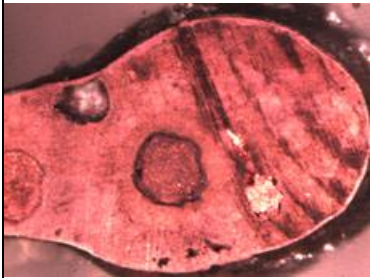
7X



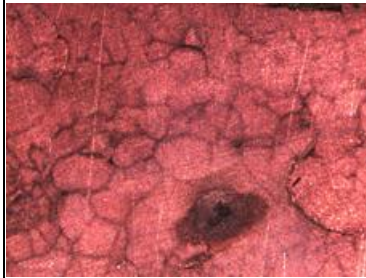
14X-1



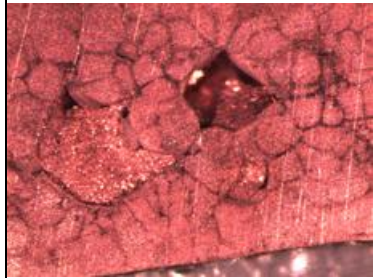
14X-2



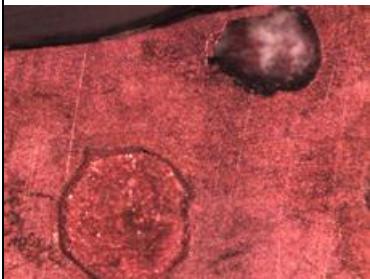
14X-3



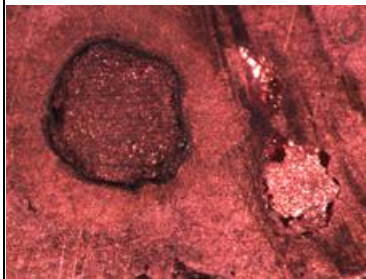
28X-1



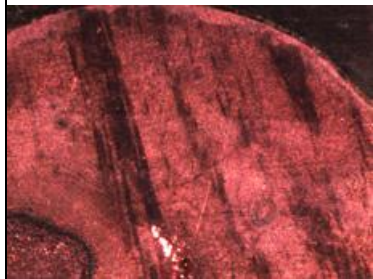
28X-2



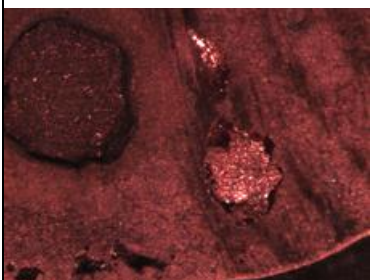
28X-3



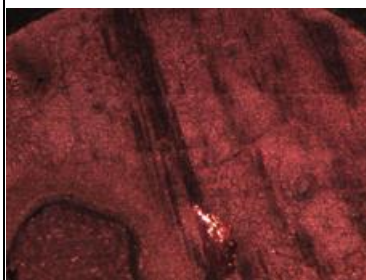
28X-4



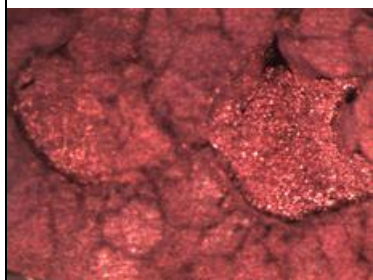
28X-5



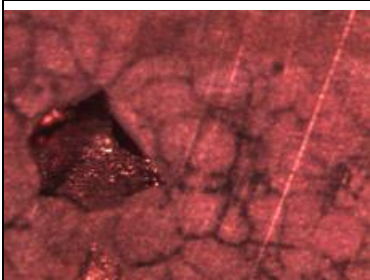
28X-6



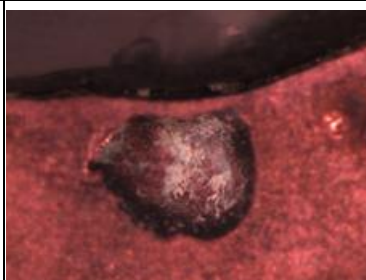
28X-7



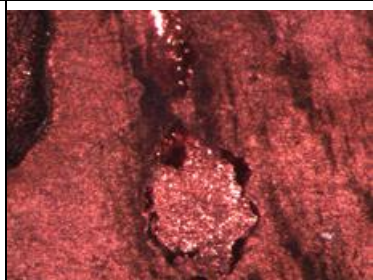
44X-1



44X-2

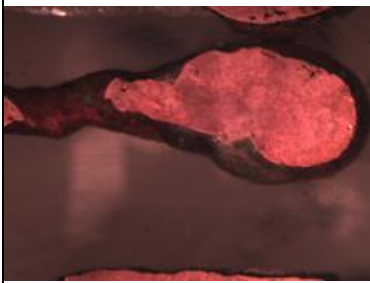


44X-3

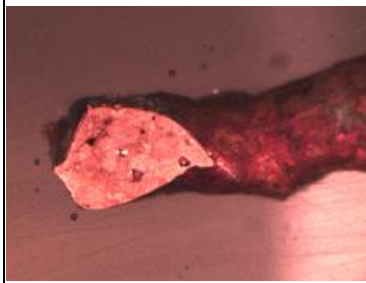


44X-4

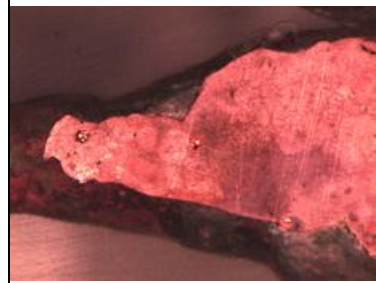
12R-NE-SC (S39)



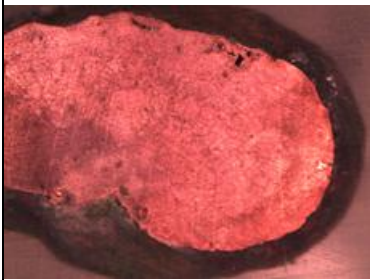
7X



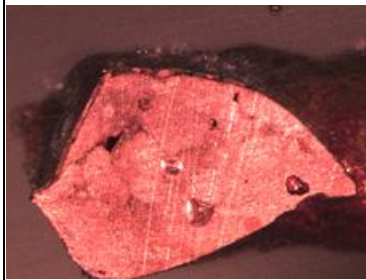
14X-1



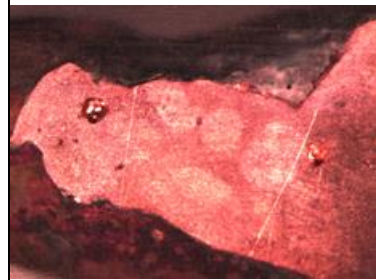
14X-2



14X-3



28X-1



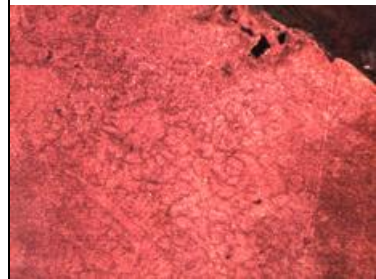
28X-2



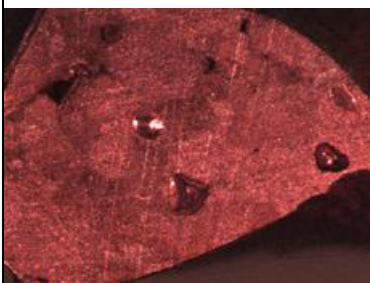
28X-3



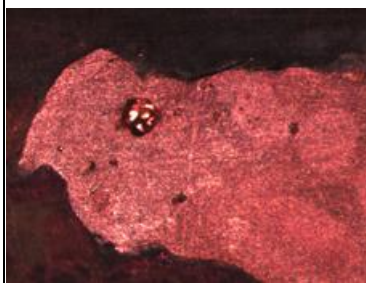
28X-4



28X-5



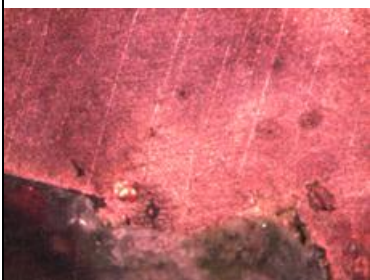
44X-1



44X-2



44X-3



44X-4



44X-5

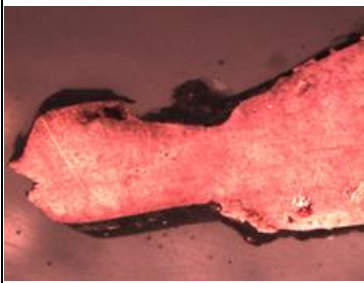


44X-6

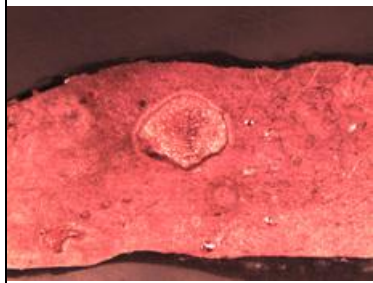
12R-NE-SC (S40)



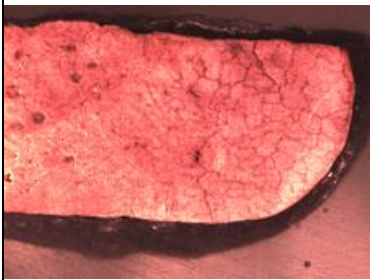
7X



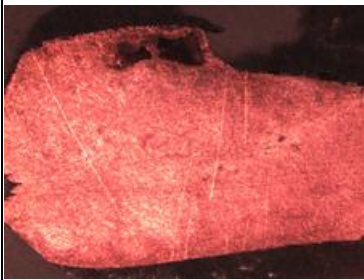
14X-1



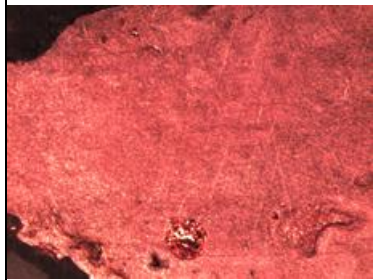
14X-2



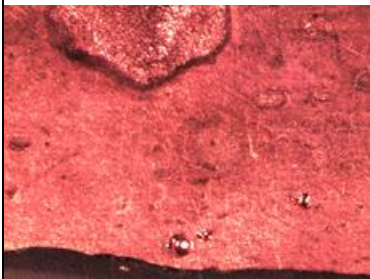
14X-3



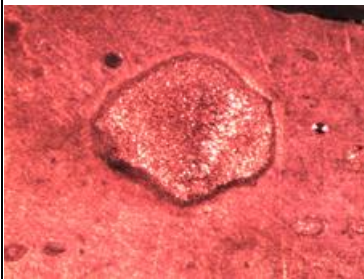
28X-1



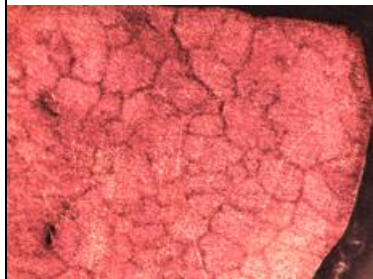
28X-2



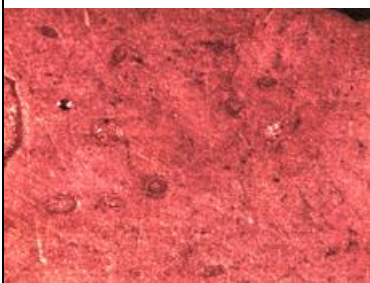
28X-3



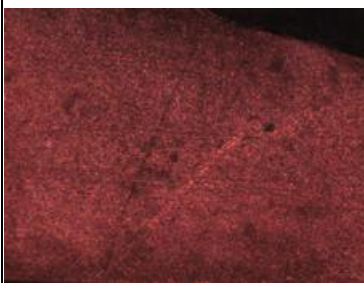
28X-4



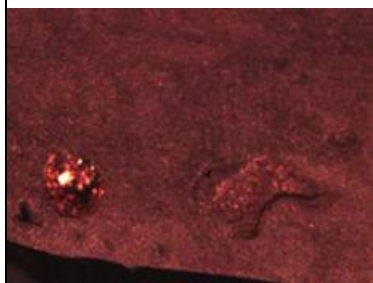
28X-5



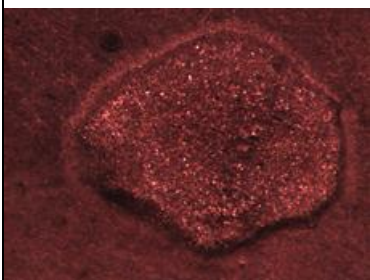
28X-6



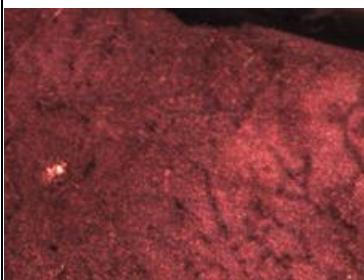
44X-1



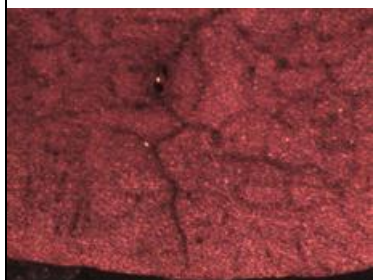
44X-2



44X-3

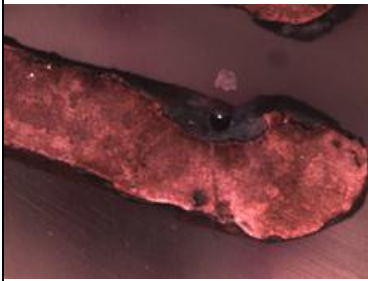


44X-4

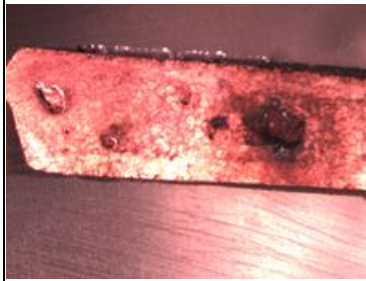


44X-5

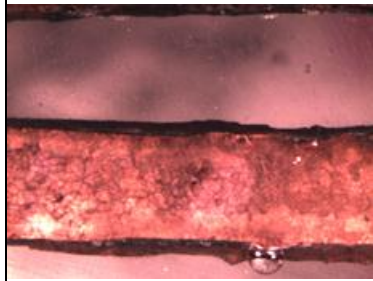
14R-NE-R (S53)



7X



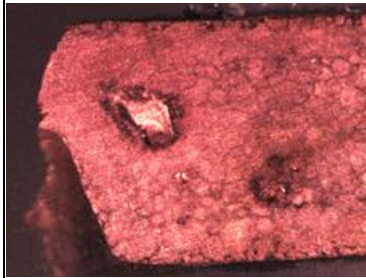
14X-1



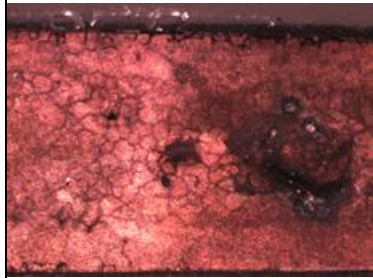
14X-2



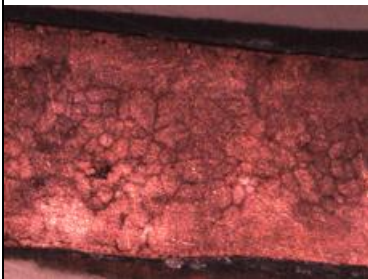
14X-3



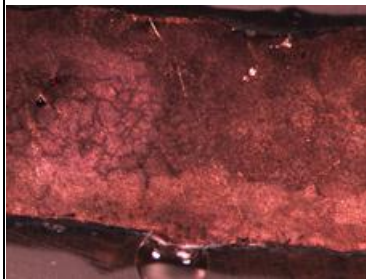
28X-1



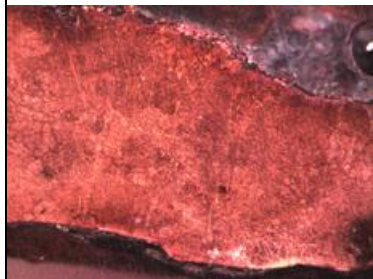
28X-2



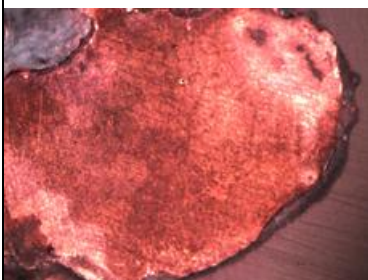
28X-3



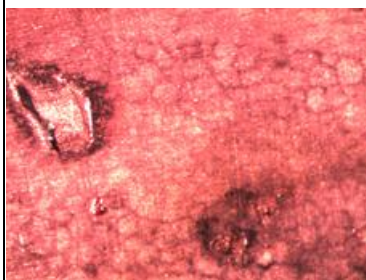
28X-4



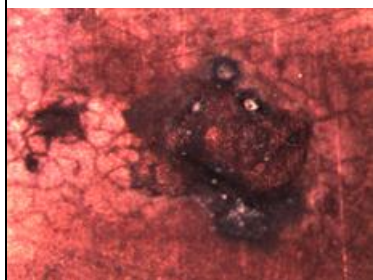
28X-5



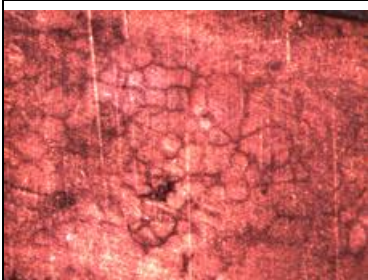
28X-6



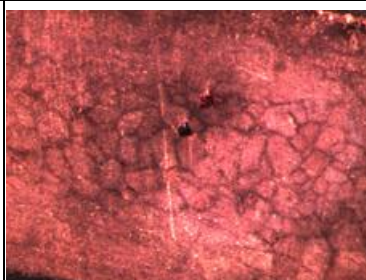
44X-1



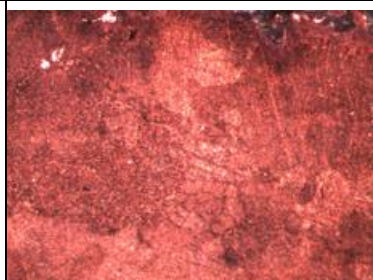
44X-2



44X-3

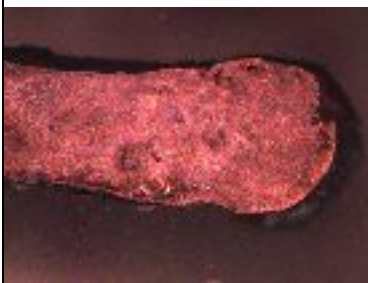


44X-4



44X-5

14R-NE-R (S54)



14X



14X-1



14X-2



14X-3



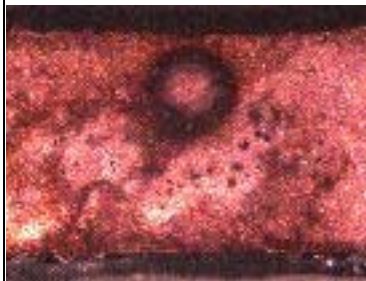
28X-1



28X-2



28X-3



28X-4



28X-5



28X-6



28X-7



44X-1



44X-2



44X-4

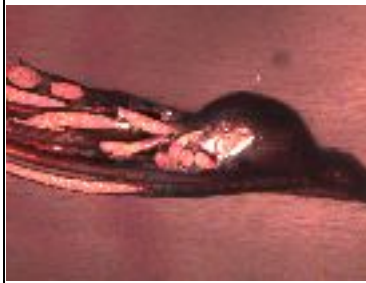


44X-5

**16MS-L-DF (S16)**



7X



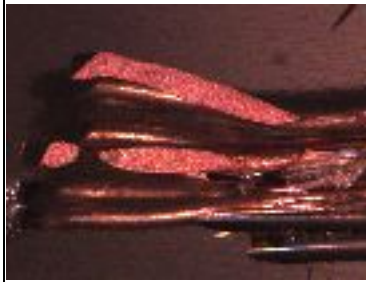
14X-1



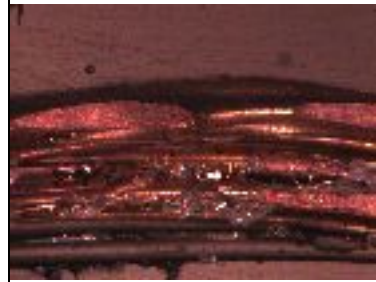
14X-2



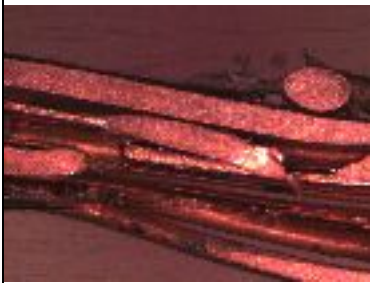
14X-3



28X-1



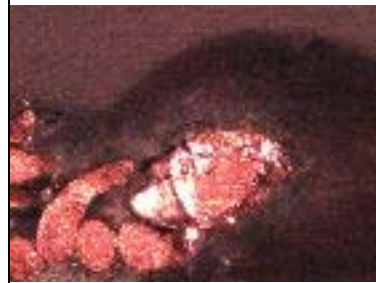
28X-2



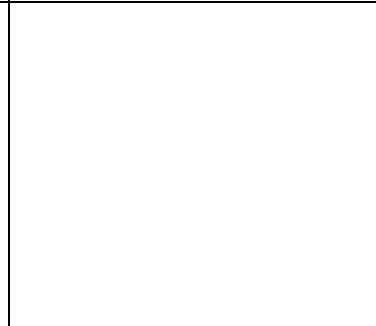
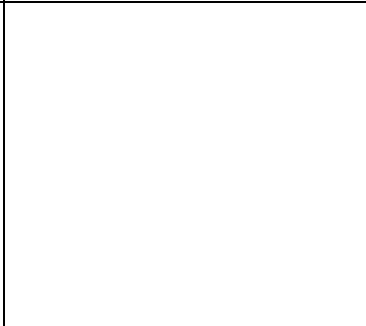
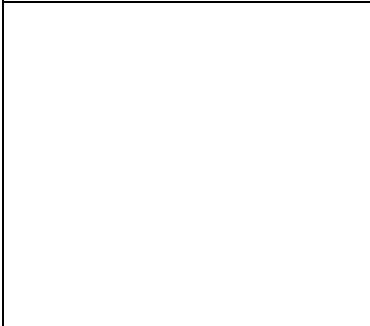
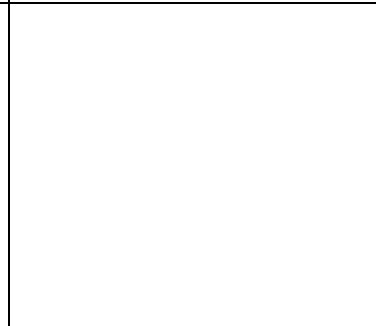
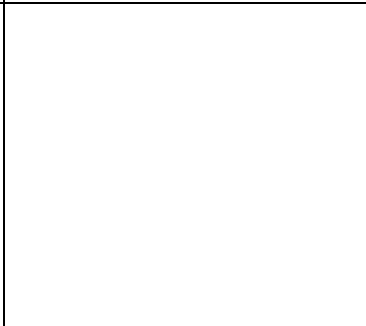
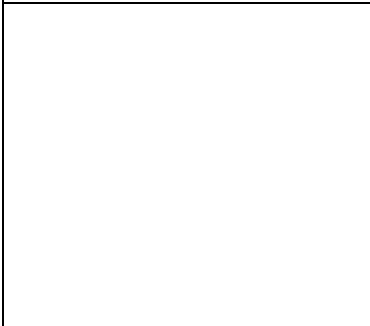
28X-3



28X-4



44X-1





**18MS-L-DF (S17)**



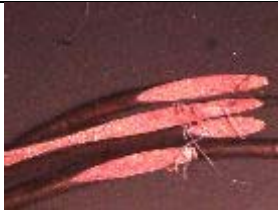
7X



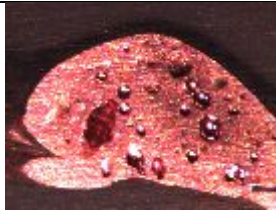
14X-1



28X-1



28X-2

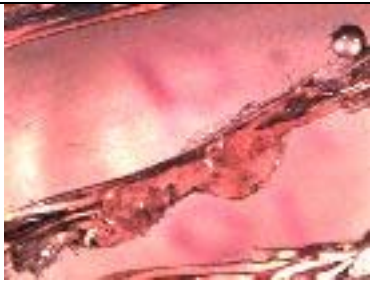


44X-1

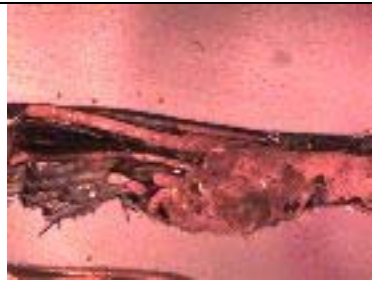


44X-2

**18MS-L-DF (S18)**



7X



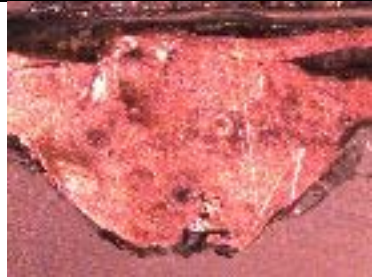
14X-1



14X-2



14X-3



28X-1



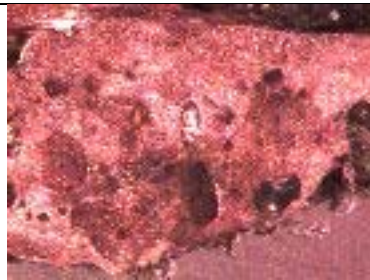
28X-2



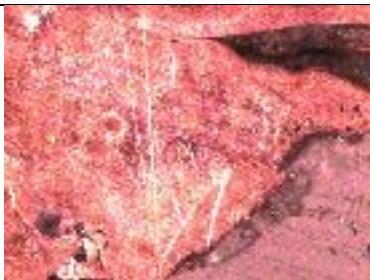
28X-3



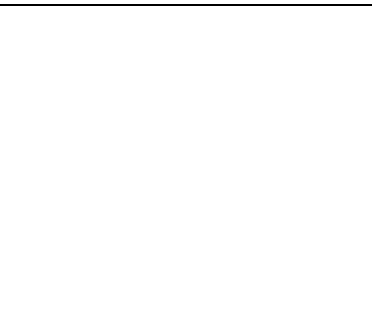
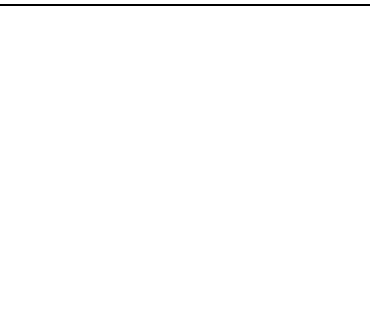
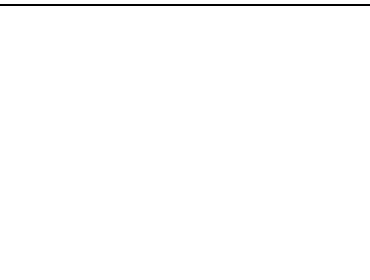
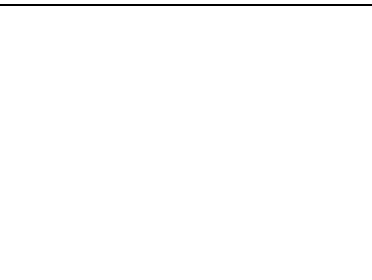
44X-1



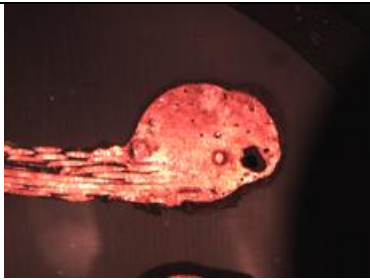
44X-2



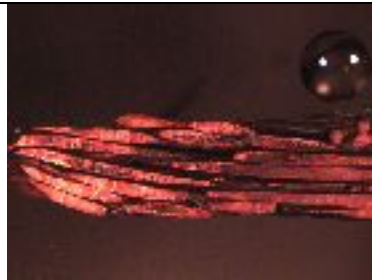
44X-3



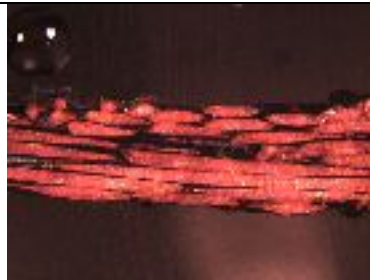
18MS-L-SC (S4)



7X



14X-1



14X-2



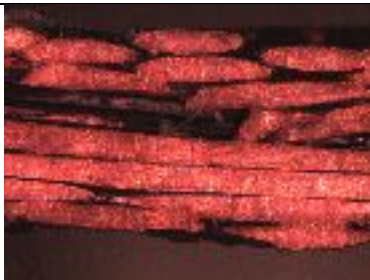
14X-3



28X-1



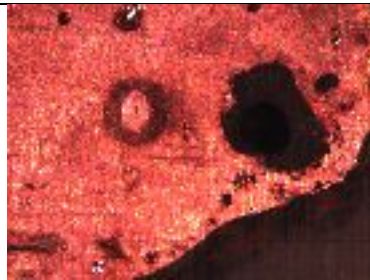
28X-2



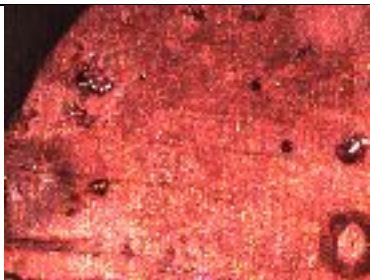
28X-3



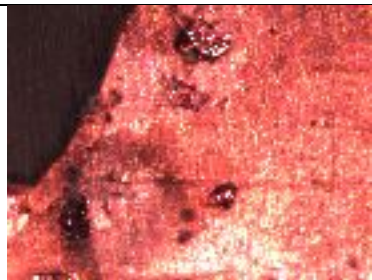
28X-4



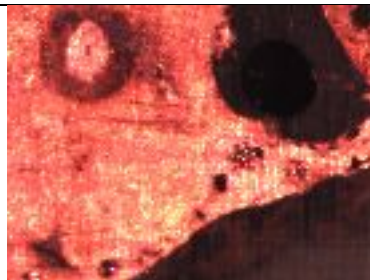
28X-5



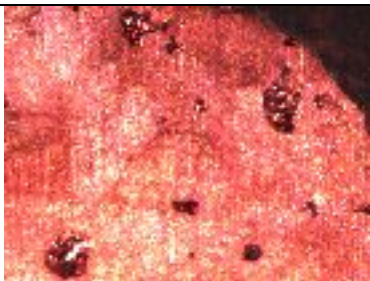
28X-6



44X-1

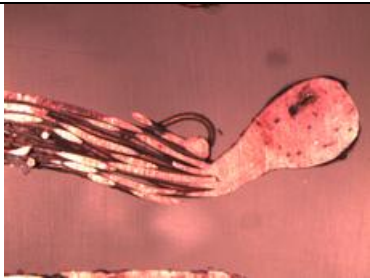


44X-2



44X-3

18MS-L-SC (S5)



7X



14X-1



14X-2



28X-1



28X-2



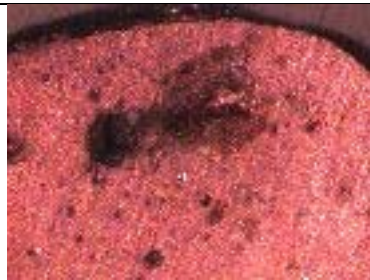
28X-3



44X-1



44X-2

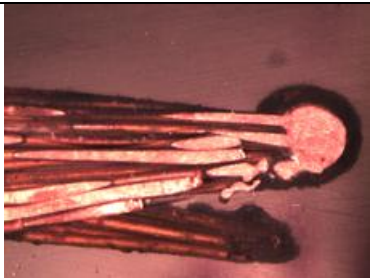


44X-3

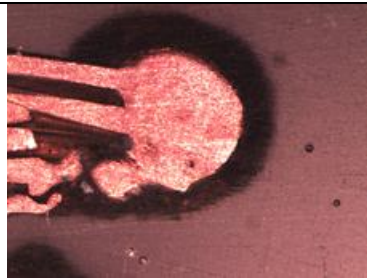


44X-4

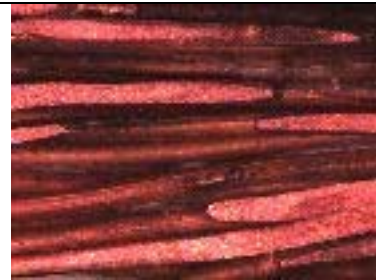
18MS-L-SC (S6)



14X



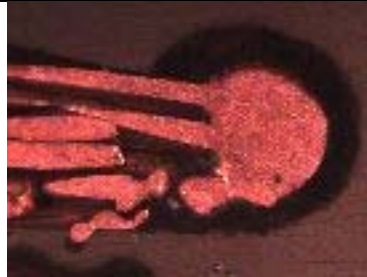
28X-1



28X-2



28X-3



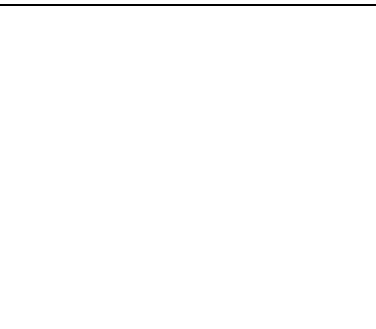
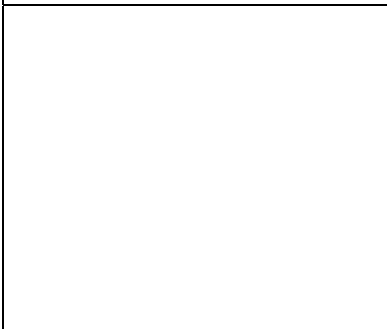
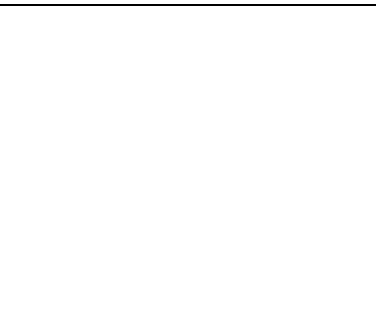
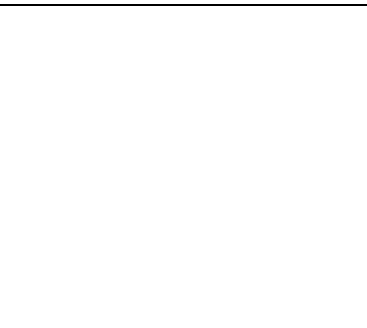
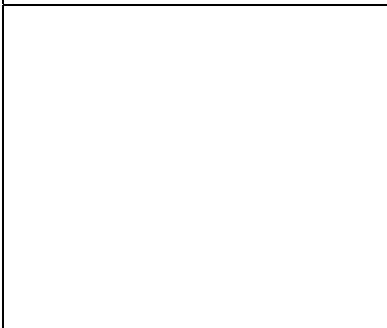
28X-1



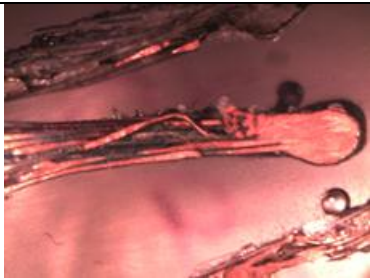
28X-2



28X-3



18MS-L-R (S19)



7X



14X-1



28X-1



28X-2



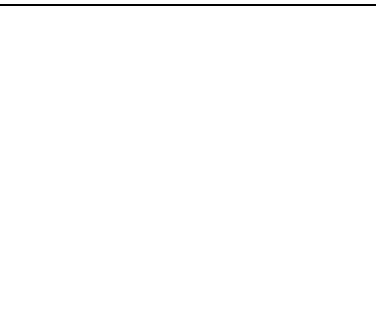
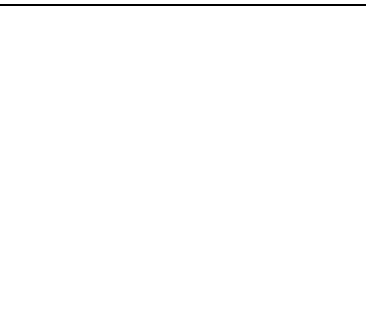
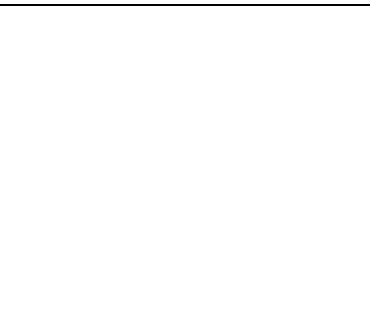
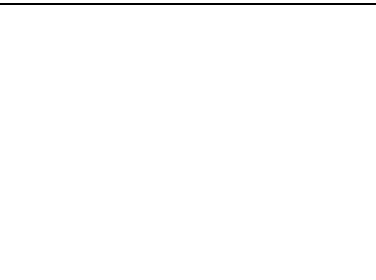
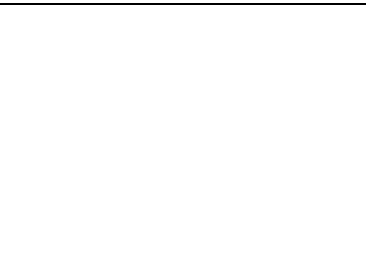
28X-3



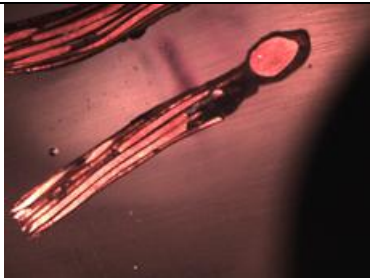
44X-1



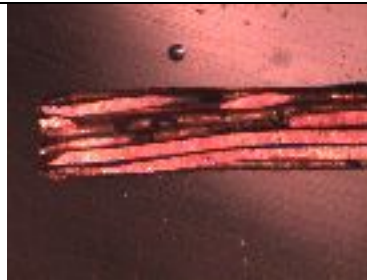
44X-2



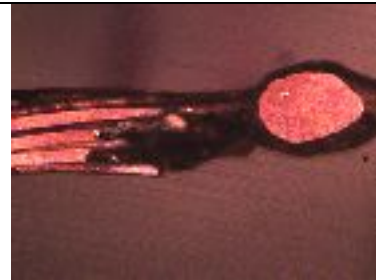
18MS-L-SC (S21)



7X



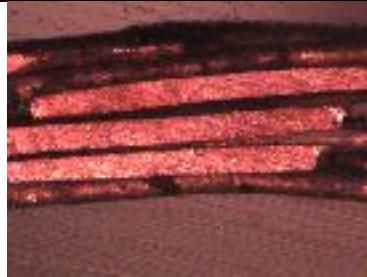
14X-1



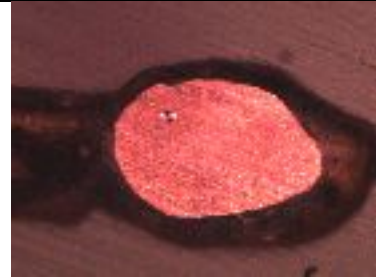
14X-2



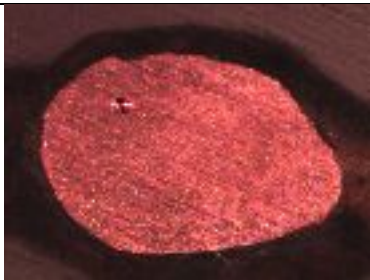
28X-1



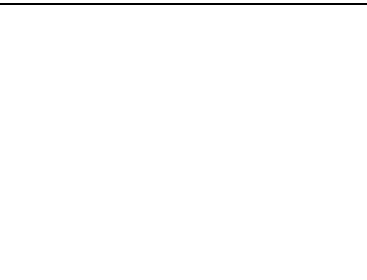
28X-2



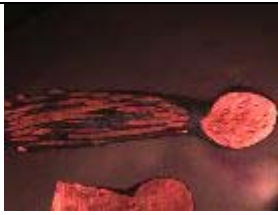
28X-3



44X-1



18MS-NE-DF (S13)



7X



14X-1



14X-2



14X-3



28X-1



44X-1



44X-2



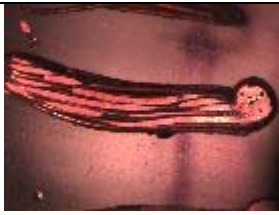
44X-3



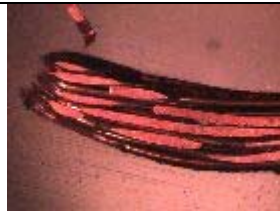
44X-4



18MS-NE-DF (S14)



7X



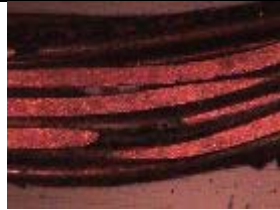
14X-1



14X-2



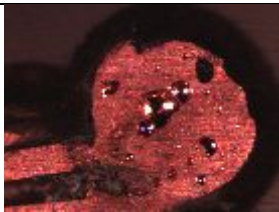
28X-1



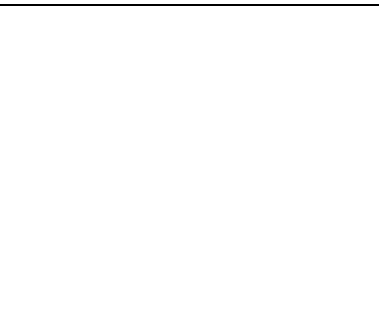
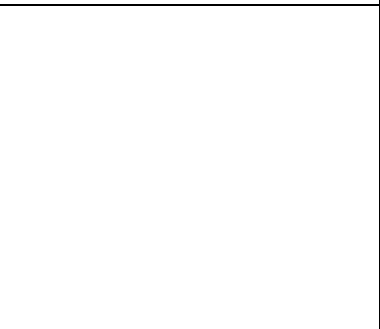
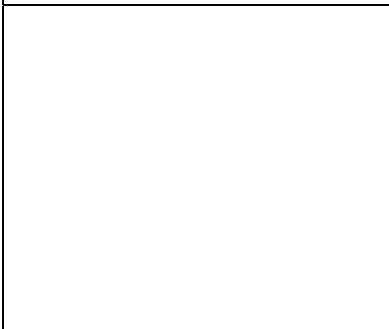
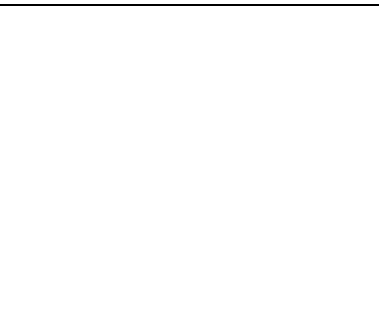
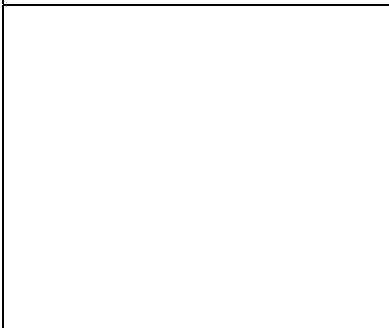
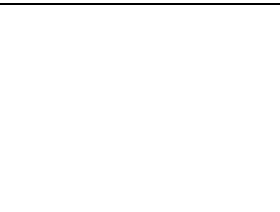
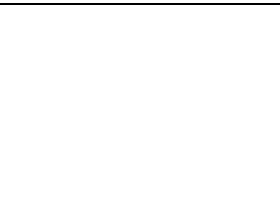
28X-2



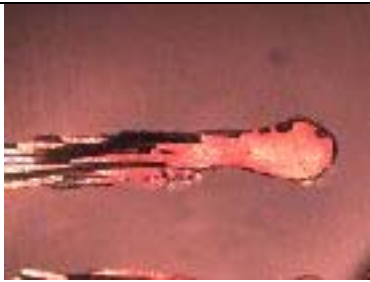
28X-3



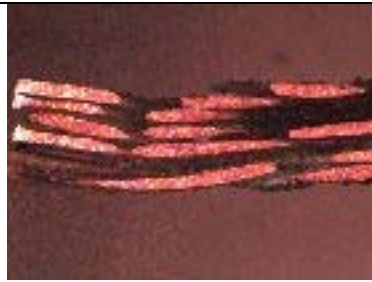
44X-1



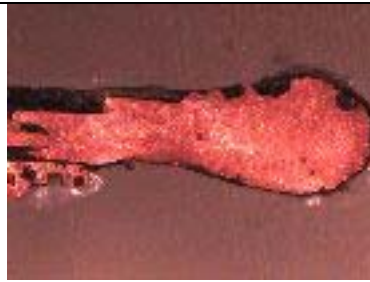
18MS-NE-DF (S15)



7X



14X-1



14X-2



28X-1



28X-2



28X-3



44X-31



44X-2

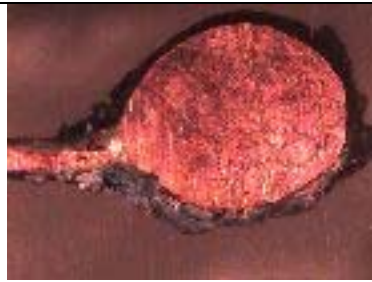


44X-3

**18MS-NE-SC (S1)**



7X



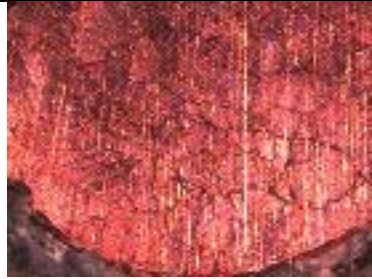
14X-1



14X-2



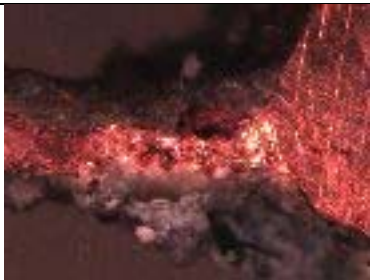
14X-3



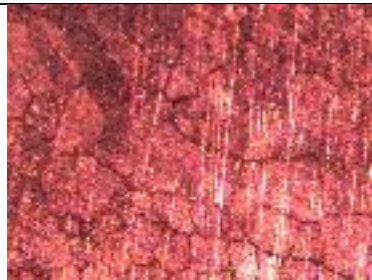
28X-1



28X-2



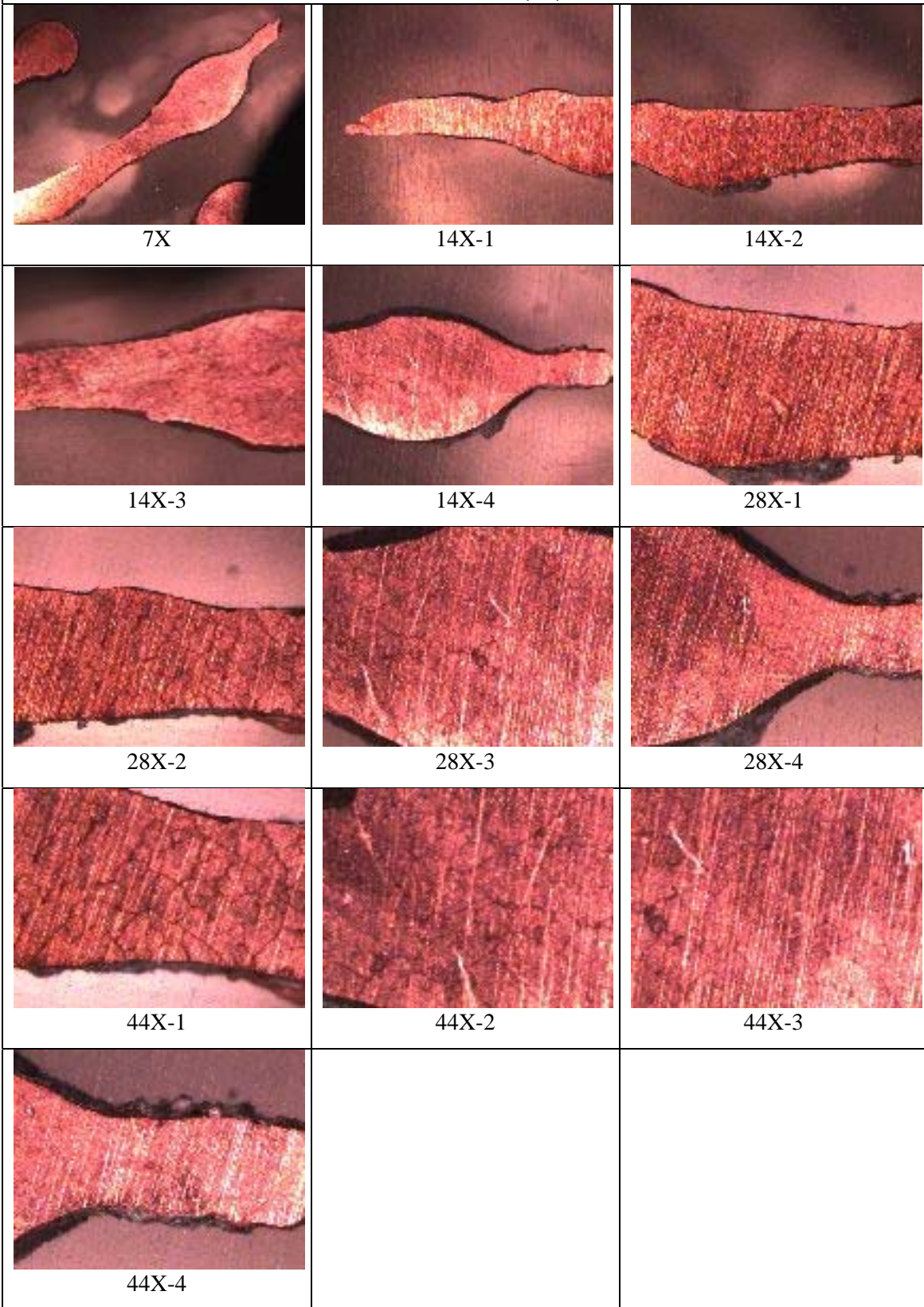
28X-3







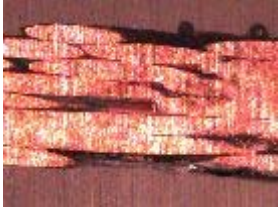
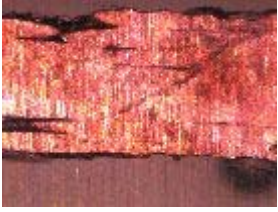
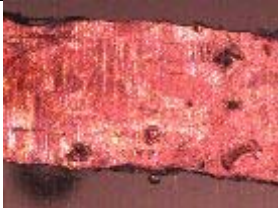
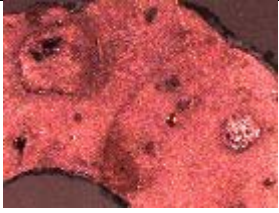
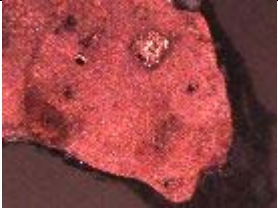
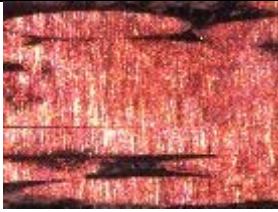
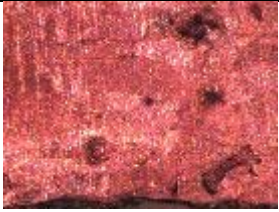
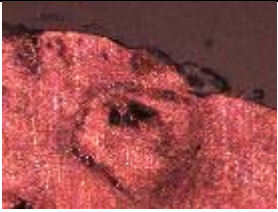
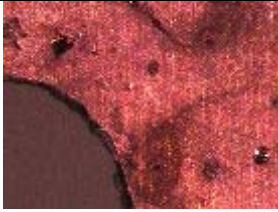
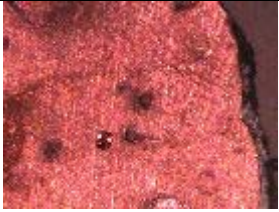

28X-4



18MS-NE-SC (S2)



**18MS-NE-SC (S3)**

 <p>7X</p>	 <p>14X-1</p>	 <p>14X-2</p>
 <p>14X-3</p>	 <p>28X-1</p>	 <p>28X-2</p>
 <p>28X-3</p>	 <p>28X-4</p>	 <p>28X-5</p>
 <p>44X-1</p>	 <p>44X-2</p>	 <p>44X-3</p>
 <p>44X-4</p>	 <p>44X-5</p>	 <p>44X-6</p>

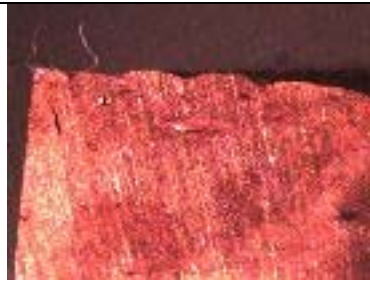
**16MS-NE-R (S25)**



14X



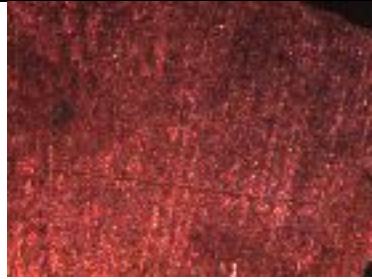
28X-1



28X-2



28X-3



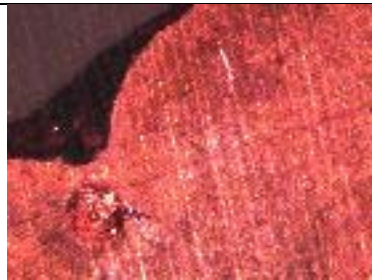
28X-4



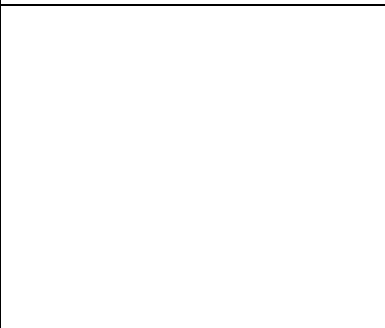
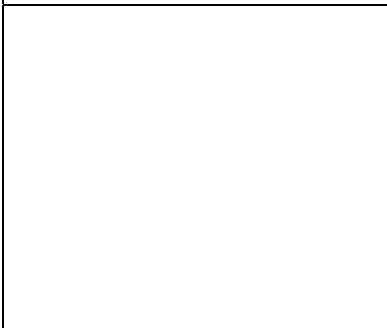
28X-5



44X-1



44X-2



## **APPENDIX 4**

### **A. Report Metallurgical Analysis**

#### **B. Metallurgical Images**

<b>DF</b>	<b>Direct Flame</b>
<b>SC</b>	<b>Scaled Compartment</b>
<b>R</b>	<b>Radiation</b>
<b>FSC</b>	<b>Full-Scale Compartment</b>
<b>L</b>	<b>Energized with Load</b>
<b>E</b>	<b>Energized no-load</b>
<b>NE</b>	<b>Non-energized</b>

## APPENDIX 4A



### **Accident Reconstruction Analysis, Inc.**

---

#### **Report of Metallurgical Findings on Copper Wire Analysis Testing Performed by Combustion Science and Engineering**

**3/23/12**

#### **Discussion**

The samples that were analyzed consist of copper wiring intended for use as electrical conductors. This copper wiring is essentially in a cold worked state, and control samples were mounted by ARAI to aid in the analysis. ARAI examined the samples using a metallurgical microscope and documented the condition using a digital camera. The individual images of each sample were then merged together into composite images and printed to allow samples to be evaluated as a group. This process greatly aided the analysis in that various physical aspects of the samples could be compared at once. Once all the samples were laid out, dramatic differences in the copper grain structure was noted. These differences are the result of grain growth due to thermal exposure. Cold worked copper (control samples) have very small grains, but as the copper is heated the grains begin to grow and can continue to grow to much larger sizes. The samples that ARAI was provided had been subjected to various test conditions. These conditions include thermal exposure from a radiant heat source, thermal exposure from convection due to the sample being within a compartment fire, and thermal exposure due to direct flame impingement. Some of the wiring was energized and some was not energized at the time of thermal exposure. All of the samples had areas of melting either due to electrical arcing or



thermal exposure. A side by side review of all samples revealed that no one physical feature would allow for conclusive determination of what the copper had experienced under test. The analysis revealed various grain sizes, various rates of grain size change, and various amounts of porosity. There was no conclusive event that could explain the variations for all samples. Furthermore, some samples contained dendritic structures within the melted areas, some did not. Dendritic structures are the result of rapid cooling of a melted metal and can be seen in various areas of the re-solidified portions of the melted copper. There are a few samples where the sharp demarcation in grain size would allow for the correct conclusion that these wires had been arced, but these were a select few of the number of samples analyzed by ARAI personnel.

### **Conclusions**

In conclusion based upon the combined effort and experience of the authors in metallurgy, engineering, and fire investigations, the following conclusions can be drawn on the metallurgical analysis of wire samples collected from fire scenes as well as the wording in NFPA 921 and used by others. Based upon the metallurgy, copper wiring will experience an enlargement of grain structure that is a direct result of the level of temperature increase and duration of exposure. Based upon this increase in grain size, it may be possible to differentiate copper wiring that has experienced an electrical arc event only. However, if a copper wire experiences an electrical arc event and then is subsequently heated, enlargement of the grain size may occur which could preclude any conclusive determination as to the nature of the event. The overwhelming conclusion is that from a metallurgical standpoint, one cannot analyze

only a copper wire and determine if melting present was the result of electrical activity or increased temperature from thermal exposure. While it holds true that localized changes to the copper's grain structure will occur as a result of electrical arcing, and this could have a clear line of demarcation as observed in several analyzed samples, subsequent heating could cause the final condition of the wire to be similar to a wire that has experienced melting when it was not energized. As an investigator and engineer, one must examine all the evidence and apply the scientific method in determining if an individual instance of melting found on copper wiring is evidence of electrical activity or thermal exposure. It is the conclusion of these authors, that the wording in NFPA 921 would need proper interpretation and could use some clarification. Specific samples that were analyzed would have the exterior lines of demarcation cited in NFPA 921 as evidence of globule or bead, but only the metallurgical analysis would differentiate between electrical activity and thermal exposure. While the metallurgical analysis would assist in many cases the determination of whether an electrical event has occurred or if a wire was only exposed to temperature sufficient to cause melting, will require knowledge of the fire scene and the application of the scientific method, not just evidence of lines of demarcation. Additional testing and analysis may reveal certain trends that may hold true as a correlation for thermal exposure.

Respectfully submitted,

Charles R. Manning, Jr. Ph.D., P.E.  
Thomas C. Wenzel M.S., P.E.  
Jonathan M. Thomas B.S.M.E.

**APPENDIX 4B**

**Note:**

**NE – Non Energized**

**EN – Energized**

**L – Loaded**

**SCALED COMPARTMENT TEST; 18-2 MULTISTRAND WIRE**

**NON ENERGIZED**

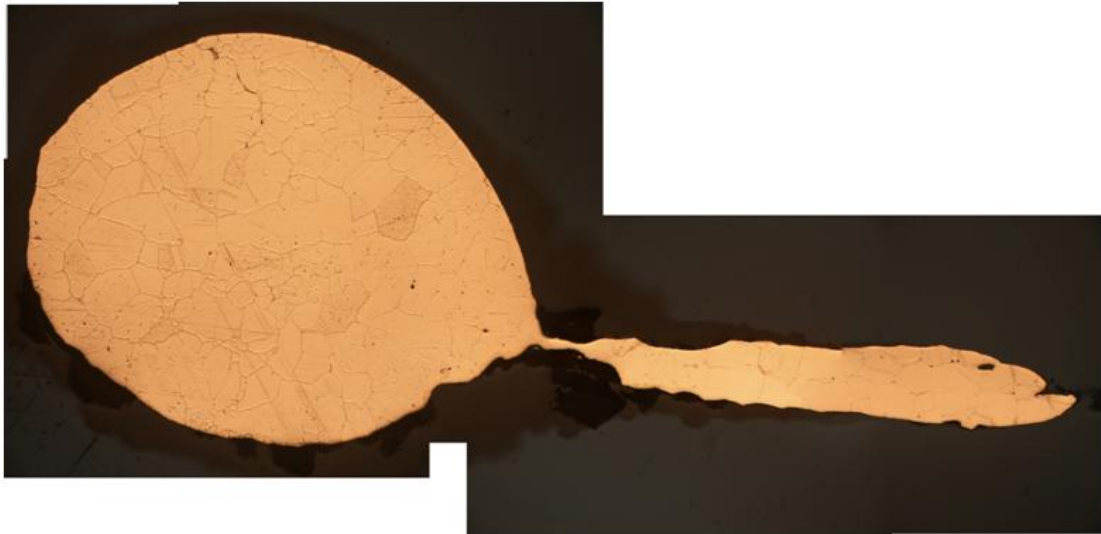


Figure 1: Compartment Tests, MS 18-2, NE (Sample # 1)



Figure 2: Compartment Tests, MS 18-2, NE (Sample # 2)



Figure 3: Compartment Tests, MS 18-2, NE (Sample # 3)

**LOADED**



Figure 4: Compartment Tests, MS 18-2, Loaded (Sample # 4)



Figure 5: Compartment Tests, MS 18-2, Loaded (Sample # 5)

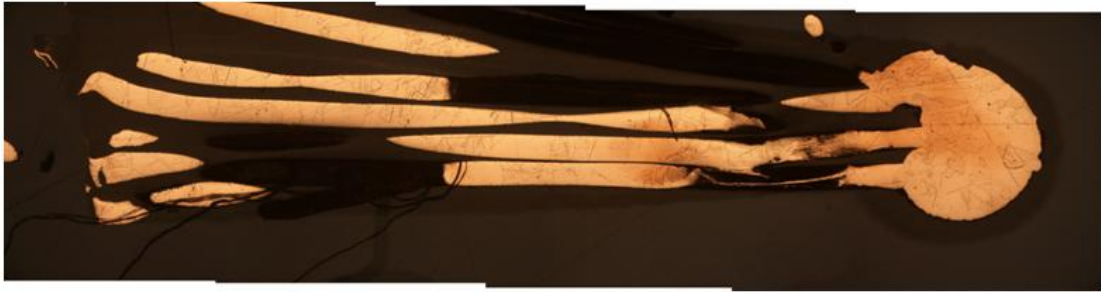


Figure 6: Compartment Tests, MS 18-2, Loaded (Sample # 6)

**SCALED COMPARTMENT TEST; 12-2 ROMEX WIRE**  
**NON ENERGIZED**



Figure 7: Compartment Tests, ROMEX 12-2, Non Energized (Sample # 38)

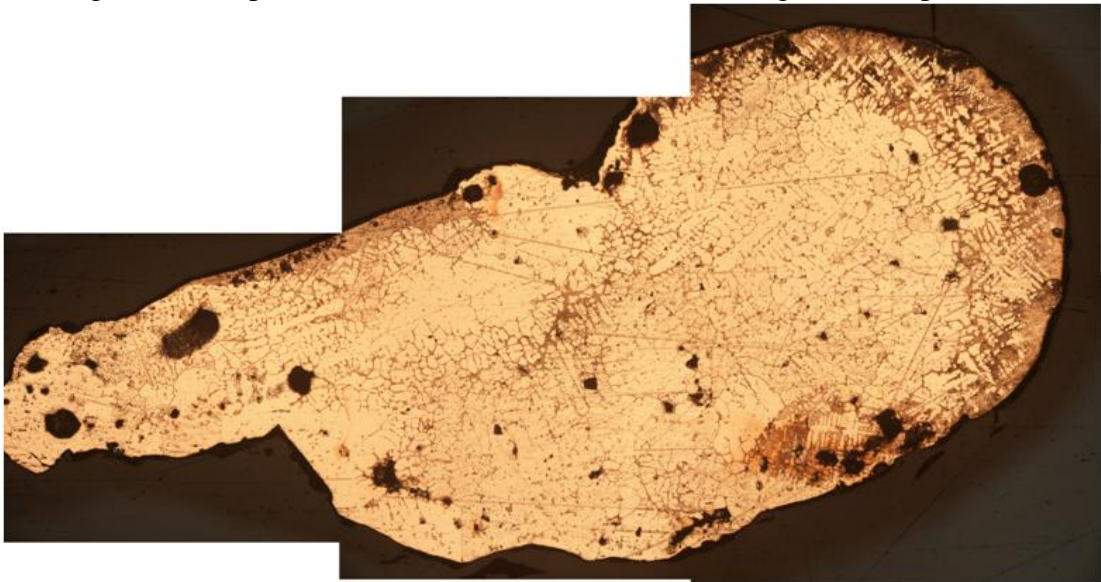


Figure 8: Compartment Tests, ROMEX 12-2, Non Energized (Sample # 39)



Figure 9: Compartment Tests, ROMEX 12-2, Non Energized (Sample # 40)

**LOADED**

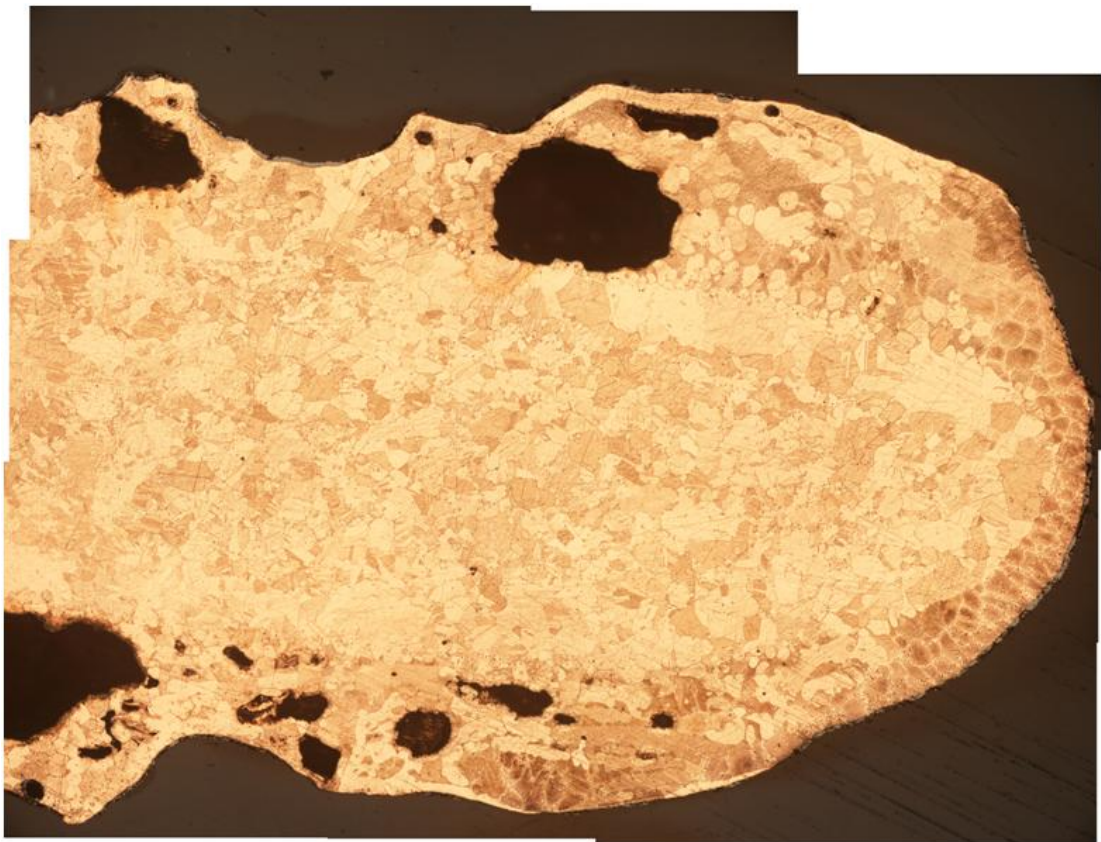


Figure 10: Compartment Tests, ROMEX 12-2, Loaded (Sample # 41)



Figure 11: Compartment Tests, ROMEX 12-2, Loaded (Sample # 42)

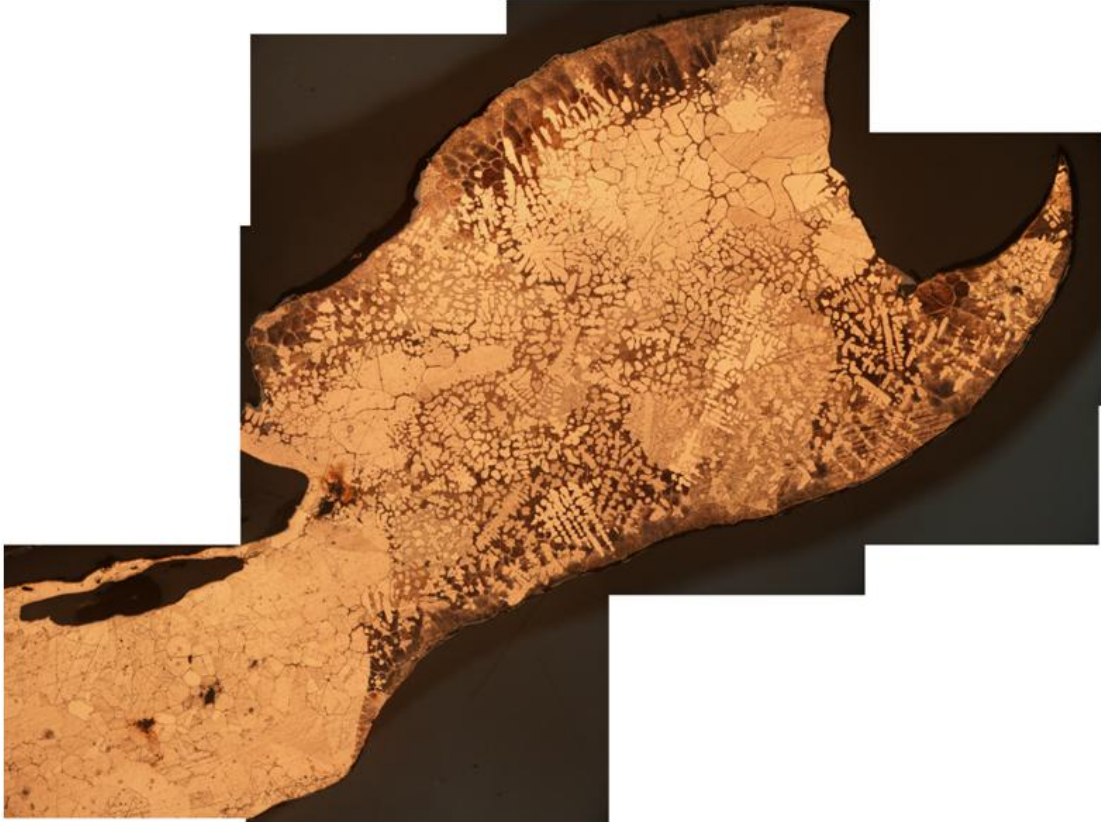


Figure 12: Compartment Tests, ROMEX 12-2, Loaded (Sample # 43)

**DIRECT FLAME TEST; 18-2 MULTISTRAND WIRE**

**NON ENERGIZED**



Figure 13: Direct Flame Tests, MS 18-2, Non Energized (Sample # 13)



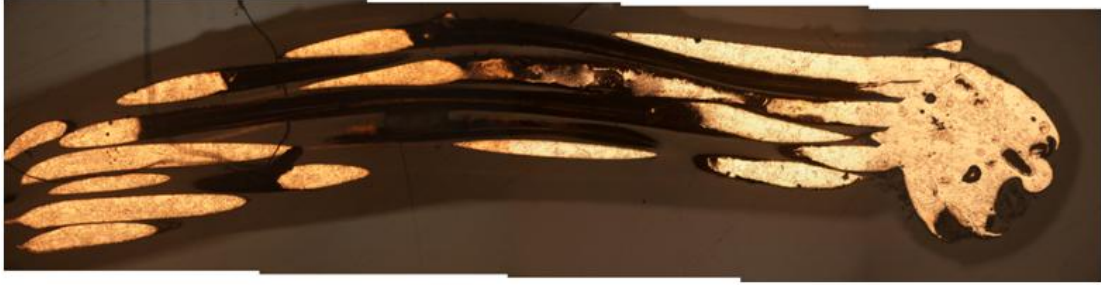


Figure 14: Direct Flame Tests, MS 18-2, Non Energized (Sample # 14)



Figure 15: Direct Flame Tests, MS 18-2, Non Energized (Sample # 15)

**LOADED**

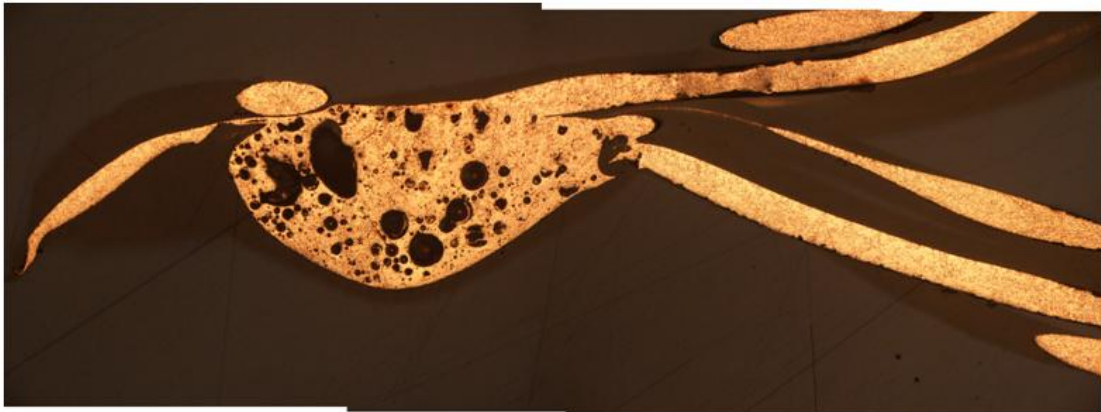


Figure 16: Direct Flame Tests, MS 18-2, Loaded (Sample # 17)

**DIRECT FLAME TEST; 12-2 ROMEX WIRE**  
**NON ENERGIZED**



Figure 17: Direct Flame Tests, MS 12-2, Non Energized (Sample # 29)

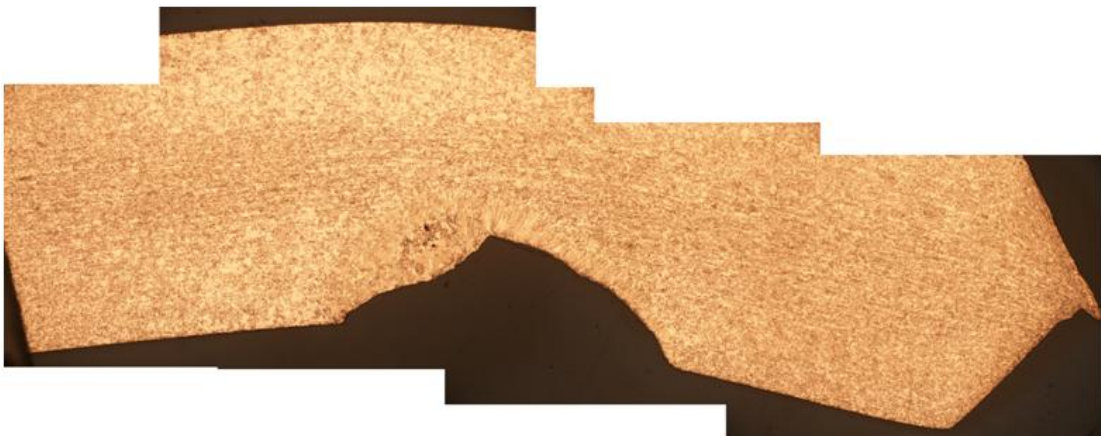


Figure 18: Direct Flame Tests, MS 12-2, Non Energized (Sample # 30)



Figure 19: Direct Flame Tests, MS 12-2, Non Energized (Sample # 31)

**LOADED**

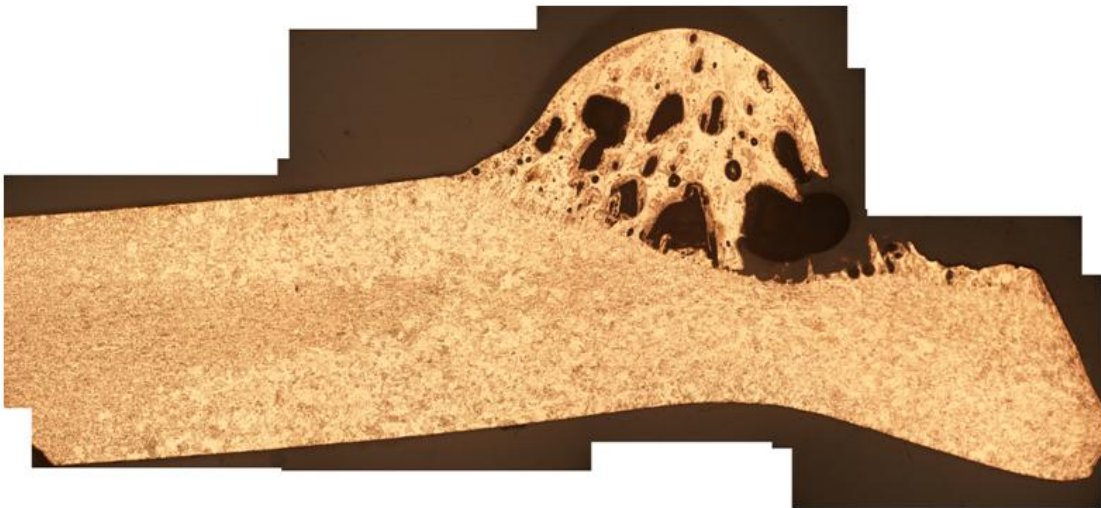


Figure 20: Direct Flame Tests, MS 12-2, Loaded (Sample # 32)

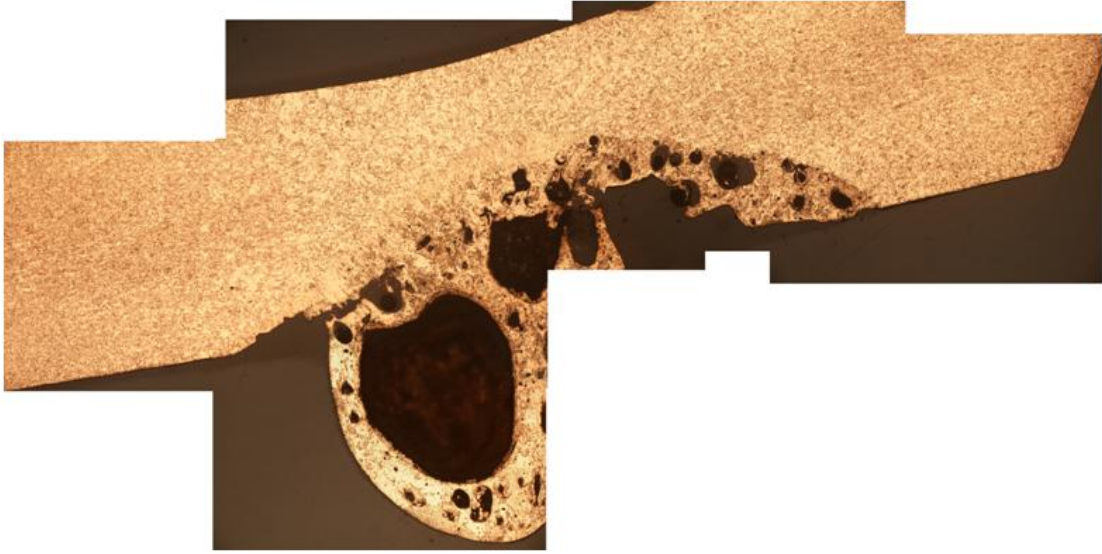


Figure 21: Direct Flame Tests, MS 12-2, Loaded (Sample # 33)



Figure 22: Direct Flame Tests, MS 12-2, Loaded (Sample # 34)

**RADIATION TEST; 18-2 MULTISTRAND WIRE**

**LOADED**



Figure 21: Radiation Tests, MS 18-2, Loaded (Sample # 21)

**RADIATION TEST; 16-2 MULTISTRAND WIRE**

**NON ENERGIZED**



Figure 22: Radiation Tests, MS 16-2, Non Energized (Sample # 25)

**RADIATION TEST; 14-2 MULTISTRAND WIRE**

**NON ENERGIZED**



Figure 23: Radiation Tests, MS 14-2, Non Energized (Sample # 53)



Figure 24: Radiation Tests, MS 14-2, Non Energized (Sample # 54)

**LOADED**

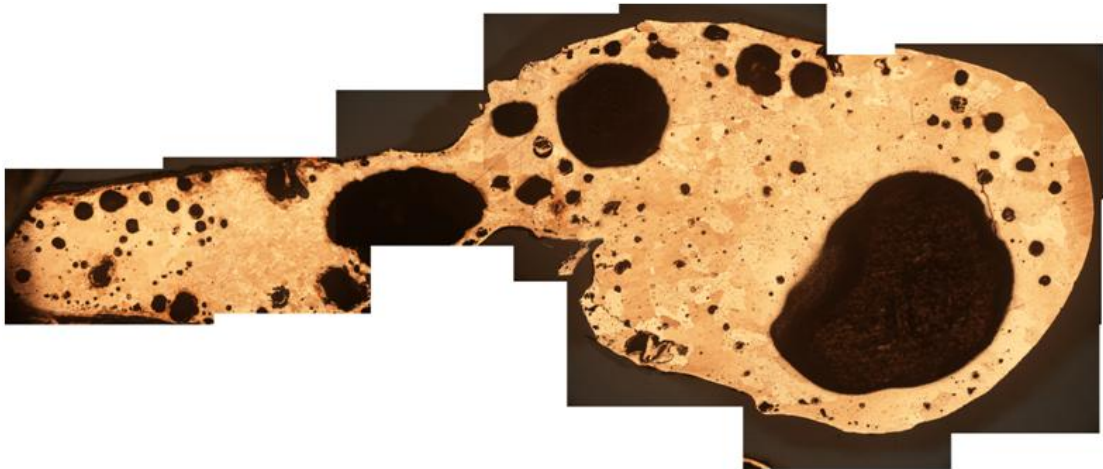


Figure 25: Radiation Tests, MS 14-2, Loaded (Sample # 50)

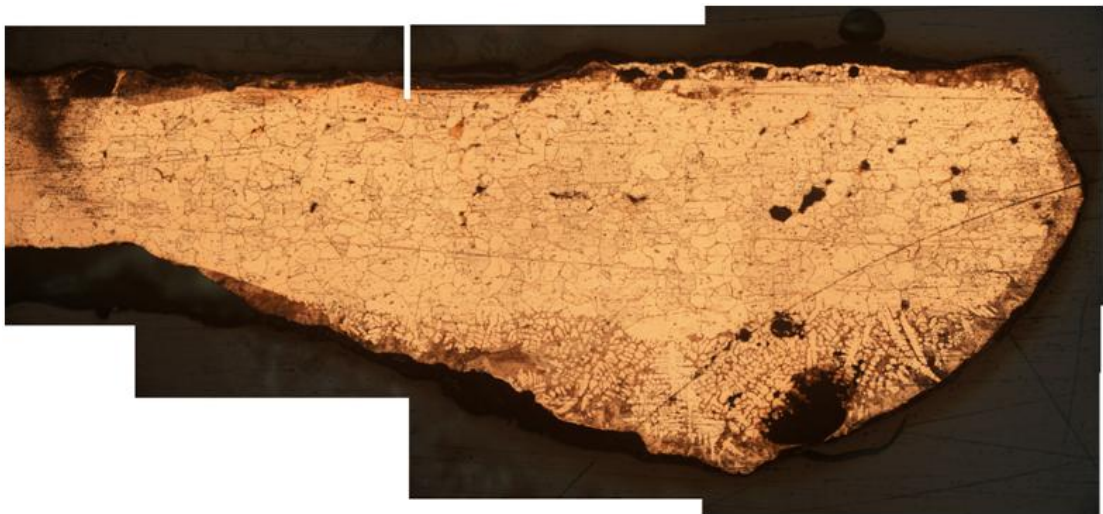


Figure 26: Radiation Tests, MS 14-2, Loaded (Sample # 51)

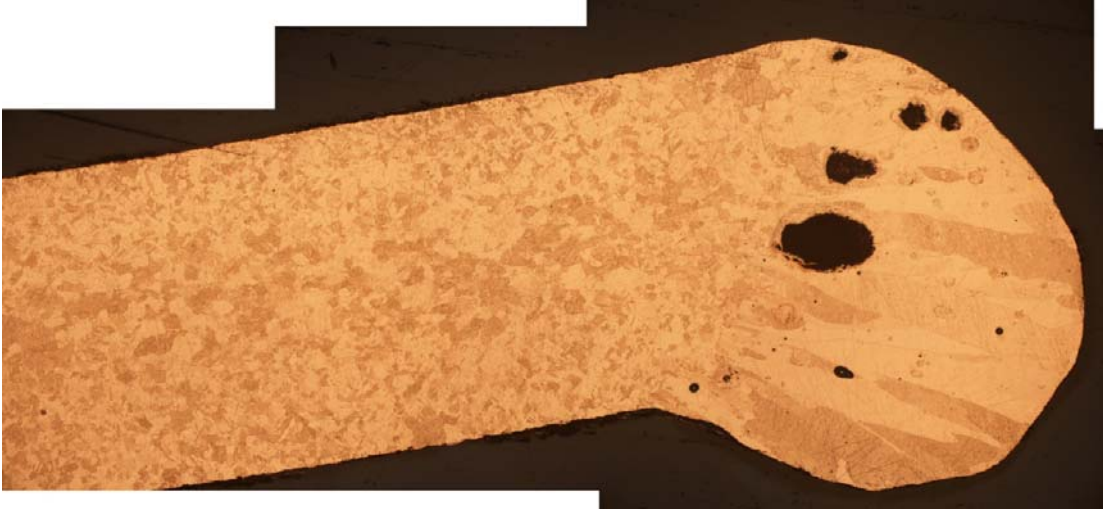


Figure 27: Radiation Tests, MS 14-2, Loaded (Sample # 52)

**NON TESTED WIRE; 16-2 MULTISTRAND WIRE**



Figure 28: Non-Tested, MS 16-2

**NON TESTED WIRE; 18-2 MULTISTRAND WIRE**



Figure 29: Non-Tested, MS 18-2



**NON TESTED WIRE; 14-2 MULTISTRAND WIRE**



Figure 30: Non-Tested; Romex 14-2

## REFERENCES

1. Anderson, R. N. (1989). Surface Analysis of Electrical Arc Residues in Fire Investigation. *Journal of Fire Sciences*, 34 (3), 633-637.
2. Anderson, R. N. (1996). Which Came First? Arcing or the Fire: A Review of Auger Analysis of Electrical Arc Residues. *Fire and Arson Investigator*, 46 (3), 38-40.
3. Andersson, P. and Van Hees, P. (2005). Performance of Cables Subjected to Elevated Temperatures. *Fire Safety Science—Proceedings of the Eighth International Symposium*, pp. 1121-1132.
4. Armstrong, W. R. (1999). Thermally Induced Failure of Low-Voltage Electrical Nonmetallic-sheathed Cable Insulation. *Fire Technology*, 35(3).
5. Babrauskas, V. (2003). How do Electrical Wiring Faults Lead to Structure Ignitions? *Fire and Materials*, 189-201.
6. Babrauskas, V. (2004), Arc Beads from Fire: Can ‘Cause’ Beads be distinguished from ‘Victim’ Beads by Physical or Chemical Testing?. *Journal of Fire Protection Engineering*, 14.
7. Beland, B. (1980). Examination of Electrical Conductors Following a Fire. *Fire Technology*, 16, 252-258.
8. Beland, B. (1981). Arcing Phenomenon as Related to Fire Investigations. *Fire Technology*, 17 (3), 180-210.
9. Beland, B. (1982). Considerations on Arcing as a Fire Cause. *Fire Technology*, 18, 188-202.
10. Beland, B. (1994). Examination of Arc Beads. *Fire and Arson Investigator*, 44 (4), 20-22.
11. Chen, C. Y. et al. SIMS Depth Profiling Analysis of Electrical Arc Residues in Fire Investigation. *Applied Surface Science*, 203-204, 779-784, 2003.
12. Churchward, D. L. and Cox, R. M. (2010). The ‘Benefits’ of Arcing. *International Symposium on Fire Investigation Science and Technology*. University of Maryland, College Park.
13. Delplace, M. and Vos, E., (1983). Electric Short Circuits Help the Investigator Determine Where the Fire Started. *Fire Technology*, 19 (3), 185-191.
14. Ettling, B. (1978). Electrical Wire in Building Fires. *Fire Technology*, 14, 317-325.
15. FEMA (2008). Residential Building Electrical Fires. 8 (2).
16. Ferrino-McAllister, J. L., Roby, R. J., Milke, J. (2006). Heating of Electrical Contacts: Characterizing the Effects of Torque, Contact Area, and Movement on the Temperature of Residential Receptacles. *Fire Technology*, 42(1), pp. 49-74.

17. Ferrino-McAllister, J. L., Roby, R. J., Klassen, M. S., Milke, J. (2005). Heating of Electrical Conductors: Characterizing the Deformation of Cable Exposed to External Radiant Heating and Internal Overload. *Fire and Arson Investigator*, 56(2).
18. Gray, D. and Lewis, F. A. (1983). Identification of Electrical Sources of Ignition in Fires. *Fire Safety Journal*, 6, 147-150.
19. Goodman, A., Schooler, C. and McAllister, J. L. (2010). Physical Characteristics of Non-energized and Energized Cables in Scaled Compartment Fires. International on Fire Investigation Science and Technology.
20. Hall Jr., J. (2012), NFPA, 'Home electrical fires'
21. Hall, J. (2009). Home Fires Involving Electrical Failure or Malfunction.
22. Henderson, R., Manning, C., and Barnhill, C. (1998). Questions Concerning the Use of Carbon Content to Identify "CAUSE" vs. "RESULT" Beads in Fire Investigation. *Fire and Arson Investigator*, Volume 48, Number 3.
23. Hirschler, M. M. (1997). Analysis of Potential Correlations between Fire Tests for Electrical Cables, and How to Use This Information for Fire Hazard Assessment. *Fire Technology*, 33(4).
24. Hoffman, D. J. (2002). Electrical Power Cord Damage from Radiant Heat and Fire Exposure and Full Scale Burn Tests of Television Sets and Electronic Appliances. DRI Fire and Casualty Seminar, (p. 223). New Orleans.
25. Hagimoto, Y., Watanabe, N. and Okamoto. (1999). Arcing Faults on PVC-covered Electrical Cords, *Proc. 1<sup>st</sup> Conf. of the Assn. of Korean-Japanese Safety Engineering Society*, Kyongju, Korea, p. 221-224.
26. Howitt, D. G. (1997). The Surface Analysis of Copper Arc Beads-A Critical Review. *Journal of Forensic Sciences*, 42 (4), 608-609.
27. Ilgevicus, A. (2004). Analytical and Numerical Analysis and Simulation of Heat Transfer in Electrical Conductors and Fuses. University of the Bundeswehr Munich. PhD in Engineering.
28. Jacobs, J. J. and Dinman, D. J. (2004). Systematic Analysis of Bicistronic Reporter Assay Data. *Nucleic Acid Research*, 32(20).
29. Karlsson, B., and Quintiere, J. (2000). *Enclosure Fire Dynamics*, Chapter 2, page 18.
30. Kehl, G. (1949). *The Principles of Metallographic Laboratory Practice*, 3<sup>rd</sup> Edition, McGraw-Hill Book Company, New York,.
31. Keski-Rahkonen, O., Mangs, J., Bertrand, R., and Rowekamp, M. Fire Induced Damage to Electrical Cables and Fire Growth on Cables.
32. Lee, E-P., Ohtani, H., Matsubara, Y., Seki, T., Hasegawa, H., Imada, S., and Yashiro, I. (2002). Study on Discrimination between Primary and Secondary Molten Marks using Carbonized Residue. *Fire Safety Journal*, 37, 353-368, 2002.

33. Lennard, C. Fire-Determination of Cause: A Review 1995-1998.
34. Levinson, D. W. (1977). Copper Metallurgy as a Diagnostic Tool for Analysis of the Origin of Building Fires. *Fire Technology*, 13 (3), 211-222, 1977.
35. Mota, C. A. A. et al. (2008). Identification of Heat Flux Imposed by an Oxyacetylene Torch. *American Institute of Aeronautics and Astronautics*.
36. NFPA. (2010). *Guide for Fire and Explosion Investigation*, Chapter 8: Electricity and Fires.
37. Singh, R. P. (1987). Scanning Electron Microscopy of Burnt Electric Wires. *Scanning Microscopy*, 1(4), 1539-1544, 1987.
38. Slenski, G. and Galler, D. (2004). Wire and Cables. *Electronic Failure Analysis Handbook*, Chapter 15.
39. WEI, M., Zhao, Z., and Liang, D. Experiment of Electrical Fire Burned copper Wire and Parameters Analysis on Metallographic Test of Melted Mark. *Procedia Engineering*, 11, 496-503.
40. White, H. E. (1948). *Modern College Physics*. Van Nostrand Reinhold Company, New York, NY.